



HAL
open science

Characterization of the new atmospheric simulation chamber CHARME, and study of the ozonolysis reaction of a biogenic VOC, the γ -terpinene

Layal Fayad

► **To cite this version:**

Layal Fayad. Characterization of the new atmospheric simulation chamber CHARME, and study of the ozonolysis reaction of a biogenic VOC, the γ -terpinene. Earth Sciences. Université du Littoral Côte d'Opale, 2019. English. NNT : 2019DUNK0550 . tel-03030246

HAL Id: tel-03030246

<https://theses.hal.science/tel-03030246>

Submitted on 30 Nov 2020

HAL is a multi-disciplinary open access archive for the deposit and dissemination of scientific research documents, whether they are published or not. The documents may come from teaching and research institutions in France or abroad, or from public or private research centers.

L'archive ouverte pluridisciplinaire **HAL**, est destinée au dépôt et à la diffusion de documents scientifiques de niveau recherche, publiés ou non, émanant des établissements d'enseignement et de recherche français ou étrangers, des laboratoires publics ou privés.



Ecole Doctorale des Sciences de la Matière, du Rayonnement et de l'Environnement
SMRE 104 (Lille, Artois, ULCO, UVHC, Centrale Lille, IMT Lille Douai)

THESE

Présentée en vue d'obtenir le grade de

DOCTEUR de l'Université du Littoral Côte d'Opale

Discipline: **Sciences de la Terre et de l'Univers (Terre, enveloppes fluides)**

Caractérisation de la nouvelle chambre de simulation atmosphérique *CHARME* et étude de la réaction d'ozonolyse d'un COV biogénique, le γ -terpinène

Layal FAYAD

Thèse soutenue le **29 novembre 2019** devant le jury d'examen :

Dr. Abdelwahid MELOUKI , Directeur de Recherche CNRS, ICARE, Université d'Orléans	Rapporteur
Prof. John WENGER , CRAC, Université Collège Cork, Irlande	Rapporteur
Prof. Alexandre TOMAS , SAGE, IMT Lille Douai, France	Examineur
Prof. Peter WIESEN , IAU, Université de Wuppertal, Allemagne	Examineur
Dr. Cécile COEUR , LPCA, Université du Littoral Côte d'Opale, France	Co-directrice de thèse
Prof. Gaël MOURET , LPCA, Université du Littoral Côte d'Opale, France	Directeur de thèse

Acknowledgments

This piece of work could not be fulfilled without a group of people who deserve a sincere THANK YOU!

*I would like to express my gratitude to the jury members: Professors **Abdelwhaid Mellouki**, **Alexandre Tomas**, **John Wenger** and **Peter Wiesen** for accepting to examine this work.*

*I would like to thank our university (Université du Littoral-Côte-d'Opale, **ULCO**) and the region (pôle métropolitain Côte d'Opale, **PMCO**) for funding the three years of my PhD.*

*I would like to address my gratitude to Professor **Gaël Mouret** for allowing me to conduct this research under his direction.*

*I owe sincere thankfulness to Dr. **Cécile Coeur** for her time, care and confidence. Without her help and guidance this work would not have been achieved.*

*I am also very grateful to LPCA director and members especially doctors: **Eric Fertein**, **Marc Fourmentin**, **Patrick Augustin**, and Professors **Weidong Chen** and **Pascal Flament** for their hospitality and kindness duration the three years of my PhD.*

*A special thank you is said to Dr. **Karine Deboud** and Dr. **Xavier Secordel** for their hard work and help with SEMS measurement and most importantly for their sympathy.*

*I would like to really thank Dr. **Allecsanedro Faccinnetto** and Dr. **Junteng Wu** as well as Professor **Denis Petitprez** from PC2A laboratory for their appreciated help and collaboration in part of this work related to hygroscopicity and CCN activity.*

*I am also very grateful to **Paul Genevray** from the CCM for his contribution to the SOA characterization tests, and to **Fabien Marteel** for his continuous technical help.*

*My sincere gratitude is reserved to **Pierre Kulinski** and **Jean Decker** for their assistance in the experiments with light characterization and for their kindness.*

*I would like to deeply thank **Thomas Fagniez** for all the help he gave me, for the continuous support and for the good friendly times we have spent together in the lab. Also, thanks for **Nicolas Houzel** for his help in the lab and for everything.*

*It was a pleasure to work with **Hichem Bouzidi** during the last year of my PhD, thanks for all the help and effort especially in the part concerning hygrosopicity and for the cheers and all the motivations at hardship.*

*My greatest thanks go to all my dear friends in LPCA and UCEIV laboratories. **Lingshuo, Meriem, Souleman, Ioanis, Gaoxuan, Tina, Rayan, Bouthayna, Lamia, Stephanie, Rebecca, Murielle, the sweetest Fengjiao, the true supporter Khaoula.** Also thanks a ton to my dear friends **Hussien and Mohammad Ali.***

*I will forever be beholden to two pieces of my heart **Ghidaa and Hadi.** THANKS FOR EVERYTHING!*

*Yes, I could not have done all this thesis without my family! I dedicate this work to my family members (**Nabil, Ilham, Iyad, Manal, Osama, Wissam, Joelle and Sandra**) who showed me endless love and support.*

Valorisation

Oral Communications

1. Layal FAYAD, Hichem BOUZIDI, Cécile COEUR, Nicolas HOUZEL, Karine DEBOUD, Xavier SECORDEL, Gaël MOURET, Paul GENEVRAY, Alexandre TOMAS, Junteng WU, Alessandro FACCINETTO, Denis PETITIPREZ. **The study of Secondary Organic Aerosols (SOAs) formed from the ozonolysis of γ -terpinene in the new simulation chamber CHARME**. Conseil Scientifique Cappa, Lille, France, 01 July 2019
2. Layal FAYAD, Cécile COEUR, Hichem BOUZIDI, Nicolas HOUZEL, Thomas FAGINEZ, and Gaël MOURET. **Ozonolysis of γ -terpinene in the new indoor atmospheric chamber CHARME: analysis of gas-phase and particulate reaction products**. 38^{EME} Edition Du Colloque annuel du groupe Français de cinétique et photochimie (GFCP), Rennes, France 6-7 June 2019
3. Layal FAYAD, Cécile COEUR, Thomas FAGINEZ, Xavier SECORDEL and Gaël MOURET. **Ozonolysis of γ -terpinene in the new indoor atmospheric chamber CHARME: analysis of gas-phase and particulate reaction products**. The EGU General Assembly, Vienne, Austria, 07-12 April 2019.
4. Layal FAYAD, Cécile COEUR, Thomas FAGNIEZ and Gaël MOURET. **The study of ozonolysis reaction of some monoterpenes in CHARME chamber**. Deuxième réunion du WP2 CLIMIBIO, Dunkerque, France, 28 January 2018

Posters

1. Layal FAYAD, Cécile COEUR, Thomas FAGNIEZ and Gaël MOURET. The study of the Ozonolysis of Biogenic Volatile Organic Compounds (BVOCs), Precursors of Secondary Organic Aerosols, in CHARME chamber. 5 Journée Scientifique Cappa, Lille, France, 06 March 2019.
2. Layal FAYAD, Cécile COEUR, Thomas FAGNIEZ, Xavier SECORDEL and Gaël MOURET. A New Environmental Simulation Chamber (CHARME) to study the Atmospheric Reactivity and the Metrology of the Environment: Design, Characterization and Preliminary Tests. The 25th International Symposium on Gas Kinetics and Related Phenomena. Lille, France 22- 26 July 2018

Papers

1. Layal FAYAD, Cécile COEUR, Thomas FAGNIEZ, Nicolas HOUZEL and Gaël MOURET. **Design and Characterization of a New Environmental Simulation Chamber for the study of Atmospheric Chemistry.** (In progress)
2. Layal FAYAD, Cécile COEUR, Thomas FAGNIEZ, Xavier SECORDEL, Nicolas HOUZEL and Gaël MOURET. **Kinetic and Mechanistic Study of the Gas-Phase Reaction of Ozone with γ -terpinene.** (In progress)
3. Hichem BOUZIDI, Layal FAYAD, Cecile Coeur, Nicolas HOUZEL, Denis PETITIPREZ, Alessandro FACCINETTO, Wu JUNTENG, Alexandre TOMAS, Ondracek JAKUB, Jaroslav SCHWARZ, Vladimir ZDIMAL and Andreas ZUEND. **Hygroscopicity properties and CCN activity of secondary organic aerosol produced from dark ozonolysis of γ -terpinene.** (In progress)

Table of Contents

List of Figures	ix
List of Tables	xv
General Introduction	1
Chapter I “Fundamentals of atmosphere: composition and interactions”	7
I.1 Atmosphere.....	8
I.1.1 Division.....	8
I.1.2 Composition.....	9
I.2 Volatile Organic Compounds.....	11
I.2.1 Definition	11
I.2.2 Importance	12
I.2.3 Sources.....	12
I.2.3.1 Anthropogenic	12
I.2.3.2 Biogenic.....	13
I.2.4 Fate of VOCs	16
I.2.4.1 Deposition.....	17
I.2.4.2 Photolysis.....	17
I.2.4.3 Oxidation	17
I.3 Atmospheric Aerosols	23
I.3.1 Sources.....	23
I.3.2 Classes	24
I.3.3 Size	24
I.3.4 Composition.....	25
I.3.4.1 Secondary Organic Aerosols (SOA).....	26
I.3.5 Sinks and transport	30
I.3.6 Impact	31
I.3.6.1 On climate.....	31
I.3.6.2 Visibility	32
I.3.6.3 On health.....	33
I.4 Atmospheric Simulation Chambers.....	34
I.4.1 Description.....	34
I.4.2 Background.....	35

I.4.3 Types.....	37
I.4.4 Benefits and Limitations.....	38
I.5 Thesis aim.....	39
References.....	41
Chapter II “Introduction to CHARME chamber”.....	51
II.1 CHARME chamber.....	52
II.1.1 Enclosure.....	53
I.1.1.1 Dimensions.....	53
I.1.1.2 Walls.....	53
I.1.1.3 Ports.....	54
I.1.1.4 Windows.....	55
I.1.1.5 Support.....	56
II.1.2 Mixing system.....	56
II.1.3 Pumping and filling system.....	57
II.1.4 Irradiation.....	58
II.1.5 Analytical instruments coupled to CHARME.....	59
II.1.5.1 Temperature & Humidity Monitoring.....	59
II.1.5.2 Pressure Monitoring.....	60
II.1.5.3 Spectroradiometer.....	61
II.1.5.4 O ₃ generator and analyzer.....	62
II.1.5.5 NO _x analyzer.....	62
II.1.5.6 PTR-TOF-MS.....	63
II.1.5.7 GC-MS/FID.....	66
II.1.5.8 SMPS.....	67
II.1.6 Other instruments.....	68
II.1.6.1 HTDMA.....	68
II.1.6.2 CCN counter.....	70
II.1.6.3 High performance liquid chromatograph (HPLC).....	71
II.1.6.4 Cryo-TSEM-EDX.....	72
II.1.6.5 TOF-SIMS.....	72
II.2 LPCA-ONE chamber.....	72
II.3 Material.....	73
II.4 Method.....	75
II.5 Summary of key features of CHARME.....	77
References.....	81

Chapter III “Characterization of CHARME”	82
III.1 Vacuum limit and leak rate	83
III.2 Dilution factor	86
III.3 Variation of relative humidity	87
III.4 Variation of temperature	91
III.5 Mixing time	92
III.6 Effect of fans	96
III.7 Wall loss	98
III.7.1 Ozone	99
III.7.2 Hydrocarbons	102
III.7.3 Particles	103
III.8 Cleaning	107
III.8.1 Daily cleaning	107
III.8.2 Ozone treatment	110
III.8.3 Manual cleaning	111
III.9 Purified air analysis	112
III.9.1 Characteristics of the purified air	112
III.9.2 Reactivity of purified air	113
III.10 Light characterization	115
III.10.1 Light intensity and spectral distribution	115
III.10.2 Photolysis frequency of NO ₂	118
III.10.2.1 Spectroradiometric measurement	118
III.10.2.2 Actinometric measurement	118
III.10.3 Homogeneity of irradiation	123
III.11 Auxiliary mechanism	124
III.12 Ozonolysis of α -pinene	128
III.12.1 Determination of rate coefficient	128
III.12.2 Determination of SOA formation yield	130
III.13 Conclusion	134

References.....	137
Chapter IV “Ozonolysis of γ-terpinene”	141
IV.1 Gas-phase study	142
IV.1.1 Rate coefficient determination.....	142
IV.1.1.1 Pseudo-first-order kinetics	143
IV.1.1.2 Relative Method.....	146
IV.1.1.3 Discussion.....	149
IV.1.2 Gas phase oxidation Products	151
IV.1.2.1 Identification of products.....	151
IV.1.2.2 Products yield determination	154
IV.1.2.3 Mechanism.....	157
IV.2 Particle-phase study	161
IV.2.1 SOA formation yields	161
IV.2.1.1 Experimental conditions	161
IV.2.1.2 Results and discussions.....	162
IV.2.2 SOA Characterization	165
IV.2.2.1 SOA sampling.....	166
IV.2.2.2 Results and discussions.....	168
IV.2.3 Hygroscopicity.....	175
IV.2.3.1 Data Analysis.....	176
IV.2.3.2 Experimentation.....	178
IV.2.3.3 Results and discussions.....	181
IV.2.4 Conclusion	188
Reference.....	191
Conclusion and Perspectives	197
Supplementary Information	200
Thesis Summary in French (Résumé de la thèse)	205
Abstracts (English and French)	221

List of Figures

• Figure i.1: The different characterization tests investigated in <i>CHARME</i>	4
• Figure i.2: Study of the ozonolysis of γ -terpinene in <i>CHARME</i>	5
• Figure I.1: Temperature profile for the atmospheric layers. Copyrights to (US Department of Commerce)	8
• Figure I.2: Scheme of the oxidation of VOCs and the different degradation products (Ziemann and Atkinson 2012).	20
• Figure I.3: Scheme of the general mechanism for the ozonolysis of olefins (Finlayson-Pitts and Pitts Jr, 2000).	22
• Figure I.4: Comparison of observed to predicted SOA ratios as determined in different studies based on the volatility of primary organic species (in red) and the traditional models (in blue) according to the photochemical age of SOA (Hodzic et al., 2010).....	27
• Figure I.5: Routes of formation of SOA from the oxidation of VOCs (Copyright: Waza, 2014).....	28
• Figure I.6: Overview of aerosol size classification together with main sources and sinks (copy rights: Schrödner, 2015).....	30
• Figure I.7: The total amount of radiative forcing (calculated in watts per square meter) caused by human activities since 1750. Copyright (US EPA, 2016)- Data source (IPCC, 2013).	32
• Figure I.8: Comparison of the 2013 Southeast Asian haze (a) during (19 June) and (b) after the episode (23 June) in Singapore (Wikipedia, 2013).	33
• Figure I.9: Size dependence of the impact of particulate matter on the respiratory system (Guariero and Guariero, 2013).....	34
• Figure II.1: The project of <i>CHARME</i> is finally realized! The chamber is installed in LPCA (IRenE Building)	52
• Figure II.2: Photo of <i>CHARME</i> chamber at the outset of installation in IRenE building.....	52
• Figure II.3: The 9 different ports of <i>CHARME</i> . Ports with letter (A) correspond to DN 450, (B) to DN 350 and (C) to DN 200.	54
• Figure II.4: The quartz widows of <i>CHARME</i>	55
• Figure II.5: The four mixing fans installed at different positions inside <i>CHARME</i> (a). One of the two-wing stainless steel fans (b).	56
• Figure II.6: (a) & (b) represent the pumping and filling valves and lines, (c) is the pure air generator and (d) is the pump coupled to <i>CHARME</i>	57
• Figure II.7: The light projectors (SKY TRACER 5000) that irradiate <i>CHARME</i>	58
• Figure II.8: Front (a) and back (b) photos for the room hosting the light projectors.....	59

- Figure II.9: The sensors (a) (Vaisala HMT330 Series HUMICAP), (b) (Sensirion EK-H5 SensorSHT75), used to measure temperature and relative humidity in *CHARME*. 60
- Figure II.10: The (a) pressure controller with two Baratron capacitance manometers and the (b) compensator connected to *CHARME* for monitoring its pressure.61
- Figure II.11: The spectroradiometer (Metcon) used with *CHARME*.61
- Figure II.12: Ozone generator (a) ana analyzer (b) utilized for monitoring O₃ in *CHARME* 62
- Figure II.13: NO_x analyzer (chemiluminescence; Thermo Scientific 42i) coupled to *CHARME*. 63
- Figure II.14: The PTR-TOF-MS (IONICON 1000), used for online measurement of gaseous concentrations. 65
- Figure II.15: The analytical system consisting of a Thermodesorber (ATD - 400, Perkin Elmer) – Gas Chromatograph (GC, Autosystem XL) – Flame Ionization Detector (FID)/ Mass Spectrometer (MS) (Turbomass), Perkin Elmer, and dedicated for VOC quantification and identification..... 66
- Figure II.16: The SMPS (Model 3081, TSI Inc.) and the (CPC Model 3775, TSI Inc.), coupled to *CHARME*. 67
- Figure II.17: The homemade HTDMA used for hygroscopicity investigation in *CHARME*.....69
- Figure II.18: Schematic set-up of the Hygroscopicity Tandem Differential Mobility Analyzer (HTDMA).70
- Figure II.19: The CCNc (DMT-100 Droplet measurement Technologies, USA) used to evaluate the CCN activity of particles in *CHARME*. 71
- Figure II.20: Photo of LPCA-ONE chamber..... 73
- Figure II.21: Injection of liquid reagents through an impinger..... 76
- Figure II.22: The setup (atomizer + drier) used to introduce seeds particles into *CHARME*..... 77
- Figure II.23: *CHARME* is operational with some analytical instruments.....80
- Figure III.1: Time profile for the evacuation process in *CHARME*..... 84
- Figure III.2: Leak rate in *CHARME*..... 85
- Figure III.3: Time profile of the pressure during the filling process..... 86
- Figure III.4: The steam reactor used for introduction of water vapour..... 88
- Figure III.5: Different injection times of water vapor corresponding to different relative humidities reached in *CHARME*..... 89
- Figure III.6: Variation of the relative humidity as a function of time in *CHARME* (RH%: 25, 50, 75 & 100)..... 90
- Figure III.7: A spot of condensed water vapor observed inside *CHARME* (a) at the end of the experiment and (b) its removal after pumping the chamber for 1 hour..... 90

- Figure III.8: Time profile of the temperature in the chamber (blue) and in the room hosting the lamps (red), with (yellow) and without irradiation (white) by the 4 xenon lamps. 92
- Figure III.9: A scheme of *CHARME* indicating the position of the injection points (A, B and C), of the PTR-MS and of O₃ and NO_x analysers..... 93
- Figure III.10: Mixing times for 3 different concentrations of isoprene (a) and acetone (b) injected at 3 different positions..... 94
- Figure III.11: Mixing times of (a) different concentrations of ozone and (b) NO₂..... 95
- Figure III.12: The mixing times for different gases injected at “Position A” of *CHARME*..... 96
- Figure III.13: Influence of the fans speed on the mixing time of ozone. 97
- Figure III.14: Influence of the fans rotation speed on the mass concentration of SOA formed from the ozonolysis reaction of γ -terpinene..... 98
- Figure III.15: Time profile of different concentrations of ozone..... 100
- Figure III.16: Determination of ozone wall loss in *CHARME* for different ozone concentrations and at different times.....101
- Figure III.17: Setup used to introduce SiO₂ particles into the *CHARME*.....104
- Figure III.18: Time profiles for the measured (solid circles) and corrected (open circles) mass concentrations of SiO₂ particles (a) and SOAs (b) formed from the ozonolysis reaction of α -pinene ([α -pinene]₀= 70 ppb and [O₃]₀= 490 ppb)..... 105
- Figure III.19: Cleaning test: Evolution of different concentrations of ozone (a); VOCs (PTR signals) (b) and SOA (ozonolysis of α -pinene) (c)..... 110
- Figure III.20: Time profile of the number and mass concentration of particles measured in the dark before and after treating the chamber by ozone (14 ppm) for 12 hours..... 111
- Figure III.21: Photo of the chamber inside contaminated with NaCl particles (a) and NO₂ (b).....111
- Figure III.22: Manual cleaning of the *CHARME* chamber..... 112
- Figure III.23: Time profile of the ozone concentration (a), NO₂ and NO concentrations (b) and mass and number concentrations for particles, before and during irradiating (yellow region) the blank chamber..... 114
- Figure III.24: Different orientations of the head of the spectroradiometer: upwards (a), downwards (b), right (c), left (d) of the chamber and towards (e) / away (f) from the lamps.....116
- Figure III.25: Emission spectra : (i) of the xenon lamps recorded inside the chamber at a single position and for different orientations of the spectroradiometer and in the housing room of the lamps; (ii) of the sun measured in Dunkerque (51°2'N 2°22' E; 16/07/2019 at 14:19 local time). *The used spectroradiometer allows to measure wavelengths from 290 nm to 660 nm..... 117

- Figure III.26: $J(\text{NO}_2)$ determination from the photolysis of NO_2 (210 ppb) in air (the yellow region corresponds to the time when lamps were switched on) 119
- Figure III.27: Time profile of NO_2 (120 ppb) and NO gases during the photolysis of NO_2 in N_2 . (Yellow region corresponds to duration when the lamps are switched on)..... 121
- Figure III.28: Actinometry in N_2 ; NO_2 consumption versus the time ($[\text{NO}_2]_0=120$ ppb)..... 122
- Figure III.29: Comparison of experimental (solid circles) and modeled (solid, dashed and dotted lines) concentrations of propene, NO , NO_2 , O_3 , formaldehyde and acetylaldehyde in propene- NO_x system. Model (0), Model (1) and Model (2) correspond to results simulated with $[\text{HONO}]_0= 0$ ppb, 1 ppb and 2 ppb, respectively. Note that $t=0$ corresponds to the time when the lights are switched on127
- Figure III.30: Plot of the pseudo-first-order rate coefficients (k') for the reaction of O_3 with α -pinene as a function of the initial ozone concentration. The error bars reflect the uncertainties (2σ) on the measurements of k' 129
- Figure III.31: Aerosol yield (Y) versus the organic aerosol mass formed (M_0) obtained in this work and literature data. Solid and empty squares correspond to data obtained with and without cyclohexane, respectively. The lines (solid in the presence and dashed in the absence of cyclohexane) represent the best fit of the data considering one semi-volatile major product.....132
- Figure IV. 1 Time profile of $\ln([\gamma\text{-terpinene}]_0/[\gamma\text{-terpinene}]_t)$ versus the time (s) for 3 different experiments: Exp.4 (green), Exp.7 (blue) and Exp.9 (red).....145
- Figure IV.2: Plot of the pseudo-first-order rate coefficients ($k'_{\gamma\text{-t}}$) for the reaction of O_3 with γ -terpinene as a function of the initial ozone concentration obtained at $294 \pm 2\text{K}$, atmospheric pressure and in the presence of an ozone scavenger (cyclohexane). The error bars reflect the uncertainties on the measurements of $k'_{\gamma\text{-t}}$145
- Figure IV.3: Relative rate plots for the reaction of γ -terpinene with ozone obtained at $294 \pm 2\text{K}$, atmospheric pressure and in the presence of an ozone scavenger (cyclohexane). Three references were used: cis-2-pentene (red squares; PTR-ToF-MS analyses), 2-methyl-2-butene (blue triangle; PTR-ToF-MS analyses) and α -pinene (green circles; GC-MS analyses)..... 147
- Figure IV.4: Relative rate plot representing (Eq. IV 6) with a slope corresponding to $k_{\gamma\text{-t}}$. The data of the three references were represented in different colors and shapes: cis-2-pentene (red squares), 2-methyl-2-butene (blue triangle) and α -pinene (green circles)..... 148
- Figure IV.5: Typical time profiles of chemical compounds ((a) reactants: γ -terpinene, acetonitrile and O_3 ; (b) major oxidation products; (c) minor oxidation products) detected by the PTR and the ozone analyzer during the ozonolysis of γ -terpinene (initial concentrations: γ -terpinene, 200 ppbv and O_3 , 2780 ppbv). m/z includes the addition of H^+ to the molar mass 153

- Figure IV.6: Typical plot for the determination of the gas-phase product yields formed from the ozonolysis of γ -terpinene (initial concentrations: γ -terpinene 200 ppbv and O₃ 2780 ppbv)..... 155
- Figure IV.7: Simplified mechanism for the formation of (POZs) and (CIs) for the reaction of γ -terpinene and ozone 158
- Figure IV.8: Partial mechanism for the ozonolysis of γ -terpinene starting from CII, yielding to products detected by the PTR-MS. Comparable schematics for the remaining CIs are provided in the supplementary information (Figure S.4)159
- Figure IV.9: Aerosol yield (Y) as a function of the organic aerosol mass concentration formed (M₀) from the ozonolysis of γ -terpinene in the presence (solid squares) and absence (open squares) of cyclohexane, respectively. The lines (solid in presence and dash in absence of cyclohexane) represent the best fit of the data considering one semi-volatile major product. 163
- Figure IV.10: Comparison of SOA yields formed from the ozonolysis of γ -terpinene, α -pinene, limonene and α -phellandrene. Experiments performed in the presence of an OH radicals scavenger (cyclohexane) under dry conditions, atmospheric pressure and at room temperature (294±2) K. The lines are the best fits of the data obtained with the single product model (Odum et al., 1996)165
- Figure IV.11: The Dekati 3-stages cascade impactor used for sampling the SOAs in *CHARME*.....167
- Figure IV.12: One collection plate of the impactor with a nucleopore membrane and 3 lacey carbon grids.....168
- Figure IV.13: Time profile of mass and number concentrations for SOAs formed from the ozonolysis of 8-terpinene (experiment 2). Green region represents the time and the duration at which the aerosols were sampled and corresponds to 3 different numbers masses and sizes of the sampled particles..... 169
- Figure IV.14: SOA size distribution at different reaction times during the ozonolysis of γ -terpinene169
- Figure IV.15: Comparison of SOA observed at ambient temperature and at -100°C for the sample collected after 120 min from the start of experiment 2.....170
- Figure IV.16: SEM images of SOAs collected on lacey film (dp50 = 30 nm) during experiment 2 at (A) t = 5 min, (B) t = 60 min and (C) t = 120 min.....172
- Figure IV.17: SEM images of SOA collected on carbon formvar film (dp50 = 30 nm) during experiment 2 at (A) t = 5 min, (B) t = 60 min and (C) t = 120 min.....172
- Figure IV.18: SEM image of SOA collected on lacey film (dp50 = 30 nm) at t = 120 min of experiment 1..... 173
- Figure IV.19 : SEM image of SOA collected on lacey film (dp50 = 30 nm) during experiment 3 at t = 120 min. 174

- Figure IV.20: Temporal evolution of the hygroscopic growth factors at RH = 90 % for SOAs produced from dark ozonolysis of γ -terpinene in absence of cyclohexane, at low (solid shapes) and high (open shapes)..... 181
- Figure IV.21: Temporal evolution of the hygroscopic growth factors at RH = 90% for SOAs produced from dark ozonolysis of γ -terpinene in the presence of trimethylbenzene, at low (solid shapes) and high (open shapes).....183
- Figure IV.22: Temporal evolution of the hygroscopic growth factors at RH = 90 % for SOAs produced from dark ozonolysis of γ -terpinene in the presence of cyclohexane, at low (solid shapes) and high (open shapes).....186
- Figure IV. 23: Temporal evolution of hygroscopic growth factor at bulk RH = 90 % of SOA internally mixed with ammonium sulfate observed in Exp. 23 and Exp. 25..... 187
- Figure IV.24: Hygroscopic growth factors for SOAs produced from the ozonolysis of γ terpinene as a function of water activity, (a) in the absence and presence of cyclohexane at low initial precursor concentrations (16 ppb; Exp. 7, 15), (b) in the absence and presence of cyclohexane at high initial precursor concentrations (~158 ppb; Exp. 1, 21), (c) in presence of TMB at 16 - 158 ppb (Exp. 14 - 17), (d) in presence of dry AS seed particles at 16 ppb and 26 ppb (Exp 23, 25)..... 188
- Figure S.1: The hygroscopic growth curve of pure AS particles d=100 nm..... 204
- Figure S.2: Time profile of acetonitrile injected and the corresponding loss in the chamber..... 205
- Figure S.3: (a) The time profile of cyclohexanone and (b) the plot of $\ln [\text{cyclohexanone}]_o/[\text{cyclohexanone}]_i$ that allows the determination of wall losses. Similarly, for (c) and (b) but for SOA formed from the ozonolysis of α -pinene (α -pinene= 70 ppb and ozone =160 ppb). Cyclohexanone represents an example of how the wall losses of gases were calculated and the SOA represents the particles wall loss determination..... 206
- Figure S.4: The different partial mechanisms proposed for CI2, CI3 and CI4 formed from the ozonolysis of γ -terpinene.....208

List of Tables

• Table I.1: Major gaseous constituents of the atmosphere (Seinfeld & Pandis, 2016).....	10
• Table I.2: Categories of non-methane BVOCs (Kesselmeier and Staudt, 1999; Guenther et al., 1995a).	14
• Table I.3: Skeletal structure of 14 most occurring monoterpenes (Geron et al., 2000).....	15
• Table I.4: The different atmospheric chambers within the frame of EUROCHAMP.....	36
• Table II.1: The different liquid, solid and gaseous chemicals used in different experiments performed in <i>CHARME</i>	74
• Table II.2: Summary of the chamber's features.....	78
• Table II.3: Summary for the instrumentations coupled to <i>CHARME</i> with their measuring parameter.....	79
• Table III.1: Wall loss of ozone and its corresponding lifetime ($\tau_{O_3} = 1/k_{O_3}$) in several simulation chambers under dark conditions.....	102
• Table III.2: The wall loss rate of several gaseous species determined in <i>CHARME</i>	103
• Table III.3: Wall loss rates of different types of particles determined in <i>CHARME</i>	105
• Table III.4: Particle wall loss rates in different simulation chambers.....	107
• Table III.5: Characterization of zero air	113
• Table III.6: The set of reactions involved in the photolysis of NO_2 and their rate constants (Atkinson et al., 2004a).	120
• Table III.7: The different NO_2 photolysis rates determined in various chambers.....	123
• Table III.8: Starting conditions for the NO_x -propene-air characterization experiment.....	124
• Table III.9: Auxiliary mechanism for the <i>CHARME</i> chamber.....	125
• Table III.10: The literature data for the rate constant of ozonolysis of α -pinene.....	130
• Table III.11: Summary of experimental conditions and results for the SOA formation from the ozonolysis of α -pinene. Add the T° , P and RH	131
• Table III.12: Comparisons of the one-product parameters (α_1 and $K_{p,1}$) obtain from this work and literature data.	133
• Table III.13: Summary of characterization tests performed in <i>CHARME</i>	135
• Table IV. 1: Summary of the conditions of pseudo-first order experiments.....	144
• Table IV.2: Rate coefficient determined for the reaction of γ -terpinene with ozone at 294 ± 2 K, atmospheric pressure and literature data.....	150
• Table IV.3: Atmospheric life time of γ -terpinene with different oxidants.....	151
• Table IV.4: Identification of the ions detected by the PTR-MS during the gas-phase reaction of γ -terpinene with ozone (m/z masses include the addition of H^+). N.D: Not Determined yield.....	156
• Table IV.5: Summary of the experimental conditions and results for the SOA formation from the ozonolysis of γ -terpinene in the presence and absence of cyclohexane at (294 ± 2) K, atmospheric pressure and $RH = (1.7 \pm 0.1)\%$	162
• Table IV. 6: The one product equation parameters obtained in this study.....	163
• Table IV.7: Summary of the experimental conditions (at $T = (297 \pm 2)$ K, $P = (1019 \pm 2)$ mbar and $RH=1.9\%$).	166

General Introduction

Air pollution has long been recognized as one of the biggest global health and environmental challenges. It ranks among the top risk factors for mortality as it accounts for 7 million deaths around the world every year (**WHO**). Along with harming human health, air pollution can cause a variety of environmental effects including acid rain, ozone depletion, global climate change, etc. Therefore, air pollution needs to be tackled at a global level through legislation and international agreements, such as the Paris Agreement (COP21) (**European Commission, 2016**) which was agreed in December 2015. Such regulations are emerged on the basis of numerous researches and several scientific publications that have investigated atmospheric pollutions and offered the latest findings regarding the sources, transformations and impacts of the pollutants introduced into the atmosphere.

Being an environment where large quantities of both biogenic and anthropogenic compounds are emitted, transported and removed whilst exposed to greatly variable physical and chemical conditions, the atmosphere is considered a complex physicochemical medium (**Finlayson-Pitts and Pitts Jr, 2000**). The need to understand the diversity of all chemical species (gases and particles) and the complexity of transformations and mechanisms occurring in the atmosphere, necessitates the presence of a new field of science that seeks to elucidate these relations and interactions. Consequently, atmospheric chemistry was found in the middle of 1980s (**Akimoto, 2016**). This new science is a multi-disciplinary path of research that involves environmental chemistry, physics, meteorology, computer modeling and other disciplines. It aims to understand the chemical and physical processes occurring in the atmosphere, in addition to the emissions, transport, lifetimes and fates of biogenic and anthropogenic chemicals (**Finlayson-Pitts and Pitts Jr, 2000**).

The study of the troposphere, particularly its chemistry, has been examined by different methods. Observations through field measurements, predictions via computer models and experimentations by laboratory studies, are powerful tools used to achieve the atmospheric research needs. Among these methodologies, atmospheric simulation chambers offer direct and simplified approaches, they have been utilized for more than 60 years and are still constructed and developed worldwide (**Akimoto, 2014**). The use of environmental chambers is one important direction that has been taken to understand the chemistry of volatile organic compounds (VOCs) and aerosols

and to investigate the gas–particle interactions in the atmosphere (Finlayson-Pitts and Pitts, 1986). A large number of experimental data studying the chemical and physical processes of emitted organic compounds has been obtained over the past three decades. However, the various classes of VOCs emitted into the troposphere are not fully investigated and there is much to be known. VOCs are produced from natural and anthropogenic sources. On regional and global scales, the emissions of biogenic VOCs exceed those produced from human activities, by a factor of about 10 (**Lamb et al., 1987; Guenther et al., 1995**). Among the different classes of BVOCs, monoterpenes ($C_{10}H_{16}$) are of great importance. The oxidation of such BVOCs is initiated by the reaction with hydroxyl radicals during daytime, nitrate radicals in the course of night and ozone throughout both night and day (**Finlayson-Pitts and Pitts Jr, 2000**). Their oxidation produces species with sufficiently low vapor pressures to be condensable, leading to the formation of Secondary Organic Aerosols (SOAs).

The study of SOAs has been of great interest due to their importance in the atmosphere. SOAs have impacts on climate via scattering and absorption of solar radiations in the atmosphere. They also alter the formation and precipitation efficiency of liquid water, ice and mixed-phase clouds and hence affect the lifetimes, amounts and albedo of clouds (**Andreae and Crutzen, 1997**). So, secondary organic aerosols affect climate both directly and indirectly and large uncertainties still remains on their radiative forcing (**IPCC, 2014**). The increase in the understanding of atmospheric species (gases and particles) and their physico-chemical interactions, is essential for properly assessing their role in pollution, climatic change and ultimately establishing effective control strategies. Despite many advances in this approach, a number of doubts still limit the knowledge about atmospheric constituents, transformations and mechanisms. Consequently, the scientific community has raised different questions including:

- What are the different mechanisms (chemical and photochemical) leading to the degradation of numerous VOCs?
- What is the contribution of some VOCs in the formation of secondary organic aerosols (SOA)?
- What is behind the discrepancies between the measured and modelled SOA concentrations?
- How hygroscopic are SOA particles generated from the oxidations of BVOCs?
- What is the impact of VOCs and SOAs on climate change and air quality?

In context of answering some of the scientific inquiries and contributing to the global knowledge of atmospheric processes, a new indoor simulation chamber “*CHARME*” (*CHamber for the Atmospheric Reactivity and the Metrology of the Environment*) has been developed at LPCA (Laboratoire de Physico-Chimie de l'Atmosphère, Dunkerque) in 2016. It aims to investigate gaseous phase (kinetic measurements, products formation, chemical mechanisms...) and particulate phase (SOAs formation, composition, hygroscopicity...) and to develop optical instruments dedicated to the in situ measurements of atmospheric species (IBBCEAS, EC-QCLPA....)

This thesis is the first research work realized within *CHARME*. The chamber (design, features, instruments...) is represented for the first time and the results of a series of characterization tests are described in the first part of this manuscript. The second session presents the study on the gas-phase ozonolysis of γ -terpinene. To our knowledge, the results related to the SOA formation from this reaction are demonstrated for the first time.

In addition to the general starting “introduction” and ending “conclusion and perspectives”, this thesis is divided into four distinct chapters:

- **Chapter I**

Chapter 1 provides an overview on the current understanding of atmospheric constituents and interactions with a focus on the oxidation of volatile organic compounds, principally, ozonolysis. The general mechanisms leading to the products in the gas phase are outlined and the formation of secondary organic aerosols is highlighted. Further, a literature review covering the background and the importance of atmospheric chambers is displayed. Finally, the aims of the thesis were stated.

- **Chapter II**

This part introduced the new simulation chamber (*CHARME*) that has been developed by the LPCA laboratory, described all the instrumentations coupled to it and explained the experimental method used in this work.

• Chapter III

This section displayed the experiments performed to characterize and validate the performances of the new chamber. The different tests sketched in **Figure i.1**, are clearly presented and their results are discussed.

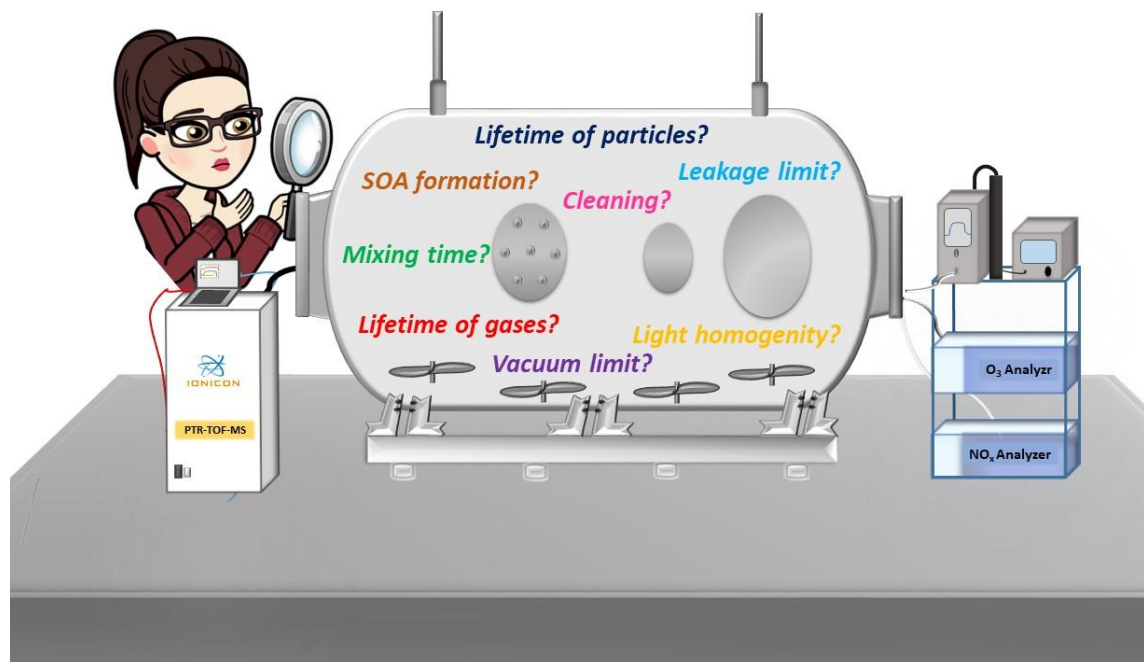


Figure i.1: The different characterization tests investigated in *CHARME*.

• Chapter IV

This chapter concerns the study of the ozonolysis of γ -terpinene (**Figure i.2**). The results obtained in the gaseous phase include: the rate constant determination, the products identification and quantification and the suggestion of a mechanism leading to these products. In addition, the particulate phase was investigated by determining the formation yields of secondary organic aerosols and characterizing their chemical and physical properties. In this part, a special emphasis was given to the hygroscopic properties of the formed SOAs.

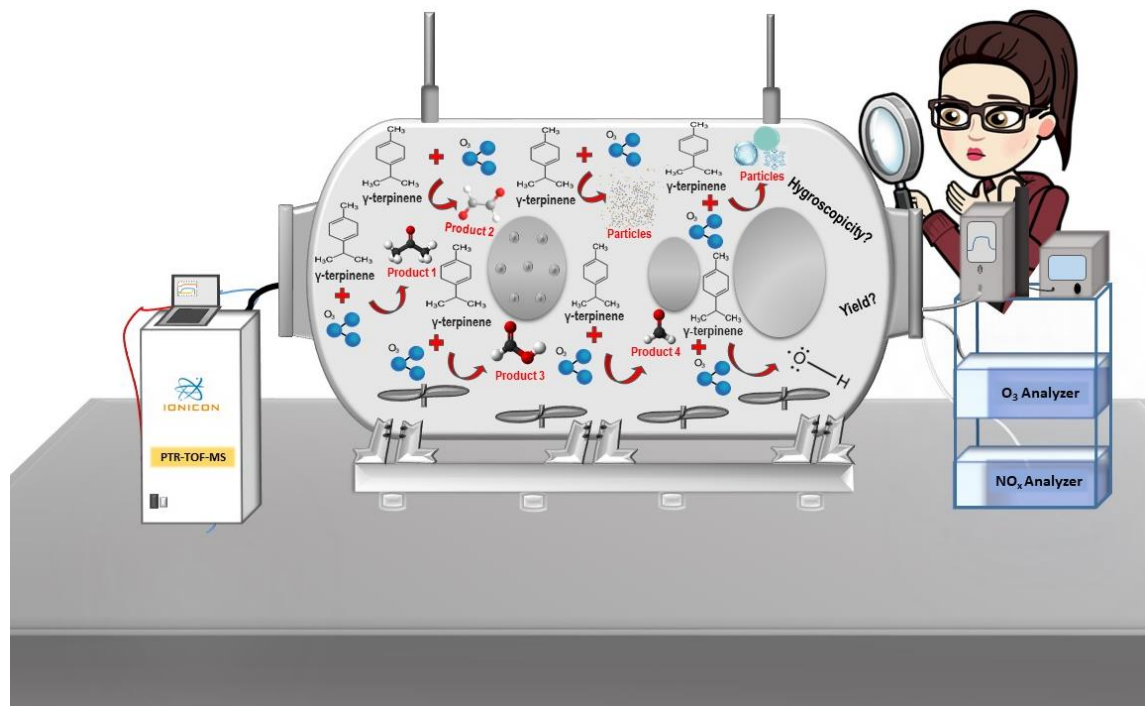


Figure i.2: Study of the ozonolysis of γ -terpinene in CHARME.

References

- Akimoto, H., 2016. Atmospheric Reaction Chemistry, Springer Atmospheric Sciences. Springer Japan, Tokyo. <https://doi.org/10.1007/978-4-431-55870-5>
- Andreae, M.O., Crutzen, P.J., 1997. Atmospheric aerosols: Biogeochemical sources and role in atmospheric chemistry. *Science* 276, 1052–1058.
- European Commission, 2016. Accord Paris 2016 [WWW Document]. Action pour le climat -European Commission. URL https://ec.europa.eu/clima/policies/international/negotiations/paris_fr (accessed 10.27.19).
- Finlayson-Pitts, B.J., Pitts, J.N., 1986. Atmospheric chemistry: fundamentals and experimental techniques. New York: Wiley.
- Finlayson-Pitts, B.J., Pitts Jr, J.N., 2000. Chemistry of the upper and lower atmosphere: theory, experiments, and applications. Elsevier.
- Guenther, A., Hewitt, C.N., Erickson, D., Fall, R., Geron, C., Graedel, T., Harley, P., Klinger, L., Lerdau, M., McKay, W.A., Pierce, T., Scholes, B., Steinbrecher, R., Tallamraju, R., Taylor, J., Zimmerman, P., 1995. A global model of natural volatile organic compound emissions. *Journal of Geophysical Research* 100, 8873. <https://doi.org/10.1029/94JD02950>
- Lamb, B., Guenther, A., Gay, D., Westberg, H., 1987. A national inventory of biogenic hydrocarbon emissions. *Atmospheric Environment* (1967) 21, 1695–1705. [https://doi.org/10.1016/0004-6981\(87\)90108-9](https://doi.org/10.1016/0004-6981(87)90108-9)
- WHO, Air pollution [WWW Document]. WHO. <http://www.who.int/airpollution/en/> (accessed 10.25.19).

Chapter I

**“Fundamentals of atmosphere:
composition and interactions”**

I.1 Atmosphere

The earth's atmosphere is the gaseous envelope surrounding the planet (Iribarne and Cho, 2012). It is a complex dynamical, physical, and chemical system held in place by the planet's gravitational attraction (Exline et al., 2008). It is driven by the interactions between the sun, the oceans and surface processes on the continents that all together form the basis of life (Salby, 2012).

I.1.1 Division

The atmosphere is divided into four layers based on its thermal structure, which determines dynamical properties of individual regions. The atmospheric layers are the troposphere, the stratosphere, mesosphere, thermosphere and exosphere (Finlayson-Pitts and Pitts Jr, 2000). The different divisions of the atmosphere are represented in Figure I.1.

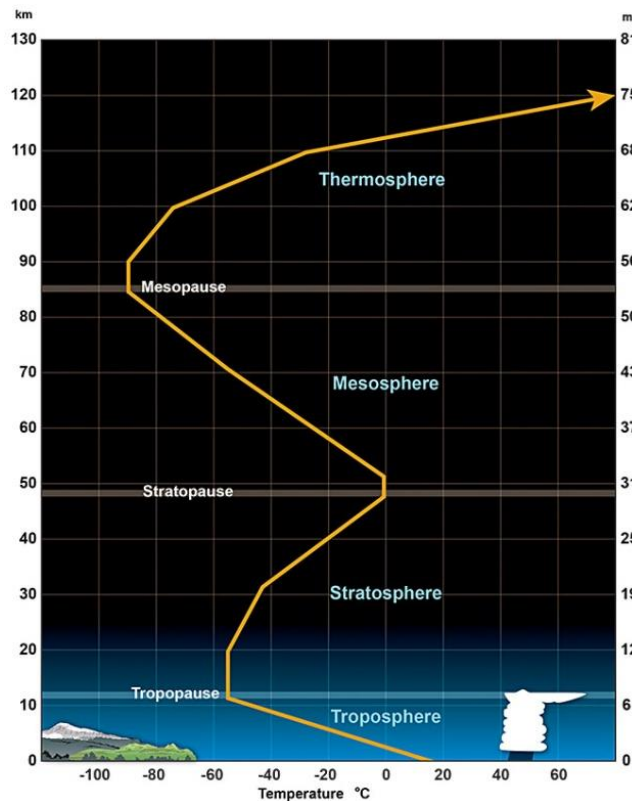


Figure I.1: Temperature profile for the atmospheric layers. Copyrights to (US Department of Commerce).

The layer immediately above the earth's surface is known as the 'troposphere', it ranges from the surface up to an altitude varying from ~ 10 - 15 km (depending on season and latitude).

The troposphere contains about 75 % of the mass of the atmospheric air and around 99 % of the atmospheric water vapor. The lowest part of the troposphere is known as the boundary layer while the upper borderline is called the ‘tropopause’. It is characterized by a temperature decrease with an increase in altitude (**Seinfeld, and Pandis, 2006**).

The region from the tropopause to an altitude of about 50 km is called the ‘stratosphere’, which means the layered sphere. In this region, temperature increases (negative lapse rate) due to a critical series of photochemical reactions involving ozone and molecular oxygen. The upper boundary of the stratosphere is called the ‘stratopause’ that lies at an altitude of 50 km where temperature reaches a maximum (**Finlayson-Pitts and Pitts, 1986**).

Above the stratopause, the ‘mesosphere’ extends from ~ 50 up to 85 km. At this level, the concentration of ozone decreases with the increase in altitude and thus ozone heating diminishes, leading to a decrease in temperature as altitude increases. The ‘mesopause’ lies at an altitude of about 85 km where a minimum of temperature is reached (**Salby, 2012**).

Over the mesopause, lies the ‘thermosphere’ at an altitude upwards of 85 km. At this layer temperature starts to rise again because of increased absorption of solar radiation at wavelengths < 200 nm by O₂, N₂, and some atomic species. Unlike lower layers, the thermosphere cannot be treated as an electrically neutral continuum because the ionization of molecules by energetic solar radiation produces a plasma of free electrons and ions.

The outermost region of the atmosphere (>500 km altitude) is called the ‘exosphere’. It is the region where gas molecules with sufficient energy can escape from earth’s gravitational attraction (**Seinfeld and Pandis, 2016**).

I.1.2 Composition

The atmosphere is a complex mixture of gases; nitrogen (~78%), oxygen (~21%) and argon (~0.93%) together make up more than 99% of the dry atmosphere, yet the remaining fraction includes a multitude of atmospheric trace gases (**Table I.1**) that are fundamental to weather and climate (**Kim, 2009**). Although present in small abundance, trace gases play important roles in the atmospheric energy cycle. For instance, methane (CH₄), carbon dioxide (CO₂), and nitrous oxide (N₂O) are known to be greenhouse gases, that play a significant role in influencing earth's surface temperature and affecting the radiation budget of the atmosphere (**Schlager et al., 2012a**). Water

vapor and ozone also play a key role in the energy balance of the earth through their involvement in radiative processes.

Trace species are treated separately from the primary atmospheric constituents, which are referred to simply as dry air (**Salby, 2012**). The sources of atmospheric minor constituent are either natural sources such as vegetation, volcanoes, oceans or anthropogenic sources like industrial emissions, transport, etc. Major sources include biomass burning and fossil fuel combustion (emissions of CO₂, SO₂, NO_x, HCs), traffic (CO₂, NO_x, CO), agriculture (N₂O, NH₃), vegetation (volatile organic compounds), oceans (N₂O, Dimethylsulfide, halocarbons), and volcanoes (SO₂, halogens) (**Schlager et al., 2012b**). After their emission, trace gases are mixed and transported vertically and horizontally by air masses and transformed in the gas phase (homogeneous chemistry), in the liquid phase and/or on the surface of particles (heterogeneous chemistry) (**Finlayson-Pitts and Pitts Jr, 2000**).

Table I.1: Major and trace gaseous constituents of the unpolluted troposphere (Seinfeld and Pandis, 2016; Dlugokencky, 2019)

Constituent	Average Mixing Ratio *
Major gases	
N ₂	78×10 ⁵ ppmv
O ₂	20×10 ⁴ ppmv
Ar	93×10 ³ ppmv
Trace gases	
H ₂ O	Variable
CO ₂	408 ppmv
Ne	18 ppmv
He	5.2 ppmv
CH ₄	1.8 ppmv
Kr	1.1 ppmv
H ₂	580 ppbv
N ₂ O	330 ppbv
CO	120 ppbv
Xe	90 ppbv
O ₃	10-100 ppbv
NO	0.1-10 ppbv
NO ₂	0.1-10 ppbv
NH ₃	0.1-1 ppbv
SO ₂	0.01-0.1 ppbv

* The units used correspond to parts per million by volume (ppmv) and parts per billion (ppbv)

The atmosphere is composed mostly of gases, but also contains liquid and solid matter suspended in the gaseous medium. These represent the atmospheric particles (0.001 and 10 μm) and are known as “aerosols”. Despite their small mass or volume fraction, atmospheric particles strongly influence the transfer of heat and radiant energy, thereby impacting the weather and climate (**IPCC, 2014**).

Nowadays, scientific research is focusing on studying the composition and processes in the atmosphere. In particular, a major attention is given to the gaseous composition of the troposphere to better understand the life cycle of these gases from their emission to their sinks and eventual removal. Consequently, this work is dedicated to the study of volatile organic gases in the atmosphere.

1.2 Volatile Organic Compounds

Large quantities of volatile organic compounds (VOCs) are continuously emitted into the atmosphere from different sources. Tens of thousands of these compounds have been detected and quantified in air at mixing ratios ranging from parts per billion (ppbv) down to parts per trillion (pptv). Consequently, their sources and fates are the subject of intensive research (**Koppmann, 2007**).

1.2.1 Definition

As defined by the European Parliament, Council of the European Union (2004), “*Volatile Organic Compounds are organic compounds, other than carbon dioxide and monoxide, having an initial boiling point lower than or equal to 250 °C (482 °F) measured at a standard atmospheric pressure of 101.3 kPa*”. In addition, the US EPA (2019) defines VOCs as “*any compound of carbon, excluding carbon monoxide, carbon dioxide, carbonic acid, metallic carbides or carbonates, and ammonium carbonate, which participates in atmospheric photochemical reaction*”.

Sometimes, VOCs are referred to as reactive organic gases (ROG) or if excluding methane, they are denoted as non-methane organic compounds (NMOCs). They consist of a large number of saturated, unsaturated, and oxygenated derivatives including aldehydes, ketones, alcohols, esters and organic acids (**Warneck, 1999**).

I.2.2 Importance

VOCs exert a strong influence on the quality, the oxidative capacity of the atmosphere, the conversion rates of nitrogen oxides (NO_x), the production of organic nitrates, the balance of global carbon cycle, etc. (Duce et al., 1983; Peñuelas and Staudt, 2010; Jain et al., 2017). These compounds are involved in the complex series of photochemical reactions with NO_x, O₃, and OH, leading to the formation of high concentrations of tropospheric ozone and secondary organic aerosols.

I.2.3 Sources

VOCs are emitted into the atmosphere from natural and anthropogenic sources. They are released into the atmosphere at a rate of nearly 10³ Tg/year (Duce et al., 1983). On regional and global scales, the emissions of natural VOCs exceed anthropogenic sources by a factor of about 10 (Lamb et al., 1987; Guenther et al., 1995a). Globally, geographical location and season determine the relative importance of anthropogenic and biogenic emissions. For instance, biogenic compounds are emitted mostly in the tropics, whereas most anthropogenic emissions occur in the northern hemisphere between 40°N and 50°N. The spatial and temporal distribution of VOCs in the atmosphere is dependent on the location of their sources, reactivity and transport phenomena (Koppmann, 2007).

I.2.3.1 Anthropogenic

The total anthropogenic VOCs (AVOCs) emissions are estimated to be 150-170 Tg/year (Müller, 1992a; Crippa et al., 2018). They are mostly dominant in urban regions where human activities such as transport, combustion and industrial processes are prevailing (Koppmann, 2007; Warneck, 1999). The major sources of these VOCs are vehicle exhaust, manufacturing plants, and chemical solvents. They are categorized into three main groups: non-methane hydrocarbons (NMHCs), oxygenated VOCs (OVOCs) and halogenated hydrocarbons. Many AVOCs are known

to be dangerous to human health and hazardous to the environment as they contribute to ozone layer depletion and photochemical smog formation (**Evuti, 2013**).

I.2.3.2 Biogenic

VOCs emitted from biogenic sources such as vegetation, fungi, microbes, animals, and oceans are called biogenic volatile organic compounds (BVOCs). The global BVOC flux is estimated to be between 377 and 1150 TgC/year (**Went, 1960a; Guenther et al., 1995b**). Compared to terrestrial sources, biogenic emissions from the ocean are less important although there are significant marine sources of dimethyl sulphide (DMS) and methyl iodide (**Koppmann, 2007**). The production of BVOCs is dependent on the amount and type of vegetation, temperature, irradiation, ambient concentration of carbon dioxide and soil humidity (**Peñuelas and Staudt, 2010a**). BVOCs are produced by a variety of physiological processes operating in many different plant tissues. In reality, they are considered as signaling chemicals released by the plants to protect them against biotic and abiotic stress, pathogens and herbivores, and to seal their wounds and damages (**Lerdau et al., 1997; Pichersky and Gershenzon, 2002; Loreto and Schnitzler, 2010**). They are also used as means to attract pollinators and to communicate with other plants and organisms (**Sherwood, Keith and Craig Idso, 2003**).

Multiple review articles on BVOC have been published over the last few decades (**Helmig et al., 1999; Lamb et al., 1987a; Peñuelas and Staudt, 2010b**) and research shows that biogenic emissions are more important than anthropogenic ones in regional and global environments as well as on the redox balance of the atmosphere (**Guenther et al., 1995a**).

Biogenic VOCs are classified into five major categories: isoprene, monoterpenes, sesquiterpenes, other reactive VOCs (ORVOC), and other VOCs (**Kesselmeier and Staudt, 1999; Guenther et al., 1995a**). Examples are given for each category in **Table I.2**.

Table I.2: Categories of non-methane BVOCs (adapted from Kesselmeier and Staudt, 1999; Guenther et al., 1995a).

Name	Chemical Lifetime *	Formula	Example
Isoprene	1 hr - 3 hrs	C ₅ H ₈	Isoprene
Monoterpene	5 min - 3 hrs	(C ₅ H _x) ₂	α-pinene, β-pinene, limonene
Sesquiterpene	< 4 min	C ₁₅ H ₂₄	β-caryophyllene, β-farnesene
Other Reactive Volatile Organic Compounds	< 1 day	C _x H _y O _z	3-methyl-3buten-2-ol
Other Volatile Organic Compounds	> 1 day	C _x H _y O _z	Methanol

* Lifetimes are estimated in relation to [NO₃] = 10 ppt, [O₃] = 20 ppb for night; and to [OH] = 10⁶ molecules.cm⁻³, [O₃] = 20 ppb for daylight conditions.

The most prominent BVOCs are isoprene (44%), and monoterpenes (11%), which both belong to the biochemical class, isoprenoids. These compounds are usually strong smelling and hardly water soluble (Guenther et al., 1995a). They, as well as their reaction products, are involved in tropospheric chemistry (Kesselmeier and Staudt, 1999).

I.2.3.2.1 Isoprene

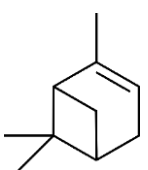
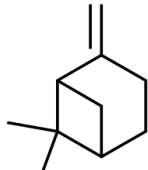
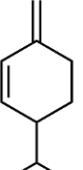
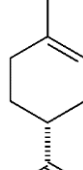
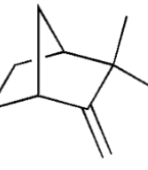
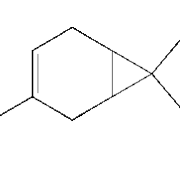
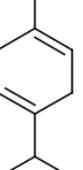
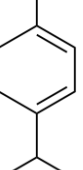
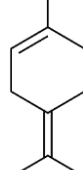
The most ubiquitous BVOC emitted in the atmosphere, is the simplest 5-carbon isoprenoid, ‘Isoprene’. It represents about half of the total global BVOCs (503 TgC/year) (Guenther et al., 2012) and is identified as a highly reactive compound, with an atmospheric lifetime on the order of few hours. Its high emission rates and reactivity allow isoprene to be recognized as the single most important reduced compound in the lower atmosphere. Emissions of isoprene from vegetation was discovered in 1960, and inventories showed that its main emitters are deciduous trees such as “Netleaf Oak” and to a lower extent coniferous trees like “Spruce” (Lamb et al., 1987a; Helmig et al., 1999).

I.2.3.2.2 Monoterpenes

The important emission rate of monoterpenes (260 TgC/year) and their contribution to the global atmospheric carbon budget have revealed the importance of this class of biogenic compounds (Guenther et al., 1995a).

Monoterpenes (MTs) are isomers of two isoprene units, they are cyclic or acyclic hydrocarbons containing at least one C=C double bond. Table I.3 shows the chemical structures for the most frequently encountered monoterpenes. The two most naturally abundant MTs in the troposphere are α -pinene and β -pinene

Table I.3: Skeletal structure of the some monoterpenes (Geron et al., 2000).

α -pinene	β -pinene	α -phellandrene	β -phellandrene	Limonene
				
Camphene	Δ^3 -carene	γ -terpinene	α -terpinene	Terpinolene
				

I.2.3.2.2.a α -pinene

α -pinene (C₁₀H₁₆) presented in Table I.3, is an important endocyclic monoterpene. It is the second most predominant contributor to the total BVOC budget after isoprene with a global emission rate estimated to be around 1.24 TgC/ year. It is responsible for 9.8% of the total BVOC emissions and 34.3% of the total monoterpene emissions (Li et al., 2012).

This monoterpene is emitted in substantial amounts by vegetation, notably by pine, coniferous trees and rosemary. α -pinene is considered as the most investigated terpene to date with

numerous studies of its emission rate (e.g **Lamb et al., 1987; Guenther et al., 2012**), kinetics and mechanism for its oxidations (e.g **Zhang and Zhang, 2005; Zhang et al., 2009**) as well as its oxidation products (e.g **Chen and Hopke, 2009; Molteni et al., 2019**).

I.2.3.2.2.b γ -terpinene

γ -terpinene is another important BVOC in the class of monoterpenes. It is one isomer of terpinene, with α and β -terpinene being the others (**Eggersdorfer, 2000**). It is an endocyclic compound with two C=C bonds located at positions 1 and 4 of the *p*-menthane skeleton. γ -terpinene is among the fourteen frequently occurring monoterpenes (**Geron et al., 2000**).

γ -terpinene is emitted from different trees including Dawn Redwood, American Beech, Sweet Gum, Loblolly Pine, Elm, Cypress, Waterhickory, Maple, *Abies religiosa* and *Pinus patula* (**Khalil and Rasmussen, 1992; Geron et al., 2000**). Most of the emission studies of this monoterpene were performed in the United States of America (USA) (**Helmig et al., 1999**). γ -terpinene is estimated to make up around 5% of all monoterpene emissions in the upper midwest and in the forests of central California (**Geron et al., 2000**). The emission of γ -terpinene was also investigated in Mexico City during the years 2002 and 2003 and reported by **Dominguez-Taylor et al., (2007)**. This study shows that the emissions change from the dry to wet season, for example, γ -terpinene contributes to 15% (dry) and 20% (rainy) of the total monoterpenes released from *Pinus patula* trees.

Besides, γ -terpinene is present in various essential oils like cumin oil. It exhibits anti-inflammatory, antimicrobial and antioxidant properties and thus is used for the production of cosmetics and pharmaceutical drugs, in perfumes and even as a fragrance and flavor in the food industry (**Natta et al., 2008; Sharifi-Rad et al., 2015**).

I.2.4 Fate of VOCs

Following their emission, volatile organic species are distributed in the atmosphere where they undergo several physico-chemical processes. The different sinks of trace gases include (1) dry and wet deposition (2) photolysis as well as (3) oxidation by OH, NO₃, halogen radical species and

ozone, (**Schlager et al., 2012b**). The overall rate of their removal from the atmosphere can be estimated by summing the rates of the mentioned sink processes. I.2.4.1 Deposition

I.2.4.1 Deposition

Among the different removal processes, dry and wet depositions are considered of minor importance for most BVOCs. However, it could be more important for chemically long-lived species such as methanol and other OVOCs (**Atkinson and Arey, 2003a**). The compounds can be eliminated physically by dry deposition to vegetation and aerosols (**Müller, 1992b**) or removed by wet deposition in rain (**Fornaro and Gutz, 2003**).

I.2.4.2 Photolysis

Direct photolysis by sunlight is known to be a significant atmospheric loss mechanism for compounds that absorb radiation in the wavelength range above 290 nm. It is an important pathway for the degradation of oxygenated volatile organic compounds (OVOCs) such as formaldehyde and acetone (**Atkinson and Arey, 2003a; Mellouki et al., 2015**). The products of photolysis, lead to the production of HO₂ radicals, which can be a source for OH radicals (**Koppmann, 2007**).

I.2.4.3 Oxidation

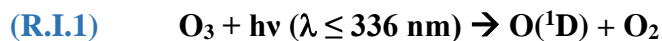
The most important sink for organic trace gases in the atmosphere is through chemical oxidation.

1.2.4.3.1 Oxidant

The major recognized oxidants for organics in the troposphere are OH and NO₃ radicals, Cl atoms and O₃.

- **Hydroxyl radical (OH)**

Hydroxyl radical (OH), has been referred to as the "tropospheric cleaner" since it reacts with hundreds of gases (**Thompson, 1992**). It is the dominant species involved in the oxidation chemistry of the troposphere together with the closely coupled species, the hydroperoxy radical (HO₂) (**Stone et al., 2012**). OH radicals are formed mainly from the photo dissociation of ozone according to the following reactions:



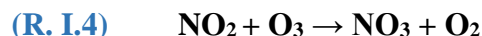
and to a lesser extent by the photolysis of nitrous acid (HONO) as seen in **(R.I.3)** (Warneck, 1999):



In addition, gas-phase ozone-alkene reactions are known to produce hydroxyl radicals in high yields (Kroll et al., 2002; Johnson and Marston, 2008).

- **(Nitrate radical) NO_3**

Although the hydroxyl radical is the main oxidant during the day, the nitrate radical may be the most important oxidizing species in the troposphere at night. In the atmosphere, NO_3 radicals are found at levels ranging from less than a few ppt in remote regions to several hundred ppt in polluted atmospheres. These radicals strongly absorb light in the visible region; thus, they are photolyzed rapidly. As a result, their concentration during the day is very low, but can be significant at night so they play an important role in the nighttime chemistry (Finlayson-Pitts and Pitts, 1986). The major source of NO_3 is the oxidation of nitrogen dioxide (NO_2) by ozone **(R. I.4)**. Then, NO_3 radicals can react with NO_2 to produce N_2O_5 **(R. I.5)**, which readily dissociates establishing an equilibrium with NO_3 .



- **Atomic chlorine (Cl)**

Although the concentration of chlorine atoms in the troposphere is generally very low, they can play a role in VOC transformations in marine and coastal areas during daylight hours (Atkinson and Arey, 2003b). The rate constants for the reaction of a number of VOCs and chlorine atoms is around 200 times larger than the equivalent reaction with OH. Consequently, its abundance, fate and cycling may considerably modify the standard daytime oxidation pathways (Tanaka et al., 2003; Le Breton et al., 2018)

- **Ozone (O₃)**

Another significant sink for VOCs especially those compounds containing C=C bonds, is through ozonolysis reaction (detailed in part [I.2.5.3.3 Ozonolysis reaction](#)). Ozone is an important participant in tropospheric chemistry throughout the day and night. It is a relatively long-lived species that can be transported and last until nighttime hours (**Finlayson-Pitts and Pitts Jr, 2000**).

I.2.4.3.2 General Mechanism

General mechanisms for the atmospheric oxidation of VOCs have been intensively studied (**Atkinson and Arey, 2003b; Ng et al., 2006; Kroll and Seinfeld, 2008a**).

There are two general mechanisms that initiate the oxidation of VOCs: through (i) the addition of oxidants to the compounds containing C=C double bond(s), or via (ii) H-atom abstraction from C-H and/or O-H bonds. The latter occurs only through the oxidation by OH, Cl and NO₃ radicals (**Atkinson and Arey, 2003a**). In most cases, the reaction mechanism involves formation of alkyl or substituted alkyl radicals (like hydroxy-alkyl or oxo-alkyl radicals). Generally, these radicals are transformed in the troposphere as shown in [Figure I.2](#), into peroxy (RO₂^{*}) and alkoxy (RO^{*}) organic radicals (**Atkinson and Arey, 2003b**). The subsequent radicals are intermediates for an array of oxygenated product species including hydroperoxides, carboxylic acids, peroxyacids, peroxy nitrates, alcohols, carbonyls (aldehydes and ketones), and 1,4-hydroxycarbonyls (**Ziemann and Atkinson, 2012**). Furthermore, successive oxidation can take place in the gas or the particle phases.

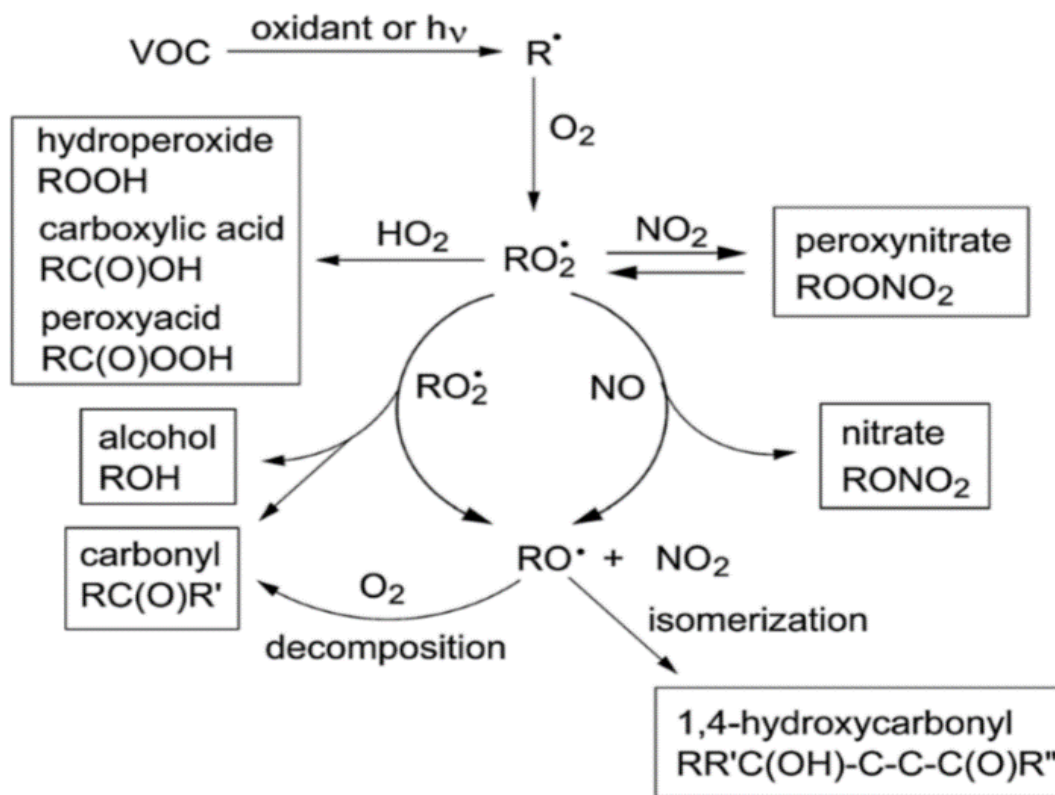


Figure I.2: Scheme for the oxidation of VOCs and the different degradation products (Ziemann and Atkinson 2012).

During the past decades, a number of research studies have investigated atmospheric reactions to better understand their mechanisms (Horie and Moortgat, 1998; Atkinson, 1997a) and to identify, as well as, to quantify their major oxidation products (Calvert and Madronich, 1987; Larsen et al., 1998).

In addition to reaction mechanisms and products examinations, rates constants for the oxidation reaction of many VOCs have been continuously reviewed, principally by Roger Atkinson (Atkinson and Carter, 1984; Atkinson, 1986; Atkinson et al., 2004, 1995, 1985b; Atkinson and Arey, 2003c). The rate constant is a quantitative measure of how fast reactions proceed or how long a given set of reactants will be present in the atmosphere. This quantification can also be expressed by the lifetime (τ), which is the approximate time it would take an atmospheric gas concentration to fall to 1/e of its initial value as a result of chemical reactivity and sink routes in the atmosphere (Finlayson-Pitts and Pitts Jr, 2000). The determination of the rate constants for atmospheric reactions has been the result of thorough laboratory experimentations using either the

relative or absolute method and structure-activity relationship (SAR) estimations (**Koppmann, 2007**).

Consequently, the high quality data sets of findings for mechanisms, degradation products and kinetics of all oxidation reactions, are put together into atmospheric computer models designed to simulate tropospheric chemistry and secondary pollutant formation.

I.2.5.3.3 Ozonolysis reaction

Among the oxidation reactions of VOCs, ozonolysis is considered as one of the most important.

In fact, ozone is recognized as a key species in the atmosphere. It is transported from the stratosphere, into the troposphere through eddy diffusion. In addition, it is formed from the photolysis of NO₂ in air as presented in **(R. I.6 and (R. I.7)** and from the photochemical reaction between VOCs and nitrogen oxides (NO_x = NO + NO₂) (**Finlayson-Pitts and Pitts, 1986; Atkinson and Arey, 2003c**).



Ozone is one of the atmospheric oxidants that drives the chemistry of the atmosphere and affects its oxidizing potential. It reacts with VOCs and yields different products in the gaseous and particulate phases (**Avzianova and Ariya, 2002**). Besides, there exists increasing evidence that ozonolysis is a significant source of radicals, such as organo-peroxy radicals (RO₂) and HO_x (HO + HO₂) in urban and rural areas (**Paulson and Orlando, 1996**). Accordingly, it offers a missing piece of the OH reactivity observed over forested areas (**Di Carlo, 2004**).

Considering the importance of the interactions between ozone and VOCs in the troposphere, the investigation of ozonolysis reactions has been of significant interest. It has been extensively studied both experimentally and theoretically. Prior to 1970, relatively few kinetic and mechanistic data were available for the reactions of O₃ with organics in the gas phase. Since then many kinetic and mechanistic studies have been performed and evaluated in several studies including (**Atkinson et al., 1990; Witter et al., 2002; Lee et al., 2006**).

The mechanisms of ozone-alkene reactions in the gas phase are detailed in apublications (Criegee, 1975; Finlayson-Pitts and Pitts, 1986; Atkinson, 1997b; Johnson and Marston, 2008). The ozonolysis of unsaturated VOCs proceeds as presented in Figure I.3 via a concerted 1,3-cycloaddition of O₃ across the C=C double bond, to form a 1,2,3- trioxolane primary ozonide denoted as a POZ. As this ozonide is known to be unstable, one of its two peroxy oxygen-oxygen bonds cleaves along with the carbon-carbon bond present from the initial alkene to form a carbonyl (aldehyde or ketone) and a carbonyl oxide intermediate, which is commonly referred to as a Criegee intermediate (CI). The formed excited CIs can be stabilized by reacting with water or other reactive oxygenated organics (SCI channel), or can be decomposed through three different path ways: (i) rearranging to an ester or an acid (ester channel) (ii) ejecting O(³P) to yield a carbonyl (oxygen-atom channel), or (iii) forming a hydroperoxide via a 1,4-hydrogen shift (hydroperoxide channel).

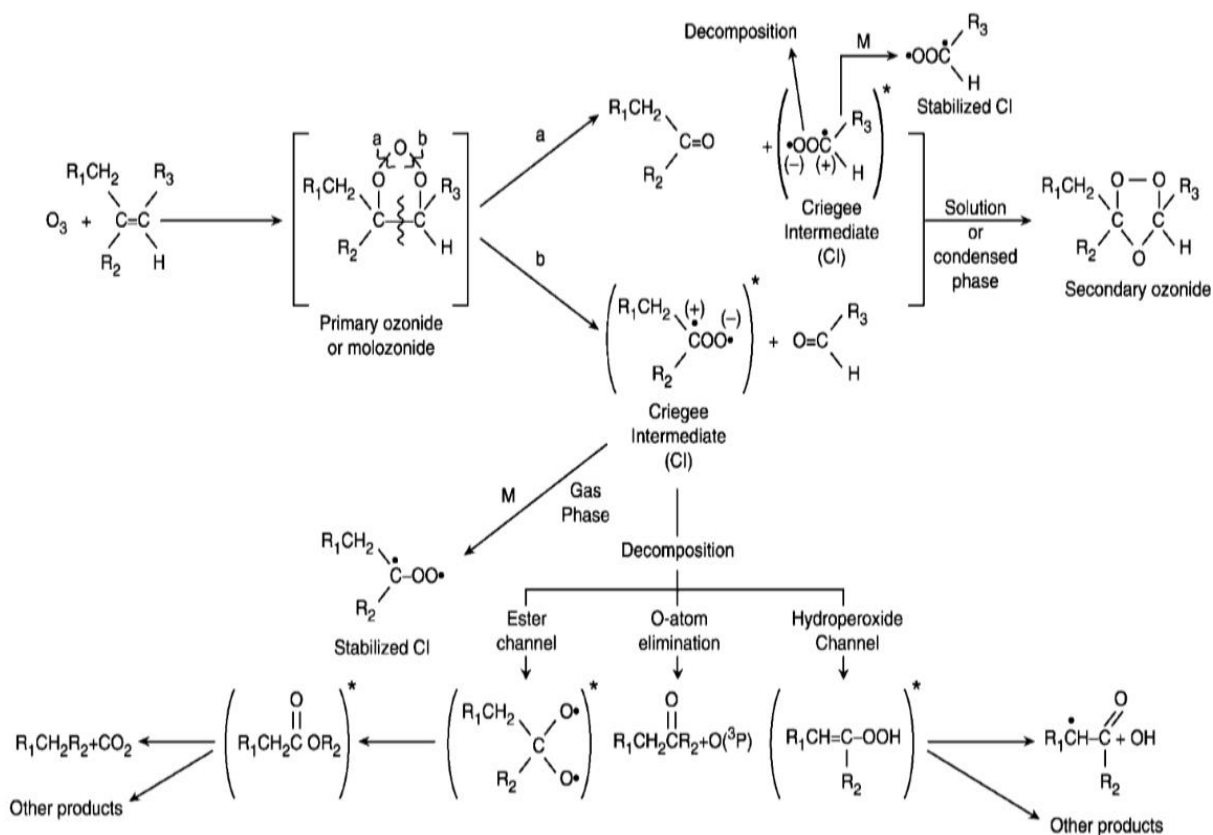


Figure I.3: General scheme for the ozonolysis mechanism of alkenes (Finlayson-Pitts and Pitts Jr, 2000).

The alkene-ozone reaction generally leads to the formation of several carbonyl compounds as main products. The carbonyl compound(s) formed from the decomposition of the POZ will be denoted as primary products, however, secondary products are usually attributed to the different reactions of CIs (**Atkinson, 1997b**).

For acyclic and exocyclic alkenes, ozonolysis leads to fragmentation processes which lead to the decrease of the carbon chain size and thus the formation of more volatile species. In contrary, for endo cyclic alkenes, there is no cut in the carbon skeleton but addition(s) of functional groups that allows the formation of secondary ozonides which are important species for Secondary Organic Aerosol (SOA) formation (**Kroll and Seinfeld, 2008b**).

In this context, ozonolysis is the most effective oxidation reaction in generating low-volatility products that can contribute significantly to the formation of SOA and thus, it has received a great deal of attention in aerosol formation studies (**Bernard et al., 2010**).

I.3 Atmospheric Aerosols

Over the past decade, atmospheric aerosols have been the subject of high scientific and political interest due to their important role on climate, atmospheric chemistry and human health (**Lanz et al., 2010**). Aerosols are defined as relatively stable suspensions of solid or liquid particles in air (**Finlayson-Pitts and Pitts Jr, 2000**).

I.3.1 Sources

Atmospheric aerosols are formed from a wide variety of natural and anthropogenic sources. Windblown soil and released rock debris (mineral dust), volcanic dust, sea spray and microbial particles (living and dead viruses, bacterial cells, fungi, spores, pollens, algae, seeds, etc.), are considered as primary sources of natural aerosol. Biogenic aerosols can sometimes account for up to 30% of the total atmospheric aerosol volume at a given location, especially in the remote tropical continental areas covered by pluvial forests (**Tomasi and Lupi, 2016**).

On the other side, human activities including transportation (cars, ships, airplanes, and other vehicles), fuel combustion, waste burning, agriculture, construction and mining, give rise to the suspension of particles in the atmosphere. These aerosols contain sulfate, ammonium, nitrate, trace metals, carbonaceous material and water. They typically contribute to at least 10% of the total tropospheric aerosol mass loading (**Tomasi and Lupi, 2016**).

I.3.2 Classes

Atmospheric aerosols are classified as either primary or secondary.

- Primary aerosols are emitted directly in the atmosphere as liquids or solids through a wide range of processes such as bulk-to-particle conversion and combustion. Their natural sources, that globally dominate emissions of aerosols, include the emission of sea spray, suspension of soil and rock debris (mineral dust) and volcanic eruptions. However, anthropogenic primary particles originate from fossil fuel combustion, waste and biomass burning and industrial activities (**Tomasi and Lupi, 2016**).
- Secondary aerosols are formed through gas-to-particle conversions such as nucleation of precursor gases, or via heterogeneous and multiphase chemical reactions including gas partitioning to pre-existing particles. They are either inorganic aerosols (SIA) formed thermodynamically (salt formation) from the main precursor gases (SO_2 , NO_x and NH_3) or organic aerosols (SOA) produced from atmospheric oxidation reactions of VOCs (detailed in **I.3.4.1 Secondary Organic Aerosols (SOA)** (**Hallquist et al., 2009; Aksoyoglu et al., 2017**).

I.3.3 Size

Among the different properties (number concentration, volume concentration, chemical composition, etc.) of the particles, size is of great importance because it is related to their effects on health, visibility and climate.

Particles are characterized by an aerodynamic diameter, corresponding to the diameter of a sphere of density 1 g.cm^{-3} and which has the same settling velocity in air as the particle under

consideration. They, as presented in **Figure I.6**, range from molecular clusters being less than one nanometer in diameter to particulate matter of 10 μm or larger. Generally, on size basis, there are three distinct groups of atmospheric aerosols (**Finlayson-Pitts and Pitts Jr, 2000**):

- **Ultrafine particles ($PM_{0.1}$)**: having an aerodynamic diameter smaller than 0.1 μm . They originate from the clustering of gas molecules through the *nucleation mode*.
- **Fine particles ($PM_{2.5}$)**: having an aerodynamic diameter smaller than 2.5 μm . They are formed from coagulation of ultrafine particles and condensation of gases through the *accumulation mode*.
- **Coarse particles (PM_{10})**: having an aerodynamic diameter between 2.5 and 10 μm . Particles in this size range are usually produced by mechanical processes such as grinding, wind, or erosion.

I.3.4 Composition

Atmospheric aerosols are composed of a complex mixture of organic matter (also termed organic aerosol or OA), inorganic species such as nitrate, mineral dust, elemental carbon (EC also referred to as black carbon) and primary biological aerosol particles (PBAPs) (**Seinfeld and Pandis, 1998**). In fact, the chemical constituents of particles depend on the source of their emissions and thus, it is characterized by their origin: soot from combustion, mineral dust from levitated crustal material, etc. (**Koppmann, 2007**). This composition directly affects how aerosols interact with solar radiation and therefore modifies the radiative balance of the atmosphere (**Kanakidou et al., 2004**). Any changes in the chemical composition might alter the properties of the particles (e.g hygroscopicity), and consequently modify the impact of aerosols on climate (**Koppmann, 2007**). Among the various chemical species, organics have been of great interest due to their importance in the atmosphere. Organic aerosols constitute approximately 10 - 70% of the total atmospheric fine particle mass (**Andrews et al., 2000**). A large and often dominant fraction of total organic particulate mass is assigned to secondary organic aerosols (SOA) (**Kroll & Seinfeld, 2008**).

I.3.4.1 Secondary Organic Aerosols (SOA)

SOAs are not emitted directly in the atmosphere, but formed from atmospheric transformations of organic species. The precursors of SOA are mainly volatile reactive biogenic (like monoterpenes) and anthropogenic (such as aromatics) VOC, with natural compounds accounting for most of the SOA formation (**Koppmann, 2007**). SOAs exhibit impacts on climate and human health similar to that of fine particles (detailed later in section **I.3.6.3 On health**). In fact, there exist uncertainties about the impact of atmospheric aerosols on climate and health due to the deficiency of knowledge on their sources, composition, physico-chemical properties and mechanisms of formation. The sources of uncertainties at each step are highlighted as areas that require further investigations (**IPCC, 2007**).

I.3.4.1.1 Modeling and Uncertainties

Present-day model simulations (e.g **Goldstein and Galbally, 2007; Yu et al., 2008**) have underestimated organic aerosol mass in both the boundary layer and aloft. The models predict that the production of SOAs, from the oxidations of BVOCs, is around 12 Tg/year (**Tsigaridis and Kanakidou, 2007**). However, some field studies indicate SOA formation in the atmosphere which is higher than predicted by models (**Volkamer et al., 2006**). In this regard, **Figure I.4** illustrates that the amount of SOA present in the atmosphere is underestimated by some models such as the traditional chemistry-transport model (concerns with the oxidation mechanisms of VOCs, and the transfer of the products formed in the gas phase to the particulate phase). However, new framework based on the volatility of primary organic species, proposed by **Robinson et al., (2007)**, constitutes a genuine revision in the understanding and prediction of SOA formation (**Hodzic et al., 2010**).

Behind the negative bias are several reported reasons (**Goldstein and Galbally, 2007; Yu et al., 2007; Carlton et al., 2009**) including:

- Large discrepancy in emission inventories of VOCs.
- Unknown SOA precursors in the atmosphere.
- Lack of knowledge in the chemical formation mechanisms of SOA.
- Limitations associated to laboratory experiments simulating the real atmospheric conditions.

- Uncertain meteorological inputs that distort the calculations of concentrations.

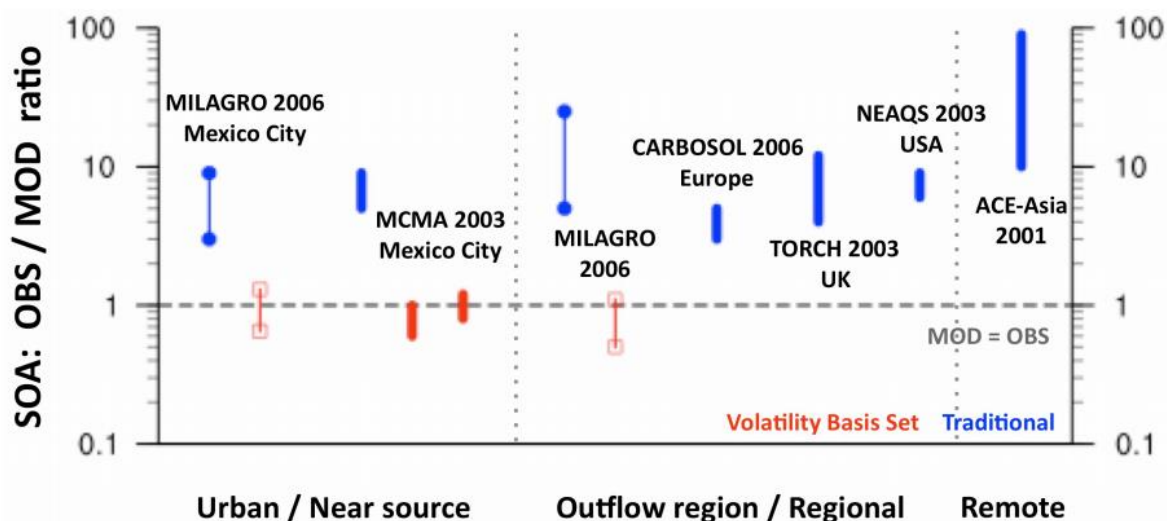


Figure I.4: Comparison of observed to predicted SOA ratios as determined in different studies based on the volatility of primary organic species (in red) and the traditional models (in blue) according to the photochemical age of SOA (Hodzic et al., 2010).

Without proper representation of aerosols in atmospheric models, improvement of operative management plans dedicated to air quality and climate effects is hindered (Carlton et al., 2009).

1.3.4.1.2 Formation mechanisms

The chemical and physical processes associated with SOA formation are diverse and complex (Hallquist et al., 2009). In general, gas-phase oxidation, initiated by the reaction of parent hydrocarbons with radicals or ozone, is the primary process by which semi-volatile oxygenated compounds are produced. These products, which tend to be highly oxidized and polar organic molecules, homogeneously nucleate to form new particles or undergo absorptive partitioning between the gas and particle phases. The equilibrium-phase partitioning is highly dependent on temperature and relative humidity (Seinfeld and Pankow, 2003). Figure I.5 displays the routes of formation of SOA from the oxidation of VOCs.

SECONDARY ORGANIC AEROSOL PRODUCTION

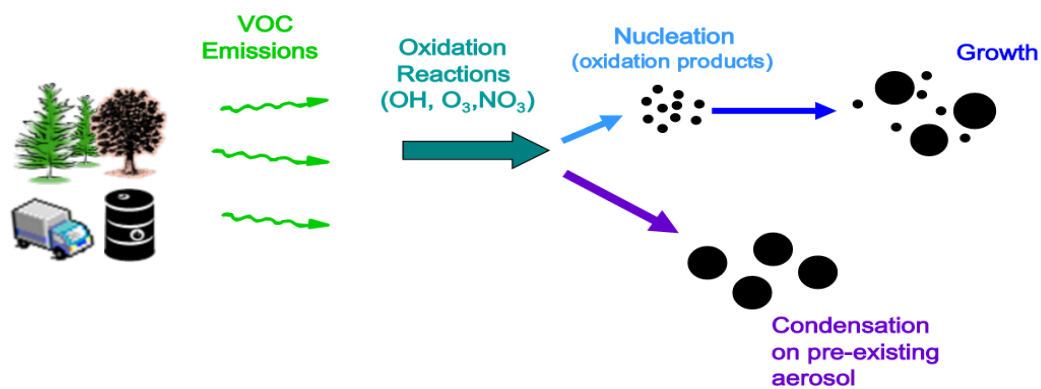


Figure I.5: Routes of formation of SOA from the oxidation of VOCs (Copyright: Waza, 2014).

Although clear progress has been made in recent years in the field of SOA, significant gaps in the scientific knowledge concerning the formation mechanisms, still exist. Consequently, many studies adopting a multidisciplinary approach are required for a better understanding of SOA formation, fate and transport and thus to properly represent aerosols in atmospheric models.

I.3.4.1.3 Formation yield

Prediction of SOA yield and speciation is challenging because of general uncertainties concerning the gas-phase chemistry that leads to formation of condensable species (Griffin, 2005). The formation yield depends on several factors such as degree of oxidation, peroxy radical (RO₂) and NO_x concentrations, the presence/absence of seed particles, light, relative humidity and temperature. A number of studies (Jonsson et al., 2008; Shilling et al., 2008; Emanuelsson et al., 2013; Schwantes et al., 2019) have been conducted to investigate the influence of these parameters on the SOA formed mostly from isoprene and monoterpenes (α - and β -pinene, sabinene, limonene, Δ 3-carene ...), but the results are highly variable and there are much to be done. New information concerning the formation and chemical nature of particulate products is needed for an improved understanding of the routes and yields of aerosol formation in the atmosphere (Carlton et al., 2009).

I.3.4.1.4 Hygroscopicity

Hygroscopicity is an important physicochemical property of aerosols as it influences radiative forcing and consequently climate (**Farmer et al., 2015**). Currently the scientific research has been focusing on this property because of its far-reaching implications (**Varutbangkul et al., 2006**).

Hygroscopicity is defined as the degree of water uptake by particles (**Tritscher et al., 2011**). It describes how aerosols interact with water vapor at different saturation conditions (**McFiggans et al., 2006**) and depends strongly on the chemical composition of the particles, their size (increasingly important for ultrafine particles), physical state and morphology (**Mikhailov et al., 2009; Krieger et al., 2012**). Therefore, it is a determining factor in the atmospheric lifetime of aerosols, gas–particle partitioning of semi-volatile compounds, and for heterogeneous chemical transformations (**IPCC, 2013**).

Hygroscopicity significantly impacts dry and wet deposition rates of aerosol particles and thus modifies their lifetimes and spatio-temporal distribution (**Fan et al., 2004**). It affects the optical properties and refractive indices of aerosols and accordingly the visibility and direct radiative forcing (**Brock et al., 2016; Haarig et al., 2017**). In addition, hygroscopicity can define the capacity of aerosols to serve as cloud condensation nuclei (CCN), thereby influencing the formation and properties of clouds and hence indirect radiative forcing (**Petters and Kreidenweis, 2007; Farmer et al., 2015**). Also, hygroscopicity significantly affects the transport and deposition of inhaled aerosol particles in the respiratory tract, so it plays an important role in the health impact of ambient aerosols (**Hofmann, 2009; Winkler-Heil et al., 2014**).

To characterize the hygroscopic properties of aerosols, instruments which monitor the size change of particles associated with humidification, have been used over the last two decades. SOA hygroscopicity has been measured either with a Tandem Differential Mobility Analyzer (HTDMA) for measurements below 100% of relative humidity or using a Cloud Condensation Nuclei counter (CCNc) above an RH of 100% or with both. The selected dried aerosols pass through the HTDMA and are exposed to a high relative humidity (~ 90%) to form humidified particles. However, aerosols drawn into the CCNc are exposed to supersaturated conditions to form activated droplets that are measured with an Optical Particle Counter (OPC).

As atmospheric aerosols contain both inorganic and organic compounds, the need to understand the hygroscopicity of both species is highly desired. However, there are still large uncertainties in the understanding of the hygroscopicity of organic species and this presents further challenges for the study of SOA and its impact (Petters et al., 2009).

I.3.5 Sinks and transport

The removal of aerosols from the atmosphere depends on their size and nature. Figure I.6, highlights the different sources and removal processes for each class of atmospheric particles. The main sink for fine particles in the Aitken and nucleation modes is via self-coagulation or coagulation with other particles and in the accumulation mode are eliminated mostly by wet precipitation (rainout, washout). However, coarse particles are removed mainly by dry deposition or sedimentation (Koppmann, 2007). Particles in the atmosphere have different residence times depending on their size. Small particles remain floating in the atmosphere for a long period of time (days). However, large particles tend to fall out of the atmosphere in few minutes or hours after being formed (Pidwirny, 2010).

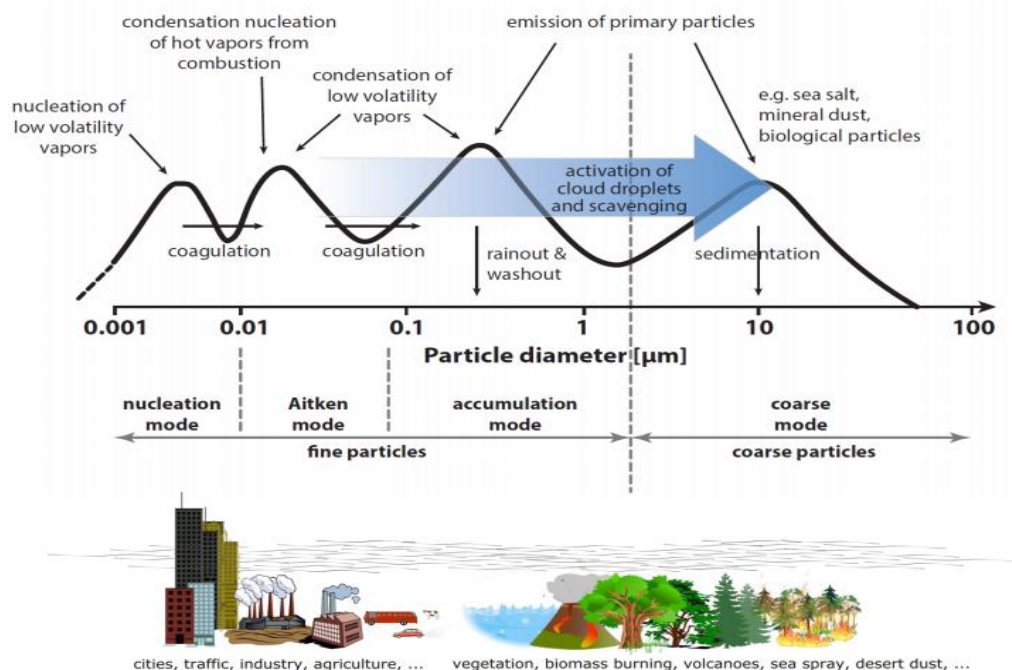


Figure I.6: Overview of aerosol size classification together with main sources and sinks (copy rights: Schrödner, 2015).

Aerosols can also be transported from their source regions into far away locations due to prevailing changes in the mean atmospheric circulation patterns. They are dispersed in the atmosphere through processes of advection, convection and turbulence (**Ramachandran, 2018**).

Global chemistry transport models are used to integrate the current knowledge of emissions and atmospheric processes of gas and aerosols, analyze remote sensing and in situ observations, and assess the impact of aerosols in the past, present, and future climate scenarios.

I.3.6 Impact

Atmospheric aerosols play a crucial role in many environmental processes. They participate in numerous meteorological, physical, and chemical phenomena occurring in the atmosphere, such as the formation of fog and cloud droplets, and they also absorb and/or scatter solar radiation (**Tomasi and Lupi, 2016**). Besides visibility and climate implications, atmospheric aerosols also have important impacts on human health which have been increasingly recognized.

I.3.6.1 On climate

Since the industrial revolution, the concentrations of atmospheric particles have generally increased primarily due to human activities. These particles interact with the incoming (from the sky) and outgoing (from the ground) radiation and therefore affect the radiative balance of the atmosphere (**IPCC, 2013; Tomasi and Lupi, 2016**). The direct influences of atmospheric particles are absorbing or scattering solar radiation, however the indirect impacts include altering the cloud microphysical, optical and radiative properties (optical thickness and cloud albedo), and changing the cloud amount, lifetime and precipitation efficiency (**Huang et al., 2007**).

The impact of the various atmospheric gases and particles (natural and anthropogenic) on the radiative forcing of climate is shown in **Figure I.7**. Some species cause positive forcing while others cause negative forcing, for instance, black carbon heats the atmosphere by absorption of solar radiation, whereas most of the organic aerosols cool the Earth's atmosphere. The direct radiative forcing summed over all aerosol types is negative (**IPCC, 2007; Boucher et al., 2013**). Hydrophilic aerosols can act as cloud condensation nuclei (CCN) and ice nuclei (IN) upon which

cloud droplets and ice crystals form and thus have an indirect climatic effect through modification of cloud properties (Kanakidou et al., 2004).

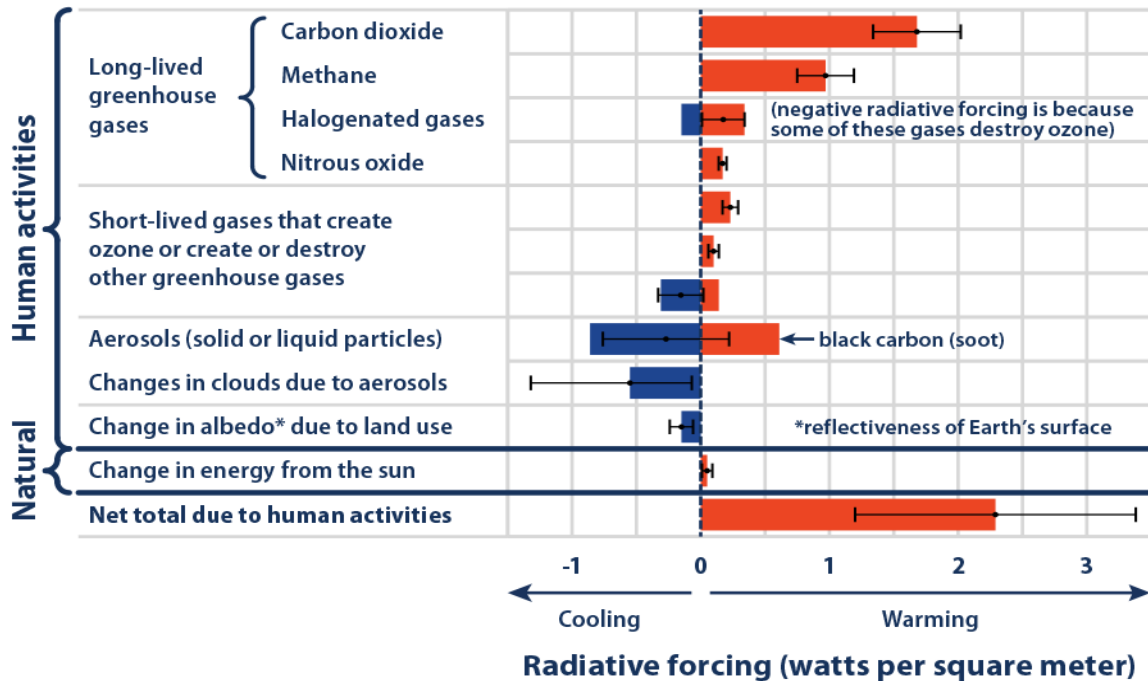


Figure I.7: The total amount of radiative forcing (calculated in watts per square meter) caused by human activities since 1750. Copyright (US EPA, 2016)- Data source (IPCC, 2013).

I.3.6.2 Visibility

The most obvious characteristic of air pollution is the loss of visibility. The term *visibility* is defined as “the farthest distance at which one can see a large, black object against a bright background at the horizon” (Seinfeld, and Pandis, 2006). The lack of visibility is primarily due to suspended airborne particles, which scatter light efficiently, giving the atmosphere a "hazy" appearance. It is well-recognized, that the concentration of aerosols, their chemical composition and size distribution, can heavily influence this parameter (Yu et al., 2016). An example of the effect of particles on air quality is illustrated in Figure I.8. It shows a severe haze with low visibility (< 10 km), caused by biomass burning aerosols in Southeast Asia (2013) (Lee et al., 2017).



Figure I.8: Comparison of the 2013 Southeast Asian haze (a) during (19 June) and (b) after the episode (23 June) in Singapore (Wikipedia, 2013).

I.3.6.3 On health

Particles have been identified as the cause of numerous negative health effects. The range of risks is broad, but predominantly associated to the respiratory, cardiovascular and even nervous system (WHO, 2006). Exposure to PM has been linked to asthma attacks, chronic bronchitis, cardiovascular diseases, cancer, premature death and much more (Kim et al., 2015).

Particle size and concentration are directly linked to their potential for causing health problems. As shown in Figure I.9, coarse particles are deposited into the airways in the head region when inhaled and cause irritation, while fine particles penetrate deeper into the lungs leading to enhanced probability of pulmonary disease and ultimately, lung damage (Guariero and Guariero, 2013). Even smaller, ultra-fine particles can reach the alveoli, pass the lung epithelium and enter the bloodstream where they can be transferred further to the liver, bone marrow, brain and heart, leading to a systematic infection. Consequently, ultra-fine particles appear to play a special role and are potentially more health hazardous than those in the coarse mode (Politis et al., 2013).

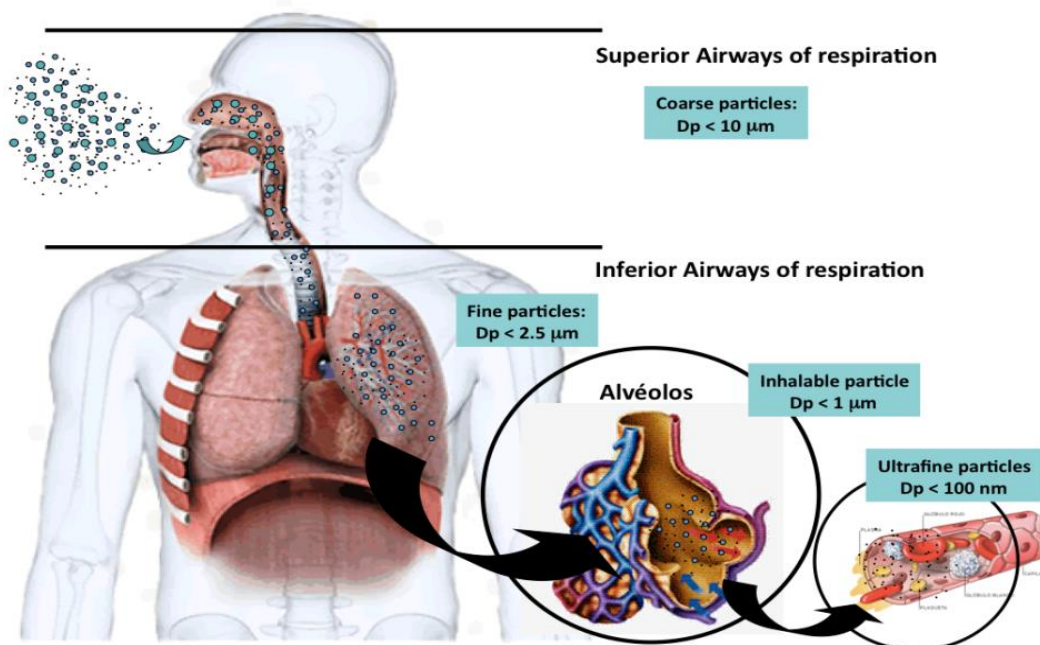


Figure I.9: Size dependence of the impact of particulate matter on the respiratory system (Guarieiro and Guarieiro, 2013).

I.4 Atmospheric Simulation Chambers

The study of the atmosphere, particularly its chemistry, has been examined through different methods. Field measurements, computer models and laboratory studies are all powerful tools used to address long-standing questions in atmospheric research. The integration of all these approaches allows scientists to better understand the atmospheric system (Kim et al., 2009). The most direct and significant way to mimic and examine the atmosphere and to simplify this extremely complex physico-chemical system is to simulate atmospheric conditions in large reactors known as atmospheric simulation chambers (Finlayson-Pitts and Pitts Jr, 2000).

I.4.1 Description

An “atmospheric simulation chamber” is a large vessel that allows the controlled study of complex chemical and physical processes which occur in the atmosphere (Finlayson-Pitts and Pitts, 1986).

The size, material, irradiation source, temperature and pressure range, as well as the analytical instruments (coupled to the chamber to investigate the gas and/or condensed phases) are characteristics to take into account while designing a chamber (**Wang et al., 2014**).

I.4.2 Background

The development of atmospheric simulation chamber studies has progressed with time. In the early 1950s, soon after the new phenomenon of photochemical air pollution had been reported, the first photochemical “smog” experiments started to be performed in small simple systems. Later in the 1960s, the understanding of atmospheric reactions took a large step forward when OH radicals were identified as the most important oxidizing agent in the troposphere and a large number of chamber experiments were subsequently carried out in more developed closed systems (**Finlayson-Pitts and Pitts Jr, 2000**). In the 1970s, studies of tropospheric reactions were initiated by laboratories in Europe and in the 1980s, gas phase kinetics and mechanistic studies were performed in both indoor and outdoor chambers (**Ackerman and Knox, 2006**). In the following years, different types of chambers were constructed worldwide, with the design characteristics depending on the aim of research and the different atmospheric conditions under which the experiments could be conducted.

Although initial advances in the application of atmospheric simulation chambers occurred in the United States and Japan, Europe now leads the world in the use of large and highly instrumented chambers for experimental investigation and atmospheric model development (**European Commission and Directorate-General for Research and Innovation, 2014**). Excluding small Teflon bags of a few hundred liters, less than 30 chambers are currently in operation around the world (**Wang et al., 2011**). At least sixteen advanced atmospheric simulation chambers are currently operating in Europe and coordinate within the framework of the European Environmental Chamber Network known as “EUROCHAMP”. The different facilities are displayed in **Table I.4**.

Table I.4: The different atmospheric simulation chambers in EUROCHAMP (www.eurochamp.org).

Name	Location	Volume (m ³)	Shape	Material	Type
<i>SAPHIR</i>	Jülich, Germany	270	Cylindrical	FEP Teflon	Outdoor
<i>EUPHORE</i>	Valencia, Spain	200	Hemisphere	FEP Teflon	Outdoor
<i>HELIOS</i>	Orléans, France	90	Hemisphere	FEP Teflon	Outdoor
<i>AIDA</i>	Hermann-von-Helmholtz-Platz 1, Germany	84.5	Cylindrical	Aluminium	Indoor
<i>ILMARI</i>	Kuopio, Finland	29	Cuboid	FEP Teflon	Indoor
<i>IASC</i>	Cork, Ireland	27	Cuboid	FEP Teflon	Indoor
<i>PACS-C3</i>	Villigen, Switzerland	27	Cubic	FEP Teflon	Indoor
<i>LEAK-LACIS</i>	Leipzig, Germany	19	Cylindrical	FEP Teflon	Indoor
<i>MAC-MICC</i>	Manchester, United Kingdom	18	Cuboid	FEP Teflon	Indoor
<i>CASC</i>	Cambridge, United Kingdom	5.5	Cubic	FEP Teflon	Indoor
<i>QUAREC</i>	Wuppertal, Germany	1.0	Cylindrical	Quartz	Indoor
<i>CESAM</i>	Créteil, France	4.2	Cylindrical	Stainless Steel	Indoor
<i>RvG-ASIC</i>	Norwich, United Kingdom	3.5	Cuboid	Glass	Indoor
<i>ChAMBRé</i>	Genoa, Italy	3	Cylindrical	Stainless steel	Indoor
<i>HIRAC</i>	Leeds, United Kingdom	2	Cylindrical	Stainless steel	Indoor
<i>ISAC</i>	Lyon, France	2	Cuboid	FEP Teflon	Indoor
<i>CERENSIM</i>	Iasi, Romania	0.78	Cylindrical	Quartz	Indoor

* The different colors correspond to the different shapes of the chambers (red: cylindrical; green: hemisphere; white: cuboid; yellow: cubic)

I.4.3 Types

The design and capacities of the different chambers vary widely, displaying large differences in factors such as shape, size, reactor wall materials, light sources, conditions (i.e. static) under which experiments can be carried out, capabilities based on connected analytical instruments and the attainable ranges of pressures and temperatures (**Finlayson-Pitts and Pitts Jr, 2000**).

Chambers have different geometry including: cubic, cuboid, cylindrical, pyramidal spherical or hemi-spherical shapes. In addition, atmospheric facilities also exhibit a wide range of volumes extending from a few to several hundred cubic meters. The volume is a crucial parameter that defines the surface-to-volume ratio (S/V) which in turn determine the extent of surface interactions in the enclosure (**Seakins, 2010**). The largest chamber in the world is SAPHIR (Volume = 270 m³) in Germany (**Barnes et al., 2006**).

In the main, Teflon, Pyrex, quartz, aluminum, and stainless steel are the materials used to construct chambers (**Barnes et al., 2006**). Glass, aluminum and stainless-steel chambers have rigid walls so they have a fixed volume, whereas a Teflon film enables the construction of a collapsible bag, whose volume decreases as a sample of air is taken out. Thus, chambers could be classified as rigid or collapsible. Rigid chambers offer the advantage of controlling and altering the temperature and pressure but they are relatively more expensive than collapsible ones. The latter enclosures are normally inert, but low molecular weight fluorocarbons can be released from FEP Teflon walls. With collapsible reactors, sampling does not dilute the gas and aerosol concentrations, unless there are inward leaks through the walls. However, the major problem with these bags is that they cannot really be used under low pressure or high temperatures (**Leskinen et al., 2015**).

Chambers are often classified into indoor or outdoor. Indoor are used to perform studies under laboratory controlled conditions of pressure, temperature, humidity and concentration. They provide control of temperature and humidity, but may suffer from the difference between the artificial light spectrum and solar spectrum, resulting in different rates of photolysis (**Carter et al., 2005**). In contrast, outdoor chambers are usually larger than the indoor ones. They are unique in the availability of real atmospheric conditions especially natural sunlight. However, diurnal variations of temperature and actinic flux make it hard to model experimental data and to reproduce experiments (**Wang et al., 2014**).

I.4.4 Benefits and Limitations

Simulation chambers provide a controlled environment to study the formation and the evolution of specific compounds of interest like gas and/or aerosols, in a closed system separately from meteorology and aside of other atmospheric interferences (**Wang et al., 2014**). Conditions such as temperature, humidity, and concentrations of the parent precursors, aerosol and oxidants can be controlled in the reactor (**Leskinen et al., 2015**). Hence, chamber based investigations play a key role in developing a more detailed understanding of lesser known processes and mechanisms in the gas phase as well as in the particulate phase and over a range of atmospheric conditions (**Glowacki et al., 2007**). They are useful for multiple species detection using several techniques on long timescales that might be in the order of hours or days, hence, reactors are capable to bridge the gap between field work and small scale kinetic studies. Besides, chambers especially large ones, provide space for analytical equipment such as cryo-trapping of radicals and Laser-induced fluorescence (LIF) and privilege the application of long path absorption spectroscopy in the UV, VIS and IR. In addition, large chamber can be used for inter-calibration campaigns to validate analytical instruments and techniques and to test new hypotheses that may arise from analysis of the field campaign (**Kim, 2009**). Moreover, chamber experiments together with knowledge gained from field campaign data, will be used to develop and improve reliable atmospheric models, and thus to better understand the tropospheric chemistry (**Seakins, 2010**).

On the other side, simulation chambers are not without any limitations. The walls represent the largest uncertainty in using chambers for atmospheric studies. For instance, it is possible for heterogeneous reactions to be initiated on the chambers surfaces resulting to the off-gassing of unexpected species (**Carter, 2006**). Background of chemicals and memory effects cannot be denied as well; they may complicate the chemical composition of the studied mixture and, hence, the reliability of the data. Also, the memory effects besides the inadequate analytical equipment employed sometimes, restrict the evaluation of chemical mechanisms in clean environments where NO_x is very low (**Kim, 2009**). Not only the surface, but also the light source might be a cause of uncertainties. For instance, artificial lights irradiating the indoor chambers, may deviate from the sunlight and create different photochemistry. Moreover, the solar spectrum of outdoor reactors varies with cloud cover and solar zenith angle and thus the distribution of the radiation is difficult to model (**Barnes et al., 2006**). Based Due to the advantages outlined above,

most of the laboratory research on the atmospheric chemistry of VOCs and SOA formation has been performed in atmospheric simulation chambers.

I.5 Thesis aim

As the bibliographic review has highlighted, the difficulty of studying the atmosphere is linked to the diversity of constituents and the complexity of the transformation processes involved in the atmospheric homogeneous and heterogeneous phases. Seeking to better understand this complex physico-chemical medium, atmospheric simulation chambers have been used since the last six decades. Today, a new built atmospheric simulation chamber named *CHARME* (*CHamber for the Atmospheric Reactivity and the Metrology of the Environment*) is founded by our laboratory.

This research work presents *CHARME* with all its basic features and important instruments. It aims at characterizing the technical and physicochemical parameters including the intensity of irradiation, mixing time of different compounds, the life time of gases and particles, the effect of walls etc. It endeavors to validate the new chamber performance and hence to make it operational.

The chamber study presented in this work aims to contribute to the understanding of the atmospheric behaviour of the monoterpene, γ -terpinene. This compound was selected based on its reactivity with major atmospheric oxidants (O_3 , OH and NO_3), its ability to release OH radicals by reaction with O_3 and its potential to form secondary organic aerosols. A number of studies have reported the gas-phase oxidation of γ -terpinene with OH (**Atkinson et al., 1986; Griffin et al., 1999a; Lee et al., 2006; Rio et al., 2010; Aschmann et al., 2011**) and NO_3 (**Atkinson et al., 1985a; Martinez et al., 1999; Fouqueau et al., 2017**). However, ozonolysis of this compound was investigated to a lesser extent with only two publications concerning kinetic studies (**Grimsrud et al., 1975; Atkinson et al., 1990**) and limited product and mechanistic information reported by **Reissell et al., (1999)** and **Aschmann et al., (2002)**. Consequently, as the knowledge of the atmospheric reactivity of this monoterpene is limited, it was necessary to improve the atmospheric chemistry knowledge, particularly to take an interest in its reactions with ozone. Furthermore, scientific research has recently been focusing on the hygroscopicity of SOA due to the importance of this property on climate and health. However, this area of study is not fully understood and there are still large uncertainties to be apprehend (**Varutbangkul et al., 2006;**

Petters et al., 2009). Thus, this research work dealing with hygroscopicity and CCN activity of aerosols formed from the ozonolysis of γ -terpinene, is considered as a representative of organic

References

- Ackerman, S., Knox, J.A., 2006. *Meteorology: Understanding the Atmosphere*. Cengage Learning.
- Aksoyoglu, S., Ciarelli, G., El-Haddad, I., Baltensperger, U., Prévôt, A.S.H., 2017. Secondary inorganic aerosols in Europe: sources and the significant influence of biogenic VOC emissions, especially on ammonium nitrate. *Atmospheric Chemistry and Physics* 17, 7757–7773. <https://doi.org/10.5194/acp-17-7757-2017>
- Andrews, E., Saxena, P., Musarra, S., Hildemann, L.M., Koutrakis, P., McMurry, P.H., Olmez, I., White, W.H., 2000. Concentration and Composition of Atmospheric Aerosols from the 1995 SEAVS Experiment and a Review of the Closure between Chemical and Gravimetric Measurements. *Journal of the Air & Waste Management Association* 50, 648–664. <https://doi.org/10.1080/10473289.2000.10464116>
- Aschmann, S.M., Arey, J., Atkinson, R., 2011. Formation of p-cymene from OH + γ -terpinene: H-atom abstraction from the cyclohexadiene ring structure. *Atmospheric Environment* 45, 4408–4411. <https://doi.org/10.1016/j.atmosenv.2011.05.044>
- Aschmann, S.M., Arey, J., Atkinson, R., 2002. OH radical formation from the gas-phase reactions of O₃ with a series of terpenes. *Atmospheric Environment* 36, 4347–4355. [https://doi.org/10.1016/S1352-2310\(02\)00355-2](https://doi.org/10.1016/S1352-2310(02)00355-2)
- Atkinson, R., 1997a. Gas-Phase Tropospheric Chemistry of Volatile Organic Compounds: 1. Alkanes and Alkenes. *Journal of Physical and Chemical Reference Data* 26, 215–290. <https://doi.org/10.1063/1.556012>
- Atkinson, R., 1986. Kinetics and mechanisms of the gas-phase reactions of the hydroxyl radical with organic compounds under atmospheric conditions. *Chemical Reviews* 86, 69–201. <https://doi.org/10.1021/cr00071a004>
- Atkinson, R., Arey, J., 2003a. Gas-phase tropospheric chemistry of biogenic volatile organic compounds: a review. *Atmospheric Environment* 37, 197–219. [https://doi.org/10.1016/S1352-2310\(03\)00391-1](https://doi.org/10.1016/S1352-2310(03)00391-1)
- Atkinson, R., Arey, J., 2003b. Atmospheric Degradation of Volatile Organic Compounds. *Chemical Reviews* 103, 4605–4638. <https://doi.org/10.1021/cr0206420>.
- Atkinson, R., Arey, J., Aschmann, S.M., Corchnoy, S.B., Shu, Y., 1995. Rate constants for the gas-phase reactions of *cis*-3-Hexen-1-ol, *cis*-3-Hexenylacetate, *trans*-2-Hexenal, and Linalool with OH and NO₃ radicals and O₃ at 296 ± 2 K, and OH radical formation yields from the O₃ reactions: Rate constants for gas-phase reactions. *International Journal of Chemical Kinetics* 27, 941–955. <https://doi.org/10.1002/kin.550271002>
- Atkinson, R., Aschmann, S.M., Pitts, J.N., 1986. Rate constants for the gas-phase reactions of the OH radical with a series of monoterpenes at 294 ± 1 K: Gas-phase reaction of OH radicals. *International Journal of Chemical Kinetics* 18, 287–299. <https://doi.org/10.1002/kin.550180303>
- Atkinson, R., Baulch, D.L., Cox, R.A., Crowley, J.N., Hampson, R.F., Hynes, R.G., Jenkin, M.E., Rossi, M.J., Troe, J., 2004. Evaluated kinetic and photochemical data for atmospheric chemistry: Volume I - gas phase reactions of O_x, HO_x, NO_x and SO_x species. *Atmospheric Chemistry and Physics* 4, 1461–1738. <https://doi.org/10.5194/acp-4-1461-2004>

- Atkinson, R., Carter, W.P.L., 1984. Kinetics and mechanisms of the gas-phase reactions of ozone with organic compounds under atmospheric conditions. *Chemical Reviews* 84, 437–470. <https://doi.org/10.1021/cr00063a002>
- Atkinson, R., Hasegawa, D., Aschmann, S.M., 1990. Rate constants for the gas-phase reactions of O₃ with a series of monoterpenes and related compounds at 296 ± 2 K. *International Journal of Chemical Kinetics* 22, 871–887. <https://doi.org/10.1002/kin.550220807>
- Atkinson, Roger., Aschmann, S.M., Winer, A.M., Pitts, J.N., 1985a. Kinetics and atmospheric implications of the gas-phase reactions of nitrate radicals with a series of monoterpenes and related organics at 294 ± 2 K. *Environmental Science & Technology* 19, 159–163. <https://doi.org/10.1021/es00132a009>
- Avzianova, E.V., Ariya, P.A., 2002. Temperature-dependent kinetic study for ozonolysis of selected tropospheric alkenes. *International Journal of Chemical Kinetics* 34, 678–684. <https://doi.org/10.1002/kin.10093>
- Barnes, I., Rudzinski, K.J., North Atlantic Treaty Organization (Eds.), 2006. Environmental simulation chambers: application to atmospheric chemical processes, NATO science series. Series IV, Earth and environmental series. Springer, Dordrecht.
- Bernard, F., Quilgars, A., Cazaunau, M., Grosselin, B., Daele, V., Mellouki, A., Winterhalter, R., Moortgat, G.K., 2010. Ozonolysis of a series of biogenic organic volatile compounds and secondary organic aerosol formation, in: EGU General Assembly Conference Abstracts. p. 822.
- Boucher, O., Randall, D., Artaxo, P., Bretherton, C., 2013. *Clouds and Aerosols*.
- Brock, C.A., Wagner, N.L., Anderson, B.E., Attwood, A.R., Beyersdorf, A., Campuzano-Jost, P., Carlton, A.G., Day, D.A., Diskin, G.S., Gordon, T.D., Jimenez, J.L., Lack, D.A., Liao, J., Markovic, M.Z., Middlebrook, A.M., Ng, N.L., Perring, A.E., Richardson, M.S., Schwarz, J.P., Washenfelder, R.A., Welti, A., Xu, L., Ziemba, L.D., Murphy, D.M., 2016. Aerosol optical properties in the southeastern United States in summer – Part 1: Hygroscopic growth. *Atmospheric Chemistry and Physics* 16, 4987–5007. <https://doi.org/10.5194/acp-16-4987-2016>
- Calvert, J.G., Madronich, S., 1987. Theoretical study of the initial products of the atmospheric oxidation of hydrocarbons. *Journal of Geophysical Research* 92, 2211. <https://doi.org/10.1029/JD092iD02p02211>
- Carlton, A.G., Wiedinmyer, C., Kroll, J.H., 2009. A review of Secondary Organic Aerosol (SOA) formation from isoprene. *Atmos. Chem. Phys.* 19.
- Carter, W., Cockeriii, D., Fitz, D., Malkina, I., Bumiller, K., Sauer, C., Pisano, J., Bufalino, C., Song, C., 2005. A new environmental chamber for evaluation of gas-phase chemical mechanisms and secondary aerosol formation. *Atmospheric Environment* 39, 7768–7788. <https://doi.org/10.1016/j.atmosenv.2005.08.040>
- Carter, W.P., 2006. The UCR EPA environmental chamber, in: *Environmental Simulation Chambers: Application to Atmospheric Chemical Processes*. Springer, pp. 27–41.
- Chen, X., Hopke, P.K., 2009. Secondary organic aerosol from α-pinene ozonolysis in dynamic chamber system. *Indoor Air* 19, 335–345. <https://doi.org/10.1111/j.1600-0668.2009.00596.x>
- Criegee, R., 1975. Mechanism of Ozonolysis. *Angewandte Chemie International Edition in English* 14, 745–752. <https://doi.org/10.1002/anie.197507451>
- Crippa, M., Guizzardi, D., Muntean, M., Schaaf, E., Dentener, F., van Aardenne, J.A., Monni, S., Doering, U., Olivier, J.G.J., Pagliari, V., Janssens-Maenhout, G., 2018. Gridded emissions of air pollutants for the period 1970–2012 within EDGAR v4.3.2. *Earth Syst. Sci. Data* 10, 1987–2013. <https://doi.org/10.5194/essd-10-1987-2018>

- Di Carlo, P., 2004. Missing OH Reactivity in a Forest: Evidence for Unknown Reactive Biogenic VOCs. *Science* 304, 722–725. <https://doi.org/10.1126/science.1094392>
- Dlugokencky Ed, NOAA/ESRL (www.esrl.noaa.gov/gmd/ccgg/trends_ch4/)
- Dominguez-Taylor, P., Ruiz-Suarez, L.G., Rosas-Perez, I., Hernández-Solis, J.M., Steinbrecher, R., 2007. Monoterpene and isoprene emissions from typical tree species in forests around Mexico City. *Atmospheric Environment* 41, 2780–2790. <https://doi.org/10.1016/j.atmosenv.2006.11.042>
- Duce, R.A., Mohnen, V.A., Zimmerman, P.R., Grosjean, D., Cautreels, W., Chatfield, R., Jaenicke, R., Ogren, J.A., Pellizzari, E.D., Wallace, G.T., 1983. Organic material in the global troposphere. *Reviews of Geophysics* 21, 921. <https://doi.org/10.1029/RG021i004p00921>
- Eggersdorfer, M., 2000. Terpenes, in: Wiley-VCH Verlag GmbH & Co. KGaA (Ed.), *Ullmann's Encyclopedia of Industrial Chemistry*. Wiley-VCH Verlag GmbH & Co. KGaA, Weinheim, Germany. https://doi.org/10.1002/14356007.a26_205
- Emanuelsson, E.U., Watne, Å.K., Lutz, A., Ljungström, E., Hallquist, M., 2013. Influence of Humidity, Temperature, and Radicals on the Formation and Thermal Properties of Secondary Organic Aerosol (SOA) from Ozonolysis of β -Pinene. *J. Phys. Chem. A* 117, 10346–10358. <https://doi.org/10.1021/jp4010218>
- European Commission, Directorate-General for Research and Innovation, 2014. Global change: towards global research infrastructures: EU support for research infrastructures in environmental and earth sciences. Updated edition 2014. Updated edition 2014. Publications Office, Luxembourg.
- European Parliament, Council of the European Union, 2004. <https://eur-lex.europa.eu/LexUriServ/LexUriServ.do?uri=OJ:L:2004:143:0087:0096>
- Evuti, A.M., 2013. A Synopsis on Biogenic and Anthropogenic Volatile Organic Compounds Emissions: Hazards and Control. *International Journal of Engineering Sciences* 10.
- Exline, J.D., Levine, A.S., Levine, J.S., 2008. *Meteorology: An educator's resource for inquiry-based learning for grades 5-9*. Hampton, VA: Langley Research Center.
- Fan, S.-M., Horowitz, L.W., Levy, H., Moxim, W.J., 2004. Impact of air pollution on wet deposition of mineral dust aerosols. *Geophysical Research Letters* 31. <https://doi.org/10.1029/2003GL018501>
- Farmer, D.K., Cappa, C.D., Kreidenweis, S.M., 2015. Atmospheric Processes and Their Controlling Influence on Cloud Condensation Nuclei Activity. *Chemical Reviews* 115, 4199–4217. <https://doi.org/10.1021/cr5006292>
- Finlayson-Pitts, B.J., Pitts, J.N., 1986. *Atmospheric chemistry: fundamentals and experimental techniques*. New York: Wiley.
- Finlayson-Pitts, B.J., Pitts Jr, J.N., 2000. *Chemistry of the upper and lower atmosphere: theory, experiments, and applications*. Elsevier.
- Fornaro, A., Gutz, I.G.R., 2003. Wet deposition and related atmospheric chemistry in the São Paulo metropolis, Brazil: Part 2-contribution of formic and acetic acids. *Atmospheric Environment* 37, 117–128. [https://doi.org/10.1016/S1352-2310\(02\)00885-3](https://doi.org/10.1016/S1352-2310(02)00885-3)
- Fouqueau, A., Cirtog, M., Quilleuc, M.L., Cazaunau, M., Pangui, E., Duncianu, M., Doussin, J.-F., Picquet-Varrault, B., 2017. Reactivity of γ -Terpinene with NO₃ radicals: experimental approach for kinetic and mechanistic study. *EGU General Assembly* 19, 2017-8444.

- Geron, C., Rasmussen, R., R. Arnts, R., Guenther, A., 2000. A review and synthesis of monoterpene speciation from forests in the United States. *Atmospheric Environment* 34, 1761–1781. [https://doi.org/10.1016/S1352-2310\(99\)00364-7](https://doi.org/10.1016/S1352-2310(99)00364-7)
- Glowacki, D.R., Goddard, A., Hemavibool, K., Malkin, T.L., Commane, R., Anderson, F., Bloss, W.J., Heard, D.E., Ingham, T., Pilling, M.J., 2007. Design of and initial results from a Highly Instrumented Reactor for Atmospheric Chemistry (HIRAC). *Atmospheric Chemistry and Physics* 7, 5371–5390.
- Goldstein, A.H., Galbally, I.E., 2007. Known and Unexplored Organic Constituents in the Earth's Atmosphere. *Environmental Science & Technology* 41, 1514–1521. <https://doi.org/10.1021/es072476p>
- Griffin, R.J., 2005. Development and initial evaluation of a dynamic species-resolved model for gas phase chemistry and size-resolved gas/particle partitioning associated with secondary organic aerosol formation. *Journal of Geophysical Research* 110. <https://doi.org/10.1029/2004JD005219>
- Griffin, R.J., Cocker, D.R., Flagan, R.C., Seinfeld, J.H., 1999. Organic aerosol formation from the oxidation of biogenic hydrocarbons. *Journal of Geophysical Research: Atmospheres* 104, 3555–3567. <https://doi.org/10.1029/1998JD100049>
- Grimsrud, E.P., Westberg, H.H., Rasmussen, R.A., 1975. Atmospheric Reactivity of Monoterpene Hydrocarbons, NO_x Photooxidation and Ozonolysis.
- Guarieiro, L.L.N., Guarieiro, A.L.N., 2013. Vehicle Emissions: What Will Change with Use of Biofuel? *Biofuels - Economy, Environment and Sustainability*. <https://doi.org/10.5772/52513>
- Guenther, A., Hewitt, C.N., Erickson, D., Fall, R., Geron, C., Graedel, T., Harley, P., Klinger, L., Lerdau, M., McKay, W.A., Pierce, T., Scholes, B., Steinbrecher, R., Tallamraju, R., Taylor, J., Zimmerman, P., 1995a. A global model of natural volatile organic compound emissions. *Journal of Geophysical Research* 100, 8873. <https://doi.org/10.1029/94JD02950>
- Guenther, A.B., Jiang, X., Heald, C.L., Sakulyanontvittaya, T., Duhl, T., Emmons, L.K., Wang, X., 2012. The Model of Emissions of Gases and Aerosols from Nature version 2.1 (MEGAN2.1): an extended and updated framework for modeling biogenic emissions. *Geoscientific Model Development* 5, 1471–1492. <https://doi.org/10.5194/gmd-5-1471-2012>
- Haarig, M., Ansmann, A., Gasteiger, J., Kandler, K., Althausen, D., Baars, H., Radenz, M., Farrell, D.A., 2017. Dry versus wet marine particle optical properties: RH dependence of depolarization ratio, backscatter, and extinction from multiwavelength lidar measurements during SALTRACE. *Atmospheric Chemistry and Physics* 17, 14199–14217. <https://doi.org/10.5194/acp-17-14199-2017>
- Hallquist, M., Wenger, J.C., Baltensperger, U., Rudich, Y., Simpson, D., Claeys, M., Dommen, J., Donahue, N.M., George, C., Goldstein, A.H., Hamilton, J.F., Herrmann, H., Hoffmann, T., Iinuma, Y., Jang, M., Jenkin, M.E., Jimenez, J.L., Kiendler-Scharr, A., Maenhaut, W., McFiggans, G., Mentel, T.F., Monod, A., Prevot, A.S.H., Seinfeld, J.H., Surratt, J.D., Szmigielski, R., Wildt, J., 2009. The formation, properties and impact of secondary organic aerosol: current and emerging issues. *Atmos. Chem. Phys.* 82.
- Helmig, D., Klinger, L.F., Guenther, A., Vierling, L., Geron, C., Zimmerman, P., 1999. Biogenic volatile organic compound emissions (BVOCs) I. Identifications from three continental sites in the U.S. *Chemosphere* 38, 2163–2187. [https://doi.org/10.1016/S0045-6535\(98\)00425-1](https://doi.org/10.1016/S0045-6535(98)00425-1)

- Hodzic, A., Jimenez, J.L., Madronich, S., Canagaratna, M.R., DeCarlo, P.F., Kleinman, L., Fast, J., 2010. Modeling organic aerosols in a megacity: potential contribution of semi-volatile and intermediate volatility primary organic compounds to secondary organic aerosol formation. *Atmospheric Chemistry and Physics* 10, 5491–5514. <https://doi.org/10.5194/acp-10-5491-2010>
- Hofmann, W., 2009. Modelling particle deposition in human lungs: modelling concepts and comparison with experimental data. *Biomarkers* 14 Suppl 1, 59–62. <https://doi.org/10.1080/13547500902965120>
- Horie, O., Moortgat, G.K., 1998. Gas-Phase Ozonolysis of Alkenes. *Recent Advances in Mechanistic Investigations* †. *Accounts of Chemical Research* 31, 387–396. <https://doi.org/10.1021/ar9702740>
- Huang, Y., Chameides, W.L., Dickinson, R.E., 2007. Direct and indirect effects of anthropogenic aerosols on regional precipitation over east Asia. *Journal of Geophysical Research: Atmospheres* 112. <https://doi.org/10.1029/2006JD007114>
- Intergovernmental Panel on Climate Change (Ed.), 2014. *Clouds and Aerosols*, in: *Climate Change 2013 - The Physical Science Basis*. Cambridge University Press, Cambridge, pp. 571–658. <https://doi.org/10.1017/CBO9781107415324.016>
- IPCC, 2013. *Anthropogenic and Natural Radiative Forcing* — IPCC. URL <https://www.ipcc.ch/report/ar5/wg1/anthropogenic-and-natural-radiative-forcing/> (accessed 5.20.19).
- IPCC, I.P. on C.C., 2013. *Fifth Assessment Report (AR5) Chapter 07: Clouds and Aerosols*.
- Iribarne, J.V., Cho, H.-R., 2012. *Atmospheric Physics*. Springer Science & Business Media.
- Jain, C.D., Gadhavi, H.S., Sahu, L.K., Jayaraman, A., 2017. Volatile Organic compounds in air their importance and measurements 16.
- Johnson, D., Marston, G., 2008. The gas-phase ozonolysis of unsaturated volatile organic compounds in the troposphere. *Chemical Society Reviews* 37, 699. <https://doi.org/10.1039/b704260b>
- Jonsson, Å.M., Hallquist, M., Ljungström, E., 2008. Influence of OH Scavenger on the Water Effect on Secondary Organic Aerosol Formation from Ozonolysis of Limonene, Δ^3 -Carene, and α -Pinene. *Environ. Sci. Technol.* 42, 5938–5944. <https://doi.org/10.1021/es702508y>
- Kanakidou, M., Seinfeld, J.H., Pandis, S.N., Barnes, I., Dentener, F.J., Facchini, M.C., Dingenen, R.V., Ervens, B., Nenes, A., Nielsen, C.J., Swietlicki, E., Putaud, J.P., Balkanski, Y., Fuzzi, S., Horth, J., Moortgat, G.K., Winterhalter, R., Myhre, C.E.L., Tsigaridis, K., Vignati, E., Stephanou, E.G., Wilson, J., 2004. Organic aerosol and global climate modelling: a review. *global climate* 171.
- Kesselmeier, J., Staudt, M., 1999. *Biogenic Volatile Organic Compounds (VOC): An Overview on Emission, Physiology and Ecology* 66.
- Khalil, M.A.K., Rasmussen, R.A., 1992b. Forest Hydrocarbon Emissions: Relationships Between Fluxes and Ambient Concentrations. *Journal of the Air & Waste Management Association* 42, 810–813. <https://doi.org/10.1080/10473289.1992.10467033>
- Kim, K.-H., Kabir, E., Kabir, S., 2015. A review on the human health impact of airborne particulate matter. *Environment International* 74, 136–143. <https://doi.org/10.1016/j.envint.2014.10.005>
- Kim, Y., Platt, U., Gu, M.B., Iwahashi, H., 2009. *Atmospheric and Biological Environmental Monitoring*. Springer Science & Business Media.

- Kim, Y.J. (Ed.), 2009. Atmospheric and biological environmental monitoring. Springer, Dordrecht ; New York.
- Koppmann, R. (Ed.), 2007. Volatile organic compounds in the atmosphere, 1st ed. ed. Blackwell Pub, Oxford ; Ames, Iowa.
- Krieger, U.K., Marcolli, C., Reid, J.P., 2012. Exploring the complexity of aerosol particle properties and processes using single particle techniques. *Chem. Soc. Rev.* 41, 6631–6662. <https://doi.org/10.1039/C2CS35082C>
- Kroll, J.H., Donahue, N.M., Cee, V.J., Demerjian, K.L., Anderson, J.G., 2002. Gas-phase ozonolysis of alkenes: formation of OH from anti carbonyl oxides. *J. Am. Chem. Soc.* 124, 8518–8519. <https://doi.org/10.1021/ja0266060>
- Kroll, J.H., Seinfeld, J.H., 2008a. Chemistry of secondary organic aerosol: Formation and evolution of low-volatility organics in the atmosphere. *Atmospheric Environment* 42, 3593–3624.
- Lamb, B., Guenther, A., Gay, D., Westberg, H., 1987. A national inventory of biogenic hydrocarbon emissions. *Atmospheric Environment* (1967) 21, 1695–1705. [https://doi.org/10.1016/0004-6981\(87\)90108-9](https://doi.org/10.1016/0004-6981(87)90108-9)
- Lanz, V.A., Prévôt, A.S.H., Alfarra, M.R., Weimer, S., Mohr, C., DeCarlo, P.F., Gianini, M.F.D., Hueglin, C., Schneider, J., Favez, O., D’Anna, B., George, C., Baltensperger, U., 2010. Characterization of aerosol chemical composition with aerosol mass spectrometry in Central Europe: an overview. *Atmospheric Chemistry and Physics* 10, 10453–10471. <https://doi.org/10.5194/acp-10-10453-2010>
- Larsen, B.R., Lahaniati, M., Calogirou, A., Kotzias, D., 1998. Atmospheric oxidation products of terpenes: A new nomenclature. *Chemosphere* 37, 1207–1220. [https://doi.org/10.1016/S0045-6535\(98\)00115-5](https://doi.org/10.1016/S0045-6535(98)00115-5)
- Le Breton, M., Hallquist, Å.M., Pathak, R.K., Simpson, D., Wang, Y., Johansson, J., Zheng, J., Yang, Y., Shang, D., Wang, H., Liu, Q., Chan, C., Wang, T., Bannan, T.J., Priestley, M., Percival, C.J., Shallcross, D.E., Lu, K., Guo, S., Hu, M., Hallquist, M., 2018. Chlorine oxidation of VOCs at a semi-rural site in Beijing: significant chlorine liberation from ClNO₂; and subsequent gas- and particle-phase Cl–VOC production. *Atmospheric Chemistry and Physics* 18, 13013–13030. <https://doi.org/10.5194/acp-18-13013-2018>
- Lee, A., Goldstein, A.H., Kroll, J.H., Ng, N.L., Varutbangkul, V., Flagan, R.C., Seinfeld, J.H., 2006a. Gas-phase products and secondary aerosol yields from the photooxidation of 16 different terpenes. *Journal of Geophysical Research* 111. <https://doi.org/10.1029/2006JD007050>
- Lee, H.-H., Bar-Or, R.Z., Wang, C., 2017. Biomass burning aerosols and the low-visibility events in Southeast Asia. *Atmospheric Chemistry and Physics* 17, 965–980. <https://doi.org/10.5194/acp-17-965-2017>
- Lerdau, M., Guenther, A., Monson, R., 1997. Plant Production and Emission of Volatile Organic Compounds. *BioScience* 47, 373–383. <https://doi.org/10.2307/1313152>
- Leskinen, A., Yli-Pirilä, P., Kuuspallo, K., Sippula, O., Jalava, P., Hirvonen, M.-R., Jokiniemi, J., Virtanen, A., Komppula, M., Lehtinen, K.E.J., 2015. Characterization and testing of a new environmental chamber. *Atmospheric Measurement Techniques* 8, 2267–2278. <https://doi.org/10.5194/amt-8-2267-2015>
- Li, M., Huang, X., Li, J., Song, Y., 2012. Estimation of biogenic volatile organic compound (BVOC) emissions from the terrestrial ecosystem in China using real-time remote sensing data.

Atmospheric Chemistry and Physics Discussions 12, 6551–6592.
<https://doi.org/10.5194/acpd-12-6551-2012>

- Loreto, F., Schnitzler, J.-P., 2010. Abiotic stresses and induced BVOCs. *Trends in Plant Science*, Special Issue: Induced biogenic volatile organic compounds from plants 15, 154–166. <https://doi.org/10.1016/j.tplants.2009.12.006>
- Martinez, E., Cabanas, B., Aranda, A., Martin, P., Salgado, S., 1999. Absolute Rate Coefficients for the Gas-Phase Reactions of NO₃ Radical with a Series of Monoterpenes at T = 298 to 433 K 18.
- Mellouki, A., Wallington, T.J., Chen, J., 2015. Atmospheric Chemistry of Oxygenated Volatile Organic Compounds: Impacts on Air Quality and Climate. *Chemical Reviews* 115, 3984–4014. <https://doi.org/10.1021/cr500549n>
- Mikhailov, E., Vlasenko, S., Martin, S.T., Koop, T., Pöschl, U., 2009. Amorphous and crystalline aerosol particles interacting with water vapor: conceptual framework and experimental evidence for restructuring, phase transitions and kinetic limitations. *Atmospheric Chemistry and Physics* 9, 9491–9522. <https://doi.org/10.5194/acp-9-9491-2009>
- Molteni, U., Simon, M., Heinritzi, M., Hoyle, C.R., Bernhammer, A.-K., Bianchi, F., Breitenlechner, M., Brilke, S., Dias, A., Duplissy, J., Frege, C., Gordon, H., Heyn, C., Jokinen, T., Kürten, A., Lehtipalo, K., Makhmutov, V., Petäjä, T., Pieber, S.M., Praplan, A.P., Schobesberger, S., Steiner, G., Stozhkov, Y., Tomé, A., Tröstl, J., Wagner, A.C., Wagner, R., Williamson, C., Yan, C., Baltensperger, U., Curtius, J., Donahue, N.M., Hansel, A., Kirkby, J., Kulmala, M., Worsnop, D.R., Dommen, J., 2019. Formation of Highly Oxygenated Organic Molecules from α -Pinene Ozonolysis: Chemical Characteristics, Mechanism, and Kinetic Model Development. *ACS Earth and Space Chemistry* 3, 873–883. <https://doi.org/10.1021/acsearthspacechem.9b00035>
- Müller, J.-F., 1992. Geographical distribution and seasonal variation of surface emissions and deposition velocities of atmospheric trace gases. *Journal of Geophysical Research* 97, 3787. <https://doi.org/10.1029/91JD02757>
- Natta, L., Orpin, K., Krittika, N., Pantip, B., 2008. 12. Natta L.pdf. *International Food Research Journal*.
- Ng, N.L., Kroll, J.H., Keywood, M.D., Bahreini, R., Varutbangkul, V., Flagan, R.C., Seinfeld, J.H., Lee, A., Goldstein, A.H., 2006. Contribution of First- versus Second-Generation Products to Secondary Organic Aerosols Formed in the Oxidation of Biogenic Hydrocarbons. *Environmental Science & Technology* 40, 2283–2297. <https://doi.org/10.1021/es052269u>
- Paulson, S.E., Orlando, J.J., 1996. The reactions of ozone with alkenes: An important source of HO_x in the boundary layer. *Geophysical Research Letters* 23, 3727–3730. <https://doi.org/10.1029/96GL03477>
- Peñuelas, J., Staudt, M., 2010. BVOCs and global change. *Trends in Plant Science* 15, 133–144. <https://doi.org/10.1016/j.tplants.2009.12.005>
- Petters, Kreidenweis, S.M., 2007. A single parameter representation of hygroscopic growth and cloud condensation nucleus activity. *Atmos. Chem. Phys.* 12.
- Pichersky, E., Gershenzon, J., 2002. The formation and function of plant volatiles: perfumes for pollinator attraction and defense. *Current Opinion in Plant Biology* 5, 237–243. [https://doi.org/10.1016/S1369-5266\(02\)00251-0](https://doi.org/10.1016/S1369-5266(02)00251-0)
- Pidwirny, M., 2010. *Atmospheric Structure and Radiation Transfer*.

- Politis, M., Pilinis, C., C. PILINIS University of Aegean, Mytilene, Greece, Lekkas, T.D., 2013. Ultrafine particles (UFP) and health effects. Dangerous. Like no other PM? Review and analysis. *Global NEST Journal* 10, 439–452. <https://doi.org/10.30955/gnj.000579>
- Ramachandran, S., 2018. *Atmospheric Aerosols: Characteristics and Radiative Effects*. CRC Press.
- Reissell, A., Harry, C., Aschmann, S.M., Atkinson, R., Arey, J., 1999. Formation of acetone from the OH radical and O₃ initiated reactions of a series of monoterpenes. *Journal of Geophysical Research: Atmospheres* 104, 13869–13879. <https://doi.org/10.1029/1999JD900198>
- Rio, C., Flaud, P.-M., Loison, J.-C., Villenave, E., 2010. Experimental reevaluation of the importance of the abstraction channel in the reactions of monoterpenes with OH radicals. *Chemphyschem* 11, 3962–3970. <https://doi.org/10.1002/cphc.201000518>
- Robinson, A.L., Donahue, N.M., Shrivastava, M.K., Weitkamp, E.A., Sage, A.M., Grieshop, A.P., Lane, T.E., Pierce, J.R., Pandis, S.N., 2007. Rethinking organic aerosols: semivolatile emissions and photochemical aging. *Science* 315, 1259–1262. <https://doi.org/10.1126/science.1133061>
- Salby, M.L., 2012. *Physics of the Atmosphere and Climate*. Cambridge University Press.
- Schlager, H., Grewe, V., Roiger, A., 2012a. Chemical Composition of the Atmosphere, in: Schumann, U. (Ed.), *Atmospheric Physics*. Springer Berlin Heidelberg, Berlin, Heidelberg, pp. 17–35. https://doi.org/10.1007/978-3-642-30183-4_2
- Schrödner, R., 2015. *Aerosols in EC EARTH*.
- Schwantes, R.H., Charan, S.M., Bates, K.H., Huang, Y., Nguyen, T.B., Mai, H., Kong, W., Flagan, R.C., Seinfeld, J.H., 2019. Low-volatility compounds contribute significantly to isoprene secondary organic aerosol (SOA) under high-NO_x conditions. *Atmospheric Chemistry and Physics* 19, 7255–7278. <https://doi.org/10.5194/acp-19-7255-2019>
- Seakins, P.W., 2010. A brief review of the use of environmental chambers for gas phase studies of kinetics, chemical mechanisms and characterisation of field instruments. *EPJ Web of Conferences* 9, 143–163. <https://doi.org/10.1051/epjconf/201009012>
- Seinfeld, J.H., Pandis, S.N., 2006. *Atmospheric Chemistry and Physics: From Air Pollution to Climate Change*. 2nd Edition, John Wiley & Sons, New York.
- Seinfeld, J.H., Pankow, J.F., 2003. Organic Atmospheric Particulate Material. *Annual Review of Physical Chemistry* 54, 121–140. <https://doi.org/10.1146/annurev.physchem.54.011002.103756>
- Sharifi-Rad, J., Sharifi-Rad, Mehdi, Hoseini-Alfatemi, S.M., Iriti, M., Sharifi-Rad, Majid, Sharifi-Rad, Marzieh, 2015. Composition, Cytotoxic and Antimicrobial Activities of Satureja intermedia C.A. Mey Essential Oil. *International Journal of Molecular Sciences* 16, 17812–17825. <https://doi.org/10.3390/ijms160817812>
- Sherwood, Keith and Craig Idso, 2003. BVOCs: What Are They? ... and How Do They Function Within the Context of Global Climate Change? *CO₂ Science*.
- Shilling, J.E., Chen, Q., King, S.M., Rosenoern, T., Kroll, J.H., Worsnop, D.R., McKinney, K.A., Martin, S.T., 2008. Particle mass yield in secondary organic aerosol formed by the dark ozonolysis of α -pinene. *Atmospheric Chemistry and Physics* 8, 2073–2088. <https://doi.org/10.5194/acp-8-2073-2008>
- Slade, J.H., de Perre, C., Lee, L., Shepson, P.B., 2017. Nitrate radical oxidation of γ -terpinene: hydroxy nitrate, total organic nitrate, and secondary organic aerosol yields. *Atmospheric Chemistry and Physics* 17, 8635–8650. <https://doi.org/10.5194/acp-17-8635-2017>

- Stone, D., Whalley, L.K., Heard, D.E., 2012. Tropospheric OH and HO₂ radicals: field measurements and model comparisons. *Chemical Society Reviews* 41, 6348. <https://doi.org/10.1039/c2cs35140d>
- Tanaka, P.L., Riemer, D.D., Chang, S., Yarwood, G., McDonald-Buller, E.C., Apel, E.C., Orlando, J.J., Silva, P.J., Jimenez, J.L., Canagaratna, M.R., Neece, J.D., Mullins, C.B., Allen, D.T., 2003. Direct evidence for chlorine-enhanced urban ozone formation in Houston, Texas. *4TMOS. ENVIRON.* 37, 1393–1400. [https://doi.org/10.1016/S1352-2310\(02\)01007-5](https://doi.org/10.1016/S1352-2310(02)01007-5)
- Thompson, A.M., 1992. The Oxidizing Capacity of the Earth's Atmosphere: Probable Past and Future Changes. *Science, New Series* 256, 1157–1165.
- Tomasi, C., Lupi, A., 2016. Primary and Secondary Sources of Atmospheric Aerosol, in: Tomasi, C., Fuzzi, S., Kokhanovsky, A. (Eds.), *Atmospheric Aerosols*. Wiley-VCH Verlag GmbH & Co. KGaA, Weinheim, Germany, pp. 1–86. <https://doi.org/10.1002/9783527336449.ch1>
- Tritscher, T., Dommen, J., DeCarlo, P.F., Gysel, M., Barmet, P.B., Praplan, A.P., Weingartner, E., Prévôt, A.S.H., Riipinen, I., Donahue, N.M., Baltensperger, U., 2011. Volatility and hygroscopicity of aging secondary organic aerosol in a smog chamber. *Atmospheric Chemistry and Physics* 11, 11477–11496. <https://doi.org/10.5194/acp-11-11477-2011>
- Tsigaridis, K., Kanakidou, M., 2007. Secondary organic aerosol importance in the future atmosphere. *Atmospheric Environment* 41, 4682–4692.
- US Department of Commerce, N., n.d. NWS JetStream - Layers of the Atmosphere [WWW Document]. URL <https://www.weather.gov/jetstream/layers> (accessed 5.3.19).
- US EPA, 2016. Climate Change Indicators: Climate Forcing [WWW Document]. US EPA. URL <https://www.epa.gov/climate-indicators/climate-change-indicators-climate-forcing> (accessed 5.22.19).
- US EPA, O., 2019. What is the definition of VOC? [WWW Document]. US EPA. URL <https://www.epa.gov/air-emissions-inventories/what-definition-voc> (accessed 7.21.19).
- Varutbangkul, V., Brechtel, F.J., Bahreini, R., Ng, N.L., Keywood, M.D., Kroll, J.H., Flagan, R.C., Seinfeld, J.H., Lee, A., Goldstein, A.H., 2006. Hygroscopicity of secondary organic aerosols formed by oxidation of cycloalkenes, monoterpenes, sesquiterpenes, and related compounds. *Atmos. Chem. Phys.* 22.
- Volkamer, R., Jimenez, J.L., San Martini, F., Dzepina, K., Zhang, Q., Salcedo, D., Molina, L.T., Worsnop, D.R., Molina, M.J., 2006. Secondary organic aerosol formation from anthropogenic air pollution: Rapid and higher than expected. *Geophysical Research Letters* 33. <https://doi.org/10.1029/2006GL026899>
- Wang, J., Doussin, J.F., Perrier, S., Perraudin, E., Katrib, Y., Pangui, E., Picquet-Varrault, B., 2011. Design of a new multi-phase experimental simulation chamber for atmospheric photosmog, aerosol and cloud chemistry research. *Atmospheric Measurement Techniques* 4, 2465–2494. <https://doi.org/10.5194/amt-4-2465-2011>
- Wang, X., Liu, T., Bernard, F., Ding, X., Wen, S., Zhang, Y., Zhang, Z., He, Q., Lü, S., Chen, J., Saunders, S., Yu, J., 2014. Design and characterization of a smog chamber for studying gas-phase chemical mechanisms and aerosol formation. *Atmospheric Measurement Techniques* 7, 301–313. <https://doi.org/10.5194/amt-7-301-2014>
- Warneck, P., 1999. *Chemistry of the Natural Atmosphere*. Elsevier.
- Waza, A.A., 2014. Effect of Green Leaf Volatiles (GLVs) on secondary organic aerosol formation.

- Went, F.W., 1960. Organic matter in the atmosphere, and its possible relation to petroleum formation. *Proc Natl Acad Sci U S A* 46, 212–221.
- WHO, 2006. WHO Air quality guidelines for particulate matter, ozone, nitrogen dioxide and sulfur dioxide.
- Wikipedia, 2013. 2013 Southeast Asian haze. Wikipedia.
- Winkler-Heil, R., Ferron, G., Hofmann, W., 2014. Calculation of hygroscopic particle deposition in the human lung. *Inhal Toxicol* 26, 193–206. <https://doi.org/10.3109/08958378.2013.876468>
- Witter, M., Berndt, T., Böge, O., Stratmann, F., Heintzenberg, J., 2002. Gas-phase ozonolysis: Rate coefficients for a series of terpenes and rate coefficients and OH yields for 2-methyl-2-butene and 2,3-dimethyl-2-butene: Gas-Phase Ozonolysis. *International Journal of Chemical Kinetics* 34, 394–403. <https://doi.org/10.1002/kin.10063>
- Yu, S., Mathur, R., Schere, K., Kang, D., Pleim, J., Otte, T.L., 2007. A detailed evaluation of the Eta-CMAQ forecast model performance for O₃, its related precursors, and meteorological parameters during the 2004 ICARTT study. *Journal of Geophysical Research* 112. <https://doi.org/10.1029/2006JD007715>
- Yu, S., Mathur, R., Schere, K., Kang, D., Pleim, J., Young, J., Tong, D., Pouliot, G., McKeen, S.A., Rao, S.T., 2008. Evaluation of real-time PM_{2.5} forecasts and process analysis for PM_{2.5} formation over the eastern United States using the Eta-CMAQ forecast model during the 2004 ICARTT study. *Journal of Geophysical Research: Atmospheres* 113. <https://doi.org/10.1029/2007JD009226>
- Yu, X., Ma, J., An, J., Yuan, L., Zhu, B., Liu, D., Wang, J., Yang, Y., Cui, H., 2016. Impacts of meteorological condition and aerosol chemical compositions on visibility impairment in Nanjing, China. *Journal of Cleaner Production* 131, 112–120. <https://doi.org/10.1016/j.jclepro.2016.05.067>
- Zhang, D., Zhang, R., 2005. Ozonolysis of α -pinene and β -pinene: Kinetics and mechanism. *J. Chem. Phys.* 13.
- Zhang, X., Chen, Z., Wang, H., He, S., Huang, D., 2009. An important pathway for ozonolysis of alpha-pinene and beta-pinene in aqueous phase and its atmospheric implications. *Atmospheric Environment* 43, 4465–4471. <https://doi.org/10.1016/j.atmosenv.2009.06.028>
- Ziemann, P.J., Atkinson, R., 2012. Kinetics, products, and mechanisms of secondary organic aerosol formation. *Chemical Society Reviews* 41, 6582. <https://doi.org/10.1039/c2cs35122f>

Chapter II

“Introduction to *CHARME* chamber”

II.1 CHARME chamber

Following the need of having a valuable scientific tool that can simulate the different atmospheric processes and contribute to a better understanding of the atmosphere, the idea of developing a new atmospheric simulation chamber was born out in 2010. The Laboratoire de Physico-Chimie de l'Atmosphère (LPCA), Dunkerque – France, was the owner of this scientific project and since 2016 the new chamber, has been developed and hosted, in the first floor of IREnE (Innovation Recherche en Environnement) building as seen in [Figure II.1](#).



Figure II.1: The project of *CHARME* is finally realized! The chamber is installed in LPCA (IREnE Building).

CHARME presented in [Figure II.2](#) is the acronym for ‘*Chamber for the study of the Atmospheric Reactivity and the Metrology of the Environment*’. It aims to be a scientific platform for national and international research work in the field of atmospheric physical chemist



Figure II.2: Photo of *CHARME* chamber at the outset of installation in IREnE building.

II.1.1 Enclosure

CHARME is an indoor evacuable reactor with a cylindrical shape and linear horizontal structure. It is made up of a chemically inert material, stainless steel type 304L. The detailed description of the enclosure is presented below.

I.1.1.1 Dimensions

The chamber has a volume of 9.2 m³. This relatively large volume for an indoor chamber, allows the performance of experiments with low concentrations (few ppb) and with long durations (few hours).

Moreover, *CHARME* has an internal surface of 30 - 32 m² area and a surface to volume ratio (S/V) of ~ 3.5 m⁻¹ which can minimize the wall effects (wall losses of particles and gas-phase species and heterogeneous reaction with the walls). The chamber is 4.4 m long, with an internal diameter of around 1.68 m and an average weight of 5850 kg.

I.1.1.2 Walls

CHARME is made up of a double layer wall, which allows the circulation of either hot or cold thermal fluids and thus the variation of temperature between -20° C and +50° C. The operation of the chamber at temperatures other than ambient is not fully realized, but it is planned for the near future.

The rigid walls with a thickness varying from 4 to 40 mm permit the reactor to guarantee vacuum and non-deformation of the flanges. Consequently, *CHARME* is considered as vacuum compatible, and it is capable to support most of the mechanical constraints when it is under vacuum. The range of pressure under which it can operate is: 0.05 mbar < P < 1000 mbar (detailed in part [III.1](#)).

The inner surface of the reactor is mechanically polished in addition to an electrochemical treatment, which enhances the light reflectivity and also reduces the interaction of gases and particles with the walls.

I.1.1.3 Ports

As shown in **Figure II.3**, the chamber has 9 different ports which are used for various tasks.

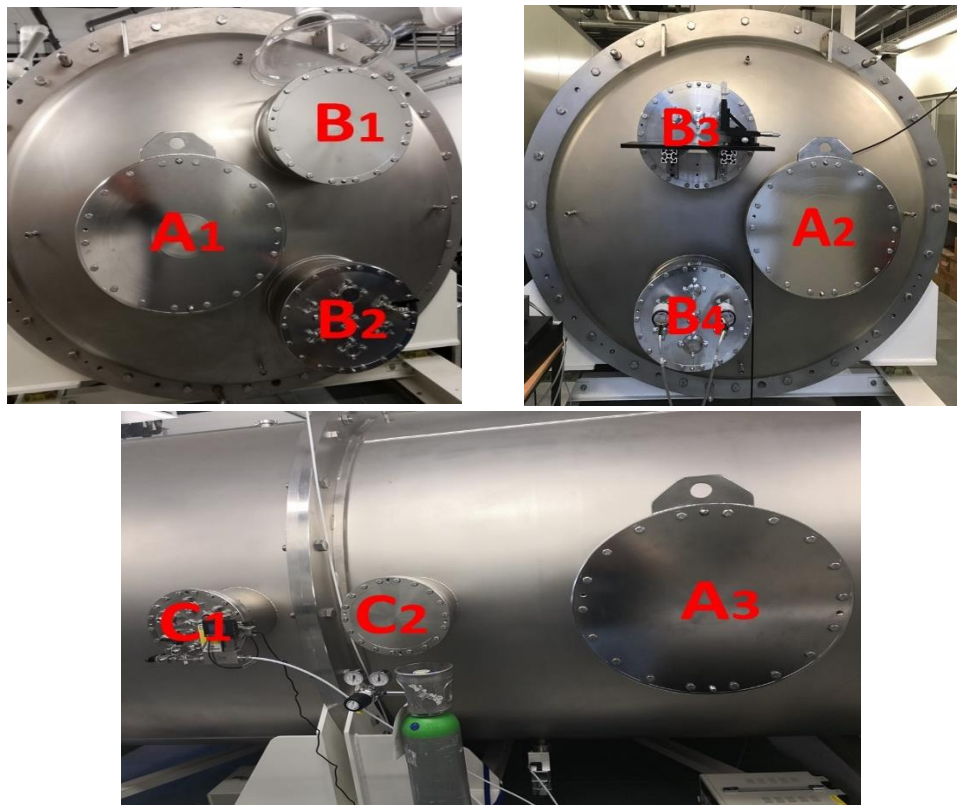


Figure II.3: The 9 different ports of *CHARME*. Ports with letter (A) correspond to DN 450, (B) to DN 350 and (C) to DN 200.

- 3 DN 450 of 45 cm diameter (letter A); two of these ports are located at the opposite ends of the chamber and are planned for a multipath- cell able to work over a very broad band of frequency (Chernin cell). The third port is placed at the longitudinal side of the reactor and used to provide physical access to the inside of the chamber.
- 4 DN 350 of 35 cm diameter (letter B); they are placed at the two peripheries and used to sample gases and particles. An IBBCEAS (Incoherent Broad Band Cavity Enhanced Absorption Spectroscopy) instrument for in-situ monitoring of NO_3 and NO_2 is installed on two facing ports. Others places are also planned to connect other IBBCEAS instruments (for gas and aerosols).

- 2 ports DN 200 of 20 cm diameter (letter C); they are positioned in the middle of the longitudinal side and are utilized to introduce gases and/or particles.

The flanges have several openings of different diameters to provide connections with a large panel of analytical instruments dedicated to gas and particulate measurements and other setups devoted for monitoring the physical parameters (temperature, relative humidity, pressure) of the chamber.

The connections between the instruments and the ports is realized by short stainless steel or teflon FEP (Fluorinated Ethylene Propylene) lines to ensure a minimum residence time (in the order of seconds) of gas and aerosols during the sampling step.

I.1.1.4 Windows

Four quartz windows shown in [Figure II.4](#), permit the introduction of radiation into the chamber. The windows located on the longitudinal side of the chamber, have diameters of 25 and thickness of 24 mm. Quartz allows transmission of the spectrum between 230 and 3600 nm and resists the vacuum with minimal leakage rate and without causing any deformation or breakage to the chamber.

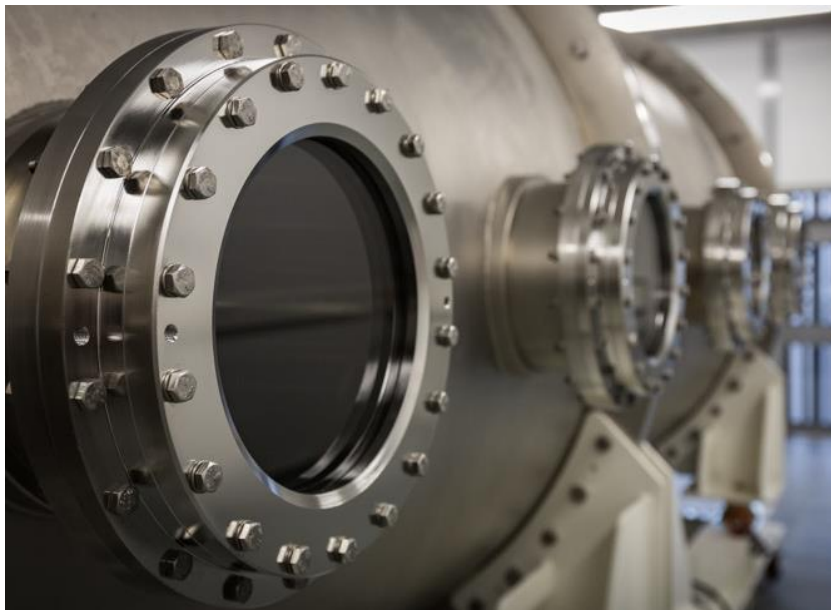


Figure II.4: The quartz windows of *CHARME*

I.1.1.5 Support

The chamber is placed on a white cradle made up of steel type S235 and S27 equipped with 8 anti-vibration supports that isolate the chamber from any perturbations coming from the ground level and the pumping system. This system has been anticipated for the future multipath cell that will equip *CHARME*.

II.1.2 Mixing system

For good homogeneity and sufficient mixing of gas species and particles, four two-blade stainless steel fans having a diameter of 50 cm are installed at the bottom of the chamber as shown in **Figure II.5**. The rotating speed of the fans can be monitored by a magnetic torque motor placed outside the chamber to avoid contaminations by oil or mechanical grease. It can be varied as a function of the input power supply with a maximum of 330 rpm for each fan.

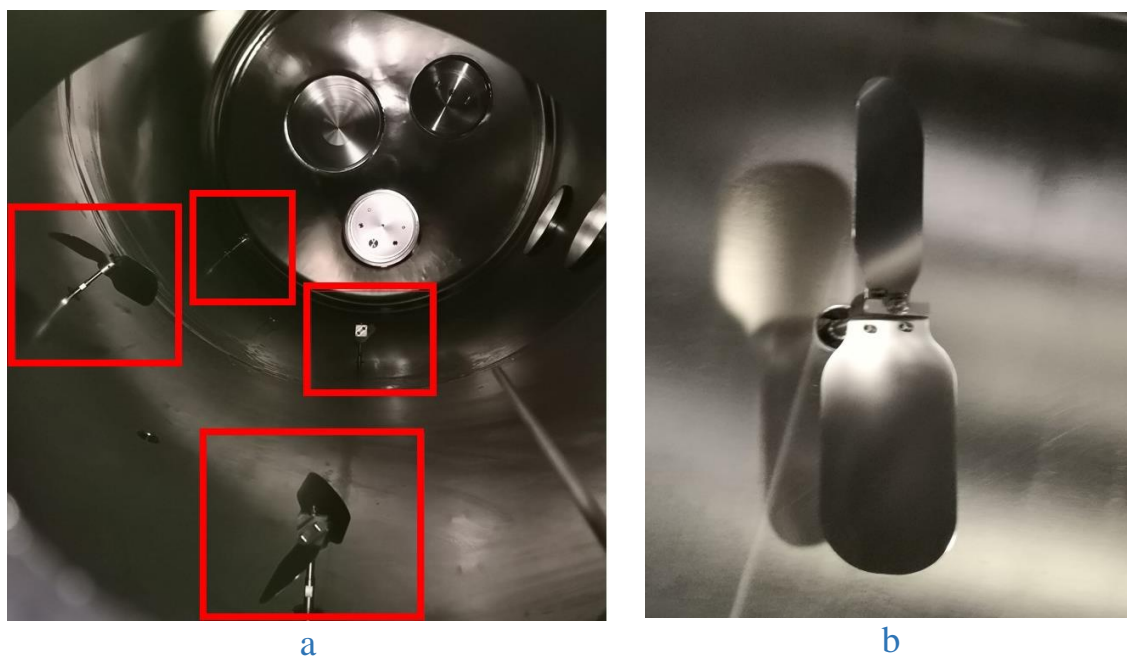


Figure II.5: The four mixing fans installed at different positions inside *CHARME* (a). One of the two-wing stainless steel fans (b).

II.1.3 Pumping and filling system

To evacuate the chamber, *CHARME* is coupled to a pumping system (Cobra NC0100-0300B) (Figure II.6-d). The unit consists of a dry screw vacuum pump that operates without lubrication and thus prevents any low vapor pressure hydrocarbons originating from it to backflush into the evacuated chamber. This pump with a speed of 110 m³/h allows to reach good vacuum limits ($P < 0.3$ mbar).



Figure II.6: (a) & (b) represent the pumping and filling valves and lines, (c) is the pure air generator and (d) is the pump coupled to *CHARME*.

Purified air produced by a compressor (SLM-S 7,5- RENNER SCROLLline) and a clean/dry air generator (Parker Zander KA-MT 1-8; flow rate (1880 L.min⁻¹) and dew-point below (-30°C)), is used to fill *CHARME* to atmospheric pressure (Figure II.6).

II.1.4 Irradiation

Light is provided by four (5 kW) Xenon high pressure arc lamps (SKY TRACER 5000) that irradiate the chamber through four quartz windows. As displayed in [Figure II.7](#), the lamps are placed on the longitudinal size of the chamber at ~70 cm away from the windows. The height of the projectors was regulated and maintained at 2.2 m from the ground to directly face the windows. It was important to have wide projected spots of light in order to minimize the concentrated warming effect on one point in the enclosure, with a maximum intensity. Thus, the focal point of the lamps was adjusted to obtain convergent or divergent beams and eventually to have homogeneous radiation with the largest possible luminous intensity.



[Figure II.7](#): The light projectors (SKY TRACER 5000) that irradiate *CHARME*.

As shown in [Figure II.8](#), the lamps were hosted inside a ventilated room. The air-conditioning, allows to limit the temperature increase due to the lamp heating within the room and in the laboratory as well. In addition, it also protects the users from the radiation.



Figure II.8: Front (a) and back (b) photos for the room hosting the light projectors.

II.1.5 Analytical instruments coupled to *CHARME*

CHARME is connected to a large panel of instruments for monitoring physical parameters and measuring gases and particles inside the chamber. The specific instruments and their related measured parameters are presented in [Table II.3](#). A brief description of each instrument is presented below.

II.1.5.1 Temperature & Humidity Monitoring

To monitor the changes in temperature and relative humidity (RH) inside *CHARME*, a special sensor (Vaisala HMT330 Series HUMICAP) is coupled to the chamber (see [Figure II.9](#)). The probe of the sensor is introduced into *CHARME* and not removed after the end of each experiment because it is ideally designed for measurement at a wide range of pressure ($0 \text{ bar} < P < 40 \text{ bar}$). The measurement range of the RH is 0 to 100 % with an accuracy of $\pm 1\%$ (for $\text{RH} < 90\%$) and $\pm 1.7\%$ (for $90\% < \text{RH} < 100\%$). The temperature interval is -70°C to $+180^\circ\text{C}$ with an accuracy of $\pm 0.2^\circ\text{C}$. In addition, another sensor (Sensirion EK-H5–Sensor SHT75) consisting of a USB

stick, single sensor cable and connector (see **Figure II.9**) is used in some experiments to follow the T & RH in the room housing the xenon lamps.



Figure II.9: The sensors (a) (Vaisala HMT330 Series HUMICAP), (b) (Sensirion EK-H5 - SensorSHT75), used to measure temperature and relative humidity in *CHARME*.

II.1.5.2 Pressure Monitoring

The pressure is continuously monitored in *CHARME* by a pressure controller with two Baratron capacitance manometers (MKS 226C) as seen in **Figure II.10 (a)**, one measures the pressure below 1 mbar while the other records the pressure up to 1000 mbar. The reading accuracy of the manometers is 0.25%. Throughout the experiments, the sampling of different instruments leads to the pressure decrease in the chamber. This decline is constantly compensated by a pressure compensator (Bronkhorst model P-602C Electronic Pressure Controllers) which is designed to accurately measure and control the input pressure of fluid (clean air or N_2) to have a desired output value in the chamber (**Figure II.10 (b)**).

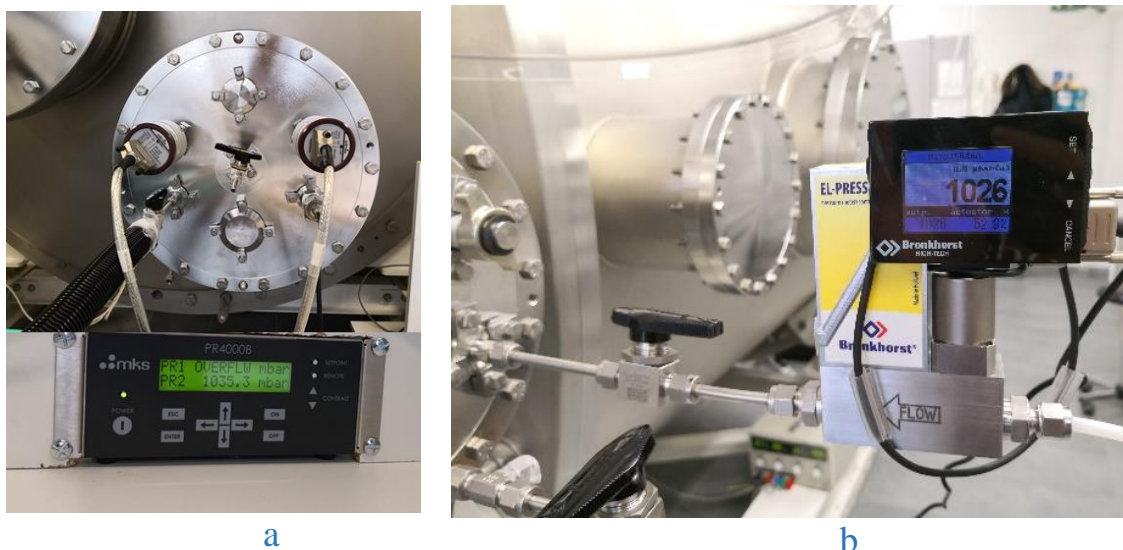


Figure II.10: The (a) pressure controller with two Baratron capacitance manometers and the (b) compensator connected to *CHARME* for monitoring its pressure.

II.1.5.3 Spectroradiometer

To characterize the spectral distribution of the irradiation source in the simulation chamber, a spectroradiometer (Ultra-fast CCD-Detector Spectrometer, Metcon) is used (**Figure II.11**). This device operates in a spectral range between 290 and 660 nm, with a spectral resolution (FWHM) lower than 1.8 nm. This device can determine the following photolysis rates constants: $j(\text{O}^1\text{D})$, $j(\text{CHO})$, $j(\text{NO}_2)$, $j(\text{HONO})$ and $j(\text{NO}_3)$ in real-time.



Figure II.11: The spectroradiometer (Metcon) used with *CHARME*.

II.1.5.4 O₃ generator and analyzer

Ozone is produced by a generator (Air Tree Ozone Technology C-L010-DTI) from zero air or pure dioxygen exposed to a corona discharge which converts O₂ into O₃. The ozone level is adjusted by changing the injection time or the flow rate of zero air or oxygen within the generator ($Q_{\max} = 5 \text{ L/min}$). In this regard, different calibrations were made regularly to check the compatibility between the different injection times and the desired ozone concentration in the chamber. Furthermore, the ozone concentration in the chamber is continuously monitored by a photometric ozone analyzer (Thermo Scientific 49i; $\lambda = 254 \text{ nm}$). Its sampling flow rate is $1.5 \text{ L}\cdot\text{min}^{-1}$ and the detection limit is 1 ppb.

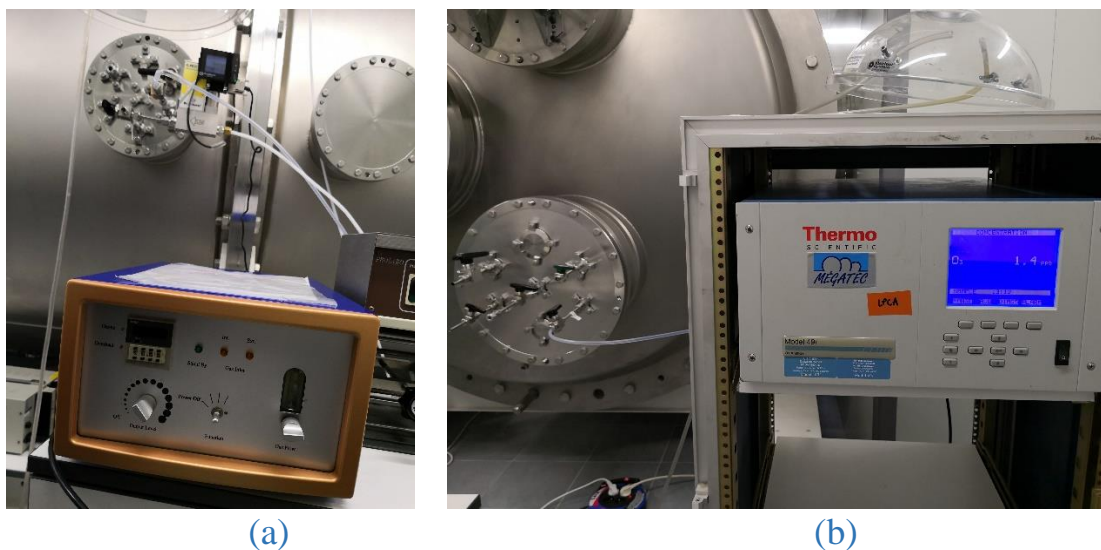


Figure II.12: Ozone generator (a) and analyzer (b) utilized for monitoring O₃ in CHARME.

II.1.5.5 NO_x analyzer

To monitor the NO_x (NO₂ + NO) concentration, CHARME is coupled to a chemiluminescence analyzer (Thermo Scientific 42i) presented in Figure II.13. The principle of this instrument is based on the reaction of NO with O₃ to produce excited NO₂. The latter molecules become de-energized and emit infrared light which is detected by a photomultiplier. The intensity of the luminescence is proportional to the concentration of NO. To measure NO₂, a Molybdenum catalyst (heated at 325 °C), is used to transform NO₂ into NO. The NO₂ mixing ratio is deduced

from the difference between the sum of the concentrations of NO₂ and NO and that of NO. The sampling flow is 0.8 L.min⁻¹.



Figure II.13: NO_x analyzer (chemiluminescence; Thermo Scientific 42i) coupled to CHARME.

II.1.5.6 PTR-TOF-MS

Proton-transfer reaction mass spectrometry (PTR-MS) is a technique developed by Professor Werner Lindinger and co-workers at the University of Innsbruck in Austria and was first introduced in the mid-1990s (**Lindinger et al., 1998**). This analytical technique has been developed for the online monitoring of volatile organic compounds (VOCs) in the atmosphere. In the PTR-MS, the sampled air is continuously pumped through a drift tube, and the VOCs are softly ionized through a proton-transfer reaction with hydronium ions (H₃O⁺) (R. II.1) which are produced from H₂O by an ion source (**de Gouw and Warneke, 2007**).



This reaction occurs for compounds having a proton affinity (PA) which is higher than that of water (i.e. 697 kJ/mol). The detection is performed at the mass corresponding to the molar mass of the species plus one (if there is no fragmentation) (**Blake et al., 2009**).

At the end of the drift tube, the ions enter a time-of-flight mass spectrometer where they are separated according to their mass to charge ratio (m/z).

The main advantages of this technique are:

- ✓ Samples do not need to be prepared and do not require special treatment, for instance, air containing VOC can be analyzed directly.
- ✓ It is a soft ionization method, that is, it generally does not lead to fragmentation of the product ions.
- ✓ H_3O^+ does not react with any major component in air (N_2 , O_2 , Ar, CO_2 , etc.) due to their proton affinity which is lower than that of H_2O , thus the air itself acts as a buffer gas and offers a soft ionization for most of the atmospheric VOCs.
- ✓ Real-time measurements for numerous VOCs, with a high sensitivity (10 –100 pptv) and rapid response time (1–10 sec).
- ✓ However, the major drawbacks are:
 - ✓ Determination of the mass of the compounds, without a clear indication of the identity.
 - ✓ Isomeric compounds cannot be distinguished.

For the online monitoring of trace gases, *CHARME* is coupled to a proton-transfer-reaction time-of flight mass spectrometer (PTR-TOF-MS, IONICON 1000) as displayed in **Figure II.14**. Within this PTR-TOF-MS (referred to as PTR throughout the thesis), the analyte is sampled by an inlet capillary line of 100 cm heated at 60°C and then ionized in the drift tube which operates at 2.2 mbar and 60°C, with a drift tube field of 600 V.cm^{-1} ($E/N=136 \text{ Td}$). After the ions are moved to the analyzing system (TOF-MS) where the mass-to-charge (m/z) ratio is determined via a time of flight measurement. The sampling flow is 50 ml.min^{-1} and the continuous VOC quantification is recorded every 10 s.

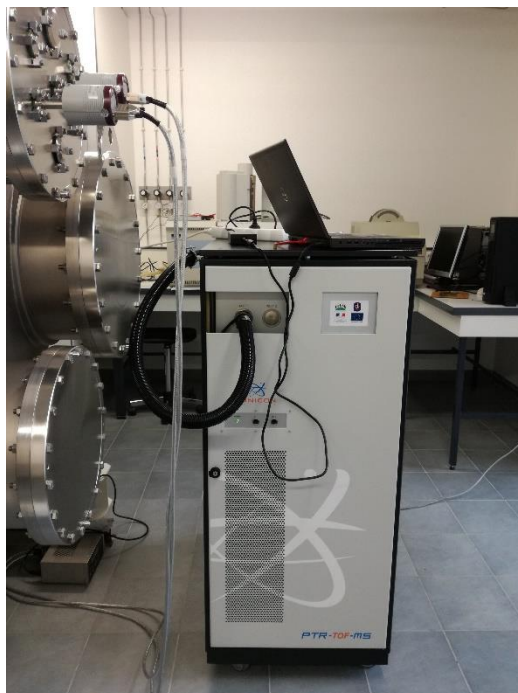


Figure II.14: The PTR-TOF-MS (IONICON 1000), used for online measurement of gaseous concentrations.

Most of the VOCs used during the experiments were calibrated by the PTR through injecting known volumes into the chamber and following their signals. However, for some chemical products which are not available commercially, their concentrations in (ppb) were estimated with the following equation:

$$\text{Eq. II. 1} \quad [R] = \frac{[RH^+]}{[H_3O^+]_0 k t}$$

where $[R]$ is the unknown concentration of the compound of interest, $[RH^+]$ the signal of the protonated compound, $[H_3O^+]$ the primary ion signal, and t the reaction time in the drift tube. Because the proton transfer reaction rate constants are not known for all compounds, an estimated generic H_3O^+ rate constant (k) of $2 \times 10^{-9} \text{ cm}^3 \text{ molecule}^{-1} \text{ s}^{-1}$ was used for those compounds whose experimental or theoretical data do not exist. The rate constants for the proton transfer reaction of most compounds are generally within $\pm 20\%$ of the estimated k .

II.1.5.7 GC-MS/FID

Off-line analysis of VOCs sampled in *CHARME* are performed with the coupling Thermodesorber (ATD - 400, Perkin Elmer) – Gas Chromatograph (GC, Autosystem XL) – Flame Ionization Detector (FID)/ Mass Spectrometer (MS) (Turbomass), Perkin Elmer. The organic compounds are sampled on Tenax TA tubes at $Q=100$ ml/min for 10 - 30 minutes. They are then thermally desorbed in the ATD for 15 minutes at 300°C under a stream of helium and cryofocused in a trap cooled to -30°C . The trap is afterwards heated within a few seconds to 300 K (flash heating) which allows a fast injection of the VOC into the chromatographic column (Restek Rxi-5Sil MS column: $30\text{ m} \times 250\ \mu\text{m} \times 1\ \mu\text{m}$). Separation of compounds was achieved through the following temperature program: 5 min isotherm at 50°C ; $5^{\circ}\text{C min}^{-1}$ to 110°C ; $45^{\circ}\text{C min}^{-1}$ to 250°C and hold at 250°C for 5 min (total programming of 25.1 min). The quantitative and qualitative analyses are realized through FID and MS, respectively. The data obtained in GC-MS was recorded in TIC (Total Ion Count) mode, with an acquisition of the masses between 33 and 500 amu (atomic mass units). The acceleration voltage used is 70 eV which allows a comparison of the detected compounds with those in the NIST library (the National Institute of Standards and Technology, 2005).

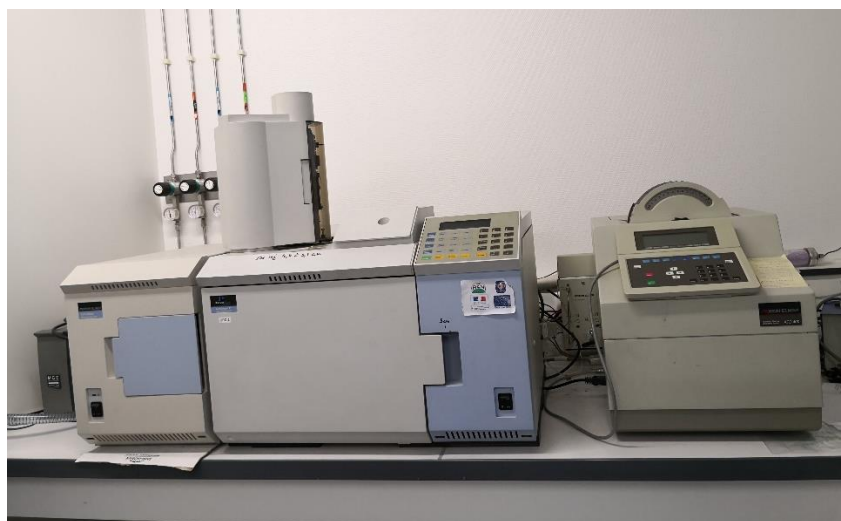


Figure II.15: The analytical system consisting of a Thermodesorber (ATD - 400, Perkin Elmer) – Gas Chromatograph (GC, Autosystem XL) – Flame Ionization Detector (FID)/ Mass Spectrometer (MS) (Turbomass), Perkin Elmer, and dedicated for VOC quantification and identification.

II.1.5.8 SMPS

A Scanning Mobility Particler Sizer (SMPS) consisting of a Differential Mobility Analyzer (Model 3081 Long DMA, TSI Inc.) and a Condensation Particle Counter (CPC Model 3775, TSI Inc.) was used to measure the number and size distribution of particles.

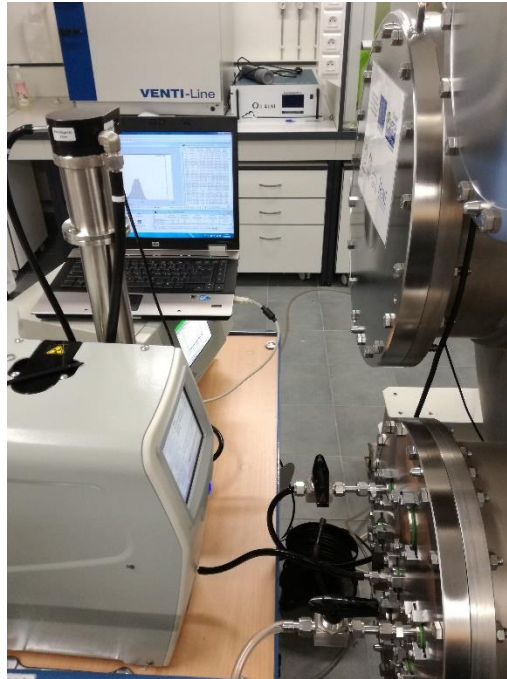


Figure II.16: The SMPS (Model 3081, TSI Inc.) and the (CPC Model 3775, TSI Inc.), coupled to *CHARME*.

The SMPS is based on the principle of the mobility of a charged particle in an electric field. The generated particles are sampled from the chamber by a short (21 cm) conductive silicon sampling line to reduce electrostatic losses. They enter, through an impactor, into the electrostatic classifier where they are neutralized with a radioactive source. Afterwards, particles with the sheath air, are introduced into the DMA which consists of two concentrically metal electrodes with the central rod being negatively charged while the outer one is electrically grounded. Due to the created electric field and according to their electrical mobility, particles drift down the annular space between the electrodes with a stable flow (to avoid uncertainties in the particle number concentration and sizing). Consequently, positively charged particles move across the sheath flow towards the central rod and then exit into the CPC, negatively charged ones are repelled to the wall and uncharged particles exit the DMA with excess air through the exhaust flow (**Wiedensohler et al., 2012**). In the particle counter, heterogeneous butanol vapor condensation takes place to grow

particles into droplets with optically detectable size. The CPC counts the number of particles to provide a particle concentration value that is displayed as the number of particles detected per cubic centimeter ($\#/cm^3$) of sampled air.

Throughout the experiments, the DMA was operated with aerosol and sheath flows of 0.3 and 3.0 liter per minute, respectively. Aerosol number concentration, size distribution, and mass concentration are sampled over a range of 20 to 680 nm mobility diameter for every 120 s. Based on the assumption that the particles are spherical, the ‘Aerosol Instrument Manager® Software for Scanning Mobility Particle Sizer™ (SMPS™) Spectrometer’, provides the volume concentration (in nm^3/cm^3) or in mass concentration ($\mu g\ m^{-3}$) if the aerosol density is assumed or known. All aerosol growth data are corrected for wall loss as described in section [III.7.3](#).

II.1.6 Other instruments

Some experiments performed in *CHARME*, necessitate the use of different instruments for analysis of samples in the gaseous and particulate phases. Such instrumentations are not permanently coupled to *CHARME*, however it possible to perform the analysis through collaboration with different teams in our laboratory or even with other laboratories.

II.1.6.1 HTDMA

A Hygroscopicity Tandem Differential Mobility Analyzer (HTDMA) instrument custom-made at the Institute of Chemical Process Fundamentals in the Czech Academy of Sciences-Czech Republic has been coupled to *CHARME* to perform investigations on the hygroscopicity of particles.

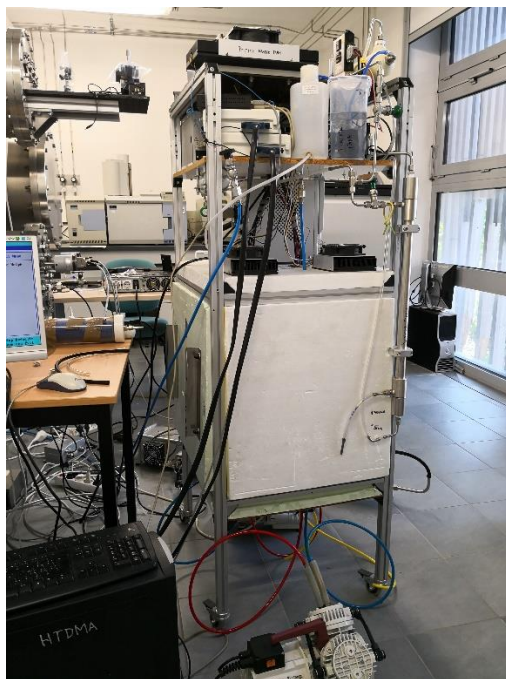


Figure II.17: The homemade HTDMA used for hygroscopicity investigation in CHARME.

The experimental setup of the HTDMA is presented in [Figure II.17](#). The particles sampled from the chamber, are dried to $RH < 4\%$ by a silica gel diffuser dryer coupled to a Nafion gas dryer (Perma Pure Inc., USA). The dry polydisperse particles are neutralized by a soft-X-Ray neutralizer and then passed through the first differential mobility analyzer (DMA1; custom-built Vienna-type). The dry diameter ($50 \pm 2 \text{ nm} < D_{\text{dry}} < 180 \pm 2 \text{ nm}$) selected by DMA1 is gradually increased with time according to the evolution of number size-distribution during SOA formation experiments. The dry particles of well-defined size are then exposed to a given RH (from 20 to $\sim 93\%$) in the humidification section consisting of a nafion membrane tube (Perma Pure Inc., USA) with a residence time of $\sim 10 \text{ s}$ (assumed to be sufficient for the particles to reach their equilibrium growth water uptake). The particle number size-distribution (40 – 350 nm) of the resulting wet particles was measured by the second custom-built Vienna-type DMA (DMA2) connected to a CPC (TSI model 3022A, USA) to measure particles. The DMAs are placed in temperature-controlled boxes, at 25°C for DMA and 23°C for DMA2; they are operated at 12:1 and 13:1 sheath-to-aerosol flow ratio, respectively. The relative humidity of the aerosol and sheath flows are measured using ROTRONIC HygroClip 2 sensors (HC2 – SH) with an uncertainty of $\pm 1.5\%$ at 90% – 93% RH. The raw data are then treated using the software TDMAinv developed by (Gysel et al., 2009). To

check the performance of the HTDMA, salt scans using ammonium sulfate particles (AS; 100 nm) were done regularly.

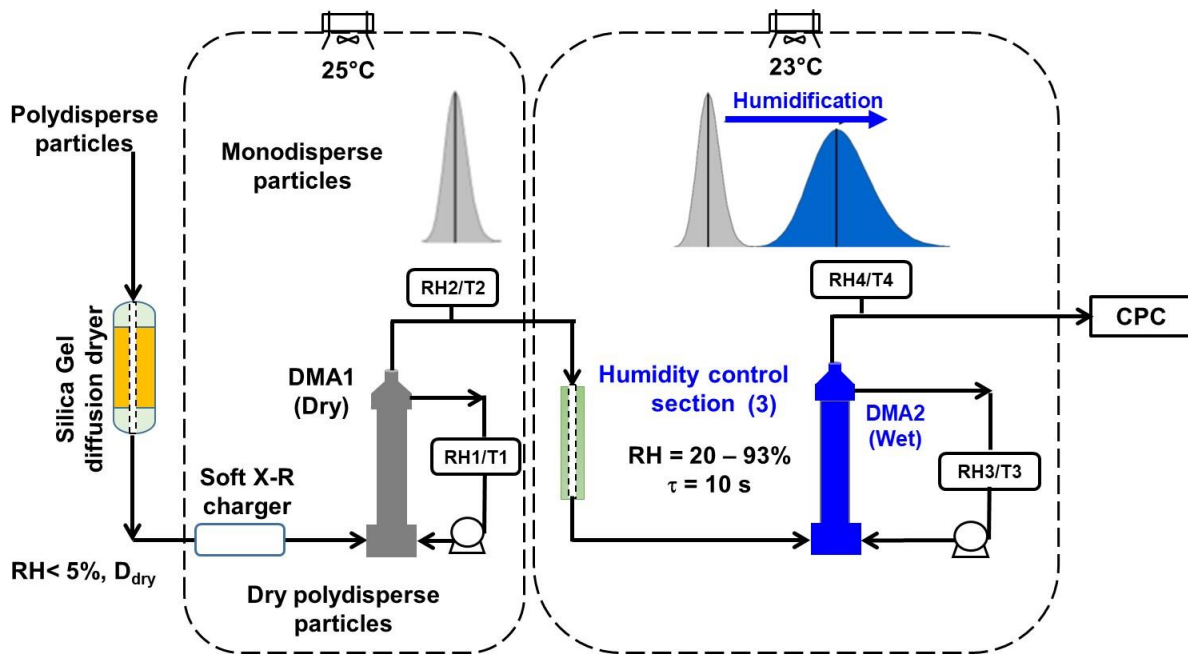


Figure II.18: Schematic set-up of the Hygroscopicity Tandem Differential Mobility Analyzer (HTDMA).

II.1.6.2 CCN counter

A Cloud Condensation Nuclei counter (CCNc, DMT-100 Droplet measurement Technologies, USA) from the PC2A laboratory (Lille University, France) was used to characterize the CCN activity in *CHARME* (see [Figure II.19](#)). The CCNc is a continuous-flow, thermal-gradient diffusion instrument that measures the count and size of individual aerosol particles which can act as cloud condensation nuclei and form cloud droplets. The CCN draws an aerosol sample into a column, where a thermodynamically unstable, supersaturated water vapor condition is created. Then, and because of the low concentration and molar mass of water vapor with respect to air, water vapor diffuses from the warm, wet column walls toward the centerline at a faster rate than the heat. After, the temperature of the column's wall gradually increases to create well-controlled and quasi-uniform centerline super-saturation. Seeking equilibrium, the supersaturated water vapor condenses on the cloud condensation nuclei in the sample air and form droplets, similar to atmospheric cloud droplets.

The instrument operates at supersaturations between 0.1% and 2%, which represents the supersaturations of different cloud types in the atmosphere. The flow rate of the CCN is 0.5 L min^{-1} with sheath-to-aerosol rate of 10 and the residence time in the column is around 18 s. Calibration of the supersaturation (SS (%)) in the CCNc was achieved using measurements of dry ammonium sulfate particles.



Figure II.19: The CCNc (DMT-100 Droplet measurement Technologies, USA) used to evaluate the CCN activity of particles in *CHARME*.

II.1.6.3 High performance liquid chromatograph (HPLC)

HPLC was used to measure the concentration of low molecular mass carbonyl compounds like formaldehyde and acetaldehyde. Samples have been collected from *CHARME* using DNPH cartridges (2,4-dinitrophenylhydrazine) which were connected to the reactor with a Teflon line. Each cartridge was sampled with a flow of 100 ml min^{-1} during 10 minutes. The DNPH cartridges were then eluted with acetonitrile (3 ml), and the solution was injected to the C18 column followed by a UV detection (at 360 nm).

II.1.6.4 Cryo-TSEM-EDX

To examine the morphology and the physical state of SOA formed in some experiments in *CHARME*, analysis by Scanning Electron Microscopy (SEM) was required. The sample analysis was performed using a field effect gun-SEM coupled with a transmitted electron detector (JEOL 7100F FEG-TSEM), equipped with three Energy Dispersive X-ray (EDS, Bruker X Flash 6/30) spectrometers and a Quorum PP3010P cryostage. Data and pictures were acquired at 15 kV, 300 pA, 10 mm for the working distance and at a temperature of 100°C.

II.1.6.5 TOF-SIMS

Time of flight secondary ion mass spectrometry (TOF-SIMS) provides detailed information on the surface chemical composition of samples. It uses a pulsed source of primary ions having an energy of a few keV (50 - 300 keV) to bombard the surface of the sample and produce secondary ions emitted from the first monolayer of the sample surface. The latter ions are focused and accelerated with the same kinetic energy in the analysis tube. The travel time of the secondary ions in the analyzer is proportional to the square root of their masses. The use of a time-of-flight analyzer makes it possible to obtain a very good mass resolution. For the SIMS analyses of the SOA sampled in *CHARME*, the samples were sputtered with a Bi^{3+} primary ion beam and the ejected secondary ions were analyzed with a time of flight mass spectrometer (resolving power around 104).

II.2 LPCA-ONE chamber

Almost all the experiments presented in this research work have been performed in *CHARME* chamber, however, some experiments dedicated to the determination of the rate coefficient for the reaction of ozone with γ -terpinene (detailed in [section IV.A.1](#)) were performed in the chamber LPCA-ONE. In this regard, this reactor which is described in details by **Lauraguais (2014)** and is only briefly presented here.

The LPCA-ONE chamber displayed in [Figure II.20](#) is a cubic, rigid PMMA (Poly(methyl metacrylate)) reactor. It has a volume of 8 m^3 ($2 \text{ m} \times 2 \text{ m} \times 2 \text{ m}$) and a S/V of 3 m^{-1} . The reagents are injected into the reactor through a liquid heating injector that is set at different temperatures

(up to 300°C) to ensure the vaporization of the gases which are then flushed by zero air into the chamber. To ensure homogeneous mixing for gases and particles, a 4 wings mixing fan (diameter of 30 cm) is installed at the mid bottom of the reactor. The chamber is operated under atmospheric pressure and temperature and is illuminated with 10 fluorescent tubes (Philips TLD 58W/965; wavelengths in the range 400 nm- 800 nm).

LPCA-ONE shares with *CHARME* most of the analytical instruments mentioned previously in section (II.1.5).



Figure II.20: Photo of LPCA-ONE chamber.

II.3 Material

To meet the objectives set for *CHARME* characterization and ozonolysis experiments, several chemical compounds in the liquid, solid and gaseous states have been used. All the compounds were utilized without further purification. **Table II.1** summarizes the chemicals that have been involved in this research work.

Besides, pure air has been used as a matrix and carrier gas during simulation experiments. The purified air is extremely dry, with relative humidity (RH) <2% and a dew-point below -30°C .

Table II.1: The different liquid, solid and gaseous chemicals used in different experiments performed in *CHARME*.

Precursors	Molar mass (g.mol ⁻¹)	Manufacturer	Purity (%)
Formaldehyde	30.03	J.T.Baker	37
Acetonitrile	41.05	SIGMA-ALDRICH	99.5
Propene	42.08	GAZ Detect	1
Formic acid	46.03	Fisher Scientific	98
Acetone	58.08	VERBIESE	≥ 99.5
Acetic acid	60.05	SIGMA-ALDRICH	≥ 99
Isoprene	68.12	SIGMA-ALDRICH	≥ 99
cis-2-pentene	70.13	SIGMA-ALDRICH	98
2-methyl-2butene	70.13	SIGMA-ALDRICH	≥ 95
Benzene	78.11	MERCK	≥ 99.7
Cyclohexane	84.16	CHEM-LAB	≥ 99.5
Dichloromethane	84.93	VERBIESE	99.9
Cyclohexanone	98.15	VERBIESE	99.8
3-methoxyphenol	124.13	ALFA AESAR	97
1,2,4 Tri-methyl-benzene	120.19	SIGMA-ALDRICH	98
α -pinene	136.23	ACROS	98
γ -terpinene	136.23	ACROS	97
Methylchavicol	148.23	ACROS	98
O ₂	15.99	PRAXAIR	99.9999
NO	30.00	MESSER	2 ppm in N ₂
NO ₂	46.00	GERLING HOL+CO	-
SiO ₂	60.08	SIGMA-ALDRICH	-
(NH ₄) ₂ SO ₄	132.12	MERCK	-
Nigrosine	618.50	SIGMA-ALDRICH	-

II.4 Method

In general, the methodology used to perform simulations is simple and almost the same in different simulation reactors.

Before the experiment is initiated, the analytical instruments are started to measure the initial concentrations of the gaseous compounds and particles and thus to verify the cleanliness of the blank chamber. The gases (VOCs, NO_x, O₃...) or/and particles are then injected into the chamber and their concentrations are monitored throughout the experiment. The time-concentration profiles of the reactants as well as the formed products are measured and the environmental parameters (irradiation, temperature, relative humidity, pressure...) are adapted to fulfill the aim of each atmospheric study.

Some processes (injection, sampling, cleaning...) within the simulation methodology are considered as particularities for each chamber depending on its features. In this regards, the experimental procedure assigned to *CHARME*, is summed up here.

Based on the physical state of the compounds (solid, liquid, gas), introduction of the chemicals into *CHARME* can be carried out in different ways:

For liquid VOCs (at atmospheric pressure and room temperature), a known volume of the reactant is injected with a micro-syringe through a septum into a glass impinger (see [Figure II.21](#)) which is then flushed with a stream of purified air. A gentle heating, for compounds with high boiling point, could be applied to speed-up the vaporization of the liquid. Another way to proceed is to inject liquids directly into the vacuumed chamber, the vacuum facilitates the vaporization of the liquid.

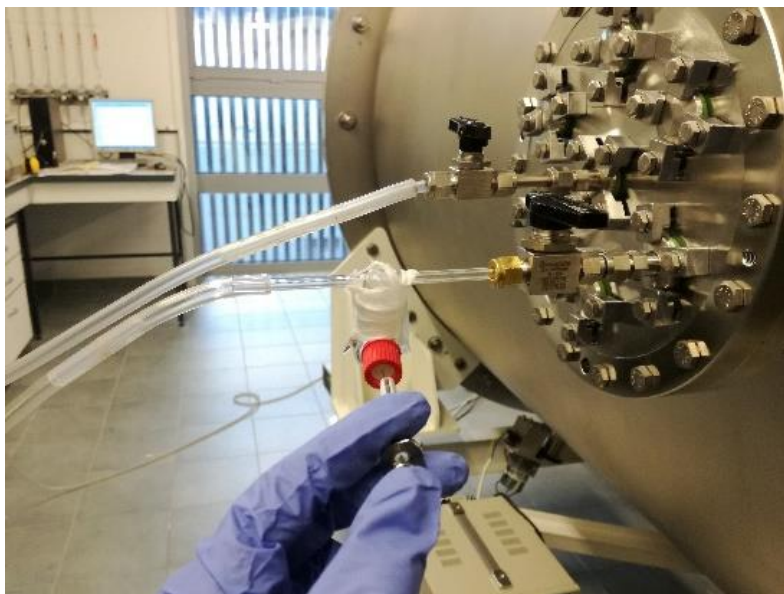


Figure II.21: Injection of liquid reagents through an impinger.

- For solid VOCs (at atmospheric pressure and room temperature), an impinger specially designed is gently heated and flushed with purified air. Another way to proceed is to dissolve a known mass of the compound of interest in a solvent and to introduce it as described above for liquids.
- NO and propene are introduced into the chamber by connecting the bottle of gas to the chamber with a flow controller to regulate the concentrations taking into account the flow and the time of injection. For NO₂, a gas syringe is used to inject known volumes directly into the chamber through a septum. O₃ is generated from the ozone generator (mentioned in part [II.1.5.4](#) O₃ generator and analyzer) and directly introduced into the chamber through a Teflon line.
- Seed particles like ammonium sulfate ((NH₄)₂SO₄), are produced by an atomizer (TSI 3076) as shown in [Figure II.22](#). Solutions at different concentrations (0.015 M - 0.3 M) are nebulized at a flow Q=3 L/min with dry pure nitrogen (P=2 bar) and then passed through a diffusion dryer TSI (3062) filled with silica gel before they are introduced into the reactor as polydispersed particles.

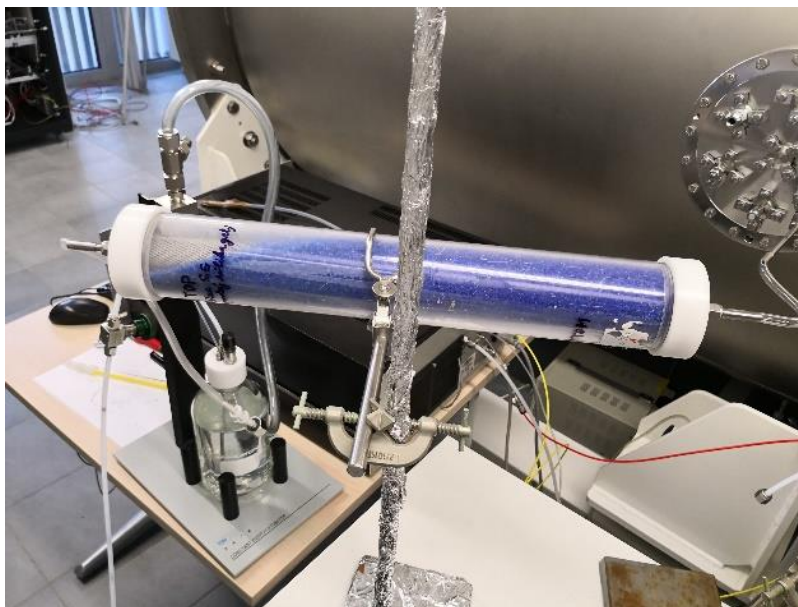


Figure II.22: The setup (atomizer + drier) used to introduce seed particles into *CHARME*.

After the reagents are injected and once they are well mixed and their concentrations are stable (or decrease steadily if there are wall losses), the investigation can start by the addition of a chemical oxidant and/or switching the lamps on. Throughout the experiment the PTR, O₃ and NO_x analyzers and/or SMPS are continuously sampling the air from the chamber. Moreover, during some experiments, it can be also useful to sample gaseous compounds on tenax and /or DNPH cartridges and particles on quartz fiber filters or other supports depending on the analytical techniques required. Depending on the initial concentration of the precursor(s), the sampling duration can be verified for gases and particles. The duration of a simulation experiment may last from a few minutes to several hours depending on the aim of the investigation.

At the end of each experiment the chamber is pumped and then filled with purified air, the efficiency of the cleaning method is presented in [chapter III.8](#).

II.5 Summary of key features of *CHARME*

In this chapter, the new atmospheric simulation chamber, *CHARME*, developed in the LPCA laboratory and the analytical techniques used to characterize the gas and particles phases are described.

Table II.2: Summary of the chamber's features.

Name	<i>CHARME</i>
Acronym	<i>CHamber for the Atmospheric Reactivity and the Metrology of the Environment</i>
Location	Indoor
Shape	Cylindrical
Position	Horizontal
Material	Stainless steel type 304L - Electropolished
Windows	4 quartz windows
Volume	9.2 m ³
Surface/Volume	3.5 m ⁻¹
Length × Diameter	4.4 m × 1.68 m
Mass	5850 kg
Temperature*	-20° C < T < +50° C
Pressure	0.4 mbar < P < 1013 mbar
Lamps	4 xenon high pressure arc lamps (=5 kW each)

**Operational in the future.*

Table II.3: Summary of the instrumentation coupled to *CHARME* with their measurement parameters.

Instrument (Model)	Species (Parameter)
Ozone monitor (UV photometric, Thermo Scientific 49i) Ozone generator (Air Tree Ozone Technology C-L010-DTI)	O ₃
NO _x monitor (Chemiluminescence, Thermo Scientific 42i)	NO, NO ₂
IBBCEAS in-situ (660 nm) ¹	NO ₃ , NO ₂
EC-QCL-MPC (8 μm) ^{1,2}	N ₂ O ₅
PTR-ToF-MS, IONICON 1000 Thermodesorber – GC (Autosystem XL) – FID / MS (Turbomass), Perkin Elmer Multipath cell (Chernin cell) connected to FTIR(Bruker)	VOCs
SMPS (DMA “TS1 3081”, CPC “TSI 3775”) SMPS (Grimm 5.404) OPC (Grimm 1108) Aerosol generator (TSI 3076) + dryer (TSI 3062)	Aerosols (size distribution, number concentration, mass concentration...) Aerosols (number concentration, particle size) Aerosols
Sensors (VAISALA HMT330) (Sensirion EK-H5 -SensorSHT75)	Humidity, Temperature
Pressure controller with MK Baratron capacitance gauges (Baratron® Basics)	Pressure
Spectroradiometer (Metcon)	Actinic flux

¹Developed in LPCA.

²Will be coupled to *CHARME* in the future.

CHARME aims at being an international research platform for researchers investigating the physico-chemistry of the atmosphere. In this regard, a large selection of experiments was performed to characterize and validate the chamber; they are described in detail in [chapter III](#).



Figure II.23: *CHARME* is operational with some analytical instruments.

References

- Blake, R.S., Monks, P.S., Ellis, A.M., 2009. Proton-Transfer Reaction Mass Spectrometry. *Chemical Reviews* 109, 861–896. <https://doi.org/10.1021/cr800364q>
- de Gouw, J., Warneke, C., 2007. Measurements of volatile organic compounds in the earth's atmosphere using proton-transfer-reaction mass spectrometry. *Mass Spectrom Rev* 26, 223–257. <https://doi.org/10.1002/mas.20119>
- Gysel, M., McFiggans, G.B., Coe, H., 2009. Inversion of tandem differential mobility analyser (TDMA) measurements. *Journal of Aerosol Science* 40, 134–151. <https://doi.org/10.1016/j.jaerosci.2008.07.013>
- Lauraguais, A., 2014. Contribution de la combustion du bois à la qualité de l'air et étude de la réactivité atmosphérique des méthoxyphénols en chambre de simulationf. ULCO.
- Lindinger, W., Hansel, A., Jordan, A., 1998. On-line monitoring of volatile organic compounds at pptv levels by means of proton-transfer-reaction mass spectrometry (PTR-MS) medical applications, food control and environmental research. *International Journal of Mass Spectrometry and Ion Processes* 173, 191–241. [https://doi.org/10.1016/S0168-1176\(97\)00281-4](https://doi.org/10.1016/S0168-1176(97)00281-4)
- Wiedensohler, A., Birmili, W., Nowak, A., Sonntag, A., Weinhold, K., Merkel, M., Wehner, B., Tuch, T., Pfeifer, S., Fiebig, M., Fjåraa, A.M., Asmi, E., Sellegri, K., Depuy, R., Venzac, H., Villani, P., Laj, P., Aalto, P., Ogren, J.A., Swietlicki, E., Williams, P., Roldin, P., Quincey, P., Hüglin, C., Fierz-Schmidhauser, R., Gysel, M., Weingartner, E., Riccobono, F., Santos, S., Gruning, C., Faloon, K., Beddows, D., Harrison, R., Monahan, C., Jennings, S.G., O'Dowd, C.D., Marinoni, A., Horn, H.-G., Keck, L., Jiang, J., Scheckman, J., McMurry, P.H., Deng, Z., Zhao, C.S., Moerman, M., Henzing, B., de Leeuw, G., Löschau, G., Bastian, S., 2012. Mobility particle size spectrometers: harmonization of technical standards and data structure to facilitate high quality long-term observations of atmospheric particle number size distributions. *Atmospheric Measurement Techniques* 5, 657–685. <https://doi.org/10.5194/amt-5-657-2012>

Chapter III

“Characterization of *CHARME*”

The new simulation chamber, *CHARME*, has to be characterized and validated in order to verify the absence of artifacts and confirm that it can be used to simulate atmospheric chemical reactions.

Characterization is essential to assess some fundamental parameters through different tests including:

- Characterization of the pumping system do determine the lowest pressure available in the chamber and the time to reach it.
- Leakage tests to verify the tightness of the chamber.
- Mixing tests to check the homogenization of the gases and particles.
- Wall loss tests to determine the life time of gases and aerosols without any reaction.
- Light tests to characterize the irradiation system by measuring its spectral distribution, determining the photolysis rates of NO₂ and O(¹D) and verifying the homogeneity of the light in the chamber.
- Propene-NO_x-air irradiation experiments to illustrate the utility of the chamber for evaluating auxiliary mechanisms.

During the characterization experiments, each test has been conducted at least twice to ensure its repeatability.

In this section, results for *CHARME* characterization are presented and discussed in details.

III.1 Vacuum limit and leak rate

The rigid material of *CHARME* makes it an evacuable chamber. As previously shown in section [II.1.1](#), the reactor is connected to a dry screw vacuum pump designed to allow the evacuation of gases as well as aerosols.

To determine the vacuum limit, the chamber was evacuated and the pressure decrease was monitored with respect to the time as presented in [Figure III.1](#). After around 40 minutes the pressure reached a value of about 1 mbar, corresponding to an average evacuation rate of ~25

mbar.min⁻¹. Then, the pressure decrease was slower with an evacuation rate of ~0.02 mbar.min⁻¹. The minimum pressure reached was ~ 0.4 mbar and this value was achieved after approximately 5 hours of pumping. For the daily cleaning procedure of the chamber, it is not required to reach such a low pressure but some cycles of evacuation and filling can be performed if the blank chamber levels are not satisfactory (detailed III.8.1). Sometimes, it is useful to reach and stay at the lowest pressure for a few hours to allow the desorption of ‘sticky’ compounds (like oxygenated aromatics, organic nitrates, etc.). In the future, the pumping system could be supported by an additional pump that permits to reach pressure around 10⁻⁴ mbar.

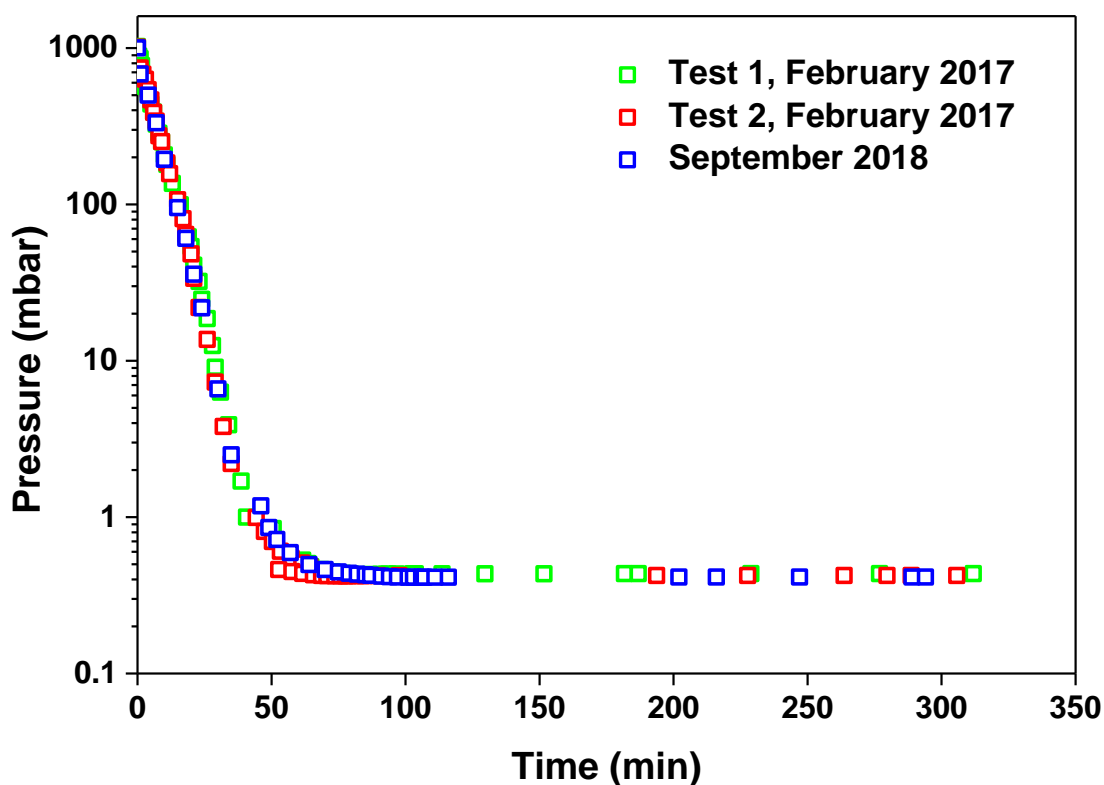


Figure III.1: Time profile for the evacuation process in *CHARME*.

The verification of the tightness of the chamber is important in order to ensure the absence of leaks of compounds injected into the chamber and also to check that there is no contamination from species that are in the atmosphere of the laboratory. The leak rate of *CHARME* was determined after stopping the pump (when it reaches the lowest value of the pressure ~ 0.4 mbar), and then monitoring the pressure increase in the chamber versus the time as shown in Figure III.2. The slope of the curve of the pressure as a function of time corresponds to the leakage rate.

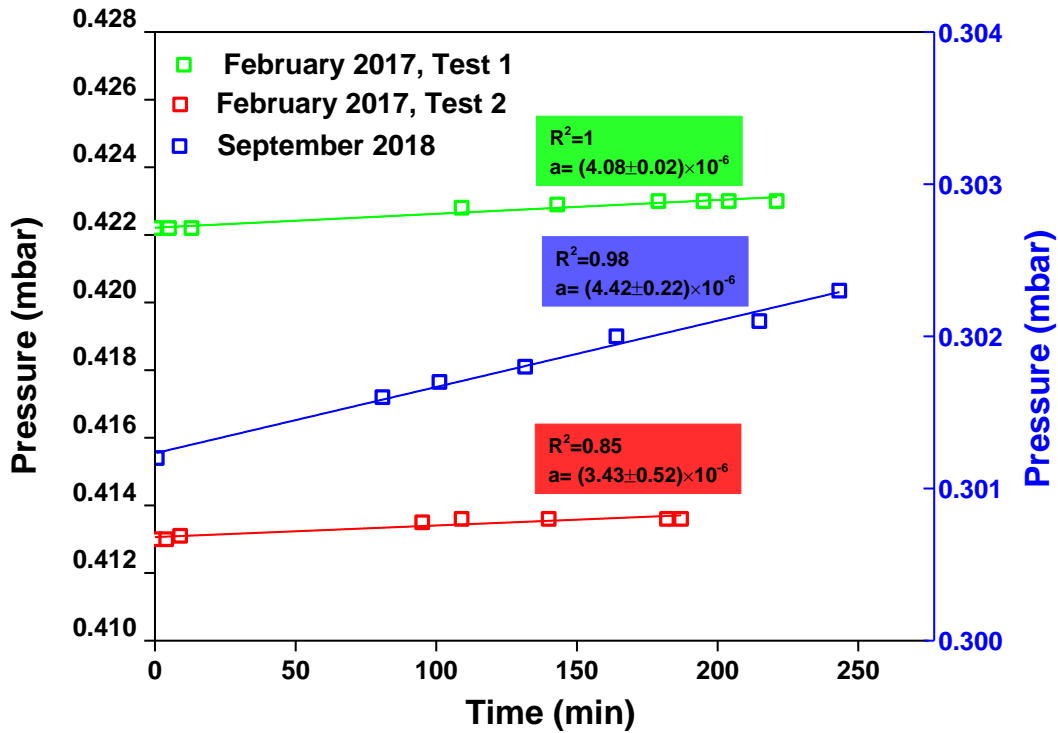


Figure III.2: Leak rate in *CHARME*.

In the low pressure range, the leakage rate with an average value $\sim 4 \times 10^{-6} \text{ mbar} \cdot \text{min}^{-1}$, was almost constant even after running experiments for a period of ~ 18 months. This rate corresponds to a very negligible concentration (~ 40 ppb) of contaminants that can enter into the chamber from the laboratory air during the filling process which last for ~ 9 minutes as shown in [Figure III.3](#). This approximation was an upper limit, as during the filling of *CHARME* the difference between the pressures of the chamber and that of the laboratory decreases, so the leak rate is reduced as well.

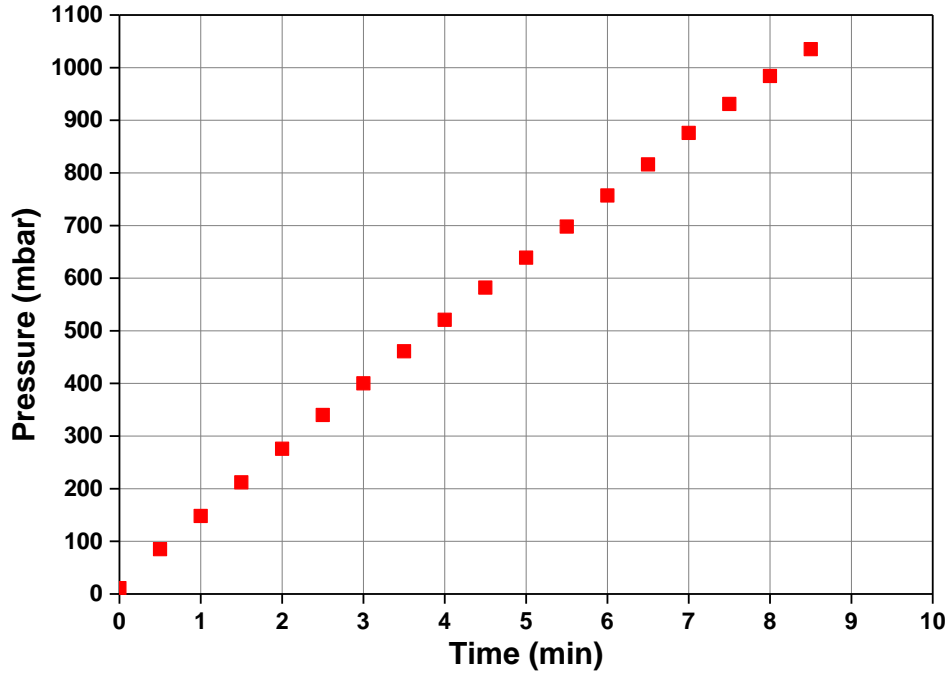


Figure III.3: Time profile of the pressure during the filling process.

In short, the small leak rate showed that *CHARME* is a tight and well-sealed chamber. To maintain a minimum contamination from the external environment, the chamber when it is not used, is kept at a slight overpressure (+5 mbar).

III.2 Dilution factor

Another parameter related to the variation of the pressure inside the chamber is the dilution factor.

This factor takes into account the amount of air lost from the chamber due to instruments sampling. The dilution rate (k_{dilution}) related to the sampling (in s^{-1}), was determined according to the following equation:

$$\text{(Eq. III. 1)} \quad k_{\text{dilution}} = \frac{\sum Q_{\text{sampling}}}{V_{\text{chamber}} \times 60}$$

where Q_{sampling} (in $\text{L} \cdot \text{min}^{-1}$) is the sampling flow rate of the instruments connected to the chamber and V_{chamber} is the volume of *CHARME* (in L).

For instance, during an experiment where the ozone analyzer ($Q = 1.5 \text{ L}\cdot\text{min}^{-1}$), the NO_x analyzer ($Q = 0.6 \text{ L}\cdot\text{min}^{-1}$), the PTR ($Q = 50 \text{ mL}\cdot\text{min}^{-1}$) and the SMPS ($Q = 0.3 \text{ L}\cdot\text{min}^{-1}$) are connected to *CHARME*, a constant dilution rate of $4.4 \times 10^{-6} \text{ s}^{-1}$ must be taken into account.

Besides, for the measurement of the total dilution rate, in some experiments, acetonitrile has been added to the reaction mixture as an inert tracer and its concentration was monitored by a PTR-ToF-MS at $m/z = 42.0$ as displayed in **Figure S.2**. The average calculated loss rate of acetonitrile over the course of each experiment was used as the dilution rate applied to all stable species in the simulations. The wall loss of acetonitrile was $k = 4.0 \times 10^{-6} \text{ s}^{-1}$ in agreement with the previously calculated dilution rate.

The dilution rate was considered as negligible (for an experiment duration of 2 hours, it was about 3%), so the measured concentrations of the species into the chamber were not corrected from the dilution. However, a pressure compensator connected to the purified air generator allowed to maintain the chamber at the initial pressure.

III.3 Variation of relative humidity

Relative humidity is an important parameter that affects the atmosphere and its constituents. Among atmospheric components, aerosols are greatly dependent on humidity conditions that impact their formation and evolution (**Hallquist et al., 2009**). At the level of aerosols, cloud cycles and rain play a central role in the particle balance, and exert globally important controls on precipitation and planetary albedo (**IPCC, 2013**). The possibility to simulate such an aqueous environment (cloud or fog) is extremely important for a better understanding of aerosol formation and transformation in the aqueous phase. Simulation chambers can afford precise control of temperature and humidity and allow the reproduction of these complicated aqueous systems. In this regard, a system (**Figure III.4**) to vary the relative humidity and to reach the relevant atmospheric conditions has been developed and tested in *CHARME*.

As shown in **Figure III.4**, water vapor was produced by a commercial stainless steel pressure cooker ($V = 5 \text{ L}$) which has been modified. The water vapor pressure was controlled by a gauge installed above the cooker. A valve was used to purge the residual air in the generator before

each steam injection. The steam reactor was connected directly to the injection port of the chamber, with a stainless steel tube.



Figure III.4: The steam reactor used for introduction of water vapor.

During the experiments, the reactor was filled with about 3 liters of ultrapure water and continuously heated to reach a pressure of 1.5 bar. At this point, residual air was purged out and water vapor was then introduced into *CHARME* through short consecutive injections (< 15 s for each). The stirring fans were operating during the injection process to promote a quick mixing of water vapor and minimize the condensation.

A total of 160 seconds divided over 20 successive introductions of water vapor each ranging from 3 to 15 s, were needed to increase the humidity in *CHARME* from $RH_0 = 1.7\%$ to $RH_{max} = 101.5\%$. As presented in **Figure III.5**, the humidity in *CHARME* increased linearly with the introduction time of the steam with a value of $0.9\% \cdot s^{-1}$ for a rise from $RH = 1.7\%$ to $RH = 96\%$ and a value of $0.08\% \cdot s^{-1}$ for a growth from $RH = 96\%$ to $RH = 101.5\%$. During the experiment the relative humidity was monitored with a RH sensor (Vaisala HMT330).

Also, the stability of the four relative humidity values (25 %, 50%, 75%, 101.5%) versus the time was also tested in *CHARME* as illustrated in **Figure III.6**. The results showed that a constant humidity could be maintained into the chamber for more than one hour.

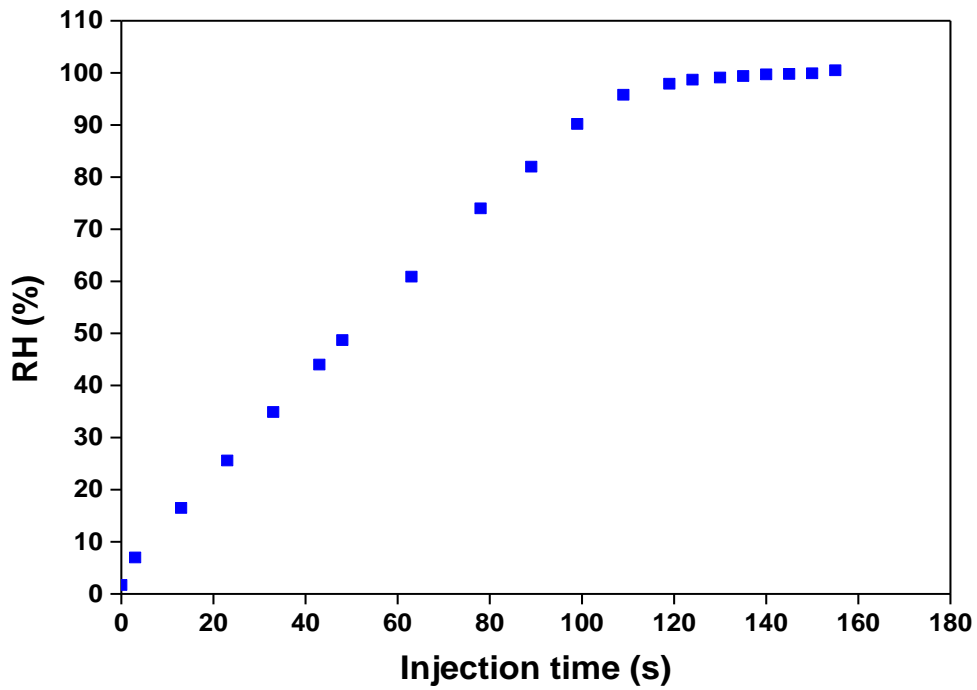


Figure III.5: Different injection times of water vapor corresponding to different relative humidities reached in *CHARME*.

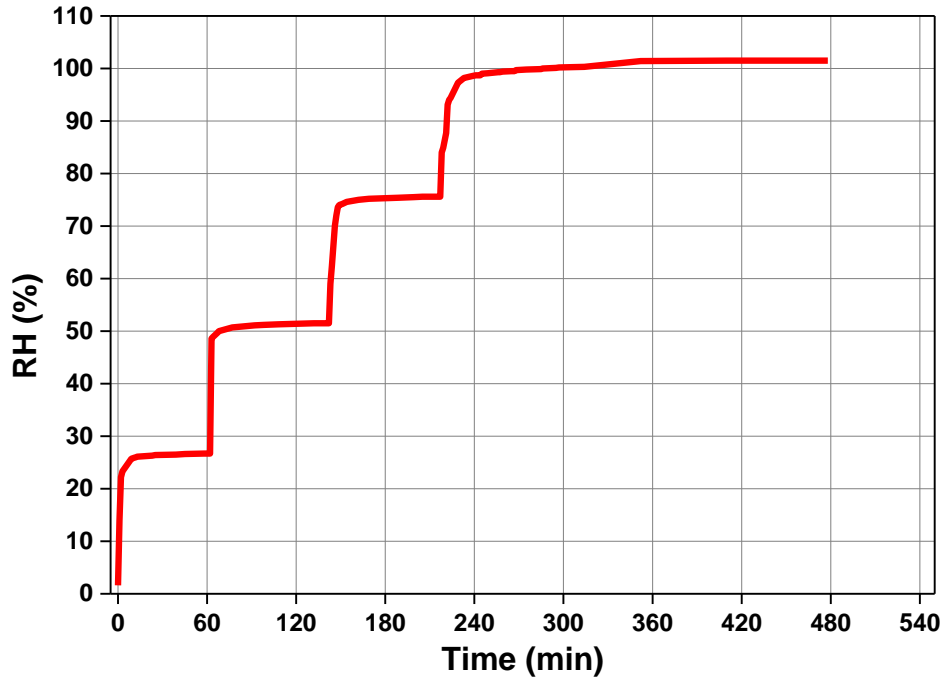


Figure III.6: Variation of the relative humidity as a function of time in *CHARME* (RH%: 25, 50, 75 & 100).

Throughout these experiments, water condensation was observed in the bottom of the chamber as seen in [Figure III.7](#), however this liquid water was removed by the pump during the cleaning procedure.

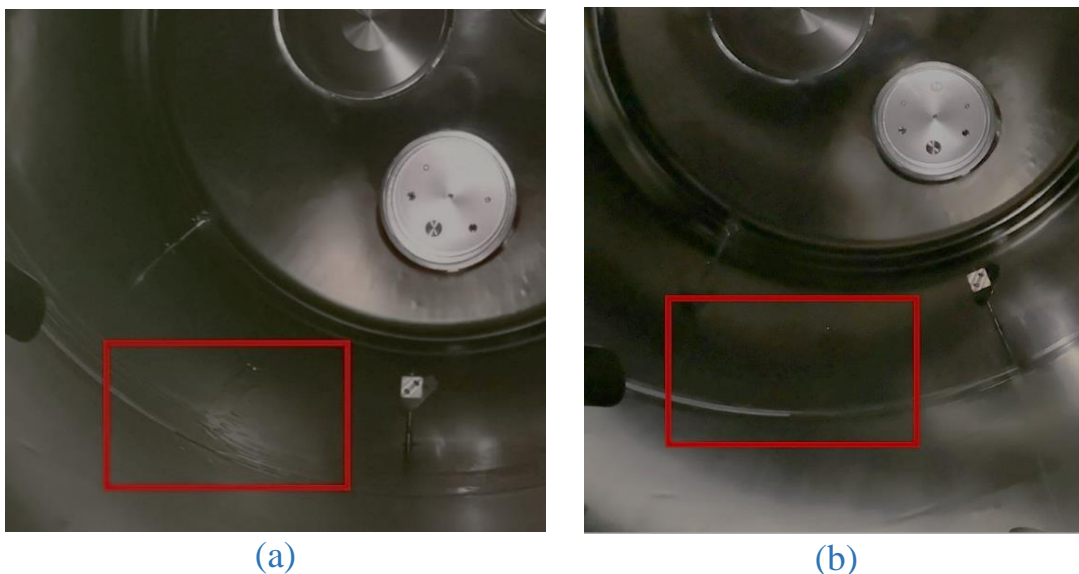


Figure III.7: A spot of condensed water vapor observed inside *CHARME* (a) at the end of the experiment and (b) its removal after pumping the chamber for 1 hour.

Therefore, the relative humidity in *CHARME* can vary from 1.7 to 101.5% and constant conditions can be maintained for more than one hour. These experiments demonstrated the ability to generate fogs and clouds and the possibility to study multiphase chemical processes in *CHARME*.

III.4 Variation of temperature

As previously mentioned, *CHARME* is irradiated by 4 xenon lamps (5 kW each). The use of this irradiation setup can lead to a temperature increase in the chamber which has to be measured as it can influence the data (e.g. rate coefficients, SOA yields, etc.) obtained during the simulations.

To determine the temperature variation in *CHARME*, the reactor was irradiated for about one hour and the temperatures, in the chamber as well as in the room hosting the lamps, were continuously monitored by the sensors VAISALA (HMT330) and Sensirion (EK-H5-Sensor SHT75) respectively. The results displayed in **Figure III.8**, showed that the irradiation led to a temperature increase in the enclosure of 2.2°C (from 20.2 °C to 22.4 °C) corresponding to an average growth rate of 0.030 °C/min. This value is acceptable but it should be reduced in the future, by the circulation of a cold fluid through the double wall of *CHARME*. Regarding the housing room, the rise up in its temperature was relatively high as it varied from 20.8°C to 40.8°C with an average rate of 0.33 °C/min. In principle, the lamps are located in a room which is well conditioned by a 12 kW air-conditioning unit. In this housing, the air is supposed to be ventilated and cooled to a temperature between -10°C and +30°C, however this seems to be insufficient indicating a system malfunction (this is probably due to the flow rate of the water-glycol mixture which has to be increased as the air-conditioning unit was well dimensioned).

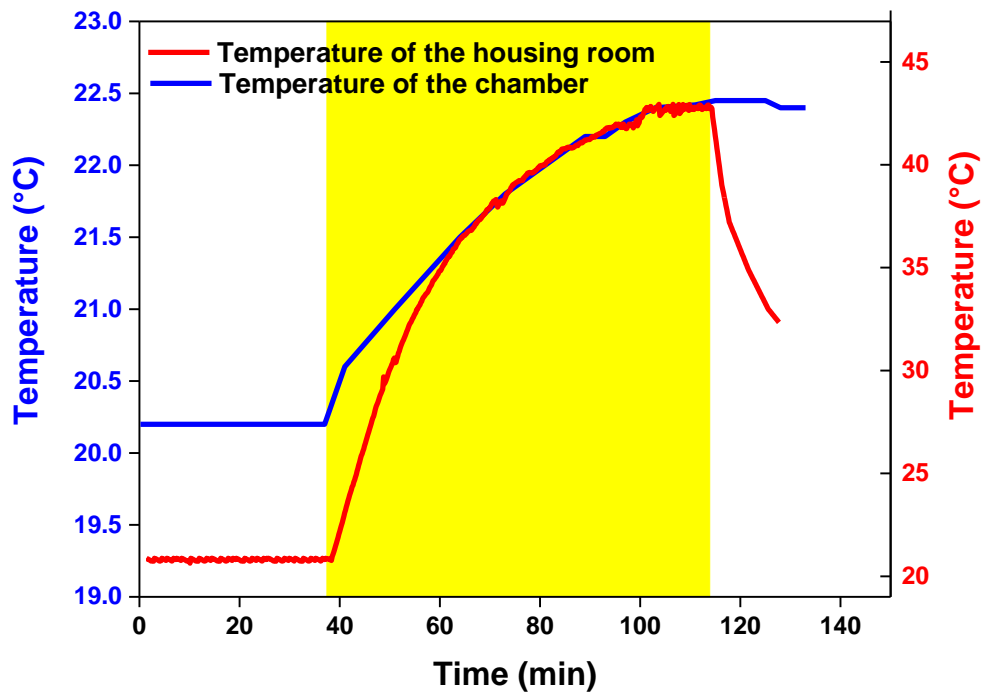


Figure III.8: Time profile of the temperature in the chamber (blue) and in the room hosting the lamps (red), with (yellow) and without irradiation (white) by the 4 xenon lamps.

III.5 Mixing time

For appropriate chemical studies, a good mixing and homogeneity of the gaseous and aerosols mixtures inside the chamber is required. The time needed for a certain compound to reach a stable concentration soon after its injection into the chamber, is known as the mixing time.

The influence of the injection position and the introduced concentration on the mixing time of gases, has been tested in *CHARME*. Three different injection positions (A, B and C) shown in [Figure III.9](#) and a range of gaseous concentrations (50 ppb - 550 ppb) were examined in this test.

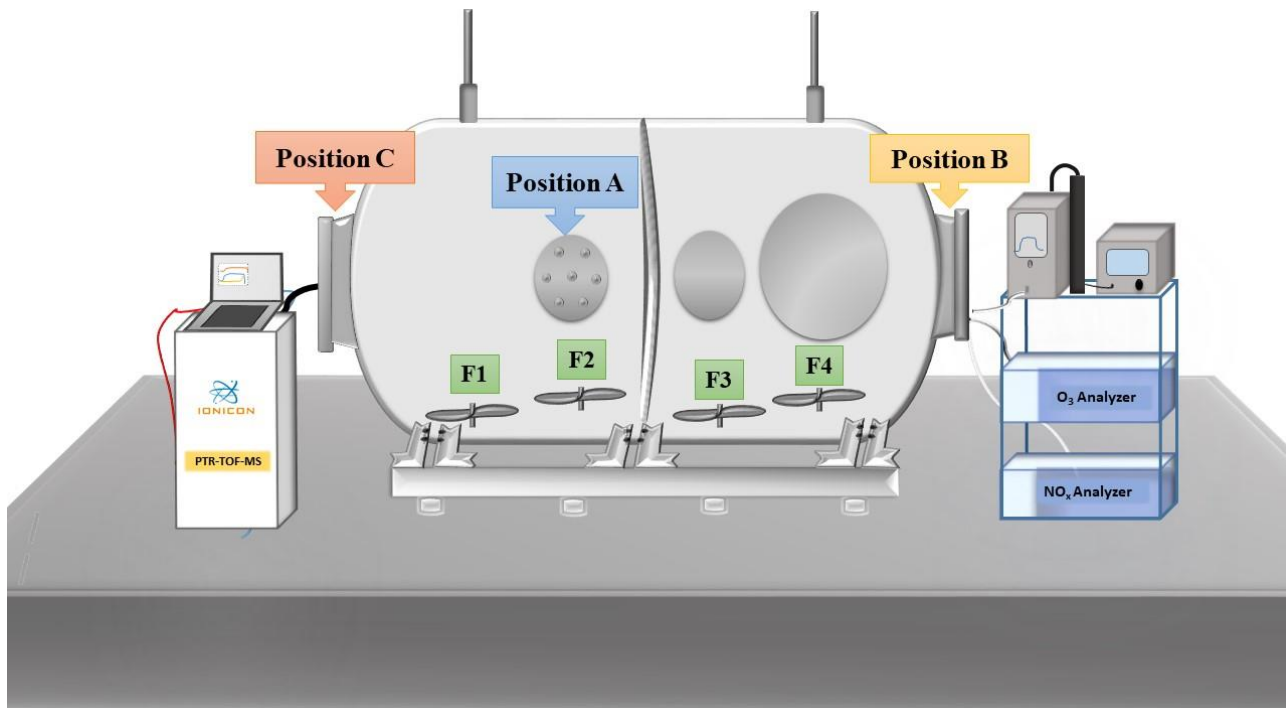


Figure III.9: A scheme of *CHARME* indicating the position of the injection points (A, B and C), of the PTR-MS and of O₃ and NO_x analysers.

During the experiments, the concentrations of the species were monitored by gas analyzers (O₃ and NO_x) and PTR-MS (VOCs) and the 4 mixing fans were continuously operating (at 190 rpm).

Acetone and isoprene were used as test compounds to determine the mixing time of VOCs. Seeking for a short injection time (few seconds), these compounds (which are liquid at room temperature) were first vaporized in a glass ampule and then known volumes were introduced into *CHARME* with a gas syringe at 3 different positions (A, B and C; see **Figure III.9**). The concentrations of the two organic compounds were monitored by a PTR-MS which was fixed at "position C".

“Position A” corresponds to the injection port placed almost at the middle of the chamber at about 2 meters from the PTR-MS. Introduction of gases at this location, is directly subjected to the influence of 3 fans, F1, F2 and F3 which are sited 130 cm, 130 cm and 80 cm, respectively away from the port.

“Position B”, is located at one periphery of the chamber at about 4 meters from the PTR-MS. Injection at this site is directly influenced by the presence of 2 fans F3 and F4, which are 170 cm and 80 cm, respectively, away from B.

“Position C”, is at the second periphery of the reactor just next to the PTR-MS. At this place, injection is mostly affected by F1 at $d = 110$ cm and F2 at $d = 160$ cm from the port.

To check the influence of the injected concentration on the mixing time, three different concentrations (50 ppb, 150 ppb and 550 ppb) have been tested for isoprene and acetone. As presented in **Figure III.10**, the mixing times for both VOCs having different concentrations, were recorded as a function of the 3 injection positions.

Injections of the different concentrations of acetone and isoprene at positions “A”, “B” and “C” led to mixing times of (100-160 s), (150-240 s) and (130-210 s). Position “A” displayed the lowest values, and this was expected as it is located to the middle of the reactor and directly influenced by the presence of 3 mixing fans. Therefore, it was retained as a site for the introduction of gaseous compounds in the chamber.

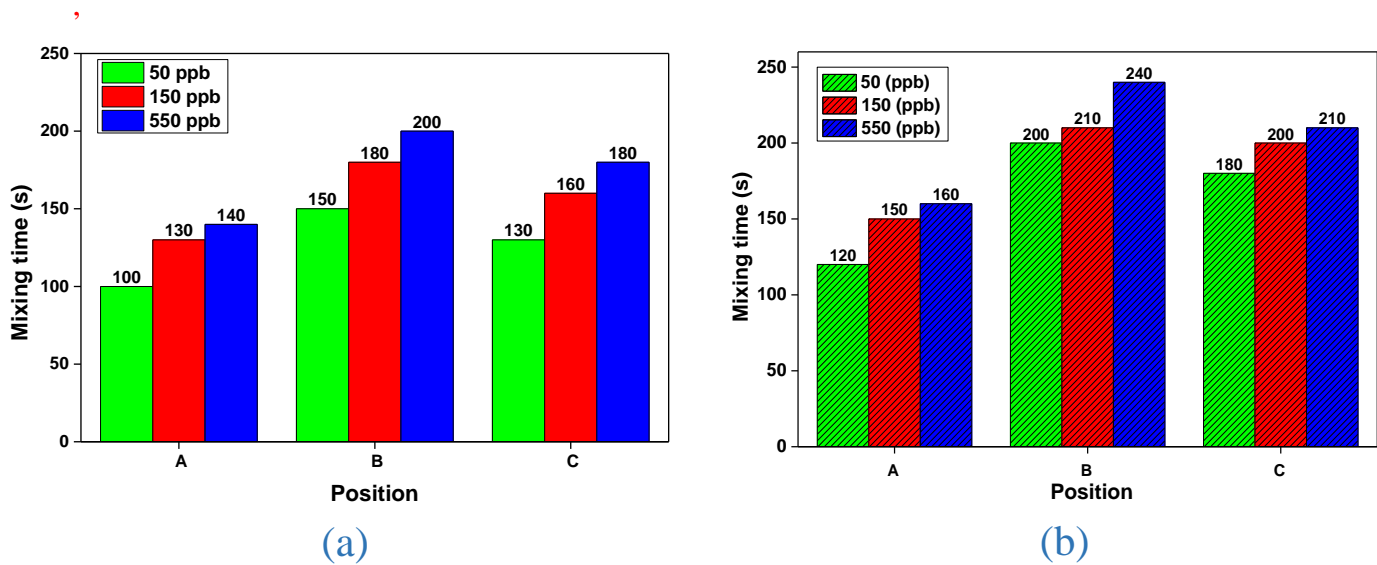


Figure III.10: Mixing times for 3 different concentrations of isoprene (a) and acetone (b) injected at 3 different positions.

In addition, **Figure III.10** also showed that the time needed to reach a homogenous concentration is related to the injected mixing ratios. For instance, for isoprene injected at position

“A”, the time needed to reach a stable concentration was maximum (140 s) for the highest concentration (550 ppb) and this mixing time was reduced (100 s) when the isoprene concentration decreased to 50 ppb. Similar profiles were observed at positions “B” and “C” for isoprene and for acetone as well.

The mixing times of O₃ and NO₂ have been also determined in *CHARME*. As observed in **Figure III.11**, three different concentrations of ozone (700 ppb, 2000 ppb, 6000 ppb) and one of nitrogen dioxide (200 ppb) was injected at “Position A”. The time needed to stabilise the different O₃ mixing ratios and those of NO₂ was around 3 minutes.

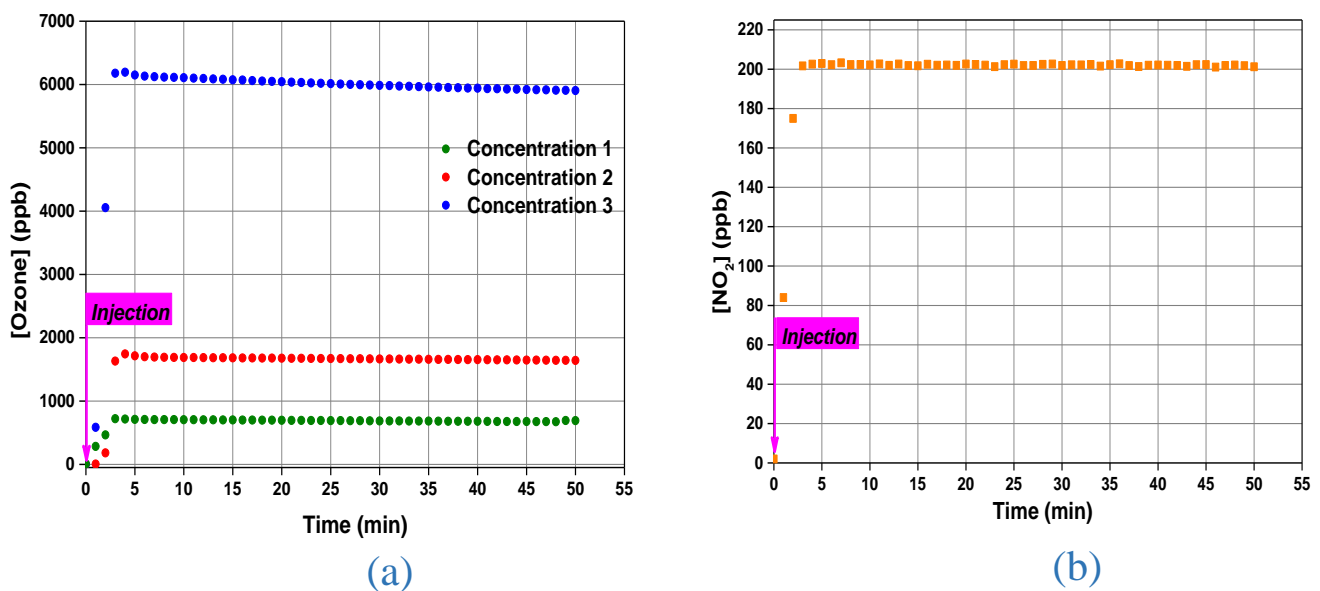


Figure III.11: Mixing times of (a) different concentrations of ozone and (b) NO₂.

Figure III.12 illustrates the time needed for different gases (VOCs, NO₂ and O₃ at ~ 100 ppb) to well mix in *CHARME*. The required time ranged between 110 and 180 seconds, depending on the nature of the injected gas (organic/inorganic, aromatic/oxygenated, low/high molecular mass...).

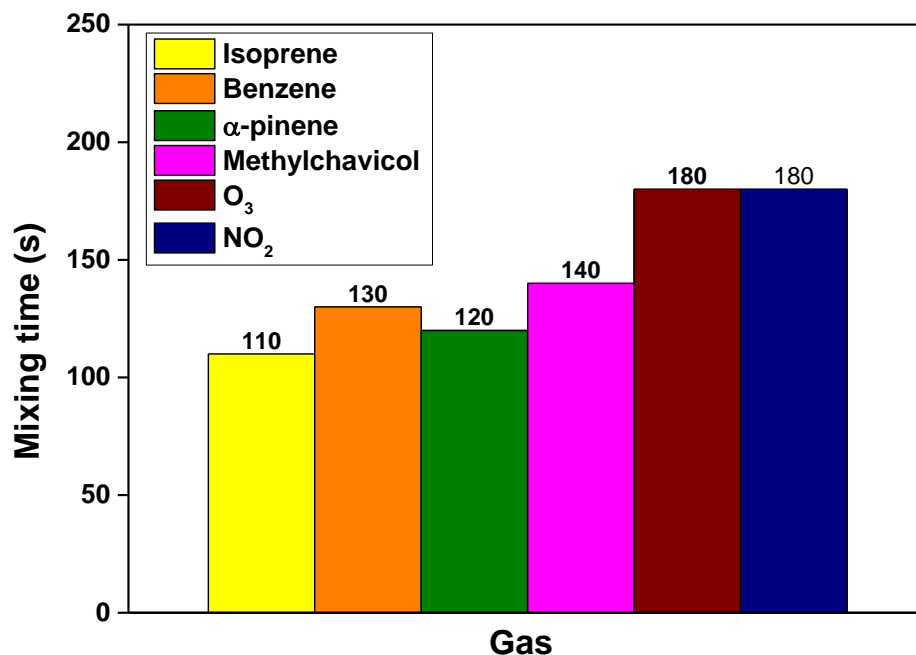


Figure III.12: The mixing times for different gases injected at “Position A” of *CHARME*.

In conclusion, position “A” is the optimum location to inject reactants in *CHARME* and the time needed for different gases to reach a stable concentration in the chamber is around 110-180 seconds. So the inhomogeneity can be considered as negligible if the pseudo-first-order rate constant is lower than $k = 5.6 \times 10^{-4} \text{ s}^{-1}$ (ten times slower than the mixing time).

III.6 Effect of fans

A good mixing in a simulation chamber is essential to provide homogeneous mixtures (gases and particles) and stable experimental conditions (temperature, relative humidity, etc.). Stirring fans are developed to offer continuously throughout the experiments, a realistic and efficient mixing system. In this respect, the stirring system of *CHARME*, was optimized to have the lowest mixing times with the minimum influence of wall exchanges.

The rotation speed of the fans can vary as a function of the input power supply. Consequently, at a maximum current supply (5A), 3 different voltages (10 V, 18 V, 30 V) corresponding to different speeds (105 rpm, 190 rpm, 320 rpm) have been examined in *CHARME*.

The aim was to study the influence of the fans on the mixing time and wall losses of particles and gases, as well as their effect on the mass concentration of SOA formed from ozonolysis reactions.

For each tested rotation speed, about 1800 ppb of ozone was introduced into the chamber. As shown in **Figure III.13 (a)**, when the four mixing fans did not operate, it took ~10 minutes to reach a stable ozone concentration in the chamber with an ozone wall loss of $1.4 \times 10^{-5} \text{ s}^{-1}$ (detailed later in **III.7.1**). The increase of the fan rotation speed at 105 rpm, 190 rpm and 320 rpm leads to reduce the ozone mixing time (from 8 minutes to 3 minutes), but increases its wall loss rate (at $2.9 \times 10^{-5} \text{ s}^{-1}$, $3.6 \times 10^{-5} \text{ s}^{-1}$ and $9.8 \times 10^{-5} \text{ s}^{-1}$, respectively). So, the balance between a short mixing time and low wall losses was achieved with the rotation speed fixed at 190 rpm.

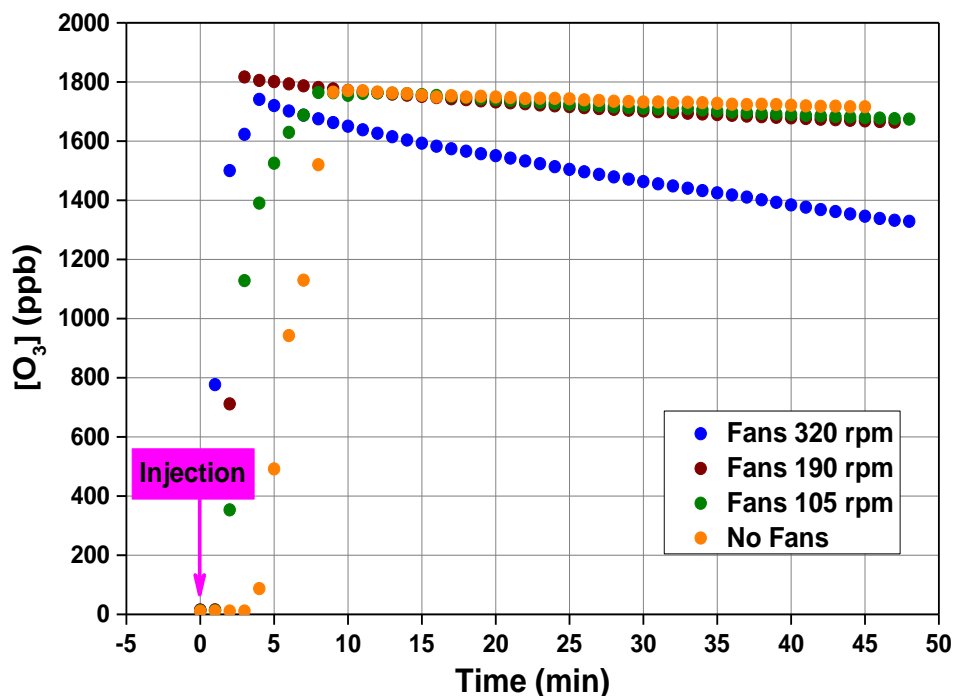


Figure III.13: Influence of the fans speed on the mixing time of ozone.

To examine the influence of the different rotation speeds on the mass concentration of the SOA, the reaction of γ -terpinene with ozone was investigated in *CHARME*. The aerosol formed was monitored with a SMPS during the course of 4 experiments involving the same initial concentrations of γ -terpinene (150 ppb) and ozone (1200 ppb). **Figure III.14** summarized the results and showed that as the rotation speed increased, the SOA mass decreased. A loss of ~ 33%

has been recorded between the SOA mass concentration obtained when the reaction takes place in the absence of fans compared to that measured in their presence with a maximum stirring speed of 320 rpm. In addition, when the fan speed was settled at the optimized value (190 rpm), the SOA mass was ~ 17% lower than without the fans rotation. A compromise has to be found between the mixing time of aerosols and the mass of the SOA which is formed.

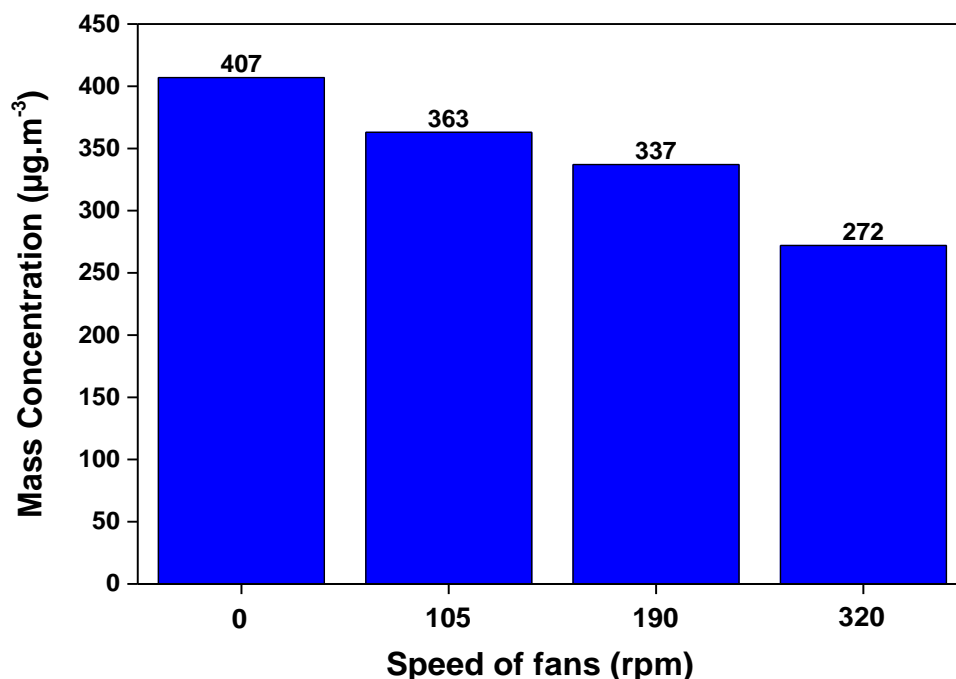


Figure III.14: Influence of the fans rotation speed on the mass concentration of SOA formed from the ozonolysis reaction of γ -terpinene

Expectedly, the variation of the stirring speed of the fans induced modifications in the mixing times of gases and particles. High rotation speeds increased turbulence inside the chamber and thus, enhanced the particles and gases deposition on the surface of the chamber. The 4 mixing fans of *CHARME* were settled at an optimized mixing speed of 190 rpm each.

III.7 Wall loss

Wall losses of gases and/or aerosols are key parameters that might limit the duration of experiments duration in simulation chambers. It is essential to determine the wall loss rates of all

the species of interest and to implement these data in model calculations of atmospheric processes. Several factors such as the chamber history, the cleaning process, the coating material and the technology used to perform the coating process, may affect the chemical reactivity of the walls of the chamber and hence the rate of gas and particle loss on its surfaces (Wang et al., 2011). The concentration decay of a certain precursor injected into a reactor as a function of time and in the absence of other gases and particles, is assumed to be the wall loss rate of this precursor. This decrease may be due to deposition and/or conversion into other species on the chamber walls.

III.7.1 Ozone

Ozone is recognized as a key oxidant that participates in atmospheric reactions. Its chemical reactivity towards surfaces and its ubiquity in chamber experiments (as reactant or as product), gives this species special importance with respect to wall reaction studies. The loss of ozone on the walls of chambers has been widely tested and many data are reported in the literature; they are summarized in [Table III.1](#).

To determine the wall loss of ozone in *CHARME*, we have introduced into the chamber different amounts of O₃. Throughout the experiment, mixing fans were operating at a speed of 190 rpm and ozone concentration was monitored by the UV photometry analyzer (Thermo Scientific 49i; λ at 254 nm). The time profiles of two different ozone concentrations (700 ppb and 4800 ppb) are shown in [Figure III.15](#).

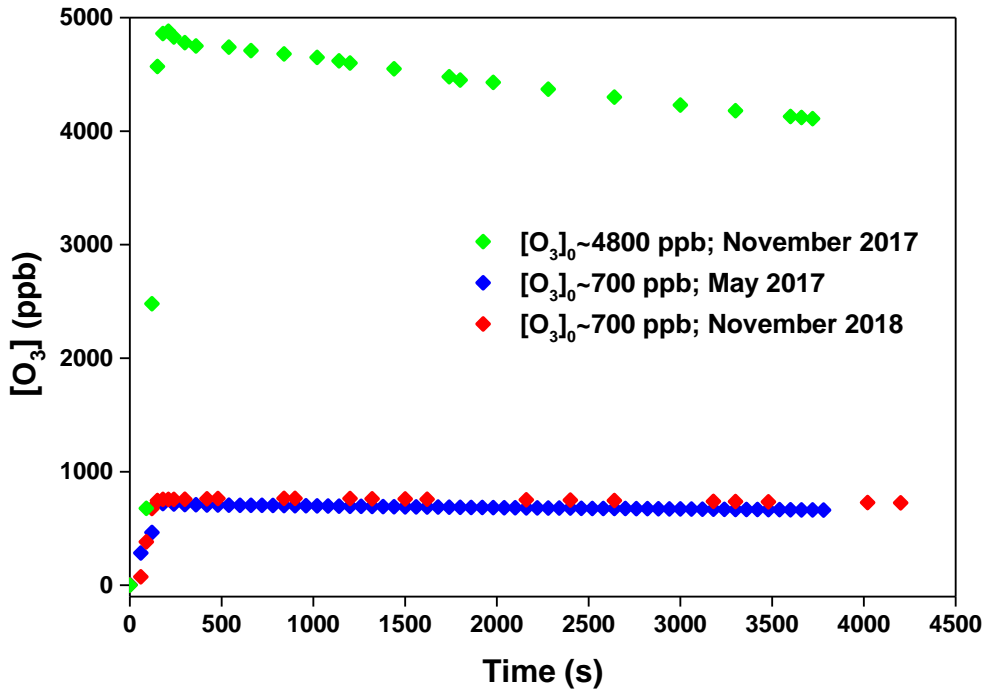


Figure III.15: Time profile of different concentrations of ozone.

To test the influence of the concentration on the rate of ozone loss, the decays of the previously mentioned concentrations, were tested in *CHARME* for a minimum of one hour. These ozone levels were chosen because they are within the range of the mostly used concentrations in our experiments. For the wall loss determination, the decay is taken into consideration after the ozone mixing time (3 minutes).

The ozone wall loss follows the kinetics of a first order process:



whose treatment leads to the following equation:

(Eq. III.2) $\ln [O_3]_0/[O_3]_t = k_{\text{wall}} \times t$

Thus, the plot of $(\ln [O_3]_0/[O_3]_t)$ versus time should be linear with zero intercept and the slope corresponds to k_{wall} (see [Figure III.16](#)).

In *CHARME*, the ozone wall losses were equal to $k = 2.0 \times 10^{-5} \text{ s}^{-1}$ for $[O_3] = 700 \text{ ppb}$ and $k = 4.5 \times 10^{-5} \text{ s}^{-1}$ for $[O_3] = 4800 \text{ ppb}$. So, this parameter is highly dependent on the initial ozone

concentration and consequently, its measurements must be carried regularly and before each set of experimental tests.

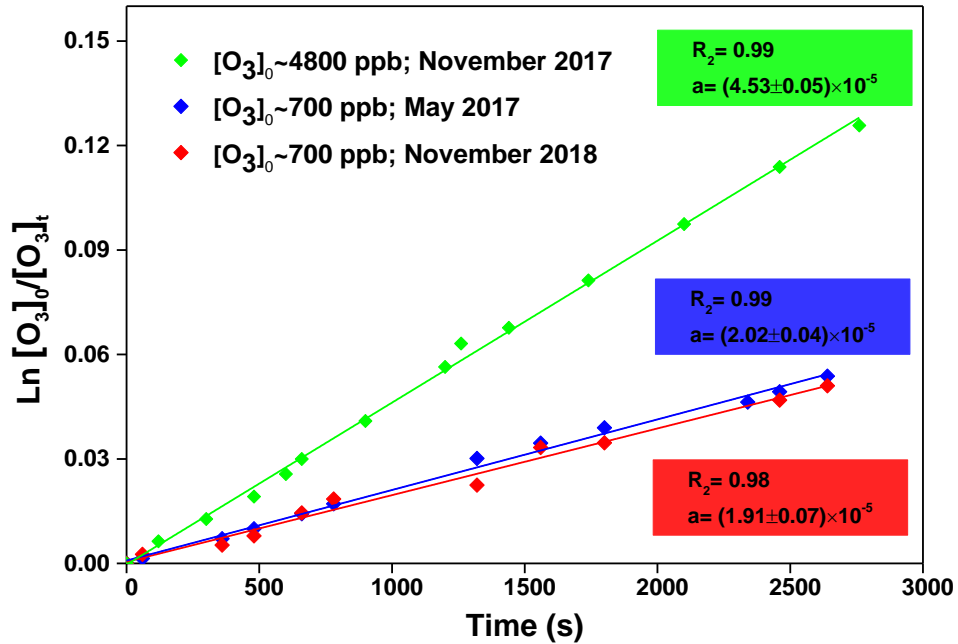


Figure III.16: Determination of ozone wall loss in *CHARME* for different ozone concentrations and at different times.

In addition, it is known that the chamber history and the state of cleanliness contribute to the uptake of reactive gases, by the reactor surface. To examine these criteria, the rate of ozone loss was tested by injecting 700 ppb of ozone in May 2017 and repeating the same experiment in November 2018. Based on the obtained results showing that the rate of ozone loss was almost kept constant ($k = 2.0 \times 10^{-5} \text{ s}^{-1}$) after a period of 18 months of experimental activity, it possible to conclude that the protocol used to clean *CHARME* is effective and the effect of the chamber history on the ozone wall losses seems to be negligible.

The values obtained in *CHARME* were in the same order of magnitude than those determined in other chambers (Table III.1) and led to an ozone life time which was in the range between 6 and 14 hours.

Table III.1: Wall loss of ozone and its corresponding lifetime ($\tau_{O_3} = 1/k_{O_3}$) measured in several simulation chambers under dark conditions.

Chamber	Material	Volume (m ³)	$k_{O_3 \text{ wall loss}}$ (s ⁻¹)	τ_{O_3} (h)	Reference
NIES	Stainless steel	6.1	1.1×10^{-5}	25.2	(Akimoto et al., 1979a)
AIDA	Aluminium	90	3.9×10^{-5}	7.1	(Bunz et al., 1996)
EUPHORE	Teflon	200	3×10^{-6}	92.6	(Martín-Reviejo and Wirtz, 2005)
UCR EPA	Teflon	90	2.2×10^{-6}	126.2	(Carter, 2006)
TSC	Teflon	2	1.0×10^{-5}	27.8	(Wu et al., 2007)
CESAM	Stainless steel	4.2	3.4×10^{-5}	8.2	(Wang et al., 2011)
GIG-CAS	Teflon	30	2.1×10^{-6}	132.3	(Wang et al., 2014)
<i>CHARME</i>	Stainless steel	9.2	$(2.0 - 4.5) \times 10^{-5}$	13.9 - 6.2	This study

III.7.2 Hydrocarbons

The wall losses of a set of organic gases having different molar masses, were measured in *CHARME* (see Table III.2). The determined rates describe the wall reactivity of the reactor and can be used as a dataset for future computer modeling.

To determine the wall losses of VOCs, a certain concentration (50 ppb - 300 ppb) of each compound was injected into *CHARME* and continuously monitored in the presence of the four mixing fans operating at a speed of 190 rpm each. The dark decay of the compounds was treated as a first order reaction as presented for some compounds in Figure S.3 and the results showed wall loss rates in the range of 10^{-6} s^{-1} - 10^{-5} s^{-1} corresponding to life times between 12 - 84 hours.

Table III.2: The wall loss rate of several gaseous species determined in *CHARME*.

VOC	Formula	Molar mass (g mol ⁻¹)	First order wall loss rate (s ⁻¹)	τ_{VOC} (hour)
Acetone	C ₃ H ₆ O	58.0	8.2×10^{-6}	34
Acetonitrile	C ₂ H ₃ N	41.0	3.5×10^{-6}	79
α -pinene	C ₁₀ H ₁₆	136.2	8.7×10^{-6}	32
Benzene	C ₆ H ₆	78.1	7.5×10^{-6}	37
cis-2-pentene	C ₅ H ₁₀	70.1	7.2×10^{-6}	39
Cyclohexanone	C ₆ H ₁₀ O	98.1	1.2×10^{-5}	23
Formaldehyde	CH ₂ O	30.0	7.1×10^{-6}	39
Formic acid	CH ₂ O ₂	46.0	8.3×10^{-6}	34
γ -terpinene	C ₁₀ H ₁₆	136.2	9.6×10^{-6}	29
Isoprene	C ₅ H ₈	68.1	3.3×10^{-6}	84
Methoxyphenol	C ₇ H ₈ O ₂	124.1	2.3×10^{-5}	12
2-methyl-2-butene	C ₅ H ₁₀	70.1	8.1×10^{-6}	34
Propene	C ₃ H ₆	42.0	3.3×10^{-6}	84
Toluene	C ₇ H ₈	92.1	9.0×10^{-6}	30

III.7.3 Particles

One of the critical parameters to be characterized before performing aerosol studies in simulation chambers is the wall loss of particles. This measurement performed in the absence of any chemical reaction, determines the maximum duration of an experiment dealing with aerosols. Thus, it is important to have low wall losses of particles, which is to have aerosols in suspension in the reactor with a sufficiently long lifetime.

A set of experiments was performed in *CHARME*, to test the influence of different parameters on the wall loss rate of particles. The aerosol type (inorganic, SOA...), the initial concentration of the seeds or SOA precursors and the particle size were investigated.

During these tests, inorganic particles were represented by crystalline silica (SiO₂) and ammonium sulfate ((NH₄)₂SO₄). As illustrated in **Figure III. 17**, SiO₂ particles were added into a beaker and mixed by a stirring plate. Meanwhile, a controlled flow of nitrogen (carrier gas) was passed to nebulise the particles, and transfer them to an Erlenmeyer flask used as a buffer volume for uniformly mixing SiO₂ particles before introducing them into *CHARME*.



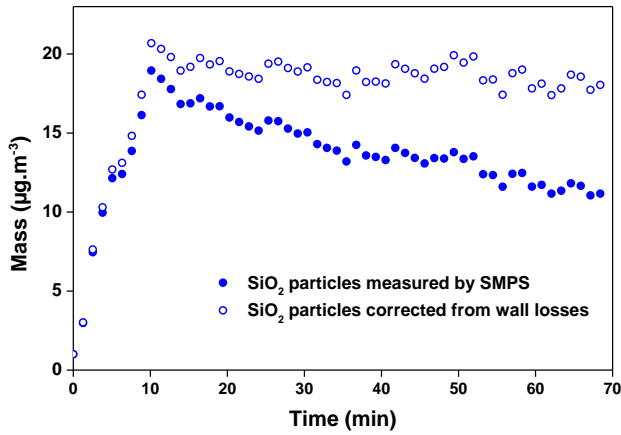
Figure III. 17: Setup used to introduce SiO₂ particles into the CHARME.

(NH₄)₂SO₄ seeds were generated by atomizing (Atomizer TSI 3076) different concentrations (2 - 6 g.L⁻¹) of the saline solutions, dried and then introduced into the chamber as polydispersed particles. Additionally, Nigrosine (C₂₂H₁₄N₆Na₂O₉S₂) was used as a primary organic aerosol. It is considered as a model for spherical and highly absorbing particles (**Washenfelder et al., 2013**). Similar to the generation method of inorganic particles, these aerosols were produced from the aqueous solutions of Nigrosine (which is water-soluble) in distilled water (at 2 g L⁻¹). Also, secondary organic aerosols formed from the ozonolysis of α-pinene (50 ppb - 320 ppb) and γ-terpinene (50 ppb - 500 ppb) were used to measure the wall loss of SOA. During these experiments the 4 mixing fans were continuously rotating with a speed of 190 rpm.

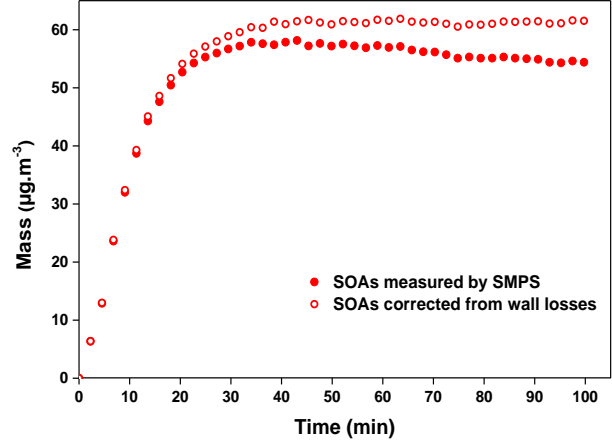
The wall loss of particles is a first-order reaction. It is determined once the mass concentration of the particles starts to decay as shown in **Figure III.18**. At the end of each experiment, the measured mass concentrations have to be corrected for wall deposition according to the following equation:

$$\text{(Eq. III.3)} \quad M_{\text{corrected}}(t) = M_{\text{measured}}(t) + (M_{\text{measured}}(t) \times k_{\text{wall}} \times t)$$

where M_{measured} is the mass concentration of the particles measured by the SMPS, k_{wall} is the calculated wall loss, (t) is the time of each scan of measurement and $M_{\text{corrected}}$ is the mass concentration corrected from the wall loss.



(a)



(b)

Figure III.18: Time profiles for the measured (solid circles) and corrected (open circles) mass concentrations of SiO₂ particles (a) and SOAs (b) formed from the ozonolysis reaction of α -pinene ([α -pinene]₀ = 70 ppb and [O₃]₀ = 490 ppb).

Table III.3 summarizes the wall losses measured in *CHARME* for different particles types.

Table III.3: Wall loss rates of different types of particles determined in *CHARME*.

Particle	Precursor(s)	Mass ($\mu\text{g}\cdot\text{m}^{-3}$)	D* (nm)	$k_{\text{particle wall loss}} (\text{s}^{-1})$	τ (hr)
Inorganic	SiO ₂	18	500	1.0×10^{-4}	2.8
		100	500	1.7×10^{-4}	1.6
		100	200	8.8×10^{-5}	3.2
	(NH ₄) ₂ SO ₄	30	50	1.4×10^{-5}	19.8
		127	102	2.7×10^{-5}	10.3
Organic	Nigrosin	25	250	3.2×10^{-5}	8.7
SOA	α -pinene + O ₃	58	83	2.2×10^{-5}	12.7
		141	95	3.7×10^{-5}	7.5
		790	133	4.4×10^{-5}	6.3
	γ -terpinene + O ₃	46	73	3.4×10^{-5}	8.2
		252	121	5.9×10^{-5}	4.7
		1220	130	8.1×10^{-5}	3.4

*D corresponds to the median diameter at maximum particle mass concentration.

Based on the presented results, it was observed that the loss rate for organic and inorganic aerosols were in a similar range.

The life time of inorganic particles injected into *CHARME*, varied from 2 hours up to 20 hours. The values were dependent on the particle size, for example by comparing the life time of SiO₂ particles having the same mass (100 µg.m⁻³) but different diameters (d₁=200 nm and d₂= 500 nm), it was shown that (d₁) revealed a higher life time than (d₂). Also, the results have shown that the wall uptake was reliant on the mass concentration of the particles, for instance the lifetime of SiO₂ particles having the same diameter (d=500 nm) but different mass concentrations (C₁=18 µg.m⁻³ and C₂= 100 µg.m⁻³) decreased with the increase in mass ($\tau_{C1} = 2.8 \text{ hour} > \tau_{C2} = 1.6 \text{ hour}$).

For experiments dealing with organic particles, Nigrosin (diameter of 250 nm and mass concentration of 25 µg.m⁻³) exhibited a life time of around 9 hours. However, the residence duration for SOA formed from ozonolysis of α -pinene and terpinene (with a size distribution centered at around 70 nm - 130 nm) ranged between 3 and 12 hours, depending on the mass of the aerosols formed which is linked to the initial concentration of the precursors.

It is apparent that the life time of aerosols is dependent on the different particle's properties including chemical composition, concentration, density, diameter, and vapor pressure (for SOA), in addition to some influencing parameters such as the material of the chamber and its surface to volume ratio (**Massabò et al., 2018**). Moreover, the mixing process inside the reactor, the turbulent and Brownian diffusion phenomena, the gravitational settling and sedimentation, and the adsorption and coagulation, one or all of these combined, explain the losses of particles on the walls (**Wu et al., 2007**).

As displayed in **Table III.4**, the aerosols lifetimes measured in *CHARME* are in the same range of the values reported for other chambers.

Table III.4: Particle wall loss rates in different simulation chambers.

Chamber	Material	Volume (m ³)	Lifetime (h)	Reference
EUPHORE	Teflon	200	5.6	(Martín-Reviejo and Wirtz, 2005)
UCR EPA	Teflon	90	3.4	(Carter, 2006)
CESAM	Stainless steel	4.2	10	(Wang et al., 2011)
GIG-CAS	Teflon	30	5.9	(Wang et al., 2014)
CMU	Teflon	12	2.5	(Donahue et al., 2012)
<i>CHARME</i>	Stainless steel	9.2	2-20	This study

In short, the determination of the wall loss rate is an important parameter to know, before performing chamber investigations for any new species (gases and aerosols) as it describes the maximum duration of the experiments. *CHARME*, displayed acceptable wall losses of gases and particles, so it can be used for relatively long (a few hours) atmospheric gas and particle investigations.

III.8 Cleaning

It is critical to have an efficient cleaning method to minimize the memory effects caused by deposition of species on the chamber walls and to ensure the absence of residual gases and particles that might interfere with new experimental results.

Three methods were considered for cleaning *CHARME*, a quick daily process (a), a chemical desorption method by ozone treatment carried out once in a while (b) and a laborious one that is performed after several days/weeks of running experiments (c).

III.8.1 Daily cleaning

Before the start of each experiment, the chamber is evacuated to a low pressure ($P < 10$ mbar) and then filled with purified air to reach atmospheric pressure. As previously shown in [Figure III.1](#), the evacuation process is fulfilled within ~50 minutes and is followed by a filling

process within 9 minutes as presented in **Figure III.3**. Thus, the daily cleaning method performed in *CHARME* is considered relatively short and accomplished in 60 minutes.

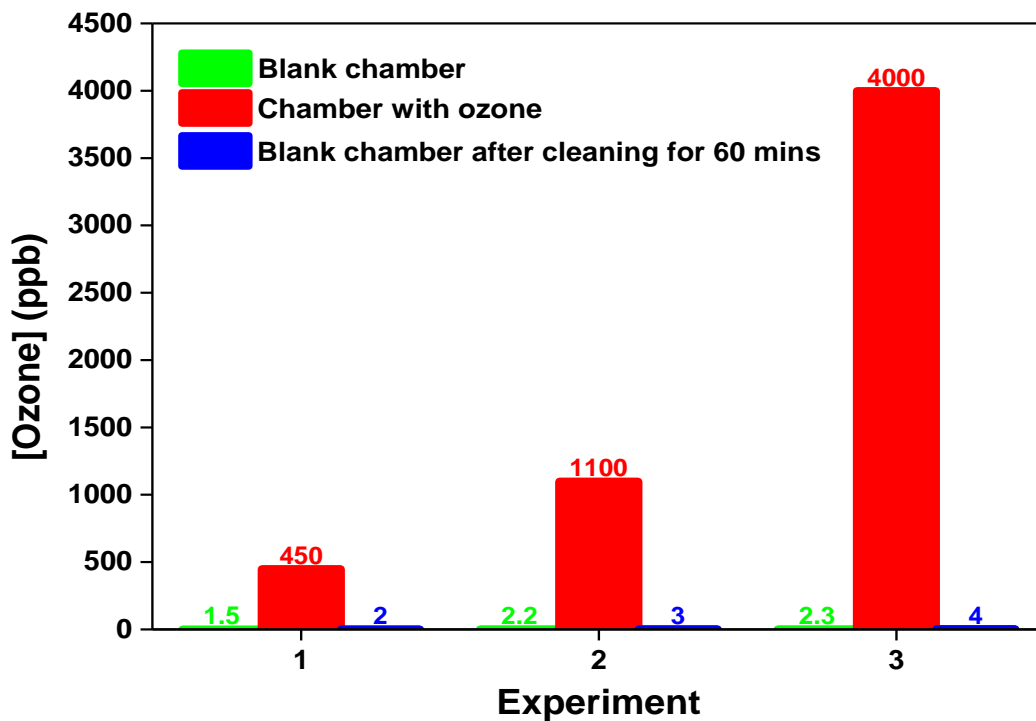
To test the efficiency of the cleaning process and to ensure that the walls of the chamber are free of any residual compounds from previous experiments, ozone (a), VOCs (b) and SOA (formed from ozonolysis of γ -terpinene) (c) have been introduced into the chamber and their concentrations were monitored before and after each experiment.

Figure III.19 (a), indicates that the cleaning process is efficient to remove ~99 % of the injected quantity of ozone regardless of its concentration (450 ppb, 1100 ppb and 4500 ppb).

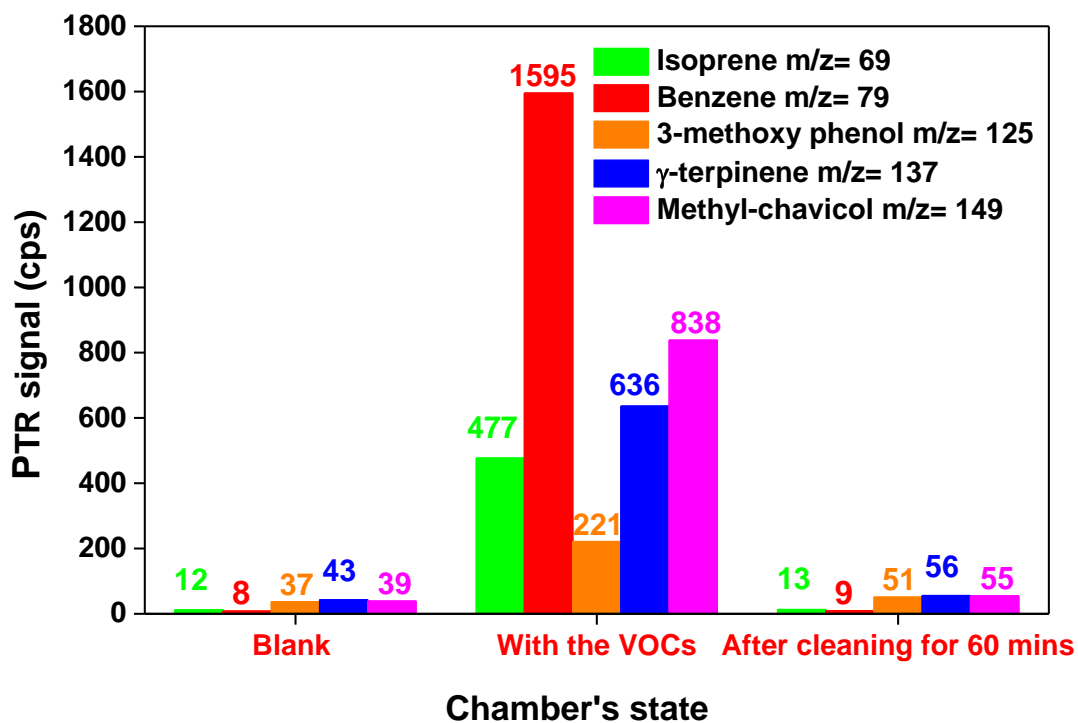
On the other hand, to examine the effectiveness of the cleaning method in removing organic gases, 100 ppb of the following VOCs (isoprene, benzene, 3-methoxyphenol, γ -terpinene and methyl chavicol) was injected in *CHARME*. The results represented in **Figure III.19 (b)**, show an efficiency of cleaning in the range of 92% - 99%. The structure and properties of the studied compounds play a major role in the efficacy of its cleaning. For instance, the PTR signal of 3-methoxyphenol, which is known to be a sticky compound, decreased from 221 to 51 cps after the cleaning method keeping ~ 6% of residuals. However, the memory effects for other VOCs like isoprene or benzene were less evident with a retention fraction of less than 1%. Nevertheless, thanks to the PTR-MS used for the online monitoring of VOCs concentration, it is possible to verify the state of cleanliness of the chamber before and after each experiment and based on the results it is possible to modify the cleaning time.

Regarding the removal of aerosols, **Figure III.19 (c)** displays three different number concentrations (24×10^3 particle/cm³, 24×10^4 particle/cm³ and 42×10^4 particle/cm³) of SOA formed from different mixing ratios of α -pinene and ozone. The particle background measured after cleaning the chamber showed low number concentration of particles (<20 particle/cm³), thus this attests that the method was capable of cleaning the chamber *CHARME* from organic aerosols, regardless, their concentrations.

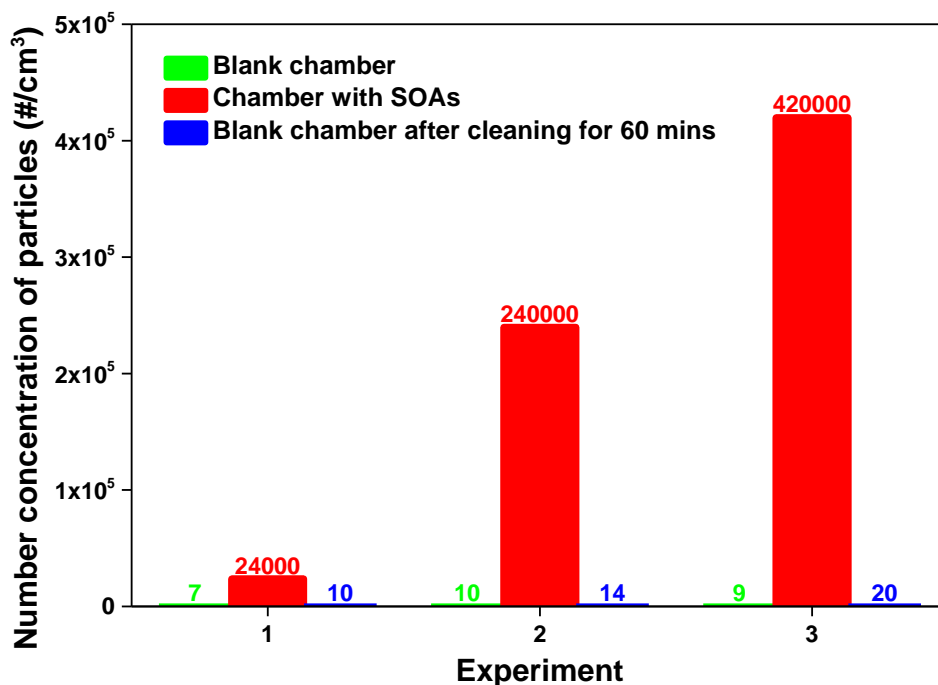
In summary, 60 minutes proved to be a sufficient time to remove the injected gases and particles, but this cleaning time could be extended or additional cycles of cleaning could be performed if it is necessary (for example for sticky compounds). The relatively short duration of the cleaning process allows the performance of 2 to 3 experiments per day.



(a)



(b)



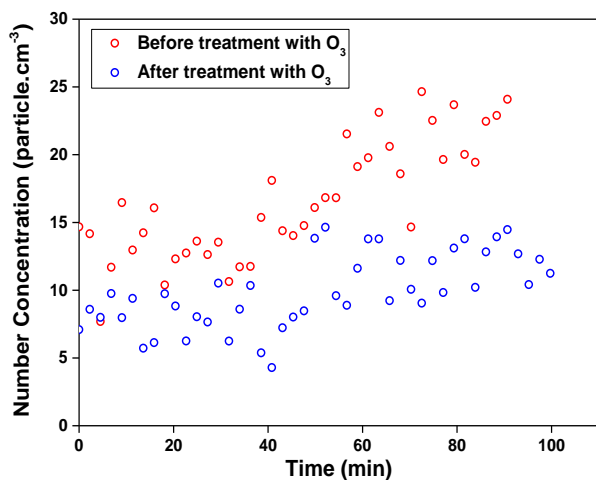
(c)

Figure III.19: Cleaning test: Evolution of different concentrations of ozone (a); VOCs (PTR signals) (b) and SOA (ozonolysis of α -pinene) (c).

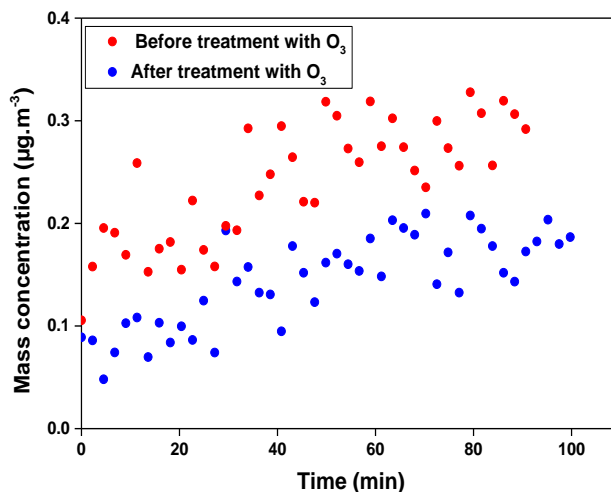
III.8.2 Ozone treatment

After performing experiments involving the use of high concentrations of VOCs, especially sticky ones, it is recommended to introduce high concentration (10-100 ppm) of ozone for several hours to activate the desorption of different impurities.

At the end of a measurement campaign involving SOAs formation from the ozonolysis of γ -terpinene, a concentration of 14 ppm of ozone was introduced into the chamber and kept for around 12 hours. The chamber blanks were checked after the exposure to ozone and compared to those recorded before O₃ treatment. **Figure III.20** illustrated the results for each blank and revealed that ozone was capable of oxidizing some of the organic compounds adsorbed on the walls and thus reduced the initial number and mass concentrations of the particles from ~ 20 particles.cm⁻³ to ~ 10 particles.cm⁻³ and from 0.25 μ g.m³ to 0.15 μ g.m³, respectively.



(a)



(b)

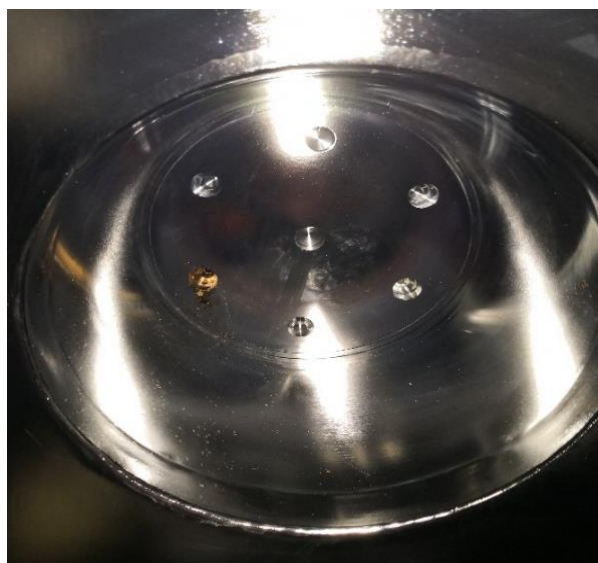
Figure III.20: Time profile of the number and mass concentration of particles measured in the dark before and after treating the chamber by ozone (14 ppm) for 12 hours.

III.8.3 Manual cleaning

Regularly and after running several manipulations, a manual cleaning of the chamber is required, especially if the performed experiments involve high concentrations of VOCs or particles (see [Figure III.21](#)).



(a)



(b)

Figure III.21: Photo of the chamber inside contaminated with NaCl particles (a) and NO₂ (b).

It is possible to enter into *CHARME* after respecting all the safety precautions of wearing a mask, gloves, and clean room clothing as seen in [Figure III.22](#). The chamber was manually cleaned with cleanroom paper and ethanol to remove all the deposited chemicals and particles. Then the walls were wiped with ultrapure water to remove the residuals of ethanol, further the chamber was pumped for 1-hour minimum to ensure the total elimination of gases or vapors.



Figure III.22: Manual cleaning of the *CHARME* chamber.

III.9 Purified air analysis

As mentioned previously in section [II.1.3](#), *CHARME* is supplied with purified air produced from an air compressor coupled to a drying and purification system (Parker Zander KAMT).

III.9.1 Characteristics of the purified air

To verify the purity and dryness of the cleaned air supplied into the laboratory, different analyses were performed at the outlet of lines carrying air directly from the generator and drier and inside the chamber. The results of the tests are shown in [Table III.5](#).

Table III.5: The different characteristics of purified air in the outlet line and in the chamber.

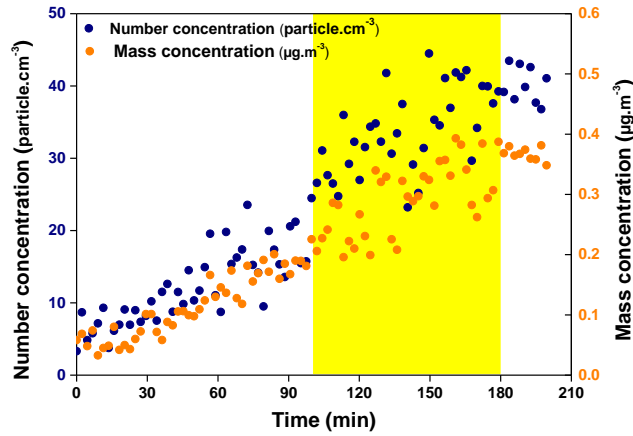
Species	Concentration/ Parameter	
	Purified air in the outlet line	Purified air in the chamber
O ₃	< 1 ppb	1.3 ppb
NO ₂	< 0.1 ppb	0.4 ppb
NO	< 0.1 ppb	0.1 ppb
CO	< 1 ppb	< 1 ppb
Particles	1 #.cm ⁻³	10 #.cm ⁻³
	< 0.1 µg.m ⁻³	0.1 µg.m ⁻³
RH	1.6%	1.7%

The findings showed that the air supplied to *CHARME* is clean and dry.

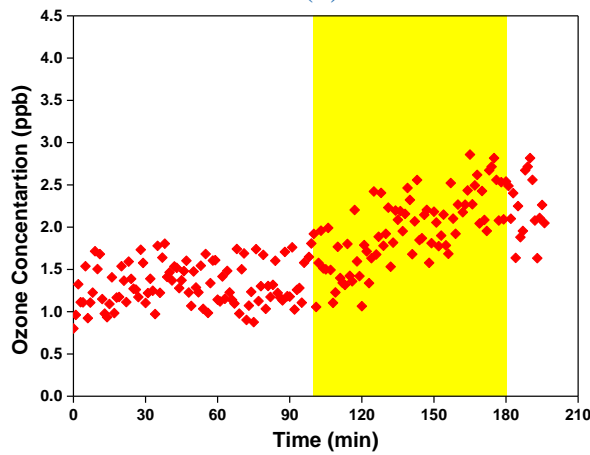
III.9.2 Reactivity of purified air

To test the background reactivity of *CHARME*, the chamber was filled with purified air and then irradiated for around 80 minutes. **Figure III.23**, shows the concentrations of ozone, NO₂, NO and particles, before and after switching on the xenon lamps. As presented in the graph **Figure III.23 (a)**, the average number and mass concentrations of particles were equivalent to ~15 particle.cm⁻³ and ~0.15 µg.m⁻³ in the dark, but they increased to reach ~ 40 particle.cm⁻³ and ~ 0.4 µg.m⁻³ upon irradiation. Also, in **Figure III.23 (b)**, it is shown that the ozone mixing ratio did not vary significantly when the lamps were off and increase to ~1.5 ppb after ~ 80 minutes of irradiation. Both findings could be explained by the occurrence of photochemical reactions involving traces of NO_y and HCs remaining in the chamber, without ignoring the possibility of desorbing these species from the walls.

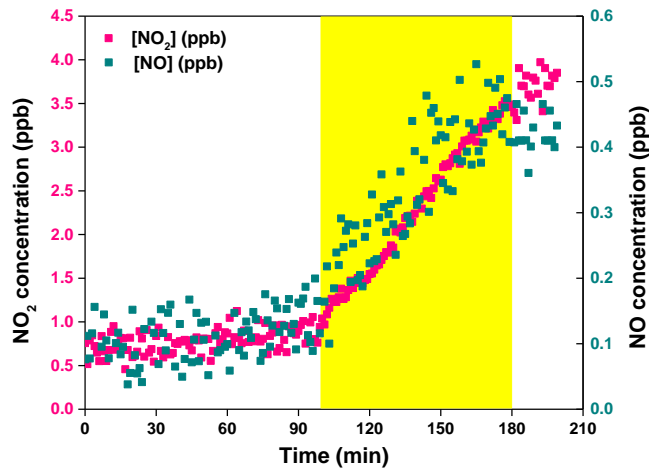
Moreover, as displayed in **Figure III.23 (c)**, the concentrations of NO and NO₂ did not rise in the dark and increase from 0.1 ppb to 0.5 ppb and from 0.5 ppb to 3.5 ppb with irradiation, respectively. These observations might be explained by the direct off-gassing of these species which are known to be sticky (especially NO₂), and/ or due to the off-gassing of some compounds like alkyl nitrates which are known to interfere with the chemiluminescence method in the measurement of the NO₂ concentrations.



(a)



(b)



(c)

Figure III.23: Time profile of the ozone concentration (a), NO₂ and NO concentrations (b) and mass and number concentrations for particles, before and during irradiating (yellow region) the blank chamber.

III.10 Light characterization

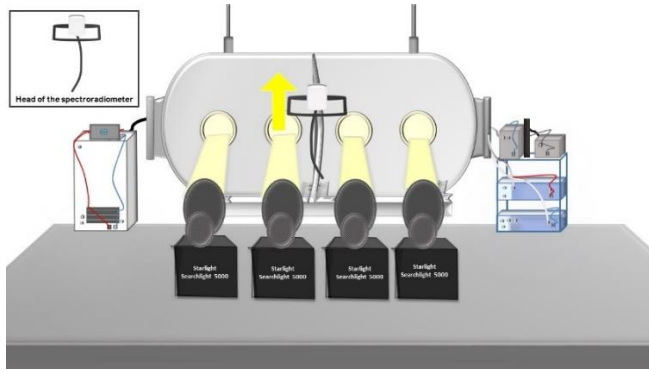
In the atmosphere, some pollutants and chemicals are photolyzed by the sun light. In fact, ultraviolet and visible solar radiations are responsible for the dissociation of several molecules into reactive species which further participate in atmospheric chemical cycles and drive much of the tropospheric chemistry (Shetter, 2003). The measurements of atmospheric photolysis frequencies are very important in the study of atmospheric chemical processes as they are directly related to the atmospheric lifetime of photolabile species.

Simulation chambers are capable of simulating photochemical processes in the troposphere, under the conditions of having a realistic and stable source of irradiation. Artificial radiation used to illuminate indoor simulation chambers might produce a spectrum different from the solar one. The irradiation intensity and the spectral distribution of the irradiation source inside the chamber must be checked periodically as the lamps may age with time.

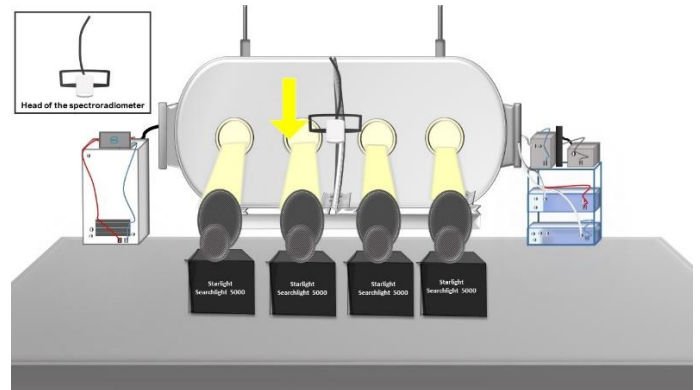
The light source used to irradiate *CHARME* is composed of four xenon lamps (5 kW each) which provide the most accurate reproduction of the solar spectrum at the earth's surface in the wavelength region 290-700 nm

III.10.1 Light intensity and spectral distribution

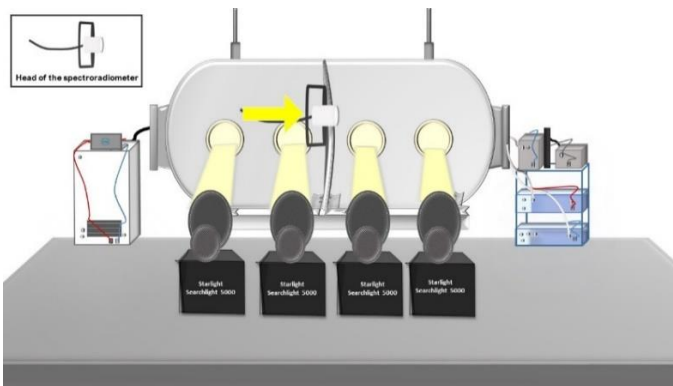
To characterize the light inside the chamber, a spectroradiometric measurement at a single point was performed with a spectroradiometer (Ultra-fast CCD-Detector Spectrometer, Metcom). The head of the spectroradiometer was introduced into the chamber from port C2 (see [Figure II.3](#)) fixed at one position (chosen to be almost at the centre of the chamber) and oriented towards different directions as presented in [Figure III.24](#). It was planned to perform similar examinations at numerous positions into the chamber, for the comparison of the different spectra and the JNO_2 and JO^1D values, however, this was not achievable due to the fragility of the detector which was broken during one of our measurements.



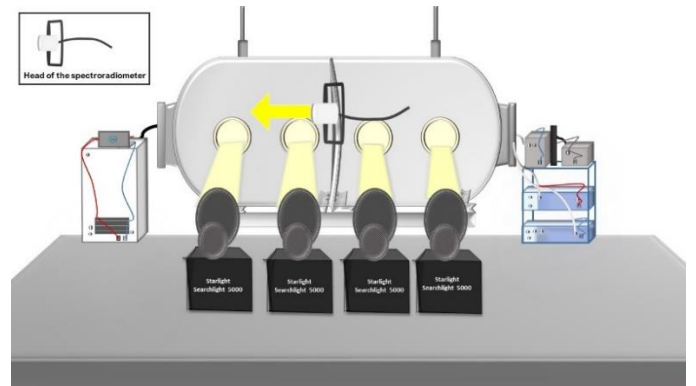
(a)



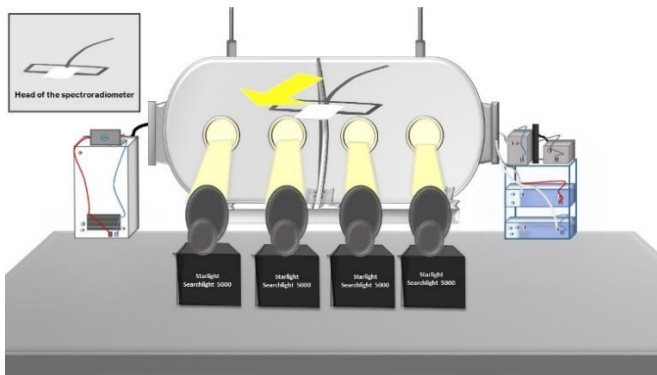
(b)



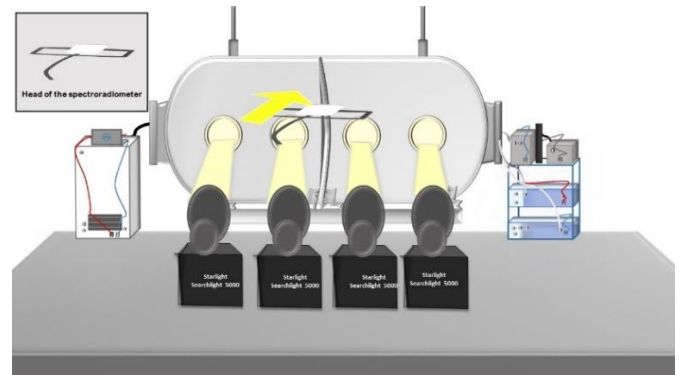
(c)



(d)



(e)



(f)

Figure III.24: Different orientations of the head of the spectroradiometer: upwards (a), downwards (b), right (c), left (d) of the chamber and towards (e) / away (f) from the lamps.

The performed experiment was not an ideal examination; however, it allowed to measure the intensity and the spectral distribution of the light in *CHARME*. As shown in [Figure III.25](#), the different orientations of the detector lead to various values of the light intensities which are recorded with the spectroradiometer. This was expected as at each position the available irradiation

corresponds to both direct and reflected light. The maximum values were monitored when the head of the instrument was positioned upwards of the chamber.

As displayed in **Figure III.25**, the lamps started to emit light at wavelength ~ 315 nm but their intensity was significant ($I \geq 0.1$) starting from $\lambda \sim 340$ nm. So, the lowest wavelength (315 nm) available in the chamber is not consistent with the value recorded in the troposphere (290 nm). Besides, all the measured spectra, unexpectedly, displayed a large absorption band between 365 nm and 420 nm. These observations allow to deduce that there is a problem with the xenon lamps and this can be overcome by changing the ampules of the projectors.

On the other side, the irradiation recorded in the chamber were the same as that measured inside the housing room indicating that the quartz windows did not filter the radiation produced by the xenon lamps.

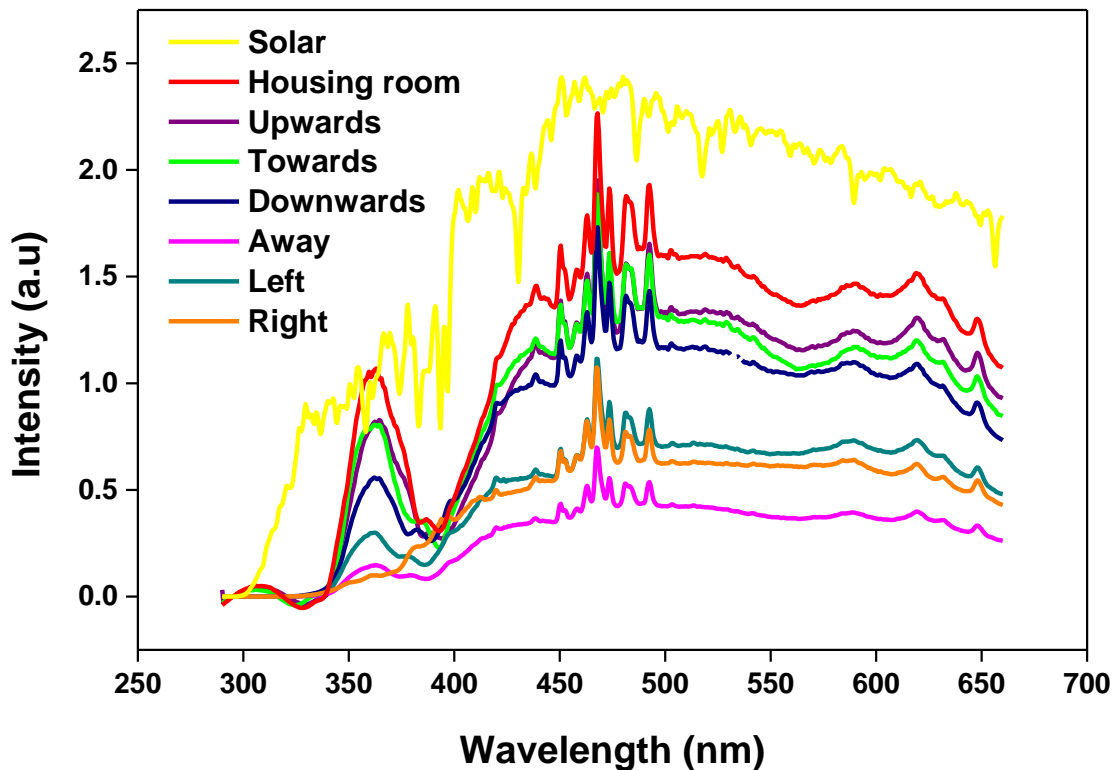


Figure III.25: Emission spectra : (i) of the xenon lamps recorded inside the chamber at a single position and for different orientations of the spectroradiometer and in the housing room of the lamps; (ii) of the sun measured in Dunkerque (51°2'N 2°22' E; 16/07/2019 at 14:19 local time). *The used spectroradiometer allows to measure wavelengths from 290 nm to 660 nm.

III.10.2 Photolysis frequency of NO₂

The majority of photolysis reactions in the troposphere occur at wavelengths between 290 nm and 400 nm. NO₂ is one of the major photolabile species in the atmosphere, this molecule strongly absorbs light in the spectral region lower than 420 nm, where most of the photochemical reactions occur. The determination of the NO₂ frequency photolysis (J_{NO_2}), is considered as a standard test to characterize the light source in simulation chambers (**Finlayson-Pitts and Pitts Jr, 1999**); it was determined in *CHARME* through spectroradiometric (i) and actinometric (ii) measurements.

III.10.2.1 Spectroradiometric measurement

The determination of J_{NO_2} in *CHARME* through spectroradiometric measurements was performed as previously detailed in section (III.10.1) dedicated to the light characterization. Depending on the orientation of the detector, the J_{NO_2} ranges from 1.8×10^{-3} to $3.7 \times 10^{-3} \text{ s}^{-1}$; however, as these values were recorded at a single position of the spectroradiometer, they are not representative of all the chamber and another determination has been done by actinometry.

III.10.2.2 Actinometric measurement

It is possible to determine the photolysis frequencies through ‘chemical actinometry’ experiments, which involve measurements of the rate of photolysing a gaseous precursor, taking into account the change in concentrations of this molecule and/or the formed product(s) (**W. Carter et al., 1995**).

III.10.2.2.1 Measurement in purified air

A series of NO₂ actinometry experiments (four) have been conducted in *CHARME*. Concentrations of NO₂ (100 ppb - 200 ppb) were introduced in the dark, stabilized for a few minutes and then irradiated with the xenon lamps. As shown for one of the experiments in **Figure**

III.26, once the irradiation was on, the dissociation of NO₂ resulted in the formation of NO and O₃ as explained by Reactions (R. III.2 to (R. III.4).

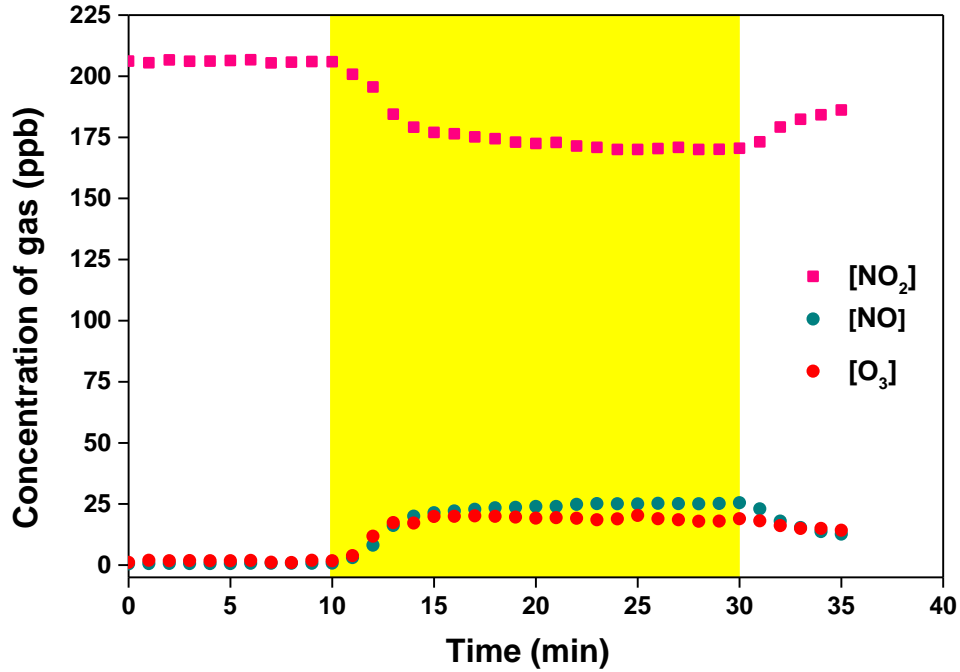


Figure III.26: JNO_2 determination from the photolysis of NO₂ (210 ppb) in air (the yellow region corresponds to the time when lamps were switched on).

After around 8 minutes of irradiation, the concentrations of NO, NO₂, and O₃ reached a photostationary state in CHARME and the value of JNO_2 can be calculated from the equation (Eq. III.4) given by Wu and Niki, (1975):

$$(Eq. III.4) \quad JNO_2 = \frac{k_{NO+O_3}[NO][O_3]}{[NO_2]}$$

where $k_{NO+O_3} = 1.8 \times 10^{-14} \text{ cm}^3 \text{ molecule}^{-1} \text{ s}^{-1}$ is the rate coefficient of the reaction between O₃ and NO at 298 K (Atkinson et al., 2004a), and [O₃], [NO] and [NO₂] are the equilibrium concentrations in (molecule.cm⁻³) given by the ozone analyzer and the chemiluminescence NO_x analyzer, respectively. Photochemical equilibrium was quickly reached and considering that the loss and formation phenomena compensate each other then:

$$\text{(Eq. III.5)} \quad \frac{d[\text{NO}_2]}{dt} = -J\text{NO}_2 + k_{\text{NO}+\text{O}_3}[\text{NO}][\text{O}_3] = 0$$

Note that the gas concentrations started to change immediately when they entered the dark sampling line before reaching the gas analyzers. Therefore, gas concentrations were corrected from the residence time into the inlet lines of the analyzers, which was estimated at 1.4 s. Consequently, the average NO₂ photolysis rate obtained in *CHARME* was equal to $1.17 \times 10^{-3} \text{ s}^{-1}$.

III.10.2.2.2 Measurement in N₂

The most widely technique used to measure $J\text{NO}_2$ in simulation chambers is to irradiate NO₂ in a nitrogen atmosphere. The photolysis of NO₂ in N₂ is not a first-order process because of a number of side reactions that occur in addition to this reaction **(R. III.2)** (Holmes et al., 1973; Bohn et al., 2004). The mechanism for NO₂ photolysis proposed by Ford and Endow, (1957) and Schuck and Stephens, (1969) is presented in **Table III.6**.

Table III.6: The set of reactions involved in the photolysis of NO₂ and their rate coefficients (Atkinson et al., 2004b).

N°	Mechanism	Rate coefficient
(R. III.2)	$\text{NO}_2 + h\nu \rightarrow \text{NO} + \text{O}$	$J\text{NO}_2$ to be determined
(R. III.3)	$\text{O} + \text{O}_2 + \text{M} \rightarrow \text{O}_3 + \text{M}$	$k_3 = 5.6 \times 10^{-34} \text{ cm}^6 \text{ molecule}^{-2} \text{ s}^{-1}$
(R. III.4)	$\text{O}_3 + \text{NO} \rightarrow \text{NO}_2 + \text{O}_2$	$k_4 = 1.8 \times 10^{-14} \text{ cm}^3 \text{ molecule}^{-1} \text{ s}^{-1}$
(R. III.5)	$\text{O} + \text{NO}_2 \rightarrow \text{NO} + \text{O}_2$	$k_5 = 1.0 \times 10^{-11} \text{ cm}^3 \text{ molecule}^{-1} \text{ s}^{-1}$
(R. III.6)	$\text{O} + \text{NO}_2 + \text{M} \rightarrow \text{NO}_3 + \text{M}$	$k_6 = 1.3 \times 10^{-31} \text{ cm}^6 \text{ molecule}^{-2} \text{ s}^{-1}$
(R. III.7)	$\text{NO}_3 + \text{NO} \rightarrow 2 \text{NO}_2$	$k_7 = 2.6 \times 10^{-11} \text{ cm}^3 \text{ molecule}^{-1} \text{ s}^{-1}$
(R. III.8)	$\text{O} + \text{NO} + \text{M} \rightarrow \text{NO}_2 + \text{M}$	$k_8 = 1.0 \times 10^{-31} \text{ cm}^6 \text{ molecule}^{-2} \text{ s}^{-1}$
(R. III.9)	$2 \text{NO} + \text{O}_2 \rightarrow 2 \text{NO}_2$	$k_9 = 2.0 \times 10^{-38} \text{ cm}^6 \text{ molecule}^{-2} \text{ s}^{-1}$
(R. III.10)	$\text{NO}_3 + \text{NO}_2 \rightarrow \text{N}_2\text{O}_5$	$k_{10} = 1.9 \times 10^{-12} \text{ cm}^3 \text{ molecule}^{-1} \text{ s}^{-1}$
(R. III.11)	$\text{N}_2\text{O}_5 \rightarrow \text{NO}_3 + \text{NO}_2$	$k_{11} = 6.9 \times 10^{-2} \text{ s}^{-1}$
(R. III.12)	$\text{NO}_2 + \text{O}_3 \rightarrow \text{NO}_3 + \text{O}_2$	$k_{12} = 3.5 \times 10^{-17} \text{ cm}^3 \text{ molecule}^{-1} \text{ s}^{-1}$

In the absence of O₂, it is possible to assume that O, O₃, NO₃, and N₂O₅ are in pseudo steady state. Also under these conditions reactions **(R. III.9)** and **(R. III.12)** can be neglected. According to these assumptions, Schuck and Stephens, (1969) have proposed the following equation:

$$(Eq. III.6) \quad \frac{-2J_{NO_2}}{\frac{d\ln[NO_2]}{dt}} = 1 + \frac{k_6[M]}{k_5} + \frac{k_8[NO][M]}{k_5[NO_2]} + \frac{k_3[M][O_2]}{k_5[NO_2]}$$

where k corresponds to the rate coefficients for the reactions presented in **Table III.6** and $[M]$ is the concentration of the collision partner (N_2).

For the determination of J_{NO_2} in N_2 , five different experiments have been carried out in *CHARME*. The chamber was filled up to atmospheric pressure by pure N_2 supplied from a liquid nitrogen tank. Concentrations of NO_2 (100 ppb - 150 ppb) were then introduced, well mixed and then irradiated as illustrated for one of the tests in **Figure III.27**.

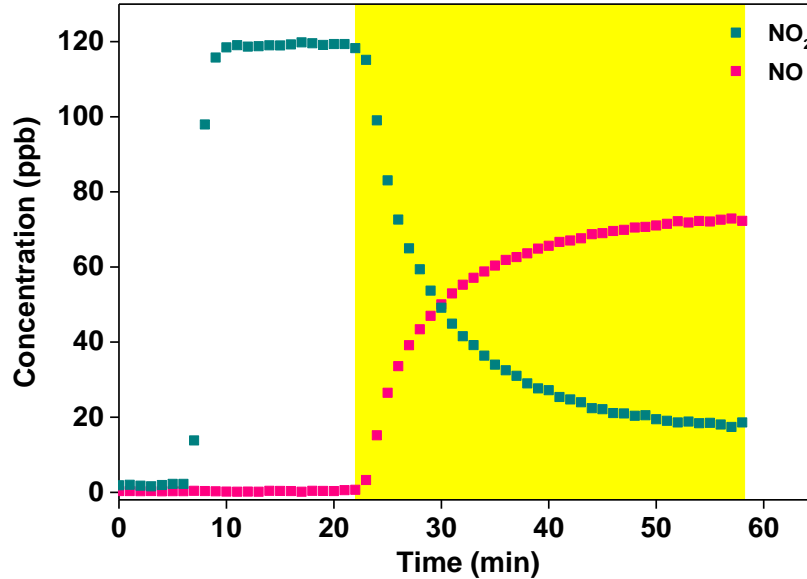


Figure III.27: Time profile of NO_2 (120 ppb) and NO during the photolysis of NO_2 in N_2 . (Yellow region corresponds to duration when the lamps are switched on).

At $[NO]_0$ and $[O_2]_0$ are equals to zero, so (Eq. III.7) is simplified to:

$$(Eq. III.7) \quad \frac{-2J_{NO_2}}{\frac{d\ln[NO_2]}{dt}} = 1 + \frac{k_5[M]}{k_4}$$

The rearrangement of (Eq. III.6) gives the following equation:

$$(Eq. III.8) \quad 2J_{NO_2} = -\frac{d \ln[NO_2]}{dt} \times \left(1 + \frac{k_5[M]}{k_4}\right)$$

Knowing that $[M] = 2.46 \times 10^{19}$ molecule cm^{-3} , $k_4 = 1.0 \times 10^{-11}$ cm^3 molecule $^{-1}$ s $^{-1}$ and $k_5 = 1.3 \times 10^{-31}$ cm^6 molecule $^{-2}$ s $^{-1}$ (Atkinson et al., 2004b), the plot of $\ln[NO_2]$ versus the time leads to the determination of (J_{NO_2}) as presented in Figure III.28.

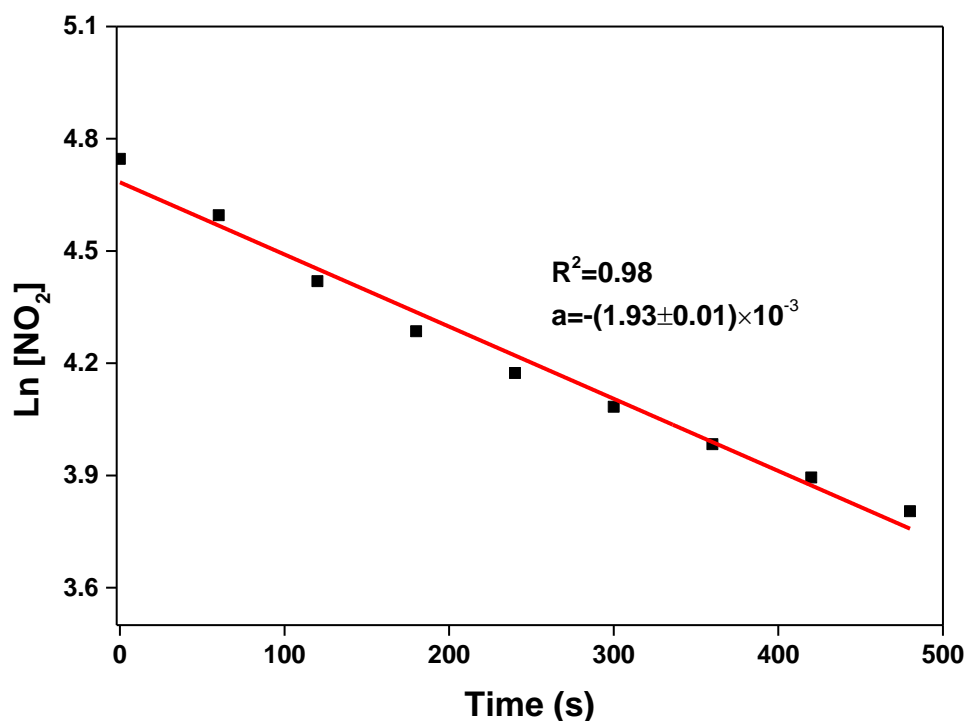


Figure III.28: Actinometry in N₂; NO₂ consumption versus the time ($[NO_2]_0 = 120$ ppb).

The average NO₂ photolysis frequency obtained through this method at full light intensity was $J_{NO_2} = 1.26 \times 10^{-3}$ s $^{-1}$.

This determination (in N₂) and the values of J_{NO_2} measured in air and with the spectroradiometer are very close as seen in Table III.7. In addition, they are also in the same order of magnitude than those measured in other chambers and in the real atmosphere as well (the J_{NO_2}) value recorded in Dunkerque (51°2N 2°22E) during a sunny day (16/07/2019 at 14:19 local time) was equal to 8.2×10^{-3} s $^{-1}$).

Table III.7: The different NO₂ photolysis rates determined in various chambers.

Chamber	Type of lamps	J _{NO₂} (s ⁻¹)	Reference
NIES (Stainless steel, 6 m ³)	Xenon arc lamps	4.2 × 10 ⁻³	(Akimoto et al., 1979a)
Caltech (Teflon, 28m ³)	Black lamps	2.5 × 10 ⁻²	(Cocker et al., 2001)
UCR-EPA (Teflon, 90 m ³)	Black lamps	3 × 10 ⁻³	(Carter et al., 2005)
HIRAC (Stainless steel, 2.2 m ³)	Black lamps	1.93 × 10 ⁻³	(Glowacki et al., 2007)
Tsinghua (Teflon, 2 m ³)	Black lamps	3.8 × 10 ⁻³	(Wu et al., 2007)
CESAM (Stainless steel, 4.4 m ³)	Xenon arc lamps	4.2 × 10 ⁻³	(Wang et al., 2011)
GIG-CAS (Teflon, 30 m ³)	Black lamps	8.1 × 10 ⁻³	(Wang et al., 2014)
Ilmari (Teflon, 29m ³)	Black lamps	10 × 10 ⁻³	(Leskinen et al., 2015)
<i>CHARME</i> (Stainless steel, 9.2 m ³)	Xenon arc lamps	1.2 × 10 ⁻³	This study, (Actinometry in zero air)
		1.3 × 10 ⁻³	This study, (Actinometry in N ₂)
		(1.8-3.7)*×10 ⁻³	This study, (Spectroradiometric measurement)
Dunkerque (51°2'N 2°22' E; 16/07/2019 at 14:19 local time)	Solar	8.2 × 10 ⁻³	This study, (Spectroradiometric measurement)

* It is a range depending on the orientation of the head of the spectroradiometer.

III.10.3 Homogeneity of irradiation

To check the light homogeneity inside *CHARME*, a mobile digital light sensor (IC BH1750FVI) was installed inside the chamber but the results are still under treatment.

III.11 Auxiliary mechanism

The simulation of atmospheric reactions in chambers requires the identification of processes which are induced by the reactor itself. The corresponding set of reactions, called "chamber auxiliary mechanism" is a key point in the validation of a simulation chamber (**Carter et al., 2005; Hynes et al., 2005**).

The propene-NO_x photo-oxidation experiment has been extensively used as a reference system for chamber qualification tests, especially for evaluating the gas-phase oxidation mechanism (**Akimoto et al., 1979b**). This photochemical system is considered as a model for the major tropospheric photochemical reactions, because propene has a well-known degradation mechanism consisting of 61 species and 202 reactions in the Master Chemical Mechanism MCMv3.2 (**Jenkin et al., 2003**). Briefly, the MCM is a near-explicit chemical mechanism that describes in detail the gas phase degradation of many VOCs and the formation of ozone and other secondary pollutants under tropospheric conditions (**Saunders et al. 2003**). The philosophy behind the construction of the MCM is to use available information on the kinetics and products of elementary reactions relevant to VOC oxidation to build up a near-explicit representation of the degradation mechanisms.

A propene-NO_x experiment was performed in *CHARME* and the initial conditions are represented in **Table III.8**.

Table III.8: Starting conditions for the NO_x-propene-air characterization experiment.

[Propene] (ppb)	[NO](ppb)	[NO ₂](ppb)	[Propene]/[NO _x]	RH (%)	T (K)
157	245	15	0.6	1.7	295

During these studies, NO and propene were injected in the chamber from gas bottles and their concentrations were followed by the NO_x analyzer and PTR-MS, respectively. Pure NO₂ was added using a gas syringe while O₃ was introduced from the ozone generator and both were monitored with NO_x and ozone analyzers, respectively. When the propene concentration was stable in the chamber, the xenon lamps were switched on to initiate the photochemical reactions. A rapid conversion of NO to NO₂ was detected and were followed by an ozone production in the reactor.

Then, a decay in the propene concentration was observed and correlated to its reaction with ozone. This oxidation was responsible for the formation of organic compounds such as formaldehyde and acetaldehyde which were sampled by DNPH cartridges (with a flow $Q = 1.2 \text{ L}\cdot\text{min}^{-1}$ for a duration of 10 min) and then quantified by HPLC with an UV detection (at 360 nm). Formaldehyde and acetaldehyde were also monitored with the PTR which was calibrated by comparison with the HPLC analyses.

The concentrations of the measured species were considered the raw data for modeling and were treated based on the auxiliary mechanism shown in **Table III.9**. Besides, some parameters including the wall loss rates for gases as well as the values of temperature, relative humidity and dilution were taken into account and integrated into the online modeling tool ‘AtChem’ (<http://mcm.leeds.ac.uk/MCMv3.2/>).

Table III.9: Auxiliary mechanism for the *CHARME* chamber.

N°	Reaction/parameter	Coefficient
(R. III.13)	$\text{NO}_2 + \text{wall-H}_2\text{O} \rightarrow \text{HONO} + \text{wall-HNO}_3$	$1.4 \times 10^{-6} \text{ (s}^{-1}\text{)}$
(R. III.14)	$\text{wall-HNO}_3 + \text{h}\nu \rightarrow \text{OH} + \text{NO}_2$	J_{HNO_3}
(R. III.15)	$\text{wall-NO}_2 + \text{h}\nu \rightarrow 0.5 \text{ NO} + 0.1 \text{ HONO}$	$1.4 \times 10^{-2} \text{ (s}^{-1}\text{)}$
(R. III.16)	$\text{wall} + \text{h}\nu \rightarrow \text{NO}_2$	$1.4 \times 10^{-3} \text{ (s}^{-1}\text{)}$
(R. III.17)	$\text{NO} \rightarrow \text{wall}$	$4.5 \times 10^{-6} \text{ (s}^{-1}\text{)}$
(R. III.18)	$\text{NO}_2 \rightarrow \text{wall}$	$3.0 \times 10^{-6} \text{ (s}^{-1}\text{)}$
(R. III.19)	$\text{O}_3 \rightarrow \text{wall}$	$2.2 \times 10^{-5} \text{ (s}^{-1}\text{)}$
	$[\text{HONO}]_0$	0 ppb - 2 ppb

The dark hydrolysis of NO_2 (**R. III.13**) on chamber wall to produce adsorbed HNO_3 and HONO which can be a source of OH radicals was taken into account and its rate coefficient was assigned at $1.4 \times 10^{-6} \text{ (s}^{-1}\text{)}$ based on the results from CASIRO chamber (**Hynes et al., 2005**).

The off-gassing of adsorbed HNO_3 leading to the formation of OH and NO_2 when the lights were switched on (**R. III.14**), was assumed to be equivalent to J_{HNO_3} (J_8 in table S1) which was calculate in *CHARME*.

The reaction that represents the transformation of NO_2 into NO and HONO on the chamber walls in the presence of light (**R. III.15**), was included in the mechanism. Except for

CESAM (Wang et al., 2011) which is a stainless steel chamber as *CHARME*, such reducing reaction was not taken into account in other chamber modules (Bloss et al., 2005; Hynes et al., 2005; Wang et al., 2014) and this particularity is explained by the material of the walls. Similar to Wang et al., (2011), the rate assigned to this reaction was equivalent to 1.4×10^{-2} (s⁻¹).

HONO is expected to be formed in the dark due to heterogeneous hydrolysis of NO₂ on the chamber walls (R. III.13), thus it could be present in experiments including NO_x. The initial concentration of HONO in *CHARME* was not measured but estimated. [HONO]₀ was the only adjustable parameter in the mechanism and the variation of its value was sensitive to the results of the modeling. Depending on the experiments, [HONO]₀ varied from 0 ppb to 2 ppb to best fit the experimental concentration profiles.

The desorption of NO₂ induced by light (R. III.16), was estimated based on simulation of experimental data and represent the NO₂ off-gassing rate which was found to be 1.4×10^{-3} (s⁻¹)

The wall losses of O₃, NO and NO₂ were measured in the dark from the decrease of their concentration (each compound was injected alone). These loss reactions presented through reactions (R. III.17) to (R. III.19) were also introduced in the numeric model.

The evaluation of the auxiliary mechanism was performed from the comparison between the observed and predicted concentrations of the investigated gaseous compounds (i.e. propene, O₃, NO, NO₂, HCHO and CH₃CHO).

The comparison of experimental and simulated concentration-time profiles of all gases (Figure III.29) showed a good agreement for the experiments performed with a HONO initial concentration of 1 ppb. It was observed that the simulations were affected when [HONO]₀ varied from 0 ppb to 2 ppb, so the initial HONO concentration is an important parameter which determines the propene oxidation rate. Wang et al., (2011), assumed that the initial HONO mixing ratio could be correlated to the time NO₂ were left in the chamber after their injection and before the start of the irradiation process. During the two performed experiments, this time was around 1 hour and could have resulted in the occurrence of minor reduction of NO₂ into HONO in the dark. A confirmation of this assumption requires the performance of additional experiments with different time for NO₂ left in the chamber. Also, a precise measurement of HONO is needed to investigate the parameters affecting the nitrous acid off-gassing (will be done by IBBCEAS in the near future).

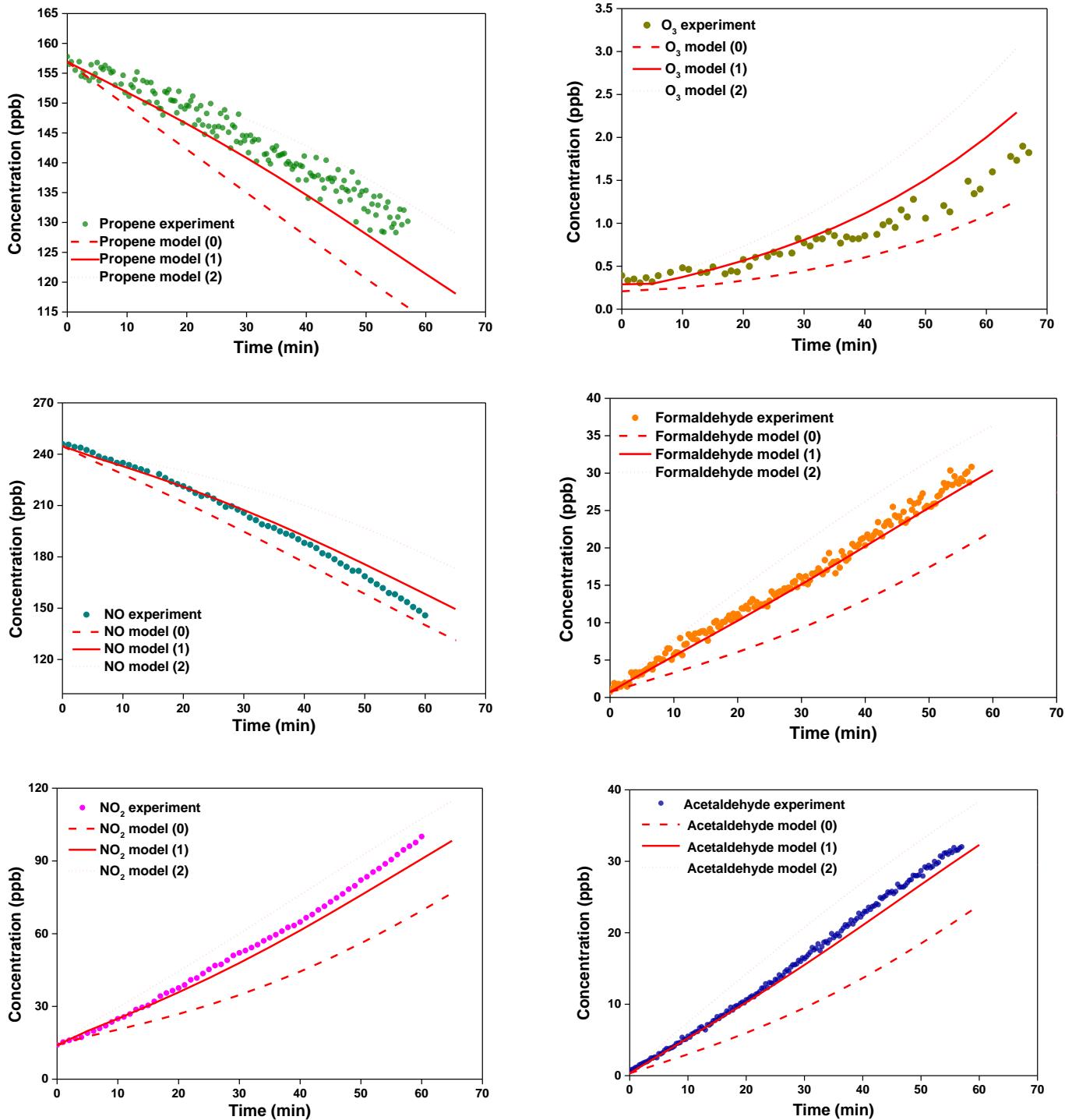


Figure III.29: Comparison of experimental (solid circles) and modeled (solid, dashed and dotted lines) concentrations of propene, NO, NO₂, O₃, formaldehyde and acetaldehyde in propene-NO_x system. Model (0), Model (1) and Model (2) correspond to results simulated with [HONO]₀= 0 ppb, 1 ppb and 2 ppb, respectively. Note that t=0 corresponds to the time when the lights are switched on.

In short, the agreement between the modeling and experimental results indicate no significant problems with the auxiliary mechanism performance. Therefore, a small number of reactions were enough to correctly reproduce the observations of the complex chemical system (chamber). In the long run, a larger number of experiments with different ranges of precursors is required to fully assess the auxiliary mechanism.

III.12 Ozonolysis of α -pinene

The ozonolysis reaction of the most abundant monoterpene, α -pinene, has been extensively studied both experimentally and theoretically; therefore, numerous data are readily found in the literature regarding its degradation and SOA formation (Nolting et al., 1988a; Atkinson et al., 1990a; Witter et al., 2002a; Zhang and Zhang, 2005; Saathoff et al., 2009; Zhang et al., 2009; Molteni et al., 2019). Thus, the investigation of this reaction is considered a way to chemically characterize and validate the performance of a simulation chamber. The reaction of α -pinene with ozone has been carried out in *CHARME* to determine (a) the rate coefficient and (b) the SOA formation yields. The obtained data were compared with those in the literature to check the ability of *CHARME* to simulate atmospheric reactions.

III.12.1 Determination of rate coefficient

The determination of the rate coefficient was performed at 294 ± 2 K, atmospheric pressure and under dark and dry conditions ($RH < 2\%$). It is well known that the ozonolysis of alkenes results in the formation of OH radicals due to the rearrangement of the Criegee biradicals (Henry and Donahue, 2011). Thus, to isolate the ozonolysis system, cyclohexane was used a scavenger for OH radicals. The cyclohexane concentrations were calculated in order to scavenge more than 95% of the OH radicals formed (i.e. the rate of “scavenger+OH” must be at least ten times higher than that of “VOC+OH”):

$$\text{(Eq. III.9)} \quad \frac{r(\text{scavenger+OH})}{r(\text{VOC+OH})} \geq 10$$

A set of eight experiments has been performed under pseudo-first-order conditions where the initial ozone concentrations were at least ten times higher than that of α -pinene. The rate is described by the following equation:

$$\text{(Eq. III.10)} \quad r = -\frac{d[\text{VOC}]}{dt} = k[\text{VOC}][\text{O}_3]$$

which is simplified as followed:

$$\text{(Eq. III.11)} \quad r = -\frac{d[\text{VOC}]}{dt} = k'[\text{VOC}]$$

where k' is the pseudo-first-order rate constant, with $k' = k[\text{O}_3]$.

So, k is determined from the plot of k' versus $[\text{O}_3]$ as displayed in **Figure III.30**.

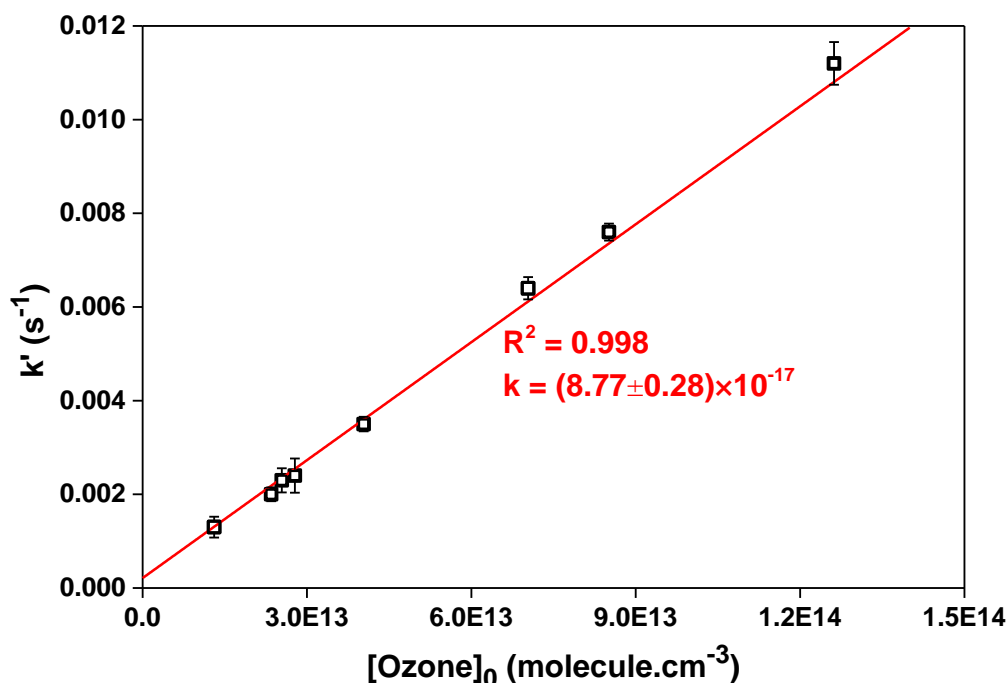


Figure III.30: Plot of the pseudo-first-order rate coefficients (k') for the reaction of O_3 with α -pinene as a function of the initial ozone concentration. The error bars reflect the uncertainties (2σ) on the measurements of k' .

The rate coefficients reported in the literature for the ozonolysis of α -pinene are listed in **Table III.10**. There is a good agreement between the previous determination and those obtained in

CHARME (excepted with the value reported by **Grimsrud et al., 1974** which is however higher than others).

Table III.10: Rate coefficients for the reaction of α -pinene with ozone.

Rate constant (molecule cm ⁻³ s ⁻¹)	Method	Reference
14.5×10^{-17}	Absolute	(Grimsrud et al., 1974)
$(8.6 \pm 1.3) \times 10^{-17}$	Relative	(Nolting et al., 1988)
$(9.7 \pm 1.1) \times 10^{-17}$	Absolute	(Atkinson et al., 1990b)
$(10.6 \pm 0.9) \times 10^{-17}$	Relative	(Witter et al., 2002)
$(9.6 \pm 0.2) \times 10^{-17}$	Recommended	(IUPAC (a), 2019)
$(8.8 \pm 0.3) \times 10^{-17}$	Pseudo First Order	This Study

III.12.2 Determination of SOA formation yield

The ozonolysis reaction is the most effective oxidation reaction occurring in the atmosphere in terms of generating low-volatility products that can contribute significantly to the formation of SOA (**Bernard et al., 2012**). SOA formation experiments were carried out in *CHARME* with α -pinene as the gaseous precursor and ozone as the oxidant. In the presence and absence of an OH scavenger, several tests have been conducted in *CHARME* to determine the SOA formation yield.

The yield (Y) is described in (**Eq. III.12**); it is determined from the ratio of M_0 (in $\mu\text{g}\cdot\text{m}^{-3}$) which is the total mass concentration of organic aerosols formed at the end of the reaction and the consumed concentration of the reactive organic gas Δvoc (in $\mu\text{g}\cdot\text{m}^{-3}$).

$$\text{(Eq. III.12)} \quad Y = \frac{M_0}{\Delta\text{voc}}$$

It is known that the ozonolysis of α -pinene produces SOA and that the aerosol mass which is formed is correlated to the initial concentration of the precursors. Thus, generally the SOA yields increase with higher starting concentrations of the hydrocarbon (**Chen and Hopke, 2009**).

In this study, the initial mixing ratios varied from 15 ppb to 330 ppb for α -pinene and from 20 ppb to 480 ppb for ozone. The experimental conditions and results are summarized in **Table III.11**.

To accurately quantify the SOA formation, particle wall losses have been taken into account. As explained previously in part in **III.7.3** and displayed in **Figure III.18**, the losses were determined at the end of each experiment from the decay of the particle mass concentration. A particle density of 1 g.cm^{-3} has been used in the whole experiments to convert the volume concentration of aerosols into mass concentration and determine the SOA yields. In the literature, no definite value has been proposed for SOA density formed from the ozone reaction with α -pinene, however, most of the recorded values were lower than 1.3 g cm^{-3} . In some experiments combining AMS and SMPS data, the reported density is 1.19 g.cm^{-3} (**Bahreini et al., 2005**), 1.30 g.cm^{-3} (**Alfarra et al., 2006**) or 1.23 g.cm^{-3} (**Shilling et al., 2008**). However, **Wirtz and Martin-Reviejo, (2003)** and **Wang et al., (2011)** have both used a value of 1.0 g.cm^{-3} in their articles dedicate to atmospheric simulation chamber validation.

Table III.11: Summary of experimental conditions and results for SOA formation from the ozonolysis of α -pinene ($T=290 \pm 2 \text{ K}$; $P=1015 \pm 3 \text{ mbar}$; $RH= 1.7 \pm 0.1$). In some experiments cyclohexane was used as an OH radical scavenger.

Experiment		[α -pinene] ₀ ^a		[O ₃] ₀ ^b	Δ voc ^c	M ₀ ^d	Yield (Y) ^e
		(ppb)	($\mu\text{g.m}^{-3}$)	(ppb)	($\mu\text{g.m}^{-3}$)	($\mu\text{g.m}^{-3}$)	
Without cyclohexane	1	16.1	91.2	96.0	87.7	10.2	0.12
	2	47.9	271.4	132.0	269.8	61.4	0.22
	3	96.03	544.1	217.0	541.1	141.4	0.26
	4	159.7	904.9	356.0	903.3	271.2	0.30
	5	204.8	1160.5	430.0	1158.3	500.0	0.36
With cyclohexane	1	17.6	99.7	20.0	99.0	7.7	0.08
	2	32.8	185.8	98.0	184.6	18.8	0.10
	3	43.8	248.2	108.0	246.6	49.4	0.20
	4	51.8	293.5	137.0	292.3	59.4	0.21
	5	82.0	465.8	150.0	464.7	102.30	0.22
	6	141.0	799.0	239.0	798.3	185.5	0.24
	7	240.5	1362.8	252.0	1361.3	375.4	0.28

^a: Initial α -pinene concentration; ^b:Ozone initial concentration; ^c:Reacted α -pinene concentration ; ^d: Organic aerosol mass concentration (corrected for wall losses); ^e: Overall SOA yield (Y) calculated as the ratio of M₀ to the total reacted α -pinene concentration (see (Eq. III.12)).

The formation of SOA is described by the gas/particle partitioning absorption model outlined by **Odum et al., (1996)**. The relationship between Y and M_0 is established through the following equation:

$$\text{(Eq. III.13)} \quad Y = \sum Y_i = M_0 \sum \frac{\alpha_i \cdot K_{p,i}}{1 + M_0 \cdot K_{p,i}}$$

where α_i is the mass-based stoichiometric coefficient of the oxidation product (i) and $K_{p,i}$ ($\text{m}^3 \cdot \mu\text{g}^{-1}$) is the gas-particle equilibrium constant that describes the partitioning of oxidation product (i) between the absorbing organic aerosol phase and the gas phase (**Odum et al., 1996**).

Yield data have been fitted to equation **(Eq. III.13)** on the basis of a one-product model and the results are listed in **Table III.12** (the model with two-products also fits the data, but the errors on α_i and $K_{p,i}$ exceed the values of the calculated parameters, so it cannot be retained).

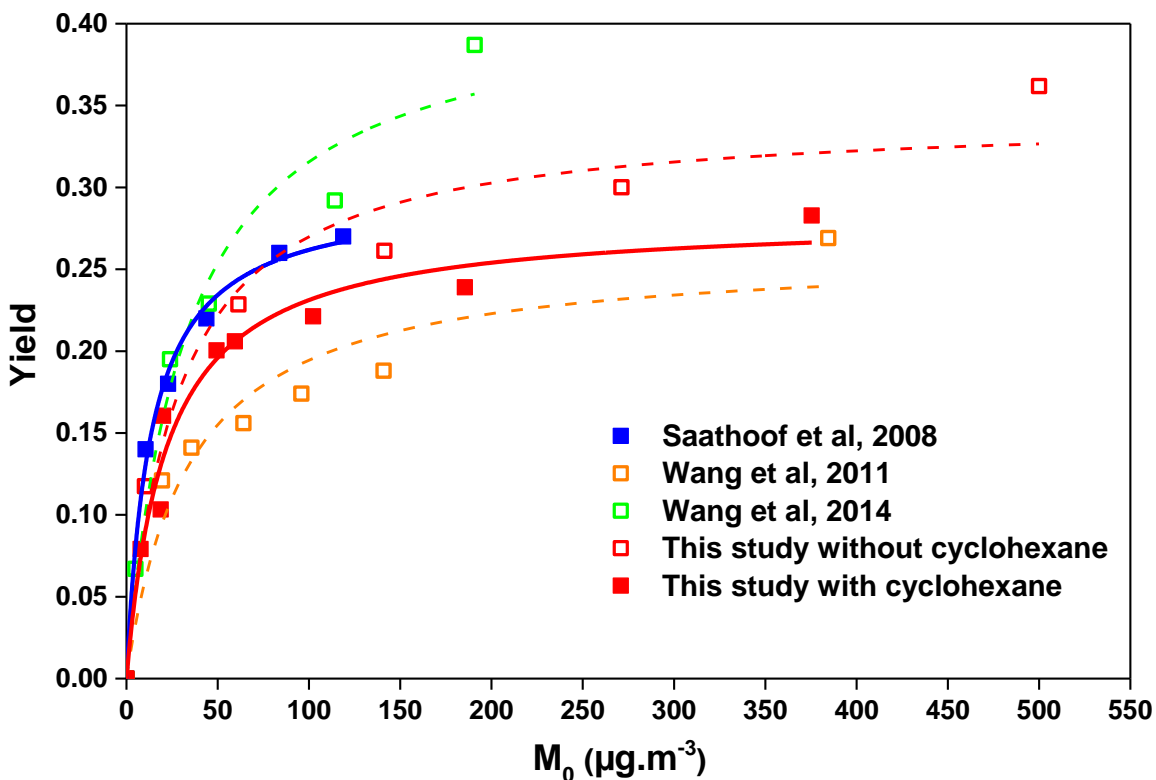


Figure III.31: Aerosol yield (Y) versus the organic aerosol mass formed (M_0) obtained in this work and literature data. Solid and empty squares correspond to data obtained with and without cyclohexane, respectively. The lines (solid in the presence and dashed in the absence of cyclohexane) represent the best fit of the data considering one semi-volatile major product.

Through the fitted plot displayed in **Figure III.31**, it is clear that for low organic mass concentrations ($< 50 \mu\text{g}\cdot\text{m}^{-3}$), the SOA yield increased with the aerosol mass concentration. However, for larger aerosol concentrations, the yields were independent of the organic mass concentration and tend to the value of α_i .

The α_1 and $K_{p,1}$ parameters obtained from the fit of the data obtained in *CHARME* are in the same range as those determined in other studies as presented in **Table III.12**. This good agreement between this work and the previous determination leads to the conclusion that *CHARME* can be used to investigate SOA formation from the gas-phase reaction of VOCs.

Table III.12: Comparisons of the one-product parameters (α_1 and $K_{p,1}$) obtain from this work and literature data.

α_1	$K_{p,1}(\text{m}^3\cdot\mu\text{g}^{-1})$	Conditions	Reference
0.29 ± 0.02	0.075 ± 0.009	T = (243-313K), RH < 78%, with cyclohexane	Saathoff et al., (2009)
0.26 ± 0.02	0.029 ± 0.011	T = 295 ± 0.5 K, RH < 1%, without scavenger	Wang et al., (2011)
0.41 ± 0.04	0.030 ± 0.010	T = 294 ± 2 K, RH < 5%, without scavenger	Wang et al., (2014)
0.28 ± 0.01	0.045 ± 0.008	T = 294 ± 2 K, RH < 2%, with cyclohexane	This study
0.44 ± 0.03	0.017 ± 0.005	T = 294 ± 2 K, RH < 2%, without scavenger	

From the comparison of the SOA yields obtained with and without an OH scavenger (cyclohexane), it was observed that the use of a scavenger has reduced (about 36%) the yield of the aerosol formation. This can be explained by the fact that the reaction of cyclohexane with OH produces alkylperoxy radicals as major radical products thus, it decreases the HO_2/RO_2 ratio inside the chamber. In their study, **Keyword et al., (2004)** have reported that the aerosol yields of alkenes with an endocyclic double bond, decrease with the decrease in HO_2/RO_2 . Similarly, **Jonsson et al., (2008)** have recorded a decrease in the numbers of particles and mass concentrations when 2-

butanol and cyclohexane were used as OH radical scavengers in the ozonolysis of α -pinene. The results in *CHARME* are in accordance with these previous observations

III.13 Conclusion

CHARME exhibited a good vacuum limit and quite negligible leaks (~40 ppb of air from the lab). The four stirring fans rotating at 190 rpm provide short (~ 3 minutes) and well mixing of chemical species. The wall properties and their minor effects, permitted relatively low wall loss rates of gases and particles which leads to lifetimes of a few hours for these species. The relatively short time for the cleaning process (~ 60 minutes) and its efficiency, displayed the advantage to perform more than one experiment per day (from 1 to 3, depending on the duration of each). The irradiation of the blank chamber for 1 hour led to the formation of gas (1 ppb of O₃ and 2 ppb of NO₂) and aerosols (15 particles), which is acceptable and comparable to those measured in other atmospheric chambers. Preliminary tests showed the capability to vary the relative humidity in the chamber, however further work is needed to define the conditions and to simulate fogs or clouds. Experiments on secondary aerosol formation from the α -pinene ozonolysis reaction, revealed a good reproducibility and an agreement with literature data. Regarding the irradiation system, although the measured spectral distribution (from 315 nm to 650 nm; this latter value corresponding to the upper limit of the spectroradiometer) was not very close to the solar emission spectrum, the determined NO₂ frequency photolysis (J_{NO_2}) was in the same order as those measured in other chambers and in the atmosphere. The propene–NO_x–air irradiation experiments have been used to identify the chamber auxiliary mechanism and an initial HONO concentration of 1 ppb allows the model to fit the measured concentrations of gases. It is important to keep in mind that all these parameters have to be characterized regularly, as they can vary due to the cleanness of the chamber's walls and/or the aging of the lamps, of the pump, etc.

Eventually, the different tests performed to characterize *CHARME* have been successful and allow to conclude that this chamber can be used to simulate atmospheric physico-chemical processes.

Table III.13: Summary of characterization tests performed in *CHARME*.

Experiment		Result	Comment(s)
Vacuum limit		0.4 mbar	Reached in 5 hours
Leak rate		4×10^{-6} (mbar.min ⁻¹)	Corresponds to a leak of ~40 ppb of contaminants of air from the lab.
Cleaning	Time	~ 60 minutes	50 minutes pumping + 10 minutes filling
	Efficiency	Satisfactory	The residual concentrations are low: - particles ($M_0 < 0.1 \mu\text{g m}^{-3}$) - gas: few ppb (depending on the nature of the examined gas)
Speed of fans		190 rpm	This is a compromise between a short mixing time and low wall losses of gases and particles
Mixing time		~ 3 minutes	Inhomogeneity is considered negligible if the pseudo-first order rate coefficient of the studied process is $< 5.6 \times 10^{-4} \text{ s}^{-1}$ (ten times slower than the mixing time).
Lifetime	Ozone	(7-14) hours	Depends on the initial ozone concentration
	Hydrocarbons	(4-84) hours	Depends on the properties of the tested VOCs
	Particles	(2-12) hours	Depends on the size and type of particles
Reactivity of purified air		Irradiation lead to an increase of O ₃ (1ppb/hour), NO ₂ (2 ppb/hour), NO (2 ppb/hour) and particles (15 particles/hour) in purified air	This formation is acceptable and comparable to those measured in other atmospheric chambers
J_{NO_2}		$(1.1-3.7) \times 10^{-3} \text{ s}^{-1}$	In the same order of magnitude as photolysis rates in other chambers and in the atmosphere

Auxiliary Mechanism			An auxiliary mechanism with an [HONO] ₀ of 1 ppb allows to simulate the gases concentrations measured in the propene/NO _x irradiation system
α-pinene ozonolysis	<i>k</i>	8.77×10^{-17} (molecule.cm ⁻³ .s ⁻¹)	Consistent with literature
	SOA Yield (α)	0.44 with cyclohexane	Consistent with literature
		0.28 without cyclohexane	

References

- Akimoto, H., Hoshino, M., Inoue, G., Sakamaki, F., Washida, N., Okuda, M., 1979a. Design and characterization of the evacuable and bakable photochemical smog chamber. *Environmental Science & Technology* 13, 471–475.
- Akimoto, H., Sakamaki, F., Hoshino, M., Inoue, G., Michio, O., 1979b. Photochemical Ozone Formation in Propylene-Nitrogen Oxide Dry Air System. *Environmental Science & Technology* 13, 53-58.
- Alfarra, M.R., Paulsen, D., Gysel, M., Garforth, A.A., Dommen, J., Prévôt, A.S.H., Worsnop, D.R., Baltensperger, U., Coe, H., 2006. A mass spectrometric study of secondary organic aerosols formed from the photooxidation of anthropogenic and biogenic precursors in a reaction chamber. *Atmospheric Chemistry and Physics* 6, 5279–5293. <https://doi.org/10.5194/acp-6-5279-2006>
- Atkinson, R., Baulch, D.L., Cox, R.A., Crowley, J.N., Hampson, R.F., Hynes, R.G., Jenkin, M.E., Rossi, M.J., Troe, J., 2004a. Evaluated kinetic and photochemical data for atmospheric chemistry: Volume I - gas phase reactions of O_x, HO_x, NO_x and SO_x species. *Atmospheric Chemistry and Physics* 4, 1461–1738. <https://doi.org/10.5194/acp-4-1461-2004>
- Atkinson, R., Baulch, D.L., Cox, R.A., Crowley, J.N., Hampson, R.F., Hynes, R.G., Jenkin, M.E., Rossi, M.J., Troe, J., 2004b. Evaluated kinetic and photochemical data for atmospheric chemistry: Volume I - gas phase reactions of O_x, HO_x, NO_x and SO_x species. *Atmospheric Chemistry and Physics* 4, 1461–1738. <https://doi.org/10.5194/acp-4-1461-2004>
- Atkinson, R., Hasegawa, D., Aschmann, S.M., 1990a. Rate constants for the gas-phase reactions of O₃ with a series of monoterpenes and related compounds at 296 ± 2 K. *International Journal of Chemical Kinetics* 22, 871–887. <https://doi.org/10.1002/kin.550220807>
- Atkinson, R., Hasegawa, D., Aschmann, S.M., 1990b. Rate constants for the gas-phase reactions of O₃ with a series of monoterpenes and related compounds at 296±2 K. *International Journal of Chemical Kinetics* 22, 871–887.
- Bahreini, R., Keywood, M.D., Ng, N.L., Varutbangkul, V., Gao, S., Flagan, R.C., Seinfeld, J.H., Worsnop, D.R., Jimenez, J.L., 2005. Measurements of Secondary Organic Aerosol from Oxidation of Cycloalkenes, Terpenes, and m-Xylene Using an Aerodyne Aerosol Mass Spectrometer. *Environ. Sci. Technol.* 39, 5674–5688. <https://doi.org/10.1021/es048061a>
- Bernard, F., Fedioun, I., Peyroux, F., Quilgars, A., Daële, V., Mellouki, A., 2012. Thresholds of secondary organic aerosol formation by ozonolysis of monoterpenes measured in a laminar flow aerosol reactor. *Journal of Aerosol Science* 43, 14–30. <https://doi.org/10.1016/j.jaerosci.2011.08.005>
- Bloss, C., Wagner, V., Bonzanini, A., Jenkin, M.E., Wirtz, K., Martin-Reviejo, M., Pilling, M.J., 2005. Evaluation of detailed aromatic mechanisms (MCMv3 and MCMv3.1) against environmental chamber data. *Atmospheric Chemistry and Physics* 5, 623–639. <https://doi.org/10.5194/acp-5-623-2005>
- Bohn, B., Rohrer, F., Brauers, T., Wahner, A., 2004. Actinometric measurements of NO₂ photolysis frequencies in the atmosphere simulation chamber SAPHIR. *Atmospheric Chemistry and Physics Discussions* 4, 8141–8170.

- Bunz, H., Möhler, O., Naumann, K.H., Saathoff, H., Schöck, W., Schurath, U., 1996. The novel aerosol chamber facility AIDA: status and first results, in: Proc. 7th European Symposium on the Physico-Chemical Behaviour of Atmospheric Pollutants. Citeseer.
- Carter, W., Cockeriii, D., Fitz, D., Malkina, I., Bumiller, K., Sauer, C., Pisano, J., Bufalino, C., Song, C., 2005. A new environmental chamber for evaluation of gas-phase chemical mechanisms and secondary aerosol formation. *Atmospheric Environment* 39, 7768–7788. <https://doi.org/10.1016/j.atmosenv.2005.08.040>
- Carter, W., Luo, D., Malkina, I., Pierce, J., 1995. Environmental chamber studies of atmospheric reactivities of volatile organic compounds: Effects of varying chamber and light source (No. NREL/TP--425-7621, 57153). <https://doi.org/10.2172/57153>
- Carter, W.P., 2006. The UCR EPA environmental chamber, in: *Environmental Simulation Chambers: Application to Atmospheric Chemical Processes*. Springer, pp. 27–41.
- Carter, W.P., Pierce, J.A., Luo, D., Malkina, I.L., 1995. Environmental chamber study of maximum incremental reactivities of volatile organic compounds. *Atmospheric Environment* 29, 2499–2511.
- Carter, W.P.L., Lurmann, F.W., 1991. Evaluation of a detailed gas-phase atmospheric reaction mechanism using environmental chamber data. *Atmospheric Environment. Part A. General Topics* 25, 2771–2806. [https://doi.org/10.1016/0960-1686\(91\)90206-M](https://doi.org/10.1016/0960-1686(91)90206-M)
- Chen, X., Hopke, P.K., 2009. Secondary organic aerosol from α -pinene ozonolysis in dynamic chamber system. *Indoor Air* 19, 335–345. <https://doi.org/10.1111/j.1600-0668.2009.00596.x>
- Cocker, D.R., Flagan, R.C., Seinfeld, J.H., 2001. State-of-the-Art Chamber Facility for Studying Atmospheric Aerosol Chemistry. *Environmental Science & Technology* 35, 2594–2601. <https://doi.org/10.1021/es0019169>
- Donahue, N.M., Henry, K.M., Mentel, T.F., Kiendler-Scharr, A., Spindler, C., Bohn, B., Brauers, T., Dorn, H.P., Fuchs, H., Tillmann, R., Wahner, A., Saathoff, H., Naumann, K.-H., Möhler, O., Leisner, T., Müller, L., Reinnig, M.-C., Hoffmann, T., Salo, K., Hallquist, M., Frosch, M., Bilde, M., Tritscher, T., Barmet, P., Praplan, A.P., DeCarlo, P.F., Dommen, J., Prevot, A.S.H., Baltensperger, U., 2012. Aging of biogenic secondary organic aerosol via gas-phase OH radical reactions. *Proceedings of the National Academy of Sciences* 109, 13503–13508. <https://doi.org/10.1073/pnas.1115186109>
- Finlayson-Pitts, B.J., Pitts Jr, J.N., 1999. *Chemistry of the upper and lower atmosphere: theory, experiments, and applications*. Elsevier.
- Ford, H.W., Endow, N., 1957. Rate Constants at Low Concentrations. III. Atomic Oxygen Reactions in the Photolysis of Nitrogen Dioxide at 3660 Å. *J. Chem. Phys.* 27, 1156–1160. <https://doi.org/10.1063/1.1743948>
- Glowacki, D.R., Goddard, A., Hemavibool, K., Malkin, T.L., Commane, R., Anderson, F., Bloss, W.J., Heard, D.E., Ingham, T., Pilling, M.J., 2007. Design of and initial results from a Highly Instrumented Reactor for Atmospheric Chemistry (HIRAC). *Atmospheric Chemistry and Physics* 7, 5371–5390.
- Hallquist, M., Wenger, J.C., Baltensperger, U., Rudich, Y., Simpson, D., Claeys, M., Dommen, J., Donahue, N.M., George, C., Goldstein, A.H., Hamilton, J.F., Herrmann, H., Hoffmann, T., Iinuma, Y., Jang, M., Jenkin, M.E., Jimenez, J.L., Kiendler-Scharr, A., Maenhaut, W., McFiggans, G., Mentel, T.F., Monod, A., Prevot, A.S.H., Seinfeld, J.H., Surratt, J.D., Szmigielski, R., Wildt, J., 2009. The formation, properties and impact of secondary organic aerosol: current and emerging issues. *Atmos. Chem. Phys.* 82.

- Henry, K.M., Donahue, N.M., 2011. Effect of the OH Radical Scavenger Hydrogen Peroxide on Secondary Organic Aerosol Formation from α -Pinene Ozonolysis. *Aerosol Science and Technology* 45, 696–700. <https://doi.org/10.1080/02786826.2011.552926>
- Holmes, J.R., O'Brien, R.J., Crabtree, J.H., Hecht, T.A., Seinfeld, J.H., 1973. Measurement of ultraviolet radiation intensity in photochemical smog studies. *Environmental Science & Technology* 7, 519–523. <https://doi.org/10.1021/es60078a002>
- Hynes, R., Angove, D., Saunders, S., Haverd, V., Azzi, M., 2005. Evaluation of two MCM v3.1 alkene mechanisms using indoor environmental chamber data. *Atmospheric Environment* 39, 7251–7262. <https://doi.org/10.1016/j.atmosenv.2005.09.005>
- IPCC, I.P. on C.C., 2013. Fifth Assessment Report (AR5) Chapter 07: Clouds and Aerosols.
- IUPAC (a), 2019. Task Group on Atmospheric Chemical Kinetic Data Evaluation – Data Sheet Ox_VOC8 [WWW Document]. URL http://iupac.pole-ether.fr/htdocs/datasheets/pdf/Ox_VOC8_O3_apinene.pdf (accessed 6.12.19).
- Jenkin, M.E., Saunders, S.M., Wagner, V., Pilling, M.J., 2003. Protocol for the development of the Master Chemical Mechanism, MCM v3 (Part B): tropospheric degradation of aromatic volatile organic compounds. *Atmospheric Chemistry and Physics* 3, 181–193.
- Jonsson, Å.M., Hallquist, M., Ljungström, E., 2008. Influence of OH Scavenger on the Water Effect on Secondary Organic Aerosol Formation from Ozonolysis of Limonene, Δ^3 -Carene, and α -Pinene. *Environ. Sci. Technol.* 42, 5938–5944. <https://doi.org/10.1021/es702508y>
- Keywood, M.D., Kroll, J.H., Varutbangkul, V., Bahreini, R., Flagan, R.C., Seinfeld, J.H., 2004. Secondary Organic Aerosol Formation from Cyclohexene Ozonolysis: Effect of OH Scavenger and the Role of Radical Chemistry. *Environmental Science & Technology* 38, 3343–3350. <https://doi.org/10.1021/es049725j>
- Leskinen, A., Yli-Pirilä, P., Kuuspallo, K., Sippula, O., Jalava, P., Hirvonen, M.-R., Jokiniemi, J., Virtanen, A., Komppula, M., Lehtinen, K.E.J., 2015. Characterization and testing of a new environmental chamber. *Atmospheric Measurement Techniques* 8, 2267–2278. <https://doi.org/10.5194/amt-8-2267-2015>
- Massabò, D., Danelli, S.G., Brotto, P., Comite, A., Costa, C., Di Cesare, A., Doussin, J.F., Ferraro, F., Formenti, P., Gatta, E., Negretti, L., Oliva, M., Parodi, F., Vezzulli, L., Prati, P., 2018. ChAMBRé: a new atmospheric simulation chamber for aerosol modelling and bio-aerosol research. *Atmospheric Measurement Techniques* 11, 5885–5900. <https://doi.org/10.5194/amt-11-5885-2018>
- Molteni, U., Simon, M., Heinritzi, M., Hoyle, C.R., Bernhammer, A.-K., Bianchi, F., Breitenlechner, M., Brilke, S., Dias, A., Duplissy, J., Frege, C., Gordon, H., Heyn, C., Jokinen, T., Kürten, A., Lehtipalo, K., Makhmutov, V., Petäjä, T., Pieber, S.M., Praplan, A.P., Schobesberger, S., Steiner, G., Stozhkov, Y., Tomé, A., Tröstl, J., Wagner, A.C., Wagner, R., Williamson, C., Yan, C., Baltensperger, U., Curtius, J., Donahue, N.M., Hansel, A., Kirkby, J., Kulmala, M., Worsnop, D.R., Dommen, J., 2019. Formation of Highly Oxygenated Organic Molecules from α -Pinene Ozonolysis: Chemical Characteristics, Mechanism, and Kinetic Model Development. *ACS Earth and Space Chemistry* 3, 873–883. <https://doi.org/10.1021/acsearthspacechem.9b00035>
- Nolting, F., Behnke, W., Zetzsch, C., 1988a. A smog chamber for studies of the reactions of terpenes and alkanes with ozone and OH. *Journal of atmospheric chemistry* 6, 47–59.
- Odum, J.R., Hoffmann, T., Bowman, F., Collins, D., Flagan, R.C., Seinfeld, J.H., 1996. Gas/Particle Partitioning and Secondary Organic Aerosol Yields 6.

- Saathoff, H., Naumann, K.-H., Möhler, O., Jonsson, A.M., Hallquist, M., Kiendler-Scharr, A., Mentel, T.F., Tillmann, R., Schurath, U., 2009. Temperature dependence of yields of secondary organic aerosols from the ozonolysis of α -pinene and limonene. *Atmospheric Chemistry and Physics* 9, 1551–1577.
- Schuck, E.A., Stephens, E.R., 1969. Oxides of nitrogen. In *Advances in Environmental Science & Technology* 1.
- Shetter, R.E., 2003. Photolysis frequency of NO₂: Measurement and modeling during the International Photolysis Frequency Measurement and Modeling Intercomparison (IPMMI). *Journal of Geophysical Research* 108. <https://doi.org/10.1029/2002JD002932>
- Shilling, J.E., Chen, Q., King, S.M., Rosenoern, T., Kroll, J.H., Worsnop, D.R., McKinney, K.A., Martin, S.T., 2008. Particle mass yield in secondary organic aerosol formed by the dark ozonolysis of α -pinene. *Atmospheric Chemistry and Physics* 8, 2073–2088. <https://doi.org/10.5194/acp-8-2073-2008>
- Wang, J., Doussin, J.F., Perrier, S., Perraudin, E., Katrib, Y., Pangui, E., Picquet-Varrault, B., 2011. Design of a new multi-phase experimental simulation chamber for atmospheric photo-smog, aerosol and cloud chemistry research. *Atmospheric Measurement Techniques* 4, 2465–2494. <https://doi.org/10.5194/amt-4-2465-2011>
- Wang, X., Liu, T., Bernard, F., Ding, X., Wen, S., Zhang, Y., Zhang, Z., He, Q., Lü, S., Chen, J., Saunders, S., Yu, J., 2014. Design and characterization of a smog chamber for studying gas-phase chemical mechanisms and aerosol formation. *Atmospheric Measurement Techniques* 7, 301–313. <https://doi.org/10.5194/amt-7-301-2014>
- Washenfelder, R.A., Flores, J.M., Brock, C.A., Brown, S.S., Rudich, Y., 2013. Broadband measurements of aerosol extinction in the ultraviolet spectral region. *Atmospheric Measurement Techniques* 6, 861–877. <https://doi.org/10.5194/amt-6-861-2013>
- Wirtz, Martin-Reviejo, 2003. Density of secondary organic aerosols. *Journal of aerosol science* 34, S223–S224.
- Witter, M., Berndt, T., Böge, O., Stratmann, F., Heintzenberg, J., 2002a. Gas-phase ozonolysis: Rate coefficients for a series of terpenes and rate coefficients and OH yields for 2-methyl-2-butene and 2,3-dimethyl-2-butene: Gas-Phase Ozonolysis. *International Journal of Chemical Kinetics* 34, 394–403. <https://doi.org/10.1002/kin.10063>
- Wu, C.H., Niki, H., 1975. Methods for measuring nitrogen dioxide photodissociation rate. Application to smog chamber studies. *Environmental Science & Technology* 9, 46–52. <https://doi.org/10.1021/es60099a005>
- Wu, S., Lü, Z., Hao, J., Zhao, Z., Li, J., Takekawa, H., Minoura, H., Yasuda, A., 2007. Construction and characterization of an atmospheric simulation smog chamber. *Advances in Atmospheric Sciences* 24, 250–258. <https://doi.org/10.1007/s00376-007-0250-3>
- Zhang, D., Zhang, R., 2005. Ozonolysis of α -pinene and β -pinene: Kinetics and mechanism. *J. Chem. Phys.* 13.
- Zhang, X., Chen, Z., Wang, H., He, S., Huang, D., 2009. An important pathway for ozonolysis of alpha-pinene and beta-pinene in aqueous phase and its atmospheric implications. *Atmospheric Environment* 43, 4465–4471. <https://doi.org/10.1016/j.atmosenv.2009.06.028>

Chapter IV

“Ozonolysis of γ -terpinene”

During the last decades, the reactions of ozone with unsaturated VOCs have been largely investigated in simulation chambers and flow reactors (**Johnson and Marston, 2008**). The ozonolysis reactions of major monoterpenes (α -pinene, β -pinene and limonene) have been deeply studied and there exist numerous data showing the rate coefficients and formation yields (of OH radicals, gaseous products and SOAs), however, the mechanism of these reactions is far from being completely understood. The investigation of the ozonolysis of any unsaturated VOC is considered an important approach to further understand and characterize such reactions. In this regard, a monoterpene, γ -terpinene, emitted into the atmosphere from various types of vegetation including Elm, Cypress, Waterhickory, and Maple trees (**Khalil and Rasmussen, 1992; Geron et al., 2000**), has been the subject of a study performed in *CHARME*. The examination of the ozonolysis of γ -terpinene is divided into three complementary parts. The first section is focused on the gas-phase chemistry including kinetic and mechanistic investigations. The second part is dedicated to the particulate phase, it concerns the determination of the formation yields of SOA and the identification of their morphology and physical state. Finally, the third unit of the chapter shed lights on the hygroscopic properties of the SOA.

IV.1 Gas-phase study

In this section, all experiments were carried out at 294 ± 2 K, atmospheric pressure, and under dark and dry (RH < 2 %) conditions. The ozonolysis reactions were performed in the presence of an excess of cyclohexane to scavenge the hydroxyl radicals produced from the Criegee rearrangement reactions. The cyclohexane concentrations were calculated based on **(Eq. IV.1)** which allows the scavenging of more than 95% of the formed OH radicals and hence the isolation of the ozonolysis system.

$$\text{(Eq. IV.1)} \quad \frac{\text{rate (scavenger+OH)}}{\text{rate (VOC+OH)}} \geq 10$$

IV.1.1 Rate coefficient determination

The study of the ozonolysis reaction of γ -terpinene has been the subject of only two studies (**Grimsrud et al., 1975; Atkinson et al., 1990a**), who reported the rate coefficient for this reaction. In this work, the determination of the rate constant has been performed through two different

kinetic methods, the pseudo-first-order (performed in *CHARME*) and the relative method (performed in *CHARME* and *LPCA-ONE*).

IV.1.1.1 Pseudo-first-order kinetics

The reaction between ozone and a VOC (here, γ -terpinene), is a second-order reaction with a rate equation described as followed:

$$\text{(Eq. IV.2)} \quad r = -\frac{d[\gamma\text{-terpinene}]}{dt} = k_{\gamma-t} \times [\gamma\text{-terpinene}] \times [\text{O}_3]$$

Under pseudo-first-order conditions, with ozone used in great excess with respect to γ -terpinene ($[\text{O}_3] > 10 \times [\gamma\text{-t}]$), the second-order rate equation is reduced to a pseudo-first-order rate equation as presented in **(Eq. IV.3)**:

$$\text{(Eq. IV.3)} \quad -\frac{d[\gamma\text{-terpinene}]}{dt} = k'_{\gamma-t} \times [\gamma\text{-terpinene}]$$

with ($k'_{\gamma-t}$) being the pseudo-first-order rate coefficient = $k_{\gamma-t} \times [\text{O}_3]$.

The integration of equation **(Eq. IV.3)**, leads to the following relationship:

$$\text{(Eq. IV.4)} \quad \frac{\ln[\gamma\text{-terpinene}]_0}{\ln[\gamma\text{-terpinene}]_t} = k'_{\gamma-t} \times t$$

where the subscripts 0 and t refer to the concentrations at the start of the reaction and at a time t , respectively.

A set of thirteen experiments summarized in **Table IV. 1**, was performed in *CHARME* with initial concentrations in the range (43 ppb - 497 ppb) for γ -terpinene and (450 ppb - 5300 ppb) for ozone.

The rate coefficient ($k'_{\gamma-t}$) was deduced according to **(Eq. IV.4)**, from the straight lines of the plots of $\ln([\gamma\text{-terpinene}]_0/[\gamma\text{-terpinene}]_t)$ versus time (t) for each experiment as presented in **Figure IV. 1**. The uncertainties on the measurement of $k'_{\gamma-t}$ are twice the standard deviation arising from linear regression analyses of the data.

Then, the rate coefficient ($k_{\gamma-t}$) was determined from the plot of the obtained $k'_{\gamma-t}$ values versus the initial ozone concentrations as shown in **Figure IV.2**. The rate coefficient determined using this method is $k_{\gamma-t} = (2.05 \pm 0.09) \times 10^{-16} \text{ cm}^3 \text{ molecule}^{-1} \text{ s}^{-1}$ (see **Table IV.2**). The indicated error is twice the standard deviation arising from linear regression analysis of the data.

Table IV. 1: Summary of the conditions of pseudo-first order experiments

Exp	$[\gamma-t]_0$ (ppb)	$[\gamma-t]_0$ (molecule.cm ⁻³)	[Ozone] ₀ (ppb)	[Ozone] ₀ (molecule.cm ⁻³)	$k'_{\gamma-t}$ (s ⁻¹)	$k_{\gamma-t}$ (cm ³ molecule ⁻¹ . s ⁻¹)
1	43	1.06×10^{12}	450	1.11×10^{13}	0.0025	2.14×10^{-16}
2	50	1.23×10^{12}	2060	5.07×10^{13}	0.0099	1.95×10^{-16}
3	75	1.85×10^{12}	1730	4.26×10^{13}	0.0079	1.86×10^{-16}
4	83	2.04×10^{12}	1100	2.71×10^{13}	0.0055	2.22×10^{-16}
5	166	4.08×10^{12}	2750	6.77×10^{13}	0.0138	2.04×10^{-16}
6	171	4.21×10^{12}	1755	4.32×10^{13}	0.0088	1.85×10^{-16}
7	190	4.67×10^{12}	1920	4.72×10^{13}	0.0100	2.11×10^{-16}
8	237	5.83×10^{12}	3945	9.70×10^{13}	0.0198	2.03×10^{-16}
9	237	5.83×10^{12}	2640	6.49×10^{13}	0.0140	2.16×10^{-16}
10	253	6.22×10^{12}	2751	6.77×10^{13}	0.0150	2.14×10^{-16}
11	316	7.77×10^{12}	3325	8.18×10^{13}	0.0171	2.03×10^{-16}
12	475	1.17×10^{12}	5300	1.30×10^{14}	0.0260	2.15×10^{-16}
13	497	1.22×10^{12}	5050	1.24×10^{14}	0.0258	2.08×10^{-16}

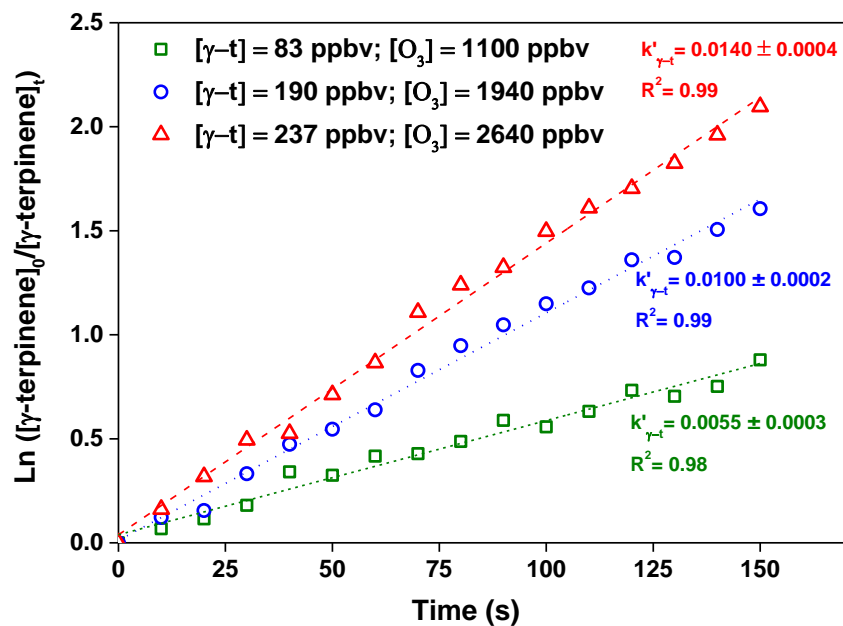


Figure IV. 1 Time profile of $\ln([\gamma\text{-terpinene}]_0/[\gamma\text{-terpinene}]_t)$ versus time (s) for 3 different experiments: Exp.4 (green), Exp.7 (blue) and Exp.9 (red).

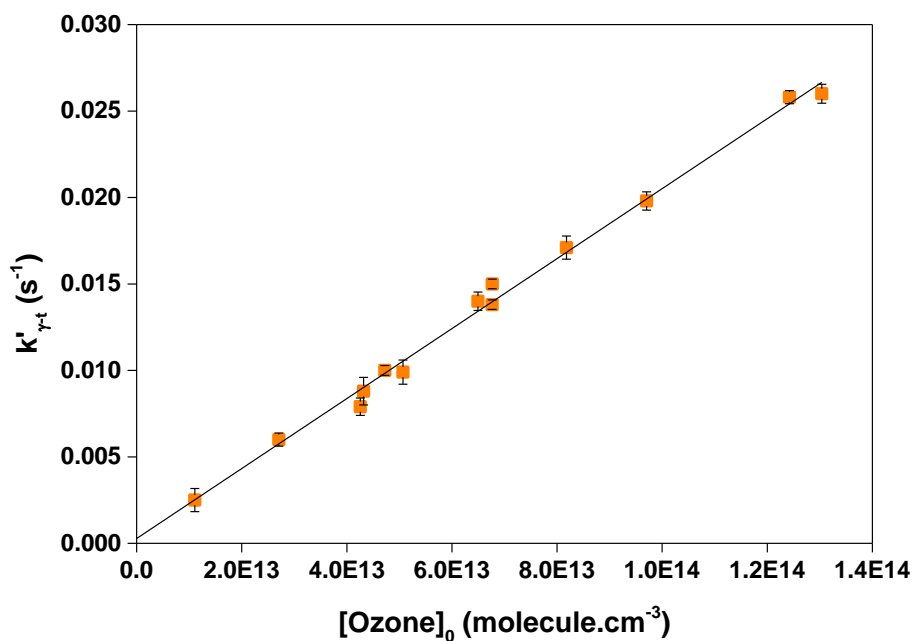


Figure IV.2: Plot of the pseudo-first-order rate coefficients ($k'_{\gamma\text{-t}}$) for the reaction of O_3 with γ -terpinene as a function of the initial ozone concentration obtained at 294 ± 2 K, atmospheric pressure and in the presence of an ozone scavenger (cyclohexane). The error bars reflect the uncertainties on the measurements of $k'_{\gamma\text{-t}}$.

IV.1.1.2 Relative Method

The rate coefficient of the ozonolysis of γ -terpinene was also obtained with the relative kinetic method performed in *CHARME* and LPCA-ONE chambers.

This method measures the decay of one reactant relative to that of a reference compound in the presence of a reactive specie (**Atkinson et al., 1986**). The chosen reference(s) must have a well-known rate constant for its reaction with the oxidant and the ratio of $k_{(\text{VOC})}/k_{(\text{ref})}$ has to be between 0.2 and 5. In this study, three reference compounds were used and a minimum of three experiments were performed for each of them. The reference compounds and their rate coefficients with ozone (in units of $\text{cm}^3 \text{ molecule}^{-1} \text{ s}^{-1}$) were: 2-methyl-2-butene (2m2b): $k_{2\text{m}2\text{b}} = (4.1 \pm 0.5) \times 10^{-16}$ (**Witter et al., 2002**), cis-2-pentene (cis-2p): $k_{\text{cis-2p}} = (1.32 \pm 0.04) \times 10^{-16}$ (**Avzianova and Ariya, 2002**) and α -pinene (α -p): $k_{\alpha\text{-p}} = (9.6 \pm 0.15) \times 10^{-16}$; (**IUPAC (a)**, current recommendation).

The determination of the γ -terpinene rate coefficient using (2m2b) and (cis-2p) was performed in *CHARME* with the use of PTR to follow their concentrations. Through these experiments, the main fragments (i.e. m/z 137.2 for γ -terpinene and m/z 71.1 for the reference compounds) were solely monitored. The organic compounds were first injected into the chamber and when their concentrations were stable, known concentrations of ozone were added using an ozone generator. O_3 concentrations were monitored by an UV photometric ozone analyzer (Thermo Scientific 49i).

In addition, α -pinene was also used as a reference compound for the rate constant measurement in LPCA-ONE with TD-GC-FID analyses as the PTR cannot distinguish isomers (here the 2 monoterpenes α -pinene and γ -terpinene). Known volumes of VOCs were injected into the chamber through a heated injector and mixed for one hour to stabilize. At that point, accurate concentrations of ozone were added to initiate the reaction, the VOCs were then sampled on Tenax TA, thermodesorbed and analyzed with a TD-GC-FID (Autosystem XL, Perkin Elmer).

The rate coefficient for reaction with ozone was determined by comparing the decay rate of γ -terpinene relative to that of the reference compounds.





Kinetic treatment of reactions **(R. IV.1)** and **(R. IV.2)** leads to the following relationship:

(Eq. IV 5) $\ln \frac{[\gamma\text{-terpinene}]_0}{[\gamma\text{-terpinene}]_t} = \frac{k_{\gamma-t}}{k_{ref}} \left(\ln \frac{[\text{Reference}]_0}{[\text{Reference}]_t} \right)$

where $k_{\gamma-t}$ and k_{ref} are the rate coefficients for the reactions of ozone with γ -terpinene **(R. IV.1)** and the references **(R. IV.2)**, and the subscripts 0 and t indicate the concentrations at the start of the reaction and at a time t, respectively.

Data obtained from the reaction were plotted in the form of **(Eq. IV 5)** and showed a good linearity with near zero intercept as shown in **Figure IV.3**. The slopes ($k_{\gamma-t}/k_{ref}$) derived from the plots and the calculated ozone rate coefficients ($k_{\gamma-t}$) are displayed in **Table IV.2**. The indicated errors are twice the standard deviations arising from the least squares linear regression of the data and do not include uncertainties on the reference rate coefficients.

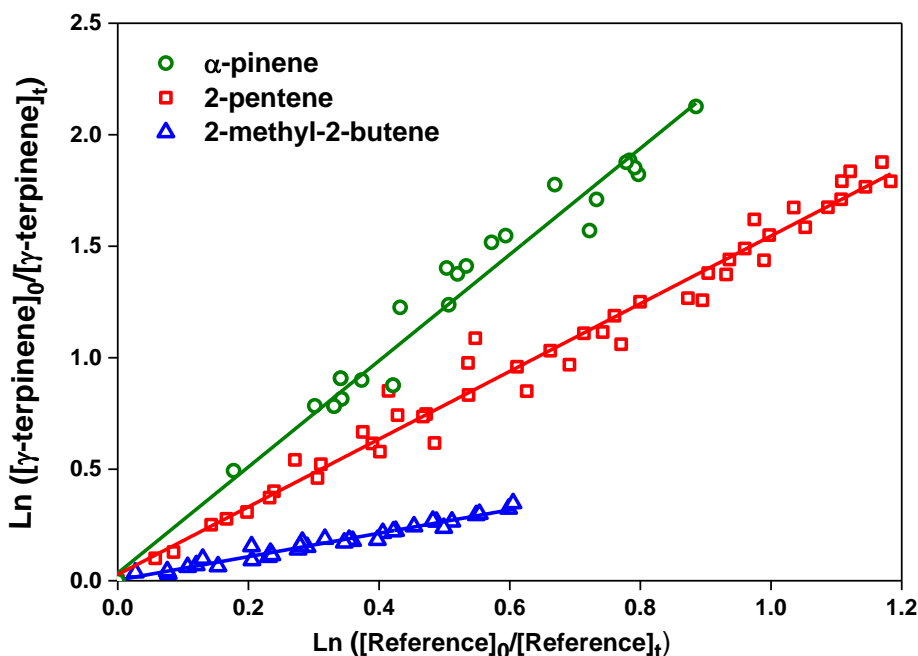


Figure IV.3: Relative rate plots for the reaction of γ -terpinene with ozone obtained at 294 ± 2 K, atmospheric pressure and in the presence of an ozone scavenger (cyclohexane). Three references were used: cis-2-pentene (red squares; PTR-ToF-MS analyses), 2-methyl-2-butene (blue triangle; PTR-ToF-MS analyses) and α -pinene (green circles; TD-GC-FID analyses).

Rather than calculating an average rate coefficient from the three used reference compounds, a more representative value for $k_{\gamma-t}$ was obtained by combining the data recorded for the three references in one plot represented by Eq. IV 6.

$$\text{Eq. IV 6} \quad \left(\ln \frac{[\gamma\text{-terpinene}]_0}{[\gamma\text{-terpinene}]_t} \right) \times k_{\text{ref}} = k_{\gamma-t} \times \left(\ln \frac{[\text{Reference}]_0}{[\text{Reference}]_t} \right)$$

The plot displayed in Figure IV.4 shows a good linearity with a near-zero intercept and a slope that corresponds to rate coefficient determined from the three different references. The uncertainties are twice the standard deviations arising from the least squares linear regression of the data.

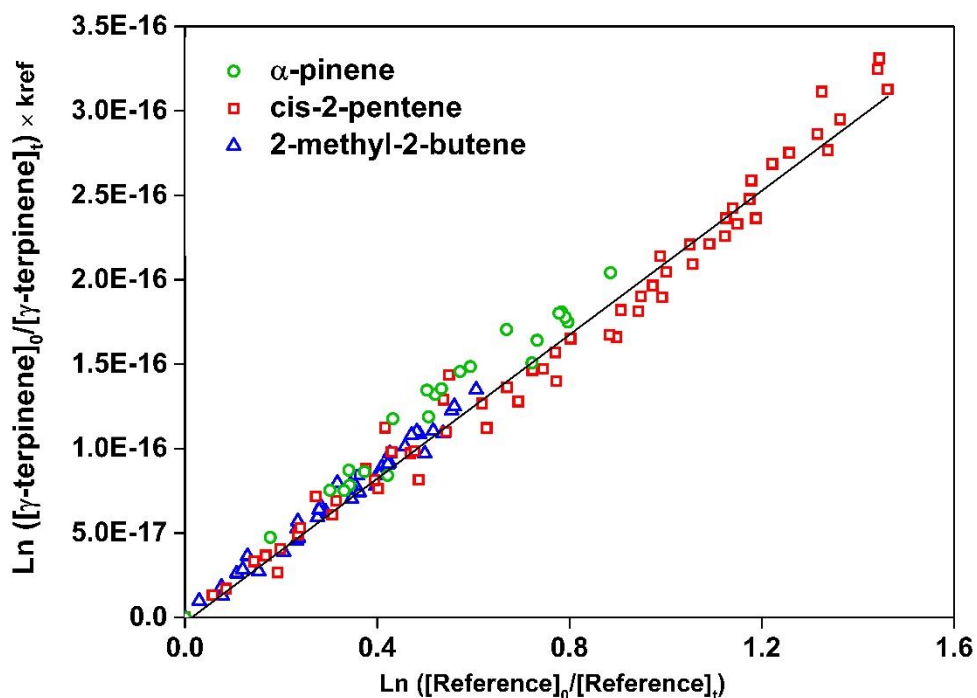


Figure IV.4: Relative rate plot representing (Eq. IV 6) with a slope corresponding to $k_{\gamma-t}$. The data of the three reference compounds were represented in different colors and shapes: cis-2-pentene (red squares), 2-methyl-2-butene (blue triangle) and α -pinene (green circles).

IV.1.1.3 Discussion

The rate coefficients for the reaction of γ -terpinene with ozone determined with the relative rate method using the three references were in accordance (relative discrepancy lower than 5 %) and gave an average value of $k_{(\gamma\text{-terpinene})} = (2.17 \pm 0.11) \times 10^{-16} \text{ cm}^3 \text{ molecule s}^{-1}$). This value was also in good agreement with the rate coefficient measured with the pseudo-first-order method ($k_{(\gamma\text{-terpinene})} = (2.03 \pm 0.11) \times 10^{-16} \text{ cm}^3 \text{ molecule s}^{-1}$). The consistency of the data determined in two chambers and using the two different methods, provided confidence in the rate constant presented in this work.

The mean rate coefficients for the reaction of γ -terpinene with ozone ($k_{(\gamma\text{-terpinene})} = (2.10 \pm 0.11) \times 10^{-16} \text{ cm}^3 \text{ molecule s}^{-1}$) is compared with literature data. Two previous determinations were reported as shown in **Table IV.2**. The rate coefficients obtained by **Grimsrud et al., (1975)** with the absolute method is ~ 39 % higher than the value determined in this study, whereas **Atkinson et al., (1995)** reported one which is ~ 22 % lower using the relative method (the value determined by Atkinson has been recalculated using the current recommended value (**IUPAC**)). In their study, **Atkinson et al., (1990)** determined consistently lower rate coefficients (by a factor of ~ 2 to 6) for monoterpenes (e.g. β -pinene, α -pinene, α -phellandrene and γ -terpinene) than **Grimsrud et al., (1975)**. **Atkinson et al., (1990)** suggested that the highest values reported by **Grimsrud et al., (1975)** were probably due to secondary reactions which occurred at atmospheric pressure in the slow flow system used to perform the experiments.

Table IV.2: Rate coefficient determined for the reaction of γ -terpinene with ozone at 294 ± 2 K, atmospheric pressure and literature data.

Method	Reference	$k_{\gamma-t}/k_{ref}^a$	$k_{\gamma-t}^{a,b}$ ($\times 10^{-16}$)	$k_{\gamma-t}^{b,c}$ ($\times 10^{-16}$)	$k_{\gamma-t(average)}^{b,d}$ ($\times 10^{-16}$)	Literature
Pseudo first order	-	-	2.03 ± 0.11			
Relative	2-methyl-2-butene ^e	0.53 ± 0.02	2.17 ± 0.08	2.17 ± 0.11	2.10 ± 0.11	This study
	cis-2-pentene ^f	1.61 ± 0.06	2.13 ± 0.13			
	α -pinene ^g	2.29 ± 0.14	2.23 ± 0.13			
	α -pinene	-	1.63 ± 0.12^h	-	-	(Atkinson et al., 1990)
Absolute	-	-	2.84	-	-	(Grimsrud, et al., 1974)

^a The indicated errors are twice the standard deviation arising from the linear regression analysis and do not include the uncertainty on the reference rate coefficients.

^b Expressed in $\text{cm}^3 \text{ molecule}^{-1} \text{ s}^{-1}$.

^c Determined using plots based on **Eq. IV 6** (see the text).

^d Average rate coefficient for both methods.

^e $k_{(2\text{-methyl-2-butene} + \text{O}_3)} = (4.1 \pm 0.5) \times 10^{-16} \text{ cm}^3 \text{ molecule}^{-1} \text{ s}^{-1}$ (Witter et al., 2002).

^f $k_{(cis\text{-2-pentene} + \text{O}_3)} = (1.32 \pm 0.04) \times 10^{-16} \text{ cm}^3 \text{ molecule}^{-1} \text{ s}^{-1}$ (Avzianova and Ariya, 2002).

^g $k_{(\alpha\text{-pinene} + \text{O}_3)} = (9.6 \pm 0.15) \times 10^{-17} \text{ cm}^3 \text{ molecule}^{-1} \text{ s}^{-1}$ at 298 K (IUPAC).

^h Recalculated using the current recommended value (IUPAC) for the α -pinene rate coefficient.

The determined rate coefficient allowed to calculate the atmospheric lifetime of γ -terpinene with respect to its reaction with ozone. Assuming a concentration of ozone of 100 ppbv ($2.46 \times 10^{12} \text{ molecule.cm}^{-3}$), the estimated lifetime of γ -terpinene in the atmosphere is 33 min (see **Table IV. 3**). The rate coefficients of γ -terpinene with hydroxyl radical and nitrate radical were previously measured and based on the current recommended values (IUPAC) their corresponding lifetimes were calculated and also provided in **Table IV. 3** for comparison. The reaction of γ -terpinene with OH and NO₃ leads to atmospheric lifetimes of about 49 min and 2 min, respectively, so the ozonolysis is also an important sink for this monoterpene.

Table IV. 3: Atmospheric life time of γ -terpinene with different oxidants.

τ OH ¹	τ O ₃ ²	τ NO ₃ ³	Reference
49 min	35 min	2 min	IUPAC ⁴
-	33 min	-	This study

¹Assumed OH radical concentration: 2.0×10^6 molecule.cm⁻³, 12-h daytime average (Atkinson and Arey, 2003a).

²Assumed O₃ concentration: 2.46×10^{12} molecule.cm⁻³, polluted atmosphere.

³Assumed NO₃ radical concentration: 2.5×10^8 molecule.cm⁻³, 12-h nighttime average (Atkinson and Arey, 2003a).

⁴Current recommended values for the rate coefficients of γ -terpinene with OH, O₃ and NO₃ (IUPAC (b); IUPAC (c); IUPAC (d)).

$\tau_{O_3} = 1/k*[O_3]$, where O₃ concentration 2.46×10^{12} molecule.cm⁻³ and $k = 2.1 \times 10^{-16}$ cm³ molecule⁻¹ s⁻¹

IV.1.2 Gas phase oxidation Products

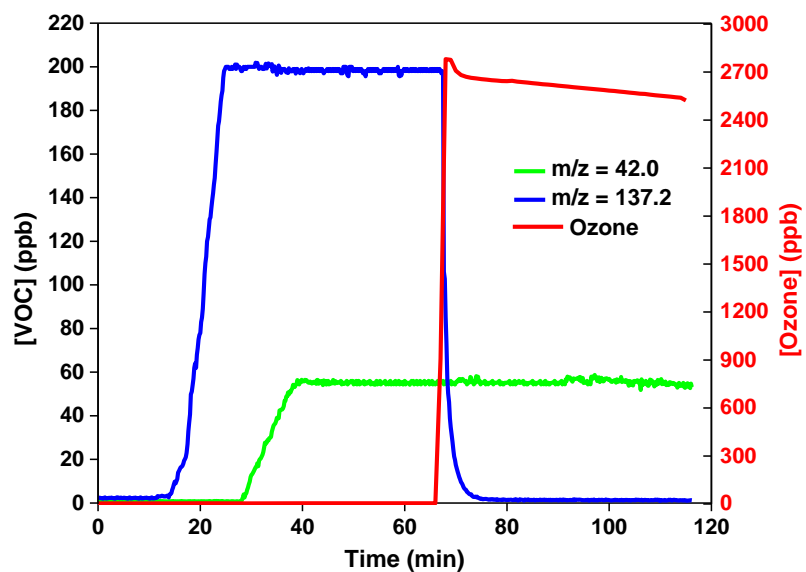
IV.1.2.1 Identification of products

A total of five experiments were carried out in the dark using CHARME to characterize the products formed from the gas phase oxidation of γ -terpinene with ozone. PTR analyses were continuously performed during the ozonolysis reaction to monitor the concentration of the organics versus time.

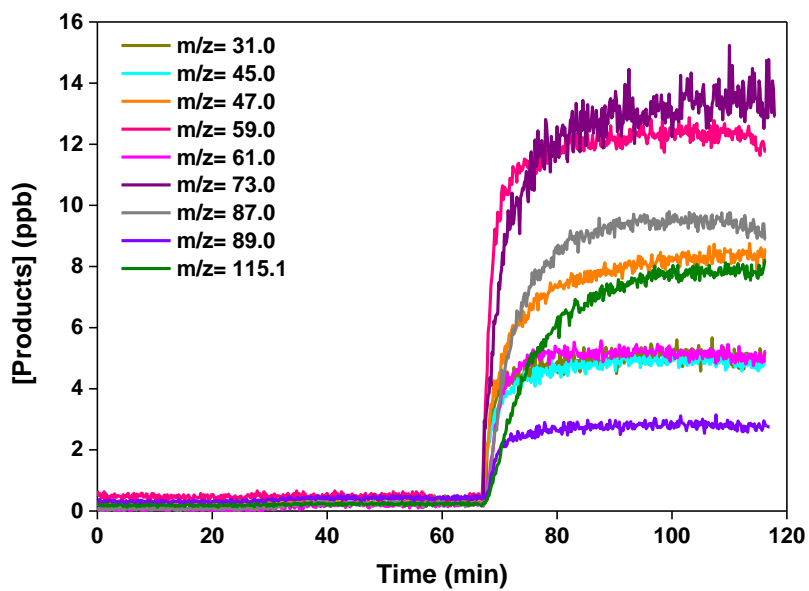
γ -terpinene was first introduced into the chamber and followed throughout the experiment with the PTR-MS at m/z 137.2. Cyclohexane was then injected and theoretically as its proton affinity is lower than that of water, it should not be detected by the PTR-MS. Acetonitrile was injected as a dilution tracer and followed throughout the experiment at m/z 42.0. Its signal remained constant indicating that the dilution was negligible in the chamber.

As soon as ozone was introduced, γ -terpinene was rapidly oxidized (within a few minutes) to form a number of oxidation products whose concentrations continuously increased during the experiment and then reached a plateau when the γ -terpinene was totally consumed. Meanwhile, the ozone concentration displayed a rapid initial consumption followed by a slow decrease due to wall losses (Figure IV.5).

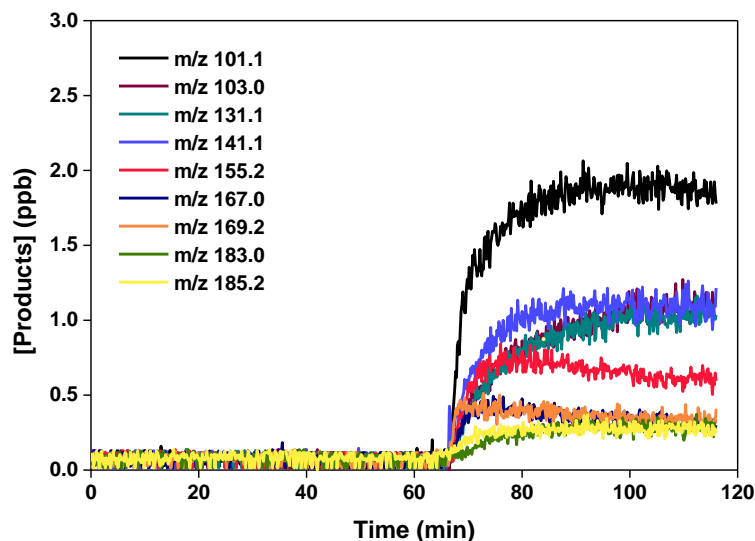
The peaks which were detected during the course of the experiments are listed in [Table IV.4](#) and their typical time profiles are displayed in [Figure IV.5](#).



(a)



(b)



(c)

Figure IV.5: Typical time profiles of chemical compounds ((a) reactants: γ -terpinene, acetonitrile and O_3 ; (b) major oxidation products; (c) minor oxidation products) detected by the PTR and the ozone analyzer during the ozonolysis of γ -terpinene (initial concentrations: γ -terpinene, 200 ppbv and O_3 , 2780 ppbv). m/z includes the addition of H^+ to the molar mass.

20 peaks corresponding to the oxidation products of γ -terpinene were observed with the PTR-MS. The major peaks were monitored at the following m/z (the indicated m/z include the addition of H^+ to the molar mass): 31.0, 45.0, 47.0, 59.0, 61.0, 73.0 and 115.1 and the minor peaks at the following m/z : 103.1, 131.1, 141.1, 155.2, 167.0, 169.2, 183.0 and 185.2.

To assign the observed signals to known compounds, separate characterization experiments were performed in *CHARME*. The standards of the compounds expected to be formed from this reaction were introduced into the chamber and followed by the PTR. The results for the tested compounds and their major fragments were: formaldehyde (m/z 31.0), acetaldehyde (m/z 45.0), formic acid (m/z 47.0), acetone and glyoxal (m/z 59.0) and acetic acid (m/z 61.0). These products were similar to those observed in other monoterpenes ozonolysis studies (**Lee et al., 2006**; **Mackenzie-Rae et al., 2017a**) that have identified the gas-phase products through PTR-MS analyses.

Other oxidation products were assigned based on the proposed mechanism (to be detailed in section **IV.1.2.3** Mechanisms such as 2-oxosuccinaldehyde (m/z 101.1) and 4-methyl-3-oxo-

pentanal (m/z 115.1). However, some products (with the corresponding m/z ratios: 73.0, 141.1, 155.2, 167.0 and 183.0) remain unidentified because they could not be explained by chemical formulae or by the formation mechanisms. Compounds at m/z 87.0, 89.0, 103.1, 131.1, 169.2, 185.2 were not assigned to a single compound because different isomers were observed in the proposed mechanism. The peaks observed at m/z 99.1 and m/z 100.1 correspond to cyclohexanone (formed from the hydroxyl radical reaction with cyclohexane) and its ^{13}C isotope, respectively.

IV.1.2.2 Products yield determination

For the most abundant oxidation products, the formation yields were determined from the plot of their concentrations versus the amount of γ -terpinene consumed ($\Delta_{\gamma\text{-terpinene}}$) as displayed in **Figure IV.6**. The concentrations of γ -terpinene and some identified products (formaldehyde, acetaldehyde, formic acid, acetone and acetic acid) were determined from calibrations performed in *CHARME* and for compounds that were not identified or for which pure commercial standards were not available, concentrations were estimated from the PTR-MS on the basis of the equation previously presented in chapter 2 (section **II.1**).

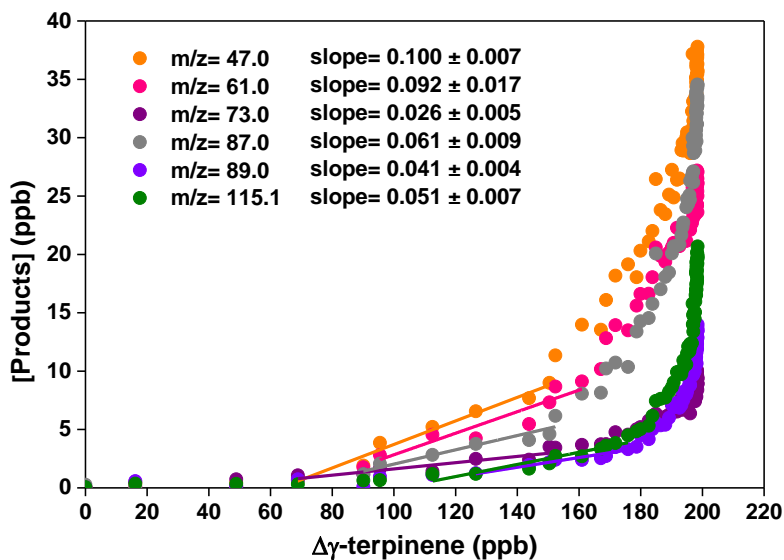
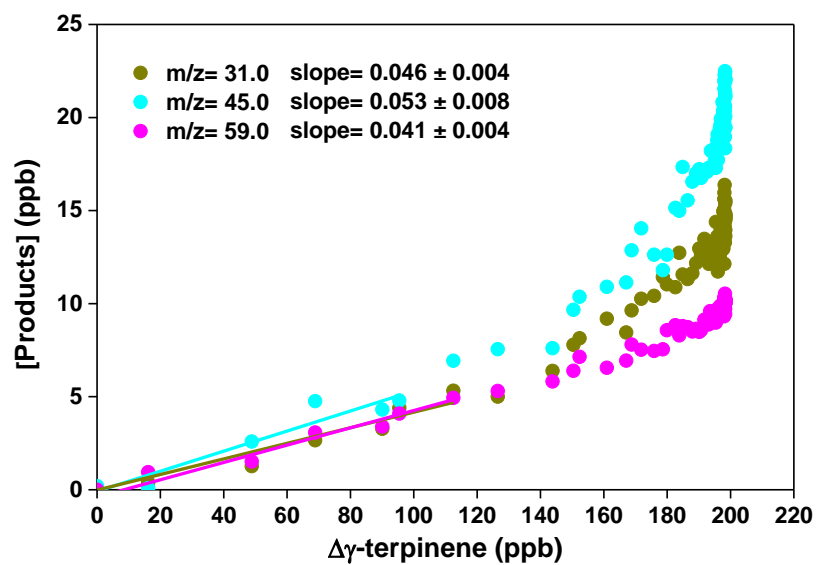


Figure IV.6: Typical plots for the determination of the gas-phase product yields formed from the ozonolysis of γ -terpinene (initial concentrations: γ -terpinene 200 ppbv and O_3 2780 ppbv).

The yields obtained from the slope of the linear least-squares fit to the data are shown in [Table IV.4](#).

Table IV.4: Identification of the ions detected by the PTR-MS during the gas-phase reaction of γ -terpinene with ozone (m/z masses include the addition of H⁺). N.D: Not Determined yield.

m/z	Formula	Assignment	Yield range (%)
31.0	CH ₂ OH ⁺	Formaldehyde	3 - 6
45.0	C ₂ H ₄ OH ⁺	Acetaldehyde	3 - 6
47.0	CH ₂ O ₂ H ⁺	Formic acid	7 - 11
59.0	C ₂ H ₂ O ₂ H ⁺	Glyoxal	6 - 9
	C ₃ H ₆ OH ⁺	Acetone	
61.0	C ₂ H ₄ O ₂ H ⁺	Acetic acid	5 - 6
73.0	Unidentified	-	2 - 3
87.0	C ₄ H ₆ O ₂ H ⁺	-	6 - 8
89.0	C ₃ H ₄ O ₃ H ⁺	-	2 - 3
99.1	C ₆ H ₁₀ OH ⁺	Cyclohexanone	N.D
100.1	¹³ C ₆ H ₁₀ OH ⁺	Cyclohexanone	N.D
101.0	C ₄ H ₄ O ₃ H ⁺	2-Oxosuccinaldehyde	< 1
103.1	C ₄ H ₆ O ₃ H ⁺	-	1 ± 2
115.1	C ₆ H ₁₀ O ₂ H ⁺	4-methyl-3-oxo-pentanal	6 - 8
131.1	C ₆ H ₁₀ O ₃ H	-	1 - 2
141.1	Unidentified	-	< 1
155.2	Unidentified	-	< 1
167.0	Unidentified	-	< 1
169.2	C ₁₀ H ₁₆ O ₂ H ⁺	-	< 1
183.0	Unidentified	-	< 1
185.2	C ₁₀ H ₁₆ O ₃ H ⁺	-	< 1

The highest yields (in %) were observed for formic acid (7 - 11), glyoxal and acetone (6 - 9), acetic acid (5 - 6), acetaldehyde (3 - 6), formaldehyde (3 - 6), 4-methyl-3-oxo-pentanal (6 - 8), and the compounds at m/z 87.0 (6 - 8), m/z 89.0 (2 - 3) and the unidentified one at m/z 73.0 (2 - 3)

The average yield for formaldehyde (~4%) is in the same range as those obtained by **Lee et al. (2006)** who studied the ozonolysis of biogenic VOCs having two endocyclic C=C double bonds: α -humulene and α -terpinene with formaldehyde yields of (3.5 ± 1) % and (4 ± 2) %, respectively. Also, the yields recorded for acetaldehyde, formic acid and acetic acid were consistent with those reported by **Lee et al. (2006)** in their study on the ozonolysis of several monoterpenes. The sum of the average yields of glyoxal and acetone was found to be ~7%, which is a factor of two lower than the value of acetone (15%) reported by **Atkinson and Arey, (2003a)**, who studied the reaction of ozone with α -pinene. The average total yield for all the measured major gaseous products was ~ 52%.

IV.1.2.3 Mechanism

Several previous studies (Atkinson, 1997; Calvert and Madronich, 1987; Herrmann et al., 2010; Zhang and Zhang, 2005) have been performed to study the products formed from the atmospheric oxidation of monoterpenes with ozone. However, to our knowledge there are no literature data describing γ -terpinene ozonolysis. γ -terpinene contains two endocyclic C=C double bonds so, mechanistic details were evolved from experimental findings and literature studies of monoterpenes having one or two endocyclic double bonds. Research works that have investigated the ozone reaction of α -phellandrene (Mackenzie-Rae et al., 2017a), limonene (Leungsakul et al., 2005), α -pinene (Zhang and Zhang, 2005) and α -terpinene (Herrmann et al., 2010) were useful guides for this study. As there are similarities between the chemical structure of γ -terpinene and these monoterpenes, comparable degradation pathways following the ozone oxidation can be expected.

The reaction mechanism of γ -terpinene with ozone leading to the products listed in [Table IV.4](#) is proposed in [Figure IV.7](#) and [Figure IV.8](#). The ozonolysis reaction is initiated by the addition of ozone across the C=C double bond to form energy rich species (1,2,3-trioxolane) referred to as primary ozonides (POZs) that rapidly decompose and form Criegee intermediates (CIs) (Johnson and Marston, 2008). The CIs contain excess energy so they are either stabilized or decomposed. Stabilization of CIs is achieved through unimolecular or bimolecular reactions with available atmospheric species and their decomposition is believed to occur via several reaction channels (Finlayson-Pitts and Pitts Jr, 2000) including the “hydroperoxide” channel which is responsible for the OH formation and the “ester” or the “hot acid” channel, leading to the formation of an ester that can further decompose into different compounds.

As shown in [Figure IV.7](#), during the ozonolysis reaction of γ -terpinene, the addition of ozone can take place either on 1-seco or 4-seco endocyclic C=C double bond, resulting in the formation of two intermediate species (POZ1) and (POZ2). Note that the term 'seco' is based on the accepted rules for terpene nomenclature and used to appoint on the bond cleavage between two atoms of the parent structure (Larsen et al., 1998). Ignoring the differences of syn- and anti-conformation, the rapid decomposition of both POZs through homolytic cleavage of the C–C and

one of the O–O bonds leads to the formation of four unique excited Criegee intermediates named CI1, CI2, CI3 and CI4. CI1 and CI2 retain the 4-seco internal C=C bond, whereas CI3 and CI4 maintain the 1-seco internal C=C bond.

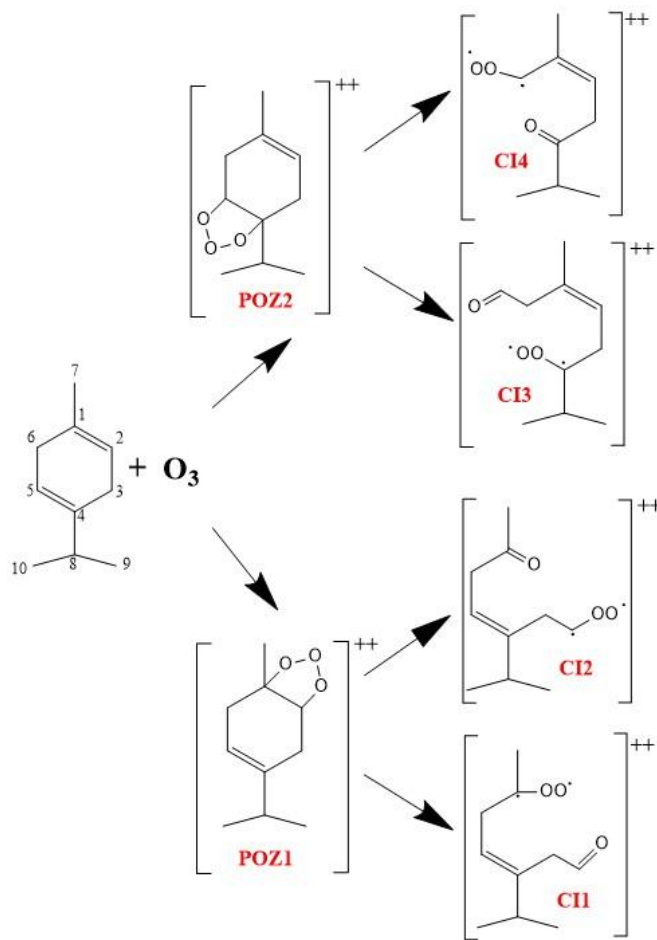


Figure IV.7: Simplified mechanism for the formation of (POZs) and (CIs) for the reaction of γ -terpinene and ozone.

The detailed degradation mechanism of CI1 is displayed in **Figure IV.8**. Comparable schematics for the remaining CIs are provided in the Supporting Information (**Figure S.4**), they lead to similar products as those produced by CI1.

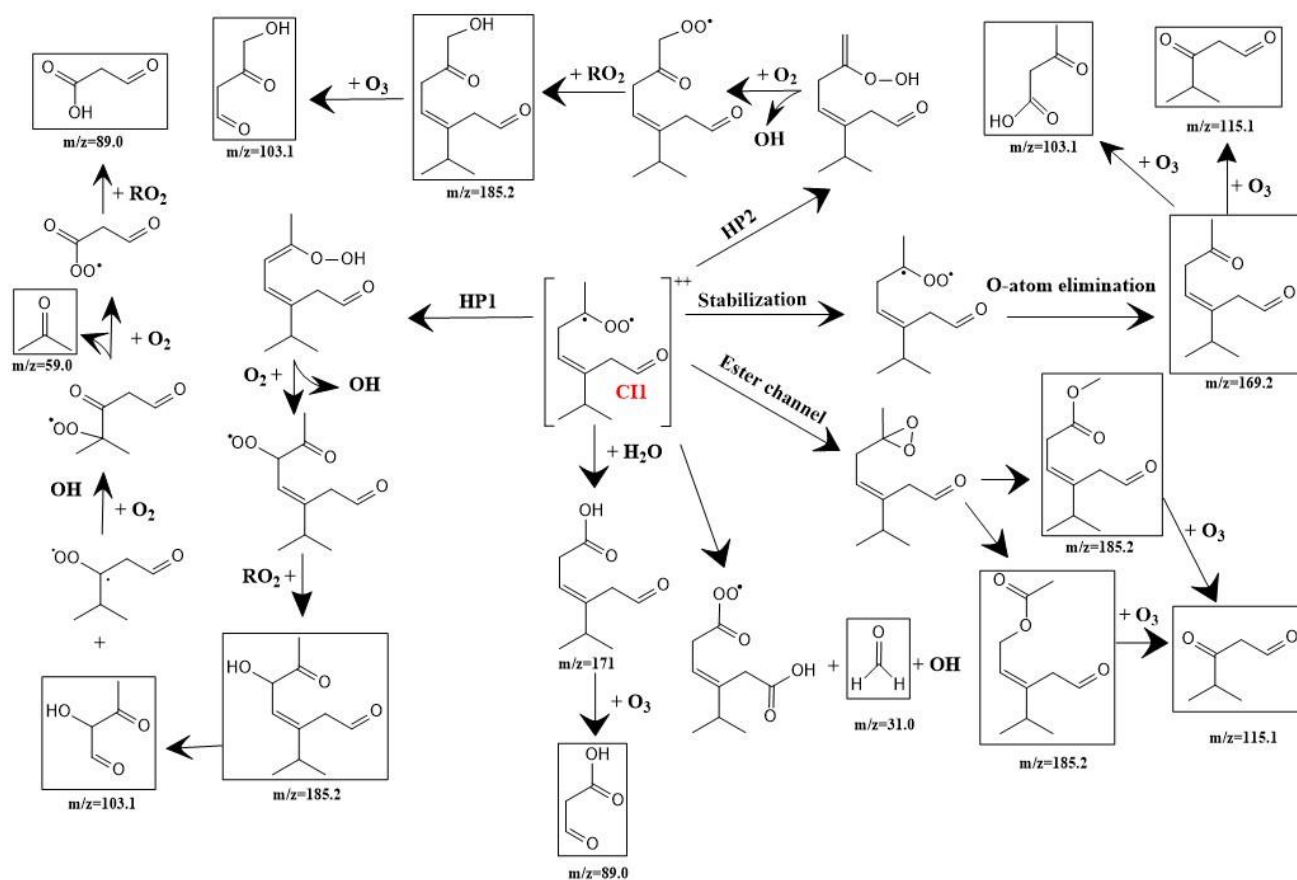


Figure IV.8: Partial mechanism for the ozonolysis of γ -terpinene starting from CII, yielding to products detected by the PTR-MS. Comparable schematics for the remaining CIs are provided in the supplementary information (Figure S.4). (Note that the shown m/z corresponds to the protonated form of the products).

Generally, the reaction of ozone with unsaturated hydrocarbons forms different oxygenated products. In the proposed mechanism for CII, an unsaturated keto-aldehyde of chemical formula $C_{10}H_{16}O_2$ (detected at $m/z = 169.2$ with the PTR-MS) probably known as 1-sec- γ -terpinonaldehyde analogous to pinonaldehyde from α -pinene or limonaldehyde from limonene may be formed from the oxygen-atom elimination channel. However, as this unsaturated compound was detected at low concentration by the PTR-ToF-MS (< 0.5 ppbv) one can assume that it was decomposed through its reaction with ozone.

The hydroperoxide channel is an important pathway for CIs decomposition and it generally explains the OH formation during alkene ozonolysis. Through this degradation pathway, CII rearranges into vinyl hydroperoxide before it loses an OH and decomposes into a vinyloxyl

radical. The latter is followed by addition of an oxygen molecule to form peroxy radicals. These radicals further react with another peroxy radical to form alkoxy radicals or dicarbonyl compounds such as α -hydroxycarbonyls having the chemical formula $C_{10}H_{16}O_3$. A set of isomeric species (esters, epoxides, secondary ozonides ...) of the same formula were also suggested from different decomposition/isomerization channels.

CII may also decompose through an ester or 'hot' acid channel to form a dioxirane intermediate. The dissociation of the O–O bond of the dioxirane leads to the formation of a diradical that rearranges to form two possible esters. The possible decomposition of the esters forms CO_2 and an alkyl biradical which can yield a variety of oxygenated and short carbon chain compounds.

It should be taken into account that this study was performed in the presence of high concentrations of reactants and in absence of NO_x ($NO+NO_2$), which means under atmospherically simplified conditions. So, the results obtained here are applicable to unpolluted atmosphere where peroxy radicals react with RO_2 or HO_2 rather than with NO_x . Besides, it is possible for NO to react with the formed alkyl and acyl peroxy radicals to give alkoxy radicals and NO_2 which might react with acyl peroxy radicals to form peroxyacyl nitrates. As a result, the proposed mechanism and the general ozonolysis chemistry of γ -terpinene can be shifted in a number of ways. However, the simplified mechanism suggested in this study can be integrated into atmospheric models such as the Master Chemical Mechanism (**Saunders et al., 2003**) to describe the chemistry of γ -terpinene and similar endocyclic monoterpenes.

IV.2 Particle-phase study

IV.2.1 SOA formation yields

Secondary organic aerosols derived from biogenic VOCs dominate the global burden of atmospheric SOA. **Griffin et al., (1999)** have estimated that 18.5 Tg of SOA is formed annually from biogenic precursors. Among the atmospheric oxidation reactions of organic precursors, ozonolysis represents the major reaction pathway (typically 80% of the hydrocarbons reacted with O₃) that yields aerosols (**Hoffmann et al., 1997**). Efforts have been made to quantify the aerosol formation (i.e. aerosol yields) of terpenes, however, there is still a lack of knowledge concerning some monoterpenes such as γ -terpinene. Previous studies have shown that the SOA formation potential of different alkenes depends strongly on their chemical structure (**Keywood et al., 2004; Jokinen et al., 2015**). Moreover, some investigations (**Lee et al., 2006; Keywood et al., 2004**) have demonstrated that the presence of an endocyclic double bond may result in an enhancement of SOA yield. For example, by comparing 2 isomers α -pinene (endocyclic monoterpene) and β -pinene (exocyclic monoterpene), the SOA yield generated from the former (41%) is ~2 times higher than the yield of the latter (17%) (**Lee et al., 2006**).

Being an alkene with two endocyclic double bonds, γ -terpinene is expected to contribute to atmospheric SOA formation. The examination of the contribution of the γ -terpinene ozonolysis on the atmospheric SOA budget was part of this research study. To our knowledge, this work is the first investigation of the SOA formation from the γ -terpinene reaction with ozone.

IV.2.1.1 Experimental conditions

A total of 15 experiments were performed in *CHARME* to determine the formation yields of SOA formed from the ozonolysis of γ -terpinene in the presence (6 experiments) and absence (9 experiments) of cyclohexane. The initial conditions of all the experiments are displayed in [Table IV.5](#).

Table IV.5: Summary of the experimental conditions and results for the SOA formation from the ozonolysis of γ -terpinene in the presence and absence of cyclohexane at (294 ± 2) K, atmospheric pressure and RH = (1.7 ± 0.1) %.

Experiment		$[\gamma\text{-terpinene}]_0^a$		$[\text{O}_3]_0^b$	Δvoc^c	M_0^d	Yield (Y) ^e
		(ppb)	($\mu\text{g}\cdot\text{m}^{-3}$)	(ppb)	($\mu\text{g}\cdot\text{m}^{-3}$)	($\mu\text{g}\cdot\text{m}^{-3}$)	
Without cyclohexane	1	15.3	87.1	60	83.5	9.7	0.12
	2	22.8	129.7	57	122.9	24.0	0.19
	3	41.3	234.2	101	227.2	69.7	0.31
	4	66.0	374.5	130	364.5	160.0	0.44
	5	82.7	468.8	211	460.6	212.6	0.46
	6	142.8	809.3	300	799.7	371.5	0.46
	7	165.3	937.2	430	926.2	440	0.47
	8	294.0	1666.2	621	1657.2	840	0.50
	9	325.2	1843.8	690	1830.9	896.6	0.49
With cyclohexane	1	37.2	211.1	91	208.3	34.3	0.16
	2	97.9	555.3	280	552.3	148.9	0.27
	3	157.0	889.9	420	887.3	260.9	0.29
	4	176.9	1002.5	445	994.5	385.1	0.39
	5	250.9	1421.9	600	1417.9	696.4	0.43
	6	285.7	1619.2	625	1610.2	719.6	0.45

IV.2.1.2 Results and discussions

The evolution of the SOA yields calculated from (Eq. III.14) was represented as a function of the formed M_0 concentrations in Figure IV.9. The experimental data obtained were processed using the semi-empirical gas / particle absorption model (previously described in section (Eq. III.15)) (Odum et al., 1996).

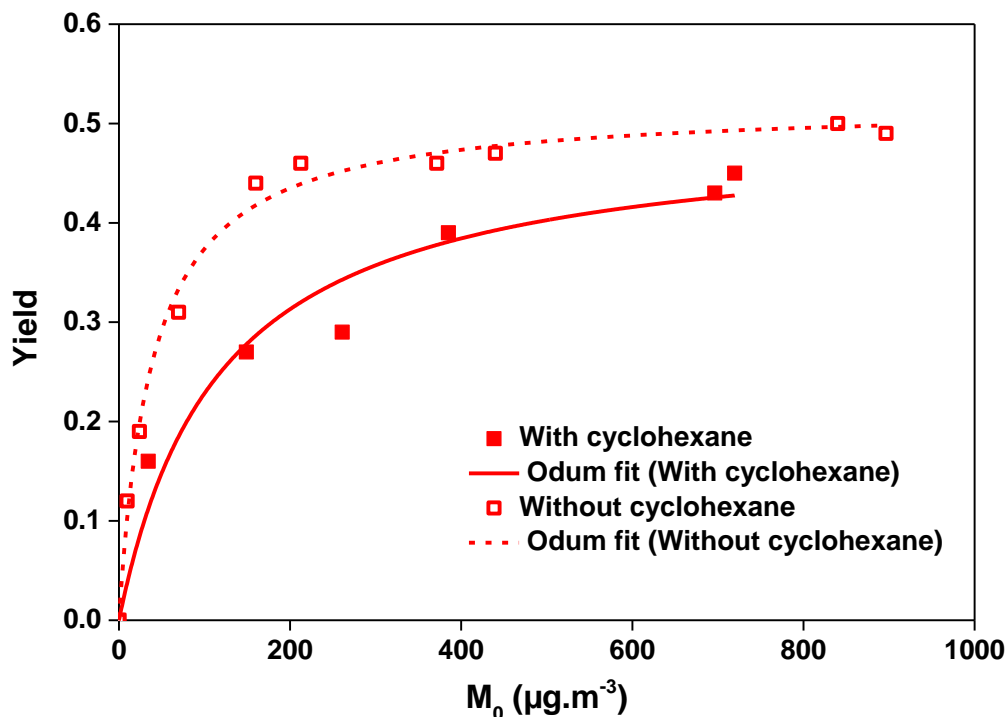


Figure IV.9: Aerosol yield (Y) as a function of the organic aerosol mass concentration formed (M_0) from the ozonolysis of γ -terpinene in the presence (solid squares) and absence (open squares) of cyclohexane, respectively. The lines (solid in presence and dash in absence of cyclohexane) represent the best fit of the data considering one semi-volatile major product.

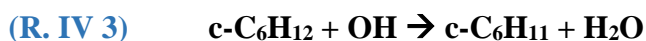
The data obtained with and without cyclohexane were fitted using the model with a single product; the corresponding parameters α and K are listed in **Table IV. 6**. The fits lead to values of $\alpha = 0.49 \pm 0.04$ and $K = (0.008 \pm 0.002) \text{ m}^3 \mu\text{g}^{-1}$ for the experiments performed in the presence of cyclohexane and $\alpha = 0.52 \pm 0.01$ and $K = (0.025 \pm 0.003) \text{ m}^3 \mu\text{g}^{-1}$ for the experiments in the absence of the OH scavenger s . The fit with two products was also tested (it is presented in **Table S. 1**). Although it allows to describe the experimental data, it was not retained as the uncertainties on the K values exceed that of K .

Table IV. 6 : The one product equation parameters obtained in this study.

α_1	$K_{p,1}(\text{m}^3 \cdot \mu\text{g}^{-1})$	Conditions	Reference
0.49 ± 0.04	0.008 ± 0.002	$T = 294 \pm 2 \text{ K}$, $\text{RH} < 2 \%$, with cyclohexane	This study
0.52 ± 0.01	0.025 ± 0.003	$T = 294 \pm 2 \text{ K}$, $\text{RH} < 2 \%$, without scavenger	

In the absence of cyclohexane, the hydroxyl radicals formed from the ozonolysis reaction will rapidly react with γ -terpinene, and as the VOC is depleted, OH will also react with the oxidation products of both γ -terpinene-O₃ and γ -terpinene-OH. Such reactions are expected to contribute to the aerosol formation, particularly due to the formation of acylperoxy radicals which are central to aerosol formation (**Keywood et al., 2004**).

Cyclohexane has been shown to reduce SOA yields in ozonolysis experiments with cyclohexene (**Keywood et al., 2004**), limonene (**Saathoff et al., 2009; Gong et al., 2018**), α -phellendrene (**Mackenzie-Rae et al., 2017**) and also in this study. An explanation for the observed effect of the scavenger could be due to the different radical products formed in the OH-scavenger reactions. In fact, when cyclohexane is used as an OH scavenger, the radical produced initially from H atom abstraction is the cyclohexyl radical (**R. IV 3**). Then upon addition of molecular oxygen, the cyclohexylperoxy radical is formed (**R. IV 4**) and further it undergoes self-reaction to give cyclohexanol and cyclohexanone (**R. IV 5**) and (**R. IV 6**) (**Bonn et al., 2002**).



The production of HO₂ radicals may also occur from the reaction of O₂ with cyclohexyloxy radicals (**R. IV 7**); however, this amount is expected to be small. The generated radicals in the OH-scavenger reactions can thus alter the peroxy radical budget in the ozonolysis system, and according to **Keywood et al., (2004)** for endocyclic alkenes (which is the case for γ -terpinene), the SOA yields decrease as the [RO₂]/[HO₂] ratio increases.

Comparing the amount of aerosols produced upon ozonolysis of different monoterpenes (**Saathoff et al., 2009; Mackenzie-Rae et al., 2017b**), **Figure IV. 10** showed that limonene and α -phellendrene contribute more the SOA formation than γ -terpinene and α -pinene. It is important to note that, the aerosol density used in this study to measure the SOA yield is 1g.cm⁻³, however, in their studies **Saathoff et al., (2009)** used 1.25 g cm⁻³ and **Mackenzie-Rae et al., (2017b)** 1.25 g

cm⁻³. Also, the number and the position of the double bonds play an important role in the production of SOA. For α -phellendrene, the formation of semi-volatile organic compounds was likely driven by the presence of two conjugated endocyclic double bonds, with functionalisation rather than fragmentation dominating the chemical mechanism of its ozonolysis reaction (Mackenzie-Rae et al., 2017). However, as previously shown in Table IV.4, the addition of ozone to γ -terpinene does not only produce products that contain two (or more) polar functional groups (low-volatility products), but also short-chain ones (C3-C4) generated from the opening and fragmentation of the ring and the latter are known to be volatile and do not contribute to aerosols formation.

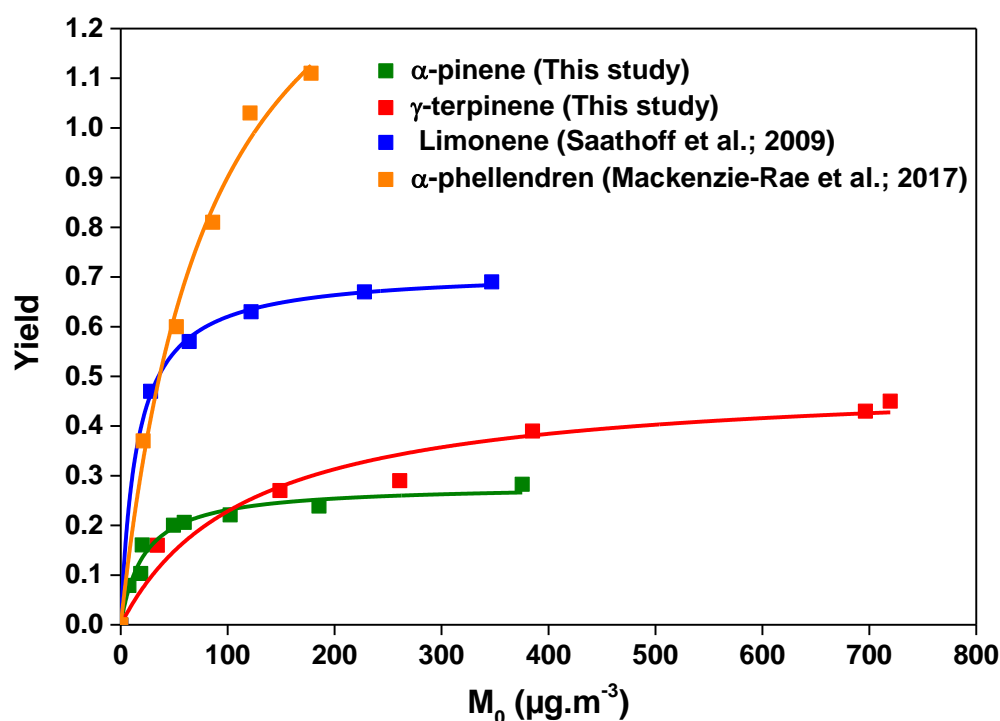


Figure IV. 10: Comparison of SOA yields formed from the ozonolysis of γ -terpinene, α -pinene, limonene and α -phellandrene. Experiments performed in the presence of an OH radicals scavenger (cyclohexane) under dry conditions, atmospheric pressure and at room temperature (294 ± 2) K. The lines are the best fits of the data obtained with the single product model (Odum et al., 1996).

IV.2.2 SOA Characterization

For the characterization of SOA formed from the reaction of γ -terpinene with O_3 , observations by Scanning Electron Microscopy (SEM) were performed. These investigations allowed the determination of the physical state and morphology of SOA.

The variation of each parameter was examined at different conditions (**Table IV. 7**) including:

1. Sampling at different stages of the experiment (experiment 2).
2. Sampling at different initial concentrations of the organic precursor (experiments 1 & 2).
3. Sampling in the presence and absence of OH radical scavenger (experiments 2 & 3).

Table IV. 7: Summary of the experimental conditions (at $T = (297 \pm 2)$ K, $P = (1019 \pm 2)$ mbar and $RH=1.9\%$).

Exp	[γ -terpinene] (ppb)	[Ozone] (ppb)	[Cyclohexane] (ppb)	Sampling time	N max(#/cm ³)	Mass max ($\mu\text{g}/\text{m}^3$)
1	16	55	×	10 min	4.18×10^4	6.6
2	158	757	×	5 min	1.09×10^6	340
3	158	924	111074	5 min	6.13×10^5	318

IV.2.2.1 SOA sampling

A Dekati 3-stage cascade impactor presented in **Figure IV. 11**, was connected to the chamber to sample the particles. Its operating principle is based on inertial size classification of the collected particles. The different stages of the impactor are:

- Stage one: highest impactor stage composed of an acceleration plate with a cut-off diameter (DP, 50%) of 10 μm and a collection plate that collects particles having an aerodynamic diameter higher than 10 μm .
- Stage two: mid impactor stage with a collection plate that collects particles having aerodynamic diameters between 10 and 1 μm .
- Stage three: lowest impactor stage with a collection plate that collects particles having aerodynamic diameters between 1 μm and 30 nm.



Figure IV. 11: The Dekati 3-stage cascade impactor used for sampling the SOA in *CHARME*.

On each collection plate, a 25 nm nuclepore track-etched polycarbonate membrane (Whatman) with sharply defined pore sizes ($0.2 \mu\text{m}$), was placed to be a smooth flat surface for collecting particles. In addition, several copper grids covered by holey carbon film known as lacey carbon films (300 Mesh Cu (50); Agar Scientific) were stuck on the membrane as shown in **Figure IV. 12** to statistically increase the chances of having a grid under an impaction spot. These grids provide the thinnest possible support film while maintaining adequate strength and give practically no background interference in the STEM. They are appropriate for determining the structure of the studied particles.



Figure IV. 12: One collection plate of the impactor with a nucleopore membrane and 3 lacey carbon grids.

Some copper grids covered by carbon formvar film were also used for some samples to allow precise measurement of the particle size.

The collection took place at different times after the start of the reaction (5 min, 60 min, and 120 min) for experiment 2, and at the end of the reaction (120 min) for experiments 1 and 3. The duration of sampling was 10 min for experiment 1 and 5 min for experiments 2 and 3; it was estimated to be efficient for collecting a representative amount of particles.

IV.2.2.2 Results and discussions

From the temporal evolution of the total mass and number concentrations (**Figure IV.13**) and the SOA number size distribution at various times (**Figure IV. 14**), it was observed that SOA were formed soon (~2 mins) after the addition of ozone in experiment 2. During the first minutes of the reaction, there was a fast increase in the particle number concentration followed by a gradual decrease throughout the experiment. This corresponds to an initial nucleation step that forms a burst of particles which then undergo coagulation resulting in an increase in the size and a decrease in the number concentration. The decline in the aerosol mass concentration at the end of the reaction corresponds to the loss of the particles on the chamber walls which was calculated to be $k = 1 \times 10^{-5} \text{ s}^{-1}$ corresponding to a lifetime of ~28 hours.

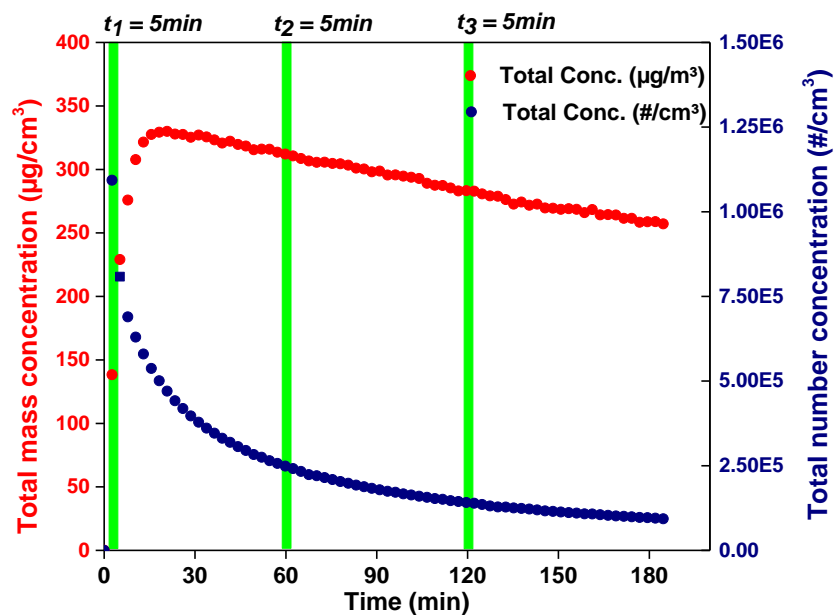


Figure IV.13: Time profile of mass and number concentrations for SOAs formed from the ozonolysis of γ -terpinene (experiment 2). Green region represents the time and the duration at which the aerosols were sampled and corresponds to 3 different numbers masses and sizes of the sampled particles.

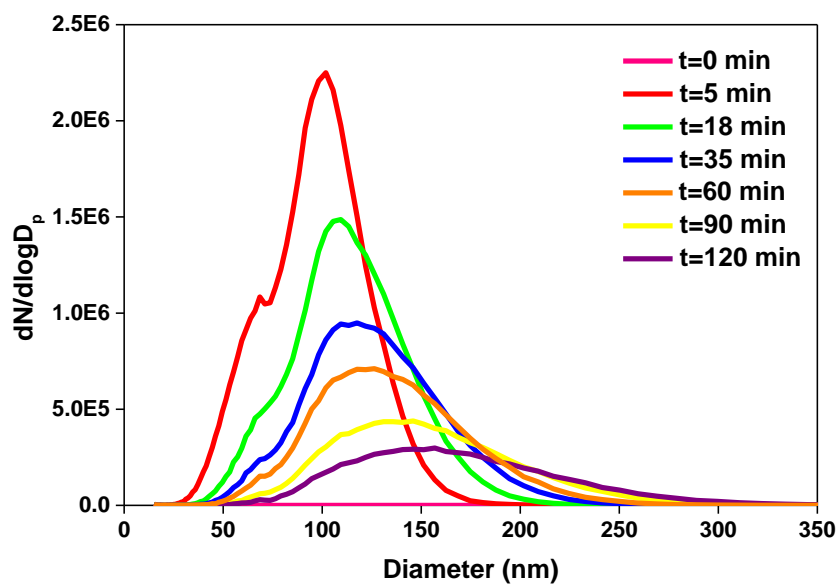


Figure IV. 14: SOA size distribution at different reaction times during the ozonolysis of γ -terpinene.

IV.2.2.2.1 Cryo-TSEM-EDX analysis

The field effect gun-SEM is coupled with a transmitted electron detector, with three Energy Dispersive X-ray spectrometers and with a cryostage. Experiments were performed using a JEOL 7100F FEG-TSEM equipped with three ultrathin-window (30 mm²) energy-dispersive X-ray detectors (Bruker XFlash 6/30) and a Quorum PP3010P cryostage. Data and pictures were acquired at 15 kV, 300 pA, 10 mm for the working distance and at 100°C. SOA are semi-volatile particles sensitive to damage by the electron beam under the vacuum of the microscope chamber (**Schmied and Poelt, 2002**). To limit this damage, SOA particles were quickly cooled in liquid nitrogen and moved into the preparation cryo-chamber for temperature stabilization at -100°C before transferred on the cryostage of the microscope for the observations. To validate this experimental protocol, the size of particles shown at ambient temperature was compared to those detected at -100°C as illustrated **Figure IV.15**. It was observed that the particle size was lower at ambient temperature, notably for the smallest ones marked by red arrows, that confirms the necessity to study particles at -100°C to avoid the beam damage of SOA. In average, particle diameter decreases by 6.4% when the temperature is lowered from ambient to -100°C (calculated from 33 particles).

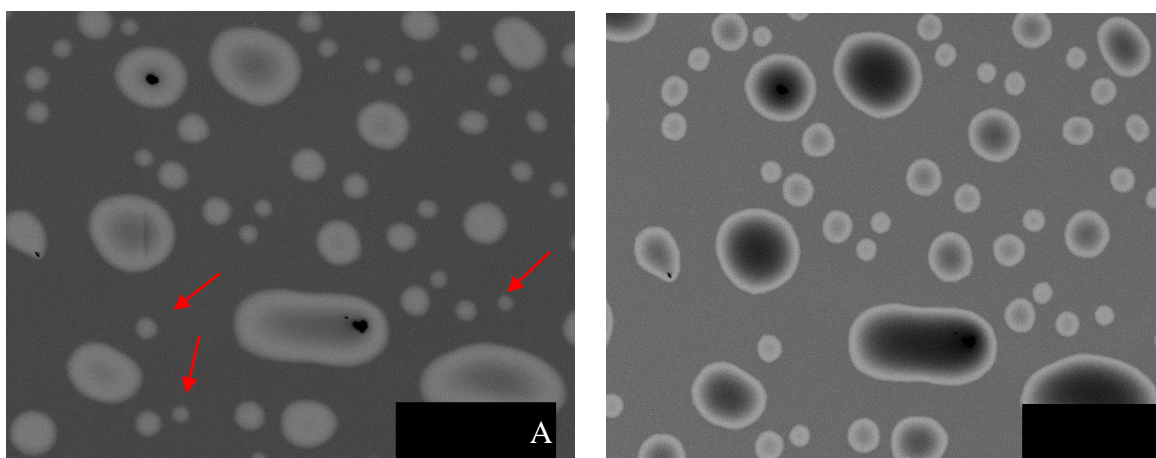


Figure IV.15: Comparison of SOA particles observed at ambient temperature and at -100°C for the sample collected after 120 min from the start of experiment 2.

Consequently, all SEM images presented below were acquired at -100°C.

IV.2.2.2.2 Physical state and morphology of the SOA

The physical state of organic particles strongly affects their formation, properties, transformation and temporal evolution (Abramson et al., 2013). The physical state and morphology of SOA were investigated, by observation of particles collected on lacey and formvar films.

A. Effect of the experiment progress

As shown in Figure IV.16, the particles collected on lacey film during experiment 2 at $t = 5$ min, 60 min and 120 min, follow the shape of the lacey film revealing that the formed SOA were not solid but viscous. If they were solid, their projected area would be perfectly circular, that was not the case.

The results were in agreement with numerous recent studies which have provided evidence that atmospheric organic aerosols may exist as semi-solid viscous particles such as Virtanen et al., (2010) and Kuwata and Martin, (2012) who have demonstrated that SOA produced from ozonolysis of α -pinene could be present in highly viscous semi-solid state at low relative humidity. The viscosity of organic particles can impact the rate of aerosol oxidation, with implications for predicting their chemical composition and hygroscopicity (Marshall et al., 2016; Reid et al., 2018).

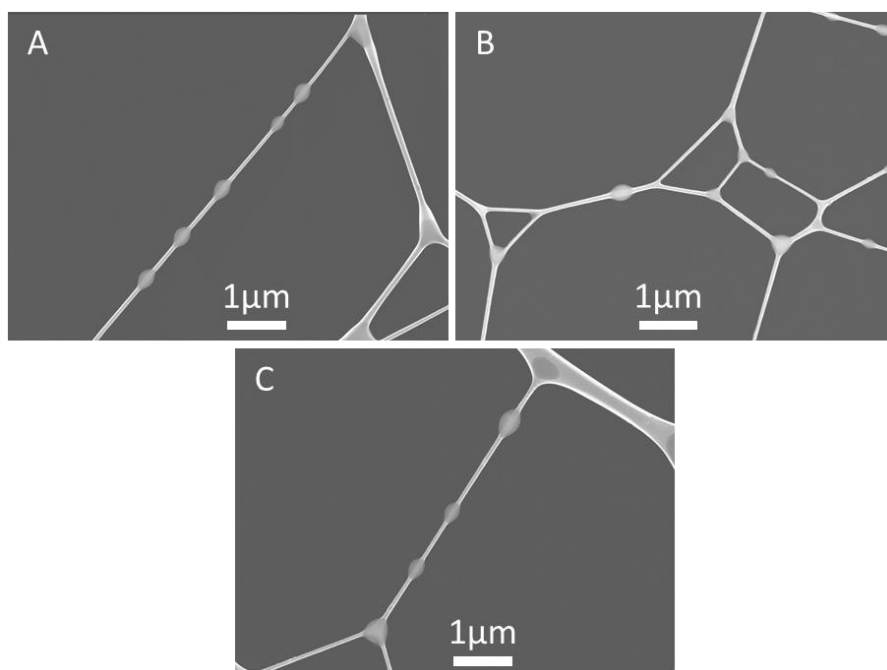


Figure IV.16: SEM images of SOAs collected on lacey film (DP50 = 30 nm) during experiment 2 at (A) $t = 5$ min, (B) $t = 60$ min and (C) $t = 120$ min.

Regarding the morphology, **Figure IV.17** showed some particles collected on carbon formvar film during experiment 2. The SOA were of rounded shapes typical of spherical particles.

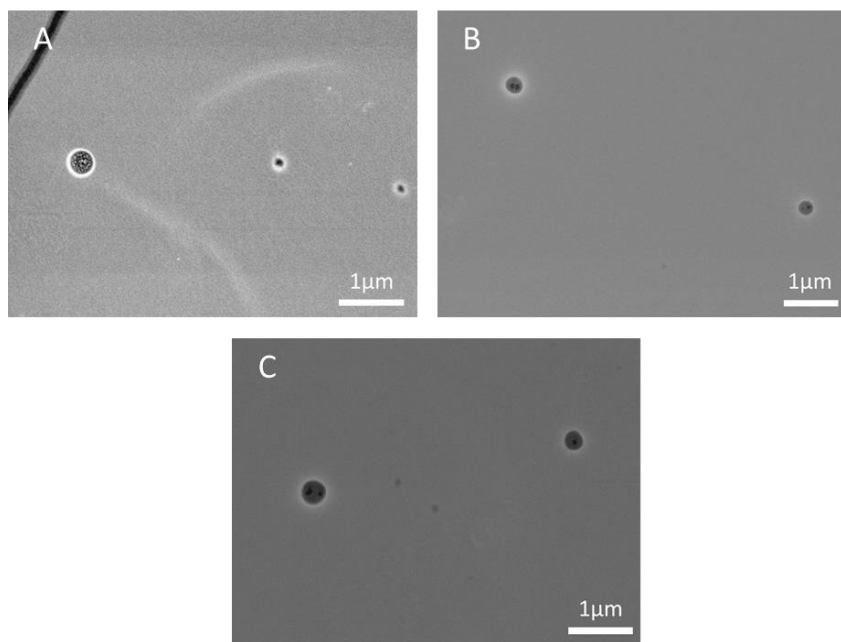


Figure IV.17: SEM images of SOA collected on carbon formvar film (DP50 = 30 nm) during experiment 2 at (A) $t = 5$ min, (B) $t = 60$ min and (C) $t = 120$ min.

There was no change of the physical state and the morphology of the SOA collected during different stages of the experiment.

B. Effect of initial precursor concentration

To assess whether the initial concentration of the organic precursor (γ -terpinene) affects the physical state of the aerosols. SOA formed in experiment 1 ($[\gamma\text{-terpinene}]_0 = 16$ ppb) are compared to those of experiment 2 ($[\gamma\text{-terpinene}]_0 = 158$ ppb).

The SEM image of particles collected on lacey film at $t = 120$ min of experiment 1 are displayed in

Figure IV.18 and showed a similar shape (round) and physical state (viscous) as SOA formed in experiment 2 at $t = 120$ min (**Figure IV.16-C**). Thus, there was no influence of the initial concentration of precursor on the morphology and physical state of the SOA.

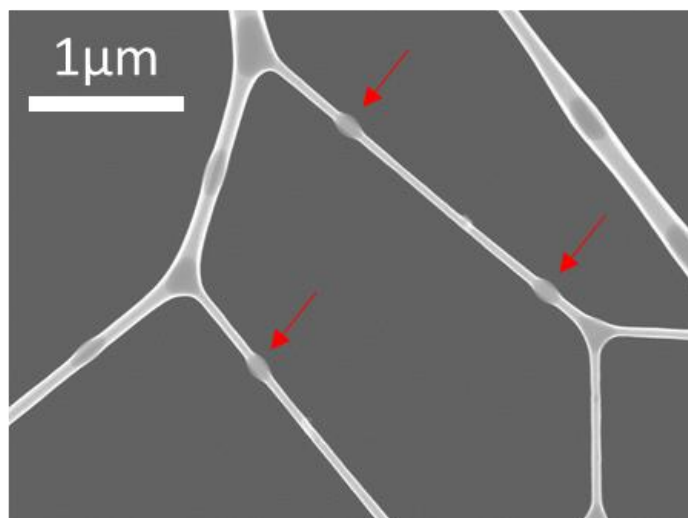


Figure IV.18: SEM image of SOA collected on lacey film (DP50 = 30 nm) at $t = 120$ min of experiment 1.

C. Effect of a OH radical scavenger (cyclohexane)

To estimate the influence of OH radical scavenger (cyclohexane) on the physical state of the formed aerosols, the SOA produced from experiment 2 and experiment 3 were compared. The particles collected on lacey film at $t = 120$ min of experiment 3 ($[\gamma\text{-terpinene}]_0 = 158$ ppb; with cyclohexane) were viscous and round shaped as presented in **Figure IV.19**, as the aerosols formed in experiment 2 ($[\gamma\text{-terpinene}]_0 = 158$ ppb; without cyclohexane) (**Figure IV.16-C**). Therefore, no influence of the cyclohexane was detected on the physical state of the SOA.

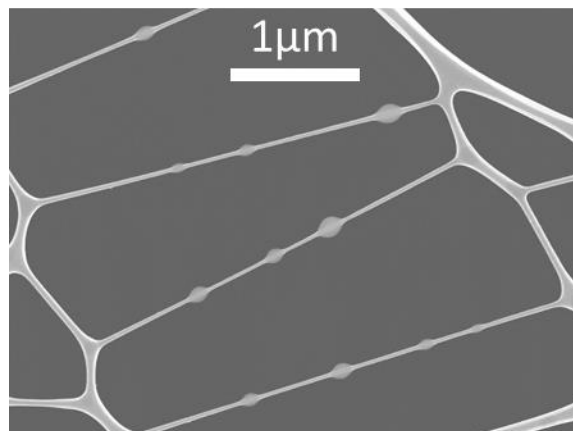


Figure IV.19 : SEM image of SOA collected on lacey film (DP50 = 30 nm) during experiment 3 at $t = 120$ min.

In short, cryo-TSEM-EDX was used to characterize the morphology and physical state of the SOA formed from the ozonolysis of γ -terpinene. The aerosols formed from this reaction were spherical and viscous particles. Under the available experimental conditions (low relative humidity), they display only one organic phase and no significant difference in the organic aerosol properties were observed when (A) the SOA were sampled at different stages of the reaction, (B) the initial precursor concentration was changed and (C) a OH radical scavenger was added.

The chemical, morphological information and phase data at the single-particle level are of crucial importance for purposes of tracing and understanding the formation and reaction mechanisms of aerosols. Thus, these primary experiments should be completed in the future by complementary experiments such as (i) evaluating the value of particles viscosity by Atomic Force Microscopy (AFM) and comparing it to standard particles of known viscosity (**Lee et al., 2017**); (ii) quantifying the particle oxygen content or the Carbon to Oxygen ratio (C/O) by collecting the SOAs on a substrate such as a boron (free of C and O).

IV.2.3 Hygroscopicity

Hygroscopicity of the aerosols represents their ability to interact with water vapor in the surrounding air. In order to understand the interaction between atmospheric aerosols and clouds, a growing number of studies have been conducted and focused on the conditions at which aerosols of different chemical compositions can serve as CCN (cloud condensation nuclei).

Measurements of water uptake and CCN activity of atmospheric particles, are needed for climate models, cloud-resolving models, and air quality predictions (Mirrieles and Brooks, 2018). The single parameter hygroscopicity κ “ κ ” (defined In the section IV.2.3.1 Data Analysis) proposed by Petters and Kreidenweis, (2007) is commonly used to represent the hygroscopicity and CCN activity of aerosol particles under sub and super-saturation conditions. The parameter κ describes the relationship between particle dry diameter and cloud condensation nuclei (CCN) activity. $\kappa \sim 1.4$ is an upper limit for the most hygroscopic species typically found in atmospheric aerosol (e.g., highly CCN active salt, NaCl), $\kappa \sim 0.1 - 0.5$ for slightly to very hygroscopic organic species, whereas $\kappa \sim 0$ is for non-hygroscopic particles (Petters and Kreidenweis, 2007). Some derived κ values for SOA from different laboratory studies are summarized in Table IV. 8.

Table IV. 8: κ values for laboratory-biogenic SOA derived from measurement in sub-saturated (HTDMA) conditions.

Precursor of SOA	κ_{GF}	Oxidation conditions	Reference
α -pinene	0.08 - 0.11	Photo-oxidation	(Duplissy et al., 2008)
α -pinene	0.07 - 0.13	Photo-oxidation	(Jurányi et al., 2009)
α -pinene	0.042 - 0.12	Photo-oxidation	(Alfarra et al., 2013)
3-carene	~ 0.026	Dark ozonolysis	(Prenni et al., 2007)
γ -terpinene	0.033 - 0.064	Photo-oxidation in the presence of $(\text{NH}_4)_2\text{SO}_4$	(Varutbangkul et al., 2006)
β -caryophyllene	0 - 0.03	Photo-oxidation	(Alfarra et al., 2012)

Most of the hygroscopicity and CCN activity studies focused on SOA derived from the oxidation of the three main monoterpenes α -pinene, β -pinene and limonene. The different studies have shown clear discrepancies depending on the experimental conditions (**Wex et al., 2009; Good et al., 2010; Alfarra et al., 2013; Hodas et al., 2016**). Motivated by this inconsistency between the different studies, further investigations of the hygroscopic properties and the CCN activity of monoterpenes under different experimental conditions in sub- and supersaturated regimes are required.

In this study, performed in collaboration between LPCA, PC2A (Lille-France), SAGE (Douai-France) and Institute of Chemical Process Fundamentals of the CAS (Czech Republic), the hygroscopic properties of SOA generated from the dark ozonolysis of γ -terpinene have been investigated in *CHARME*. The measurements were performed under sub-saturated conditions using a hygroscopic tandem differential mobility analyzer (HTDMA) to measure the hygroscopic growth factor (*GF*) and the derived (*K_{GF}*).

IV.2.3.1 Data Analysis

Throughout this section a number of terms and equations describing the hygroscopic properties of the particles will be frequently mentioned, thus they are well defined in this paragraph.

The saturation ratio ‘S’, in a thermodynamic equilibrium over a spherical aqueous solution droplet, can be described by classical Köhler theory (**Köhler, 1936; Brechtel and Kreidenweis, 1999; Kreidenweis et al., 2005**) demonstrated in the following equation:

$$\text{Eq. IV.7} \quad S = \frac{\text{RH}}{100 \%} = a_w \cdot \exp\left(\frac{4 \cdot M_w \cdot \sigma_{s/a}}{R \cdot T \cdot \rho_w \cdot D_p}\right)$$

where a_w is water activity of the solution droplet, $\sigma_{s/a}$ is the surface tension of the solution/air interface, often assumed to be equal to that of water (0.072 J m^{-2}), ρ_w and M_w are the density and the molar mass of water, respectively. R and T are the universal gas constant and absolute temperature, respectively. D_p is the wet particle diameter related to the growth factor determined by the HTDMA according to (**Eq. IV.8**)

$$\text{Eq. IV.8} \quad \text{GF} = \frac{D_{(\text{RH})}}{D_{(\text{Dry})}}$$

where $D_{(\text{RH})}$ and D_{dry} are the mobility diameters of the particle at a given RH% value and at RH < 5%, respectively.

For continuous water uptake humidograms, the HTDMA growth factors can be parameterized according to **Dick et al., (2000)** and **Kreidenweis et al. (2005)**, using a three-parameter curve fit in terms of water activity defined as:

$$\text{Eq. IV.9} \quad \text{GF} = \left[1 + (a + b \cdot a_w + c \cdot a_w^2) \frac{1 - a_w}{a_w} \right]^{1/3}$$

where a, b and c are the three adjustable coefficients determined by fitting the measured GF data obtained at different RH levels to an expression in a_w . From these parameters, the GF can be computed at a given RH using **Eq. IV.9**.

Köhler theory represented in (**Eq. IV.7**) is the combination of the water activity term and the Kelvin effect. It defines a thermodynamic barrier to the growth of a dry particle into a cloud droplet by condensation of water (**Köhler, 1936**). The water activity term (governed by the chemical composition, solubility and non-ideal mixing) is known as the solute or “Raoult effect”. As reported by **Davies et al. (2019)**, this effect describes the lowering of the equilibrium water vapor pressure above a liquid surface due to the presence of dissolved (hygroscopic) species, which can reduce the water activity value below 1. The second term, known as the Kelvin effect or curvature effect (determined by surface tension and the size), describes an increase in the equilibrium water vapor pressure above a microscopic curved surface. (**Davies et al., 2019**). In order to describe the relationship between the particle dry diameter and the cloud condensation nuclei (CCN) activity, **Petters and Kreidenweis, (2007)** have proposed a single-parameter expression for hygroscopicity and CCN activity defined through its effect on the water activity of the solution:

$$\text{Eq. IV.10} \quad \frac{1}{a_w} = 1 + \kappa \frac{V_s}{V_w}$$

where V_s and V_w are the volumes of dry particulate matter and water, respectively and κ is the hygroscopicity parameter kappa. This simple form of κ assumes perfect dissolution and no change

in the gas-particle partitioning of particle constituents upon variation of RH (i.e., non-volatile solutes) (Rastak et al., 2017). Assuming volume additivity (and spherical shape) and by combining Eq. IV.7 and Eq. IV.10, an equation defining the “κ-Köhler theory” is yielded (Petters and Kreidenweis, 2007):

$$\text{Eq. IV.11} \quad S(D) = \frac{D_p^3 - D_{\text{dry}}^3}{D_p^3 - D_{\text{dry}}^3 (1 - \kappa)} \exp\left(\frac{4M_w \sigma_s}{RT \rho_w D_p}\right)$$

where D_{dry} is the dry particle diameter and the other parameters are previously defined.

Eq. IV.11 can be used to predict the water uptake in the sub-saturated ($S < 1$) regime, as well as to expect the conditions for cloud droplet activation (Petters and Kreidenweis, 2007).

The rearrangement of Eq. IV.11 allows the calculation of κ_{GF} (Eq. IV.12), which is an approximation for the bulk solution water activity, under sub-saturated conditions (Cai et al., 2018):

$$\text{Eq. IV.12} \quad \kappa_{GF} = \frac{(GF^3 - 1)(1 - a_w)}{a_w}$$

where GF is the growth factor of the particle and a_w is the water activity represented according to the following equation:

$$\text{Eq. IV.13} \quad a_w = 0.01 \times RH / \exp\left(\frac{4 \cdot M_w \cdot \sigma_s / a}{R \cdot T \cdot \rho_w \cdot D_p}\right)$$

IV.2.3.2 Experimentation

A set of 25 experiments on the dark ozonolysis of γ -terpinene, were conducted at RH < 2%, under atmospheric pressure and at temperature (296 ± 2) K. The experimental conditions were varied to characterize the effects on the measured GF upon:

- (1) Changing the initial precursor (γ -terpinene) concentration.
- (2) Adding:
 - i. Trimethylbenzene (TMB) as anthropogenic SOA precursor,

- ii. Cyclohexane as OH radical scavenger.
- iii. Ammonium sulfate (AS) as seed particles.

Depending on the studied parameter the experimental protocol slightly changed, however the basic procedures were performed according to the following sequence:

- A. Introduction of known concentrations of organic compounds (γ -terpinene alone, γ -terpinene and TMB or γ -terpinene and cyclohexane).
- B. Injection of AS particles (for experiments involving seeds)
- C. Introduction of ozone to initiate the formation of SOA.
- D. Monitoring the particle properties through SMPS (size distribution and concentrations) and HTDMA (hygroscopicity).

A hygroscopic tandem differential mobility analyzer (HTDMA) previously presented in section [II.1.6.1](#), was used to measure online the hygroscopic properties of SOA formed from the ozonolysis of γ -terpinene. Then, the humidification section and the second DMA were set to constant RH in the range 87-93% in order to measure the GF at 90 % RH. For some experiments, when the particle nucleation has stopped and the mass of the particles have reached the maximum, the RH in the humidification section was varied from 93% to ~20%. The GFs were then plotted versus water activity (bulk equilibrium RH) to obtain a humidogram.

The different performed experiments with their conditions are summarized in [Table IV. 8](#).

Table IV.9: Summary of the different experimental conditions. The “white” rows corresponds to the experiments performed in the absence of any additive; “red” refers to tests in the presence of TMB; “yellow” indicates the tests in the presence of cyclohexane and “green” corresponds to experiments in the presence of ammonium sulfate. ^a The GF (90%) of pure AS; ^b The maximum reached mass of AS seeds; ^c The maximum reached mass of SOA+AS.

Exp N°	[GT] (ppb)	[Ozone] (ppb)	[Cyclohexane] (ppb)	[TMB] (ppb)	AS Seeds (#/cm ³)	Number Conc. (#/cm ³)	Mass Conc. (µg/m ³)	GF (90%) (D _{dry})	K _{GF}
1	158	1229	-	-	-	1.2×10 ⁶	358	1.050 (100-140 nm)	0.017 ± 0.001
2	402	1165	-	-	-	1.0×10 ⁷	433	1.045 (100-180 nm)	0.015 ± 0.001
3	150	1243	-	-	-	9.3×10 ⁵	298	1.049 (100-140 nm)	0.017 ± 0.001
4	8	58	-	-	-	3.9×10 ³	0.35	1.092 (55-60 nm)	0.033 ± 0.001
5	8	53	-	-	-	3.7×10 ³	0.27	1.110 (50-60 nm)	0.040 ± 0.001
6	16	33	-	-	-	7.5×10 ³	0.95	1.090 (60 nm)	0.031 ± 0.001
7	16	48	-	-	-	1.2×10 ⁴	2.25	1.109 (50-90 nm)	0.040 ± 0.001
8	16	42	-	-	-	1.5×10 ⁴	2.64	1.106 (50-90 nm)	0.039 ± 0.001
9	16	45	-	-	-	1.5×10 ⁴	1.96	1.088 (57-82 nm)	0.030 ± 0.001
10	158	1982	-	-	-	1.1×10 ⁶	400	1.048 (80-150 nm)	0.016 ± 0.001
11	320	2193	-	-	-	1.4×10 ⁶	909	1.045 (80-150 nm)	0.015 ± 0.001
12	16	52	-	-	-	1.5×10 ⁴	2.01	1.085 (50-80 nm)	0.029 ± 0.001
13	16	50	-	7	-	1580	0.8	1.092 (66-100 nm)	0.033 ± 0.001
14	48	500	-	50	-	1.5×10 ⁵	106	1.084 (80-150 nm)	0.030 ± 0.001
15	158	1240	-	50	-	5.9×10 ⁵	506	1.045 (140 nm)	0.015 ± 0.001
16	16	50	-	5	-	550	0.15	1.077 (150 nm)	0.027 ± 0.001
17	110	500	-	34	-	1.1×10 ⁵	205	1.053 (150 nm)	0.018 ± 0.001
18	410	1245	84000	-	-	1.2×10 ⁷	485	1.027 (150 nm)	0.009 ± 0.001
19	404	1204	84000	-	-	1.1×10 ⁷	457	1.024 (150 nm)	0.008 ± 0.001
20	16	53	7243	-	-	1.6×10 ³	0.52	1.048 (55-70 nm)	0.016 ± 0.001
21	154	1208	760000	-	-	9.7×10 ⁵	0.52	1.025 (100 nm)	0.008 ± 0.001
22	4	43	1200	-	-	35	0.08	-	-
23	16	52	-	-	1.5×10 ⁴	1.5×10 ⁴	14.9 ^b 21.1 ^c	1.70 ^a 1.44 (90 nm)	0.210 ± 0.020
24	16	47	-	-	1.7×10 ⁴	1.6×10 ⁴	15.3 ^b 21.8 ^c	1.45 (60-95 nm)	0.220 ± 0.020
25	26	54.3	-	-	1.6×10 ⁴	1.6×10 ⁴	15.4 ^b 38.2 ^c	1.72 ^a (110 nm) 1.20 (105 nm)	0.090 ± 0.001

IV.2.3.3 Results and discussions

In this section the results of the performed experiments are presented and discussed.

IV.2.3.3.1 HTDMA measurement

A. Influence of initial concentration

To examine whether the initial concentration of the precursor can affect the hygroscopic property of the formed SOA, a set of 12 experiments were performed in *CHARME*. Throughout the following tests, the initial concentrations of γ -terpinene range between low (4 ppb -16 ppb) and high (158 ppb - 400 ppb) while that of ozone vary between 33 ppb and 2913 ppb.

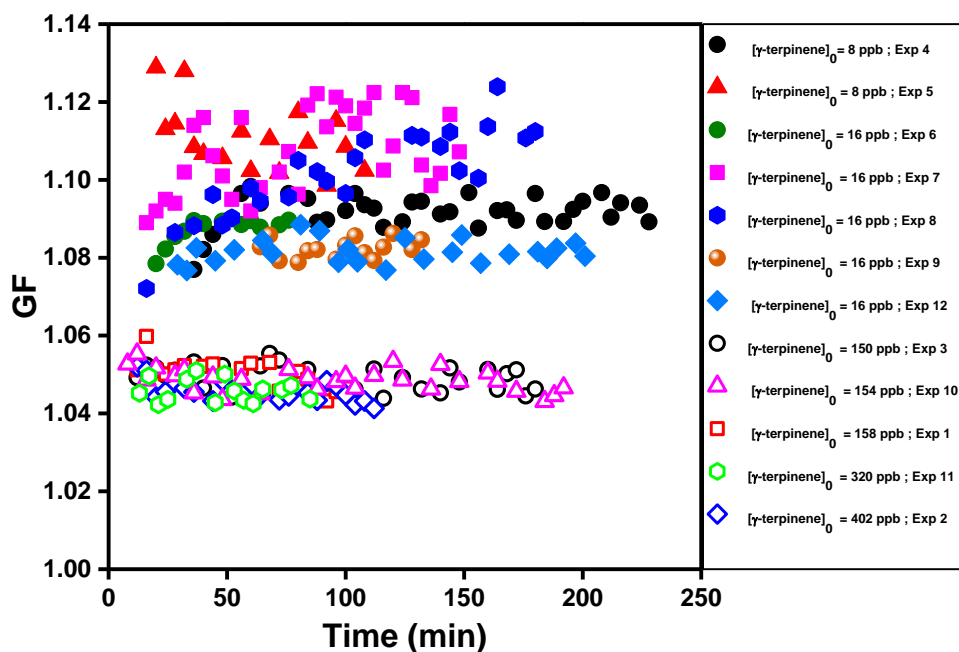


Figure IV.20: Temporal evolution of the hygroscopic growth factors at $\text{RH} = 90\%$ for SOA produced from dark ozonolysis of γ -terpinene in absence of cyclohexane, at low (solid shapes) and high (open shapes).

As shown in **Figure IV.20**, the hygroscopicity of SOA produced from the dark ozonolysis of γ -terpinene at low and high initial precursor concentrations showed similar measured GF values within a range of $GF \sim 1.05 - 1.12$. Small differences of the measured GF s were found for γ -terpinene experiments using 8 and 16 ppb with an average GF of 1.097 ± 0.027 corresponding to $\kappa_{GF} = 0.035 \pm 0.003$. In addition, the measured GF s remain constant for the different experiments

at high initial precursor concentrations in the range of 150 – 400 ppb, with an average measured GF of 1.047 ± 0.015 equivalent to $\kappa_{GF} = 0.016 \pm 0.001$. These findings were consistent with previous measurements of 1.07 ± 0.01 at 84% (**Virkkula et al., 1999**), 1.07 ± 0.02 at 85% (**Prenni et al., 2007**) and 1.04 at 90% for SOA produced from the ozonolysis of α -pinene (**Denjean et al., 2015**). The decrease of γ -terpinene concentration led to the enhancement of the SOA water uptake and indicated that the hygroscopicity of SOA formed from the ozonolysis of γ -terpinene depends on the initial precursor concentration. A similar observation has been previously done for several chamber studies (**Duplissy et al., 2008; Shilling et al., 2008**). **Duplissy et al., (2008)**, have found that at high precursor concentration, the decrease of the hygroscopicity of the SOAs is the result of partitioning of more volatile, less oxygenated components towards the particle phase. Moreover, **Tritscher et al., (2011)** have found that experiments with high initial precursor concentration (high SOA mass) have generally higher volatility and lower hygroscopicity.

Note that in some experiments, the GF was measured for two or three diameters, however, no significant difference was found, suggesting that the measured GF and the derived κ_{GF} values were relatively insensitive to the selected particle size. Also, no temporal variation of the measured GF has been detected in this study although it has been observed by previous investigations (**Baltensperger et al., 2005; Varutbangkul et al., 2006**). This study was consistent with other ozonolysis studies of monoterpenes (**Denjean et al., 2015; Prenni et al., 2007**).

B. Influence of TMB

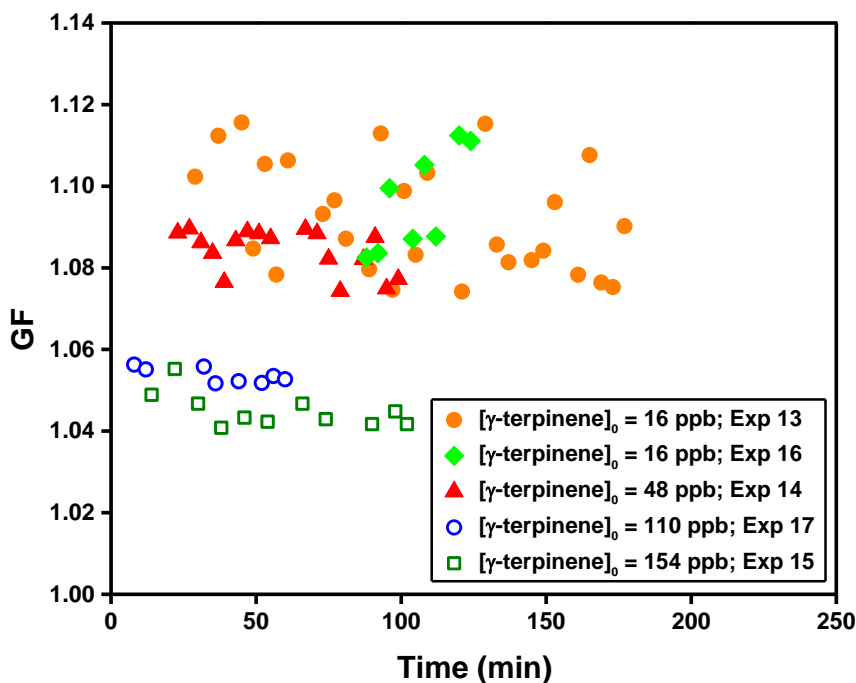
Natural VOCs including terpenes and sesquiterpenes, as well as anthropogenic species like aromatic VOCs, have been found to be precursors of SOA (**Baltensperger et al., 2005; Kari et al., 2019**). Aromatics are emitted by fuel combustion and evaporation and therefore influence SOA formation mainly in polluted urban areas. Among the most abundant aromatic hydrocarbons are alkyl benzenes such as toluene, xylenes and trimethylbenzene (TMB).

It has been shown that the interaction between anthropogenic (VOCs) and biogenic (VOCs) can significantly affect the properties of SOA (**Setyan et al., 2014; Ahlberg et al., 2017**). To investigate this interaction and the influence of anthropogenic precursors on the hygroscopicity

of SOAs formed from the ozonolysis of γ -terpinene, 1,3,5 trimethylbenzene was used as an aromatic representative in this study.

Five experiments (Experiments 13 through 17) have been performed in *CHARME* in the presence of TMB. A fraction of about (1:3) of [γ -terpinene] to [TMB] was used in all the experiments in order to respect the ratio $\nu_{(\text{OH}+\gamma\text{-terpinene})}/\nu_{(\text{OH}+\text{TMB})} \sim 1$.

As shown in **Figure IV.21**, the hygroscopic behavior of the different experiments showed the same behavior as the one observed for SOAs formed only from γ -terpinene (Exp. 1 – 12). The SOAs produced from lower initial precursor concentrations (16 ppb and 48 ppb; Exp. 13, 14 and 16) were more hygroscopic ($\text{GF} = 1.084$) than those formed from higher initial concentrations (110 and 154 ppb; Exp. 17 and 15) ($\text{GF} = 1.049$). These measured values were equivalent to κ_{GF} of 0.030 ± 0.003 and 0.017 ± 0.001 , and were in the same range of the hygroscopic growth factors observed for SOAs produced from dark ozonolysis of γ -terpinene.



C. Influence of OH scavenger

As presented in **Figure IV.22**, experiments in the presence of cyclohexane (Exp. 18–21) showed the lowest water uptake compared to measurements of SOA generated from ozonolysis of γ -terpinene and γ -terpinene -TMB at a_w of 90%. The GFs were 1.048 ± 0.012 and 1.025 ± 0.010 for initial precursor concentrations 16 and 158 ppb, respectively. These values were slightly lower (<5%) than the measured GFs of SOA derived from low (16 ppb) or high (158 ppb) γ -terpinene initial concentrations. This is consistent with the study of **Wex et al., (2009)**, who found that the addition of butanol as an OH radical scavenger decreases the hygroscopicity of SOA generated from the ozonolysis of α -pinene. The suppression of OH radicals affects the ratio HO_2/RO_2 , which could influence the SOA chemical composition (**Henry and Donahue, 2011**).

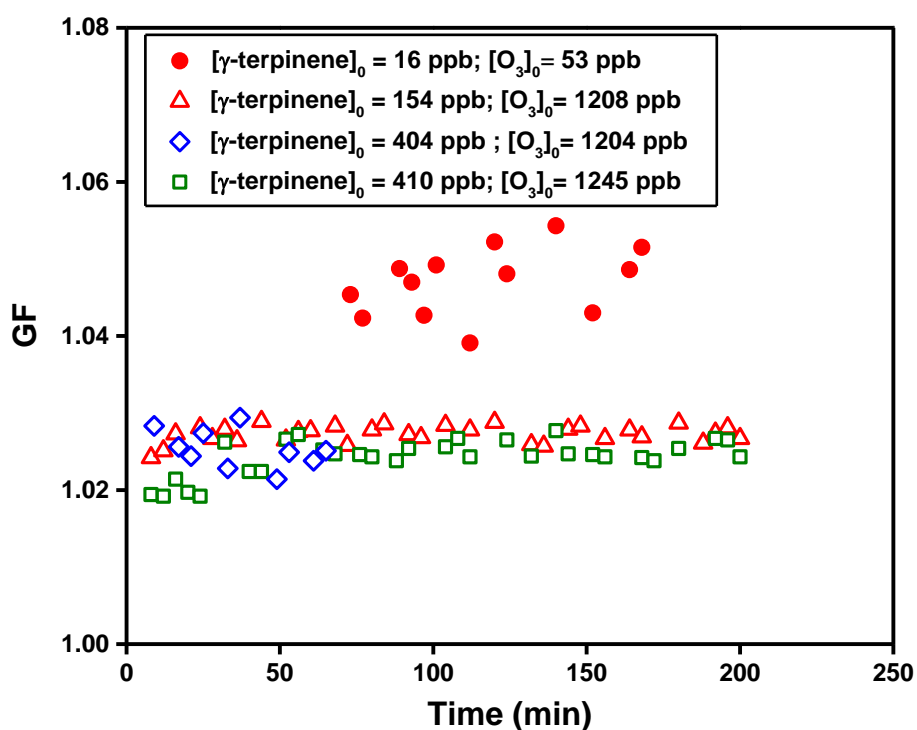


Figure IV.22: Temporal evolution of the hygroscopic growth factors at $\text{RH} = 90\%$ for SOA produced from dark ozonolysis of γ -terpinene in the presence of cyclohexane, at low (solid shapes) and high (open shapes).

D. Influence of AS seed particles

As displayed in **Figure IV. 23**, at the beginning of the ozonolysis reaction, the average GF measured by the HTDMA at $a_w = 90\%$ was equal to that of pure AS ($\text{GF} = 1.72$). As soon as

the ozonolysis reaction started, the measured GFs decreased as the semi-volatile compounds produced (with less-hygroscopic properties than ammonium sulfate) condensed onto the seed particles. A similar behavior was observed previously during the hygroscopic measurements of SOA produced in the presence of ammonium sulfate from different monoterpenes and oxygenated terpenes (Virkkula et al., 1999; Saathoff et al., 2003; Varutbangkul et al., 2006). During the experiment a single narrow mode of growth factor distribution was observed for each selected size, indicating that particles generated from the dark ozonolysis of γ -terpinene in the presence of seeds are in an internally mixed state.

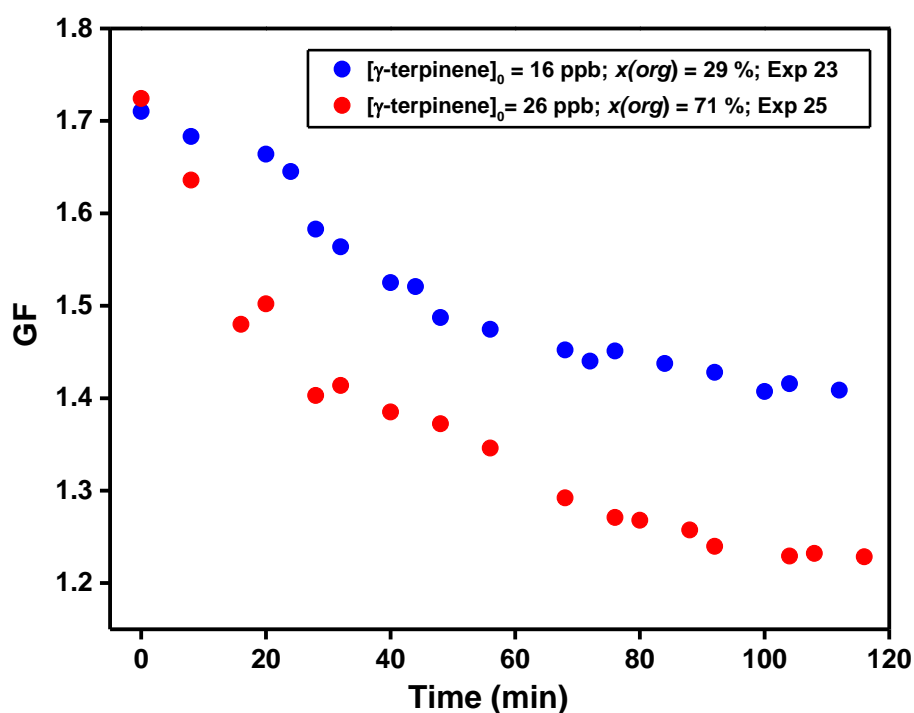


Figure IV. 23: Temporal evolution of hygroscopic growth factor at bulk RH = 90% of SOA internally mixed with ammonium sulfate observed in Exp. 23 and Exp. 25.

IV.2.3.3.2 Humidogram Representation

During hydration regime (RH = ~20 – 93%), the hygroscopic growth curves of the SOA formed in the absence and presence of cyclohexane (Figure IV.24 a and b), and in the presence of TMB (Figure IV.24 c) showed small but continuous water uptake with no visible deliquescence transition. These observation were in agreement with the humidograms measured for SOA produced from the oxidation of monoterpenes and sesquiterpenes (Varutbangkul et al., 2006).

The coefficients a , b and c of the fitted GF-parameterization of the continuous hygroscopic growth curves according to (Eq. IV.9) and are summarized in Table S. 3.

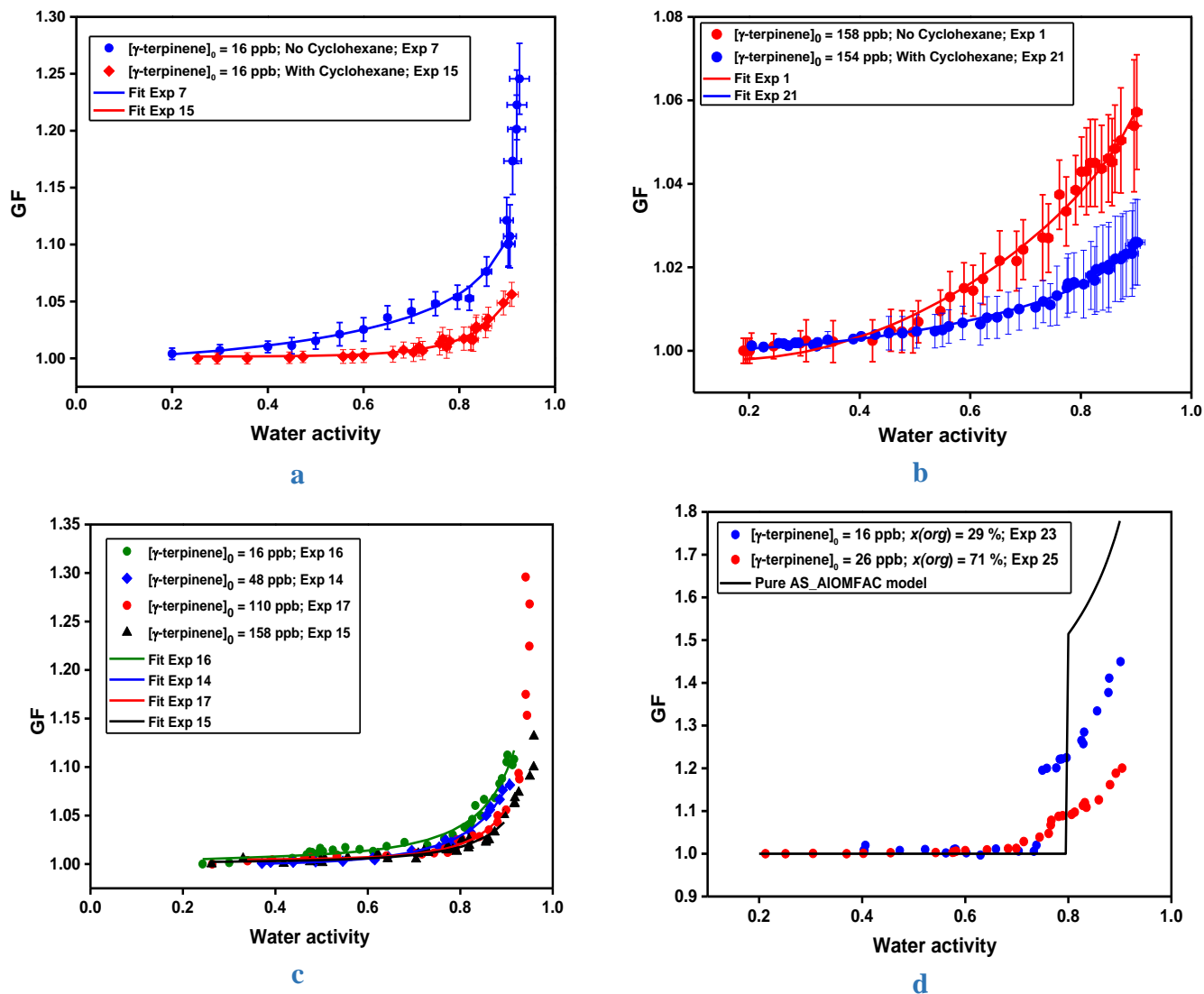


Figure IV.24: Hygroscopic growth factors for SOA produced from the ozonolysis of γ -terpinene as a function of water activity, (a) in the absence and presence of cyclohexane at low initial precursor concentrations (16 ppb; Exp. 7, 15), (b) in the absence and presence of cyclohexane at high initial precursor concentrations (\sim 158 ppb; Exp. 1, 21), (c) in presence of TMB at 16 - 158 ppb (Exp. 14 - 17), (d) in presence of dry AS seed particles at 16 ppb and 26 ppb (Exp 23, 25).

As shown in Figure IV.24 d, upon hydration, the hygroscopic behavior observed for Exp. 23 ($[\gamma\text{-terpinene}]_0 = 16$ ppb, organic mass fraction $x(\text{org}) \sim 0.3$) and Exp. 25 ($[\gamma\text{-terpinene}]_0 = 26$ ppb, organic mass fraction $x(\text{org}) \sim 0.7$) were similar and showed little to no water uptake ($\text{GF} \sim 1$)

at low and moderate a_w (~73%). However, the humidogram showed an increase in particle diameter corresponding to the full deliquescence (dissolution and liquification of solids) at RH ~76% (DRH). The presence of secondary organic compounds produced by ozonolysis of γ -terpinene slightly shifted the deliquescence of pure AS from 80% to 76%. This was in agreement with previous studies (Meyer et al., 2009; Smith et al., 2012), which reported that secondary organic compounds produced from biogenic precursors could affect the deliquescence transition of pure AS. For Exp. 25, with particles having an organic mass fraction ~0.7, a gradual increase in water uptake was observed at RH ~73% - 76%, however this behavior was not observed in Exp. 23 having organic mass fraction ~0.3. Thus, the increase of organic mass fraction promotes the partial dissolution of AS. This is in agreement with previous studies (Choi and Chan, 2002; Marcolli et al., 2004) of mixed organic-ammonium sulfate aerosol particles, which observed that organic compounds could affect the solubility of AS prior to deliquescence.

As expected, the two humidograms for mixed particles showed a reduced water uptake compared to pure AS at water activity (a_w) \geq 80% (Figure IV.24 d). The measured GFs at bulk RH = 80%, were 1.20 and 1.08 for particles derived from Exp. 23 and Exp. 25, respectively. These values were ~23% and ~37% lower than the measured GFs of pure AS at a_w =80% (GF = 1.47). The GFs measured at a_w = 90% were equal to 1.43 and 1.22 for Exp. 23 and Exp. 25, respectively. These GF values were 20% and 44 % lower than that of pure AS (GF = 1.75 at a_w = 90%), and equivalent to κ_{GF} values of 0.250 ± 0.001 and 0.100 ± 0.001 , respectively. The later κ values were lower than that of pure AS ($\kappa_{AS} = 0.620$) (Petters and Kreidenweis, 2007).

In short, the different experiments performed to examine the hygroscopic properties (growth factor and its corresponding κ) of SOA in this study allow to derive the following deductions:

- The growth of SOA formed in the presence and absence of the OH scavenger (cyclohexane) are slightly hygroscopic (GF = 1.024 – 1.011) in agreement with the hygroscopicity of aerosols produced from ozonolysis of other monoterpenes (Prenni et al., 2007; Denjean et al., 2015).
- The presence of TMB showed no significant effect on the growth factor of the formed SOA under the performed experimental conditions (ratio $v_{(OH+\gamma\text{-terpinene})} / v_{(OH+TMB)} \sim 1$).

- SOAs internally mixed with AS showed little to no water uptake at low and moderate RH (~ 73%), followed by a deep increase in diameter of the particle at $\sim 75 \pm 1\%$, corresponding to the full deliquescence transition.
- It was observed that the growth factor was slightly dependent on the initial concentration of γ -terpinene (higher concentrations lead to lower hygroscopic SOA).
- The hygroscopic growth curves of all SOA formed from seedless γ -terpinene ozonolysis exhibited continuous water uptake in the range 20 – 93% (**Figure IV.24**).

It should be noted that HTDMA measurements only are not enough to map out the global hygroscopic behavior and CCN activity of the formed SOA. Complementary measurements are useful to assess the CCN activity under supersaturation conditions. In these regards, a set of manipulations in the framework of postdoctoral project (Hichem BOUZIDI) have been performed but the results are still progress.

IV.2.4 Conclusion

A research work to study the reaction of ozone with γ -terpinene, an important monoterpene containing two endo-cyclic double bonds, has been carried out in the *CHARME* (mainly) and LPCA-ONE chambers and the obtained results are summarized in **Table IV. 10**.

The kinetic investigation has been performed at 294 ± 2 K, atmospheric pressure, under dry conditions ($\text{RH} < 2\%$) and in the presence of cyclohexane as OH scavenger. Two different methods, the pseudo-first-order and the relative method were used to determine the γ -terpinene rate coefficient with ozone. The values obtained with both methods are in good agreement and lead to a rate coefficient of $(2.1 \pm 0.11) \times 10^{-16} \text{ cm}^3 \text{ molecule s}^{-1}$ for the ozonolysis reaction of γ -terpinene. The oxidation products formed in the gas-phase were analyzed with a PTR-TOF-MS. 20 oxidation products were observed and quantified and 9 of them were identified. A mechanism proposing the formation of some of the observed oxidation products was presented for the first time.

In addition, the study of the particulate phase has revealed a formation yield of SOA over a mass range ($\sim 10 - 890 \mu\text{g m}^{-3}$) in the presence ($\sim 49\%$) and absence ($\sim 52\%$) of an OH scavenger (cyclohexane). The examination of the physical state and morphology of the formed SOA particles

showed that they are viscous and spherical. Moreover, the hygroscopic properties and CCN activity of the SOA were investigated using an HTDMA at RH 93%. These parameters were characterized under different experimental conditions including: (1) the effect of initial precursor concentrations, (2) the presence of an anthropogenic VOC (TMB), (3) the presence of OH scavenger and (4) the presence of dry AS seed particles.

Table IV. 10: Summary of the experiments performed to characterize the gas and particulate phases of the reaction of ozone and γ -terpinene.

Parameter	Result	Comment
Gaseous-Phase		
Rate coefficient	$(2.1 \pm 0.11) \times 10^{-16}$ $\text{cm}^3 \text{ molecule}^{-1} \text{ s}^{-1}$	A new determination revealed from 2 methods (pseudo first order and relative (with 3 references) in 2 different chambers \rightarrow high confidence
Gaseous products	20 observed products and 9 identified ones including: formaldehyde, acetaldehyde, formic acid, acetone, glyoxal, acetic acid...	An average total yield ~52%
Particulate-Phase		
SOA yield	~49 % (With cyclohexane)	The reaction of γ -terpinene and ozone is considered a new contributor to the atmospheric SOA formation.
	~52% (Without cyclohexane)	
Morphology	Spherical	Independent of the initial concentration of the precursor and the presence/absence of cyclohexane.
Physical state	Viscous	
Growth factor (RH=90%)	1.024 – 1.11	Dependent on the initial concentration of the γ -terpinene, presence of OH radicals and TMB.
	1.20 - 1.44	Affected by the presence of AS seeds and the initial concentration of γ -terpinene
KGF	0.008 – 0.2	Dependent on the initial concentration of the γ -terpinene, presence of OH radicals, TMB and seeds.

Future research concerning this reaction requires a set of investigations including: the determination of OH formation yields and the identification / quantification of the SOA molecular composition using different methods (ToF-SIMS, ESI-LC-MS...).

Reference

- Abramson, E., Imre, D., Beránek, J., Wilson, J.I., Zelenyuk, A., 2013. Experimental determination of chemical diffusion within secondary organic aerosol particles. *Physical chemistry chemical physics: PCCP* 15, 2983–2991. <https://doi.org/10.1039/c2cp44013j>
- Ahlberg, E., Falk, J., Eriksson, A., Holst, T., Brune, W.H., Kristensson, A., Roldin, P., Svenningsson, B., 2017. Secondary organic aerosol from VOC mixtures in an oxidation flow reactor. *Atmospheric Environment* 161, 210–220. <https://doi.org/10.1016/j.atmosenv.2017.05.005>
- Alfarra, M.R., Good, N., Wyche, K.P., Hamilton, J.F., Monks, P.S., Lewis, A.C., McFiggans, G., 2013. Water uptake is independent of the inferred composition of secondary aerosols derived from multiple biogenic VOCs. *Atmospheric Chemistry and Physics* 13, 11769–11789. <https://doi.org/10.5194/acp-13-11769-2013>
- Atkinson, R., 1997. Gas-Phase Tropospheric Chemistry of Volatile Organic Compounds: 1. Alkanes and Alkenes. *Journal of Physical and Chemical Reference Data* 26, 215–290. <https://doi.org/10.1063/1.556012>
- Atkinson, R., Arey, J., 2003. Gas-phase tropospheric chemistry of biogenic volatile organic compounds: a review. *Atmospheric Environment* 37, 197–219. [https://doi.org/10.1016/S1352-2310\(03\)00391-1](https://doi.org/10.1016/S1352-2310(03)00391-1)
- Atkinson, R., Arey, J., Aschmann, S.M., Corchnoy, S.B., Shu, Y., 1995. Rate constants for the gas-phase reactions of *cis*-3-Hexen-1-ol, *cis*-3-Hexenylacetate, *trans*-2-Hexenal, and Linalool with OH and NO₃ radicals and O₃ at 296 ± 2 K, and OH radical formation yields from the O₃ reactions: Rate constants for gas-phase reactions. *International Journal of Chemical Kinetics* 27, 941–955. <https://doi.org/10.1002/kin.550271002>
- Atkinson, R., Aschmann, S.M., Pitts, J.N., 1986. Rate constants for the gas-phase reactions of the OH radical with a series of monoterpenes at 294 ± 1 K: Gas-phase reactions of OH radicals. *International Journal of Chemical Kinetics* 18, 287–299. <https://doi.org/10.1002/kin.550180303>
- Atkinson, R., Hasegawa, D., Aschmann, S.M., 1990a. Rate constants for the gas-phase reactions of O₃ with a series of monoterpenes and related compounds at 296 ± 2 K: Gas-phase reactions of O₃. *International Journal of Chemical Kinetics* 22, 871–887. <https://doi.org/10.1002/kin.550220807>
- Avzianova, E.V., Ariya, P.A., 2002. Temperature-dependent kinetic study for ozonolysis of selected tropospheric alkenes. *International Journal of Chemical Kinetics* 34, 678–684. <https://doi.org/10.1002/kin.10093>
- Baltensperger, U., Kalberer, M., Dommen, J., Paulsen, D., Alfarra, M.R., Coe, H., Fisseha, R., Gascho, A., Gysel, M., Nyeki, S., Sax, M., Steinbacher, M., Prevot, A.S.H., Sjögren, S., Weingartner, E., Zenobi, R., 2005. Secondary organic aerosols from anthropogenic and biogenic precursors. *Faraday Discussions* 130, 265. <https://doi.org/10.1039/b417367h>
- Bonn, B., Schuster, G., Moortgat, G.K., 2002. Influence of Water Vapor on the Process of New Particle Formation during Monoterpene Ozonolysis. *The Journal of Physical Chemistry A* 106, 2869–2881. <https://doi.org/10.1021/jp012713p>
- Brechtel, F.J., Kreidenweis, S.M., 1999. Predicting Particle Critical Supersaturation from Hygroscopic Growth Measurements in the Humidified TDMA. Part I: Theory and Sensitivity Studies. *J. Atmos. Sci.* 57, 1854–1871. [https://doi.org/10.1175/1520-0469\(2000\)057h](https://doi.org/10.1175/1520-0469(2000)057h)

- Cai, M., Tan, H., Chan, C.K., Qin, Y., Xu, H., Li, F., Schurman, M.I., Liu, L., Zhao, J., 2018. The size-resolved cloud condensation nuclei (CCN) activity and its prediction based on aerosol hygroscopicity and composition in the Pearl Delta River (PRD) region during wintertime 2014. *Atmospheric Chemistry and Physics* 18, 16419–16437. <https://doi.org/10.5194/acp-18-16419-2018>
- Calvert, J.G., Madronich, S., 1987. Theoretical study of the initial products of the atmospheric oxidation of hydrocarbons. *Journal of Geophysical Research* 92, 2211. <https://doi.org/10.1029/JD092iD02p02211>
- Choi, M.Y., Chan, C.K., 2002. The effects of organic species on the hygroscopic behaviors of inorganic aerosols. *E and T Contents* 36, 2422–2428. <https://doi.org/10.1021/es0113293>
- Davies, J.F., Zuend, A., Wilson, K.R., 2019. Technical note: The role of evolving surface tension in the formation of cloud droplets. *Atmospheric Chemistry and Physics* 19, 2933–2946. <https://doi.org/10.5194/acp-19-2933-2019>
- Denjean, C., Formenti, P., Picquet-Varrault, B., Camredon, M., Pangui, E., Zapf, P., Katrib, Y., Giorio, C., Tapparo, A., Temime-Roussel, B., Monod, A., Aumont, B., Doussin, J.F., 2015. Aging of secondary organic aerosol generated from the ozonolysis of α -pinene: effects of ozone, light and temperature. *Atmos. Chem. Phys.* 16. <https://doi:10.5194/acp-15-883-2015>
- Dick, W.D., Saxena, P., McMurry, P.H., 2000. Estimation of water uptake by organic compounds in submicron aerosols measured during the Southeastern Aerosol and Visibility Study. *J Geophysical Research* 105, 1471–1479. <https://doi.org/10.1029/1999JD901001>
- Duplissy, J., Gysel, M., Alfarra, M.R., Dommen, J., Metzger, A., Prevot, A.S.H., Weingartner, E., Laaksonen, A., Raatikainen, T., Good, N., Turner, S.F., McFiggans, G., Baltensperger, U., 2008. Cloud forming potential of secondary organic aerosol under near atmospheric conditions. *Geophysical Research Letters* 35. <https://doi.org/10.1029/2007GL031075>
- Finlayson-Pitts, B.J., Pitts Jr, J.N., 2000. *Chemistry of the upper and lower atmosphere: theory, experiments, and applications*. Elsevier.
- Geron, C., Rasmussen, R., R. Arnts, R., Guenther, A., 2000. A review and synthesis of monoterpene speciation from forests in the United States. *Atmospheric Environment* 34, 1761–1781. [https://doi.org/10.1016/S1352-2310\(99\)00364-7](https://doi.org/10.1016/S1352-2310(99)00364-7)
- Gong, Y., Chen, Z., Li, H., 2018. The oxidation regime and SOA composition in limonene ozonolysis: roles of different double bonds, radicals, and water. *Atmospheric Chemistry and Physics* 18, 15105–15123. <https://doi.org/10.5194/acp-18-15105-2018>
- Good, N., Topping, D.O., Duplissy, J., Gysel, M., Meyer, N.K., Metzger, A., Turner, S.F., Baltensperger, U., Ristovski, Z., Weingartner, E., Coe, H., McFiggans, G., 2010. Widening the gap between measurement and modelling of secondary organic aerosol properties? *Atmospheric Chemistry and Physics* 10, 2577–2593. <https://doi.org/10.5194/acp-10-2577-2010>
- Griffin, R.J., Cocker, D.R., Flagan, R.C., Seinfeld, J.H., 1999. Organic aerosol formation from the oxidation of biogenic hydrocarbons. *Journal of Geophysical Research: Atmospheres* 104, 3555–3567. <https://doi.org/10.1029/1998JD100049>
- Grimsrud, E.P., Westberg, H.H., Rasmussen, R.A., 1975. *Atmospheric Reactivity of Monoterpene Hydrocarbons, NO_x Photooxidation and Ozonolysis*.

- Henry, K.M., Donahue, N.M., 2011. Effect of the OH Radical Scavenger Hydrogen Peroxide on Secondary Organic Aerosol Formation from α -Pinene Ozonolysis. *Aerosol Science and Technology* 45, 696–700. <https://doi.org/10.1080/02786826.2011.552926>
- Herrmann, F., Winterhalter, R., Moortgat, G.K., Williams, J., 2010. Hydroxyl radical (OH) yields from the ozonolysis of both double bonds for five monoterpenes. *Atmospheric Environment* 44, 3458–3464. <https://doi.org/10.1016/j.atmosenv.2010.05.011>
- Hodas, N., Zuend, A., Schilling, K., Berkemeier, T., Shiraiwa, M., Flagan, R.C., Seinfeld, J.H., 2016. Discontinuities in hygroscopic growth below and above water saturation for laboratory surrogates of oligomers in organic atmospheric aerosols. *Atmospheric Chemistry and Physics* 16, 12767–12792. <https://doi.org/10.5194/acp-16-12767-2016>
- Hoffmann, T., Odum, J.R., Bowman, F., Collins, D., Klockow, D., Flagan, R.C., Seinfeld, J.H., 1997. Formation of organic aerosols from the oxidation of biogenic hydrocarbons. *Journal of Atmospheric Chemistry* 26, 189–222.
- IUPAC (a), Task Group on Atmospheric Chemical Kinetic Data Evaluation – Data Sheet Ox_VOC8 [WWW Document]. URL http://iupac.pole-ether.fr/htdocs/datasheets/pdf/Ox_VOC8_O3_apinene.pdf (accessed 6.12.19).
- IUPAC (b), Task Group on Atmospheric Chemical Kinetic Data Evaluation – Data Sheet Ox_VOC30 [WWW Document]. URL http://iupac.pole-ether.fr/htdocs/datasheets/pdf/Ox_VOC30_O3_gterpinene.pdf
- IUPAC (c), IUPAC Task Group on Atmospheric Chemical Kinetic Data Evaluation HOx_VOC85_OH_g-terpinene [WWW Document]. URL http://iupac.pole-ether.fr/htdocs/datasheets/pdf/HOx_VOC85_OH_g-terpinene.pdf (accessed 10.26.19).
- IUPAC (d), IUPAC Task Group on Atmospheric Chemical Kinetic Data Evaluation – Data Sheet NO₃_VOC41 2.
- Johnson, D., Marston, G., 2008. The gas-phase ozonolysis of unsaturated volatile organic compounds in the troposphere. *Chemical Society Reviews* 37, 699. <https://doi.org/10.1039/b704260b>
- Kari, E., Hao, L., Ylisirniö, A., Buchholz, A., Leskinen, A., Yli-Pirilä, P., Nuutinen, I., Kuuspallo, K., Jokiniemi, J., Faiola, C., Schobesberger, S., Virtanen, A., 2019. Dual effect of anthropogenic emissions on the formation of biogenic SOA. *Atmospheric Chemistry and Physics Discussions* 1–35. <https://doi.org/10.5194/acp-2019-330>
- Keywood, M.D., Kroll, J.H., Varutbangkul, V., Bahreini, R., Flagan, R.C., Seinfeld, J.H., 2004. Secondary Organic Aerosol Formation from Cyclohexene Ozonolysis: Effect of OH Scavenger and the Role of Radical Chemistry. *Environmental Science & Technology* 38, 3343–3350. <https://doi.org/10.1021/es049725j>
- Khalil, M.A.K., Rasmussen, R.A., 1992. Forest Hydrocarbon Emissions: Relationships Between Fluxes and Ambient Concentrations. *Journal of the Air & Waste Management Association* 42, 810–813. <https://doi.org/10.1080/10473289.1992.10467033>
- Köhler, H., 1936. The nucleus in and the growth of hygroscopic droplets. *Trans. Faraday Soc.* 32, 1152–1161. <https://doi.org/10.1039/TF9363201152>
- Kreidenweis, S.M., Koehler, K., DeMott, P.J., Prenni, A.J., Carrico, C., Ervens, B., 2005. Water activity and activation diameters from hygroscopicity data - Part I: Theory and application to inorganic salts. *Atmospheric Chemistry and Physics* 5, 1357–1370. <https://doi.org/10.5194/acp-5-1357-2005>
- Kuwata, M., Martin, S.T., 2012. Phase of atmospheric secondary organic material affects its reactivity. *PNAS* 109, 17354–17359. <https://doi.org/10.1073/pnas.1209071109>

- Larsen, B.R., Lahaniati, M., Calogirou, A., Kotzias, D., 1998. Atmospheric oxidation products of terpenes: A new nomenclature. *Chemosphere* 37, 1207–1220. [https://doi.org/10.1016/S0045-6535\(98\)00115-5](https://doi.org/10.1016/S0045-6535(98)00115-5)
- Lee, A., Goldstein, A.H., Kroll, J.H., Ng, N.L., Varutbangkul, V., Flagan, R.C., Seinfeld, J.H., 2006. Gas-phase products and secondary aerosol yields from the photooxidation of 16 different terpenes. *Journal of Geophysical Research* 111. <https://doi.org/10.1029/2006JD007050>
- Lee, H.-H., Bar-Or, R.Z., Wang, C., 2017. Biomass burning aerosols and the low-visibility events in Southeast Asia. *Atmospheric Chemistry and Physics* 17, 965–980. <https://doi.org/10.5194/acp-17-965-2017>
- Leungsakul, S., Jaoui, M., Kamens, R.M., 2005. Kinetic Mechanism for Predicting Secondary Organic Aerosol Formation from the Reaction of *d*-Limonene with Ozone. *Environmental Science & Technology* 39, 9583–9594. <https://doi.org/10.1021/es0492687>
- Mackenzie-Rae, F.A., Liu, T., Deng, W., Saunders, S.M., Fang, Z., Zhang, Y., Wang, X., 2017a. Ozonolysis of α -phellandrene – Part 1: Gas- and particle-phase characterisation. *Atmospheric Chemistry and Physics* 17, 6583–6609. <https://doi.org/10.5194/acp-17-6583-2017>
- Mackenzie-Rae, F.A., Liu, T., Deng, W., Saunders, S.M., Fang, Z., Zhang, Y., Wang, X., 2017b. Ozonolysis of α -phellandrene – Part 1: Gas- and particle-phase characterisation. *Atmospheric Chemistry and Physics* 17, 6583–6609. <https://doi.org/10.5194/acp-17-6583-2017>
- Marcolli, C., Luo, B., Peter, T., 2004. Mixing of the Organic Aerosol Fractions: Liquids as the Thermodynamically Stable Phases. *J. Phys. Chem. A* 108, 2216–2224. <https://doi.org/10.1021/jp036080l>
- Marshall, F.H., Miles, R.E.H., Song, Y.-C., Ohm, P.B., Power, R.M., Reid, J.P., Dutcher, C.S., 2016. Diffusion and reactivity in ultraviscous aerosol and the correlation with particle viscosity. *Chem. Sci.* 7, 1298–1308. <https://doi.org/10.1039/C5SC03223G>
- Meyer, N.K., Duplissy, J., Gysel, M., Metzger, A., Dommen, J., Weingartner, E., Alfarra, M.R., Prevot, A.S.H., Fletcher, C., Good, N., McFiggans, G., Jonsson, Å.M., Hallquist, M., Baltensperger, U., Ristovski, Z.D., 2009. Analysis of the hygroscopic and volatile properties of ammonium sulphate seeded and unseeded SOA particles. *Atmospheric Chemistry and Physics* 9, 721–732. <https://doi.org/10.5194/acp-9-721-2009>
- Mirrieles, J.A., Brooks, S.D., 2018. Instrument artifacts lead to uncertainties in parameterizations of cloud condensation nucleation. *Atmospheric Measurement Techniques* 11, 6389–6407. <https://doi.org/10.5194/amt-11-6389-2018>
- Odum, J.R., Hoffmann, T., Bowman, F., Collins, D., Flagan, R.C., Seinfeld, J.H., 1996. Gas/Particle Partitioning and Secondary Organic Aerosol Yields 6.
- Petters, Kreidenweis, S.M., 2007. A single parameter representation of hygroscopic growth and cloud condensation nucleus activity. *Atmos. Chem. Phys.* 12.
- Petters, M.D., Kreidenweis, S.M., 2007. A single parameter representation of hygroscopic growth and cloud condensation nucleus activity. *Atmospheric Chemistry and Physics* 7, 1961–1971. <https://doi.org/10.5194/acp-7-1961-2007>
- Prenni, A.J., Petters, M.D., Kreidenweis, S.M., DeMott, P.J., Ziemann, P.J., 2007. Cloud droplet activation of secondary organic aerosol. *Journal of Geophysical Research: Atmospheres* 112. <https://doi.org/10.1029/2006JD007963>

- Reid, J.P., Bertram, A.K., Topping, D.O., Laskin, A., Martin, S.T., Petters, M.D., Pope, F.D., Rovelli, G., 2018. The viscosity of atmospherically relevant organic particles. *Nat Commun* 9, 956. <https://doi.org/10.1038/s41467-018-03027-z>
- Saathoff, H., Naumann, K.-H., Möhler, O., Jonsson, A.M., Hallquist, M., Kiendler-Scharr, A., Mentel, T.F., Tillmann, R., Schurath, U., 2009. Temperature dependence of yields of secondary organic aerosols from the ozonolysis of α -pinene and limonene. *Atmospheric Chemistry and Physics* 9, 1551–1577.
- Saathoff, H., Naumann, K.-H., Schnaiter, M., Schöck, W., Möhler, O., Schurath, U., Weingartner, E., Gysel, M., Baltensperger, U., 2003. Coating of soot and (NH₄)₂SO₄ particles by ozonolysis products of α -pinene. *Journal of Aerosol Science, Intercomparison of Soot Measurement Techniques* 34, 1297–1321. [https://doi.org/10.1016/S0021-8502\(03\)00364-1](https://doi.org/10.1016/S0021-8502(03)00364-1)
- Saunders, S.M., Jenkin, M.E., Derwent, R.G., Pilling, M.J., 2003. Protocol for the development of the Master Chemical Mechanism, MCM v3 (Part A): tropospheric degradation of non-aromatic volatile organic compounds. *Atmos. Chem. Phys.* 21.
- Schmied, M., Poelt, P., 2002. Particle Analysis by SEM/EDXS and Specimen Damage. *Microchimica Acta* 139, 171–177. <https://doi.org/10.1007/s006040200057>
- Setyan, A., Song, C., Merkel, M., Knighton, W.B., Onasch, T.B., Canagaratna, M.R., Worsnop, D.R., Wiedensohler, A., Shilling, J.E., Zhang, Q., 2014. Chemistry of new particle growth in mixed urban and biogenic emissions – insights from CARES. *Atmospheric Chemistry and Physics* 14, 6477–6494. <https://doi.org/10.5194/acp-14-6477-2014>
- Shilling, J.E., Chen, Q., King, S.M., Rosenoern, T., Kroll, J.H., Worsnop, D.R., McKinney, K.A., Martin, S.T., 2008. Particle mass yield in secondary organic aerosol formed by the dark ozonolysis of α -pinene. *Atmospheric Chemistry and Physics* 8, 2073–2088. <https://doi.org/10.5194/acp-8-2073-2008>
- Smith, M.L., Bertram, A.K., Martin, S.T., 2012. Deliquescence, efflorescence, and phase miscibility of mixed particles of ammonium sulfate and isoprene-derived secondary organic material. *Atmospheric Chemistry and Physics* 12, 9613–9628. <https://doi.org/10.5194/acp-12-9613-2012>
- Tritscher, T., Dommen, J., DeCarlo, P.F., Gysel, M., Barmet, P.B., Praplan, A.P., Weingartner, E., Prévôt, A.S.H., Riipinen, I., Donahue, N.M., Baltensperger, U., 2011. Volatility and hygroscopicity of aging secondary organic aerosol in a smog chamber. *Atmospheric Chemistry and Physics* 11, 11477–11496. <https://doi.org/10.5194/acp-11-11477-2011>
- Varutbangkul, V., Brechtel, F.J., Bahreini, R., Ng, N.L., Keywood, M.D., Kroll, J.H., Flagan, R.C., Seinfeld, J.H., Lee, A., Goldstein, A.H., 2006. Hygroscopicity of secondary organic aerosols formed by oxidation of cycloalkenes, monoterpenes, sesquiterpenes, and related compounds. *Atmos. Chem. Phys.* 22.
- Virkkula, A., Dingenen, R.V., Raes, F., Hjorth, J., 1999. Hygroscopic properties of aerosol formed by oxidation of limonene, α -pinene, and β -pinene. *Journal of Geophysical Research: Atmospheres* 104, 3569–3579. <https://doi.org/10.1029/1998JD100017>
- Virtanen, A., Joutsensaari, J., Koop, T., Kannosto, J., Yli-Pirilä, P., Leskinen, J., Mäkelä, J.M., Holopainen, J.K., Pöschl, U., Kulmala, M., Worsnop, D.R., Laaksonen, A., 2010. An amorphous solid state of biogenic secondary organic aerosol particles. *Nature* 467, 824–827. <https://doi.org/10.1038/nature09455>

- Wex, H., Petters, M.D., Carrico, C.M., Hallbauer, E., Massling, A., McMeeking, G.R., Poulain, L., Wu, Z., Kreidenweis, S.M., Stratmann, F., 2009. Towards closing the gap between hygroscopic growth and activation for secondary organic aerosol: Part 1 – Evidence from measurements. *Atmospheric Chemistry and Physics* 9, 3987–3997. <https://doi.org/10.5194/acp-9-3987-2009>
- Witter, M., Berndt, T., Böge, O., Stratmann, F., Heintzenberg, J., 2002. Gas-phase ozonolysis: Rate coefficients for a series of terpenes and rate coefficients and OH yields for 2-methyl-2-butene and 2,3-dimethyl-2-butene: Gas-Phase Ozonolysis. *International Journal of Chemical Kinetics* 34, 394–403. <https://doi.org/10.1002/kin.10063>
- Zhang, D., Zhang, R., 2005. Ozonolysis of α -pinene and β -pinene: Kinetics and mechanism. *J. Chem. Phys.* 13.

Conclusion and Perspectives

To understand atmospheric pollution that affects the global terrestrial climate, it is essential to know the processes that lead to transformation of pollutants in the environment. These atmospheric chemical mechanisms and interactions have been much studied through different scientific approaches including observations, modeling and laboratory research. Atmospheric simulation chambers are considered as important laboratory tools that allow the investigation of physicochemical mechanisms under controlled conditions. Chamber investigations contribute to the foundations for air quality and climate models and help in interpretation of field measurements. Chambers have been used over the last six decades and they are still evolving today.

In this context, a new atmospheric simulation chamber '*CHARME*' (*Chamber for the study of the Atmospheric Reactivity and the Metrology of the Environment*) has been designed in FRANCE and hosted in the Laboratory of Physical Chemistry of the Atmosphere (LPCA) of the University of Littoral – Côte d'Opale (ULCO, Dunkirk). *CHARME* consists in an electropolished stainless steel cylinder with a volume of about 9.2 m³ (S/V = 3.5 m⁻¹). It is evacuable down to 0.4 mbar, currently it is operating at room temperature (i.e. 293 ± 1 K) and under various conditions of relative humidity (~1-100%). *CHARME* is equipped with 4 xenon arc lamps (5 kW each) to simulate solar irradiation and is coupled (online and offline) to many instruments dedicated to atmospheric measurements (spectroradiometer, temperature / relative humidity probe, PTR-ToF-MS, O₃ and NO_x analysers, SMPS, thermal desorber-GC-FID/MS, IBBCEAS for NO₃ and NO₂...).

The first objective of this thesis was to characterize and validate the *CHARME* chamber by performing a wide range of preliminary experiments. These investigations demonstrate that *CHARME* exhibits a good vacuum limit (0.4 mbar), negligible leaks (~40 ppb of air from the lab), short mixing times for gases and aerosols (~ 3 mins) and sufficiently long lifetimes for atmospheric species (~3 hrs - 84 hrs). The chamber displays minor wall effects which have been well characterized through the auxiliary mechanism. In addition, the four xenon lamps used to irradiate the chamber provide wavelengths in the range 340 - 1100 nm and a NO₂ photolysis rate constant (J_{NO_2}) of $1.1 \times 10^{-3} \text{ s}^{-1}$ allowing to simulate photochemical reactions occurring in the troposphere. The preliminary tests performed in *CHARME* have demonstrate that this chamber is a useful tool to study physico-chemical processes occurring in the atmosphere. Other developments are planned

for *CHARME* in the near future. In 2020, a Chernin multipath cell will be installed into the chamber and connected to an FTIR spectrometer (Bruker) and a THz source (for rotational spectroscopy analyses). Other optical techniques will be also coupled to *CHARME* (IBBCEAS for HONO and aerosols extinction coefficients, photoacoustic spectroscopy for aerosols absorption coefficients, EC-QCL-MPC for N₂O₅...). Lastly, a setup to accurately introduce VOCs in the reactor and a temperature regulation system (from -20 to 50 °C) will be installed.

The second part of this research was focused on the study of the ozonolysis reaction of γ -terpinene. The experiments were performed in the dark, under dry conditions (RH <2%), atmospheric pressure and room temperature (294 ± 2 K). The rate coefficient ($k = 2.1 \times 10^{-16} \text{ cm}^3 \text{ molecule}^{-1} \text{ s}^{-1}$) determined using both the pseudo-first-order and the relative methods lead to an atmospheric lifetime of ~ 33 mins for γ -terpinene with respect to its reaction with ozone.

In addition, the products formed in the gas-phase were identified and quantified for the first time and the mechanism leading to these oxidation products was proposed. The formation potential of secondary organic aerosols from the γ -terpinene reaction with ozone has also been studied with and without an OH radical scavenger and provide a new source of SOA which can be included in atmospheric models. Scanning Electron Microscopy (SEM) images show that the aerosols formed from this reaction are spherical and viscous and that only one organic phase is present in the aerosol under the applied experimental conditions (relative humidity < 2%).

Finally, the hygroscopic properties of the SOA were investigated using a HTDMA. The measurements of the growth factor (GF = 1.024 – 1.11) and the kappa (0.008 – 0.2) indicate that these aerosols are slightly hygroscopic. The influence of several parameters including the presence of an OH radical scavenger (cyclohexane), an anthropogenic VOC precursor of SOAs (TMB) and seed particles (AS) on the aerosol hygroscopicity, was also evaluated. Regardless of the presence of AS seeds, the results revealed no significant effects.

The chemical characterization of SOA formed from the ozonolysis of γ -terpinene was also tentatively investigated. Analyses were performed using different techniques: thermodesorption / GC / MS (in LPCA), solvent extraction followed by ES / LC / QToF-MS (in CCM, ULCO) and ToF-SIMS (in PhLAM, Lille University). The former did not allow to clearly characterize some organic compounds in the particle phase and the two others which are not carried out in LPCA are not finished yet. The derivatization followed by GC/MS analyses could also be tested for the

analysis of (multi)-functionalized compounds. The investigation of hygroscopicity of SOA using a CCNc is already started but the results are still in progress and after it is possible to have closure analysis for kappa values obtained from CCNc and HTDMA data. On the other hand, the reactivity of γ -terpinene with other oxidants OH, NO₃ and Cl is planned to be investigated in *CHARME*. Also, the reactivity of different VOCs (Furan, Sesquiterpenes...) precursors of SOA is intended to be studied in the future.

Finally, *CHARME* is a leading instrument of the region "Hauts-de-France". It has recently been associated to the European project EUROCHAMP 2020 and aims to become a national and international platform for physico-chemists of the atmosphere.

Supplementary Information

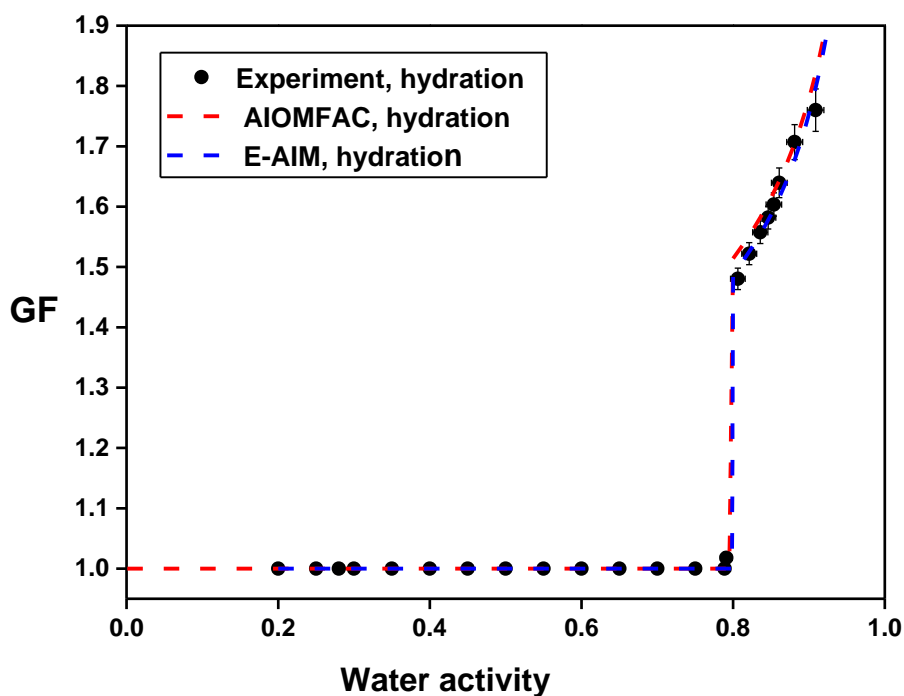


Figure S.1 The hygroscopic growth curve of pure AS particles $d=100$ nm.

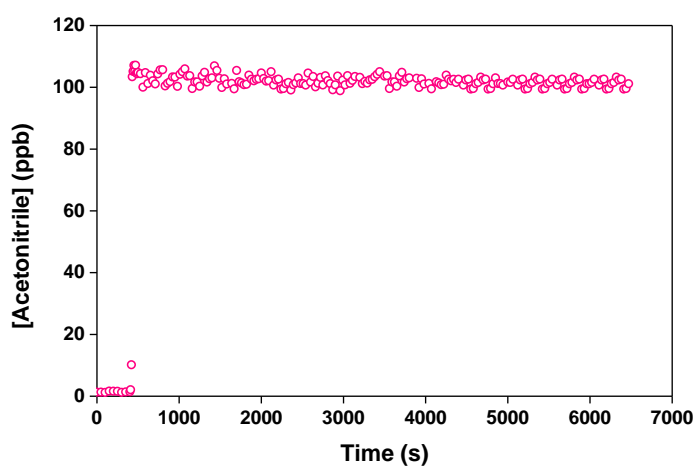
Figure S.1 shows typical behavior of crystalline inorganic salts with a deliquescence relative humidity point (DRH) at $\sim 80\%$ RH, in good agreement with thermodynamic models (AIOMFAC) and (E-AIM). GFs uncertainties in our experiments are estimated to be less than 3.5% at RH 93%, 2.5% and $< 1.5\%$ for 90% and $< 80\%$ RH, respectively.

Table S. 1: The two-product parameters (α_1, α_2 and $K_{p,1}, K_{p,2}$) obtained from ozonolysis of α -pinene.

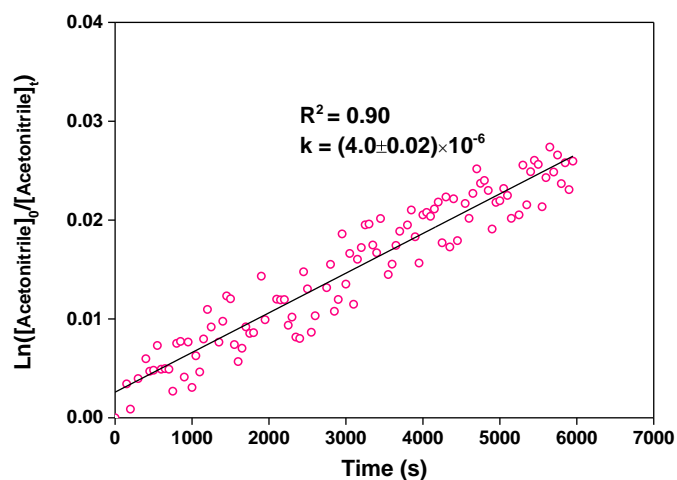
α_1	$K_{p,1}(\text{m}^3 \cdot \mu\text{g}^{-1})$	α_2	$K_{p,2}(\text{m}^3 \cdot \mu\text{g}^{-1})$	Reference
0.25 ± 0.08	0.06 ± 0.04	0.27 ± 0.1	0.01 ± 0.03	This study, with cyclohexane
0.24 ± 0.01	0.08 ± 0.01	0.30 ± 0.5	0.009 ± 0.005	This study, without cyclohexane

Table S. 2 : The two-product parameters (α_1, α_2 and $K_{p,1}, K_{p,2}$) obtained from ozonolysis of γ -terpinene.

α_1	$K_{p,1} (\text{m}^3 \cdot \mu\text{g}^{-1})$	α_2	$K_{p,2} (\text{m}^3 \cdot \mu\text{g}^{-1})$	Reference
0.48 ± 0.03	0.03 ± 0.9	0.11 ± 0.02	0.002 ± 0.02	This study, with cyclohexane
0.50 ± 0.02	0.02 ± 0.004	0.52 ± 0.03	0.02 ± 0.03	This study, without cyclohexane

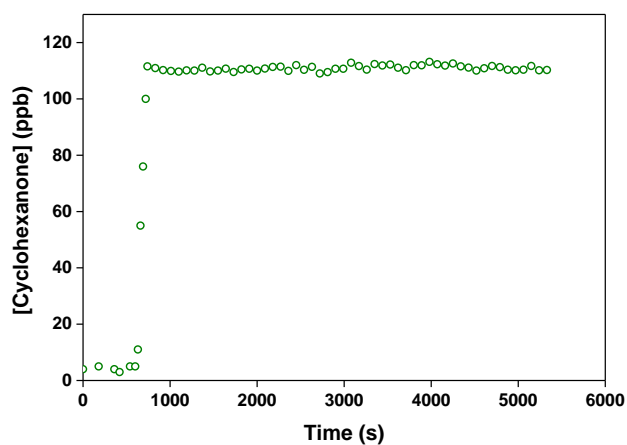


a

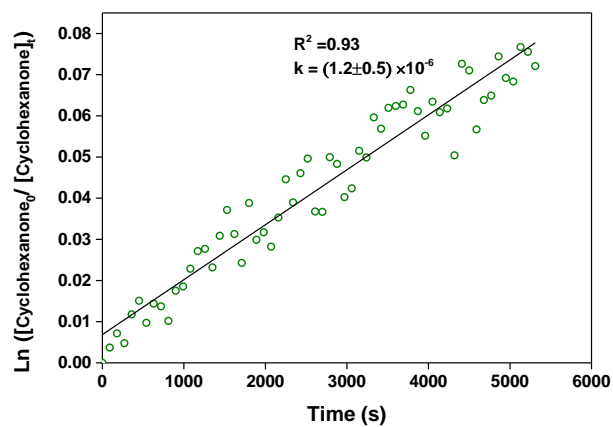


b

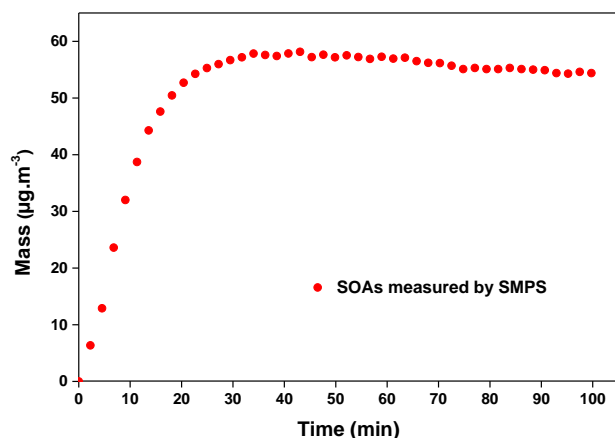
Figure S.2: Time profile of acetonitrile injected and the corresponding loss in the chamber.



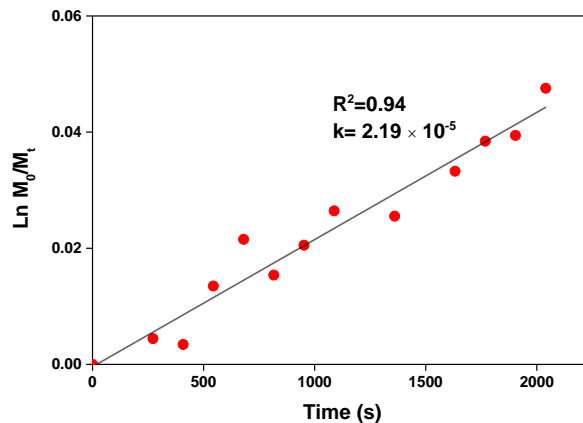
a



b



c



d

Figure S.3: (a) The time profile of cyclohexanone and (b) the plot of $\ln [cyclohexanone]_0/[cyclohexanone]_t$ that allows the determination of wall losses. Similarly, for (c) and (d) but for SOA formed from the ozonolysis of α -pinene (α -pinene= 70 ppb and ozone =160 ppb). Cyclohexanone represents an example of how the wall losses of gases were calculated and the SOA represents the particles wall loss determination.

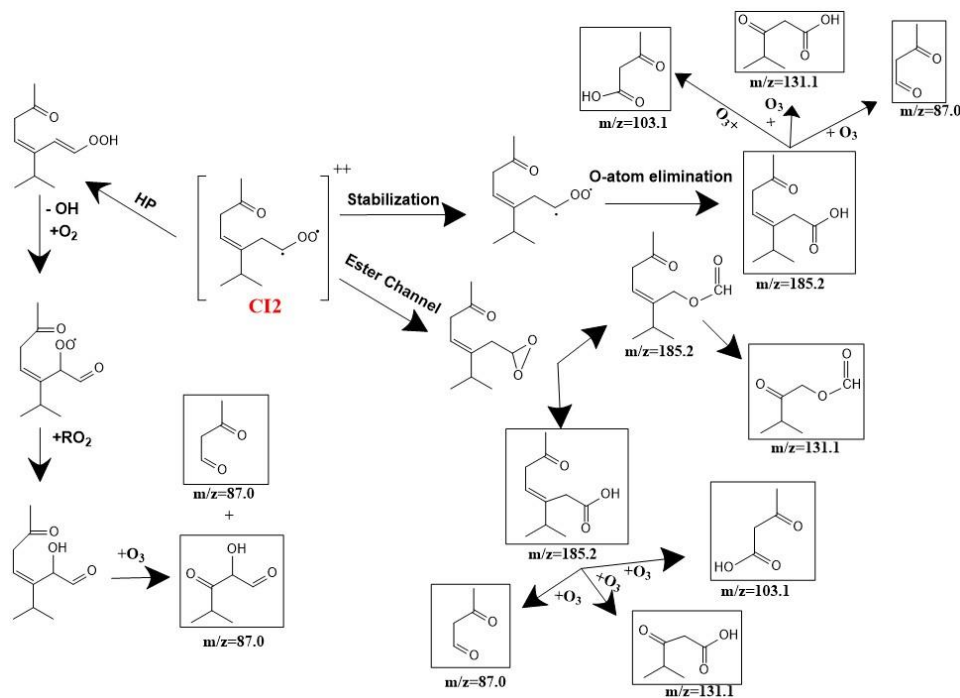


Table S. 3: Coefficients (a, b, c) of the fitted growth factor parameterization (Eq. IV.9).

SOA produced from ozonolysis of	Exp Number	$[\gamma\text{-terpinene}]_0$ (ppb)	a	b	c
γ -terpinene	7	16	0.0270	0.0985	-0.0954
γ -terpinene + Cyclohexane	15	16	0.0306	-0.0893	0.0836
γ -terpinene	1	158	-0.0835	0.3506	-0.2613
γ -terpinene +Cyclohexane	21	154	-0.0044	0.0662	-0.0569
γ -terpinene +TMB	16	16	0.0776	-0.1528	0.1171
γ -terpinene +TMB	14	48	-0.0038	0.0030	0.0370
γ -terpinene +TMB	17	110	0.0712	-0.1746	0.1313
γ -terpinene +TMB	15	158	0.0321	-0.0660	0.0534

Thesis Summary in French

(Résumé de la thèse)

Contexte scientifique

Les interactions importantes entre l'atmosphère et les organismes vivants nécessitent la présence d'un nouveau domaine scientifique qui cherche à élucider ces relations et interactions. Par conséquent, la chimie atmosphérique a été découverte au milieu des années 1980 (**Akimoto, 2016**).

La chimie atmosphérique est devenue une voie de recherche multidisciplinaire qui implique la chimie environnementale, la physique, la météorologie, la modélisation informatique et d'autres disciplines. Elle cherche à comprendre les processus chimiques et physiques qui se produisent dans l'atmosphère, en plus des émissions, du transport, des durées de vie et du devenir des produits chimiques biogènes et anthropiques (**Finlayson-Pitts et Pitts Jr, 1999**).

L'étude de l'atmosphère, en particulier de sa chimie, a été examinée par différentes méthodes. Les mesures sur le terrain, les modèles informatiques et les études cinétiques en laboratoire sont les outils puissants utilisés pour répondre aux besoins de recherche atmosphérique. L'intégration de tous ces outils permet aux scientifiques de mieux comprendre le système atmosphérique (**Kim, 2009**).

La façon la plus directe et la plus significative d'examiner les processus et mécanismes se produisant dans l'atmosphère et de simplifier ce système physico-chimique extrêmement complexe consiste à simuler les conditions atmosphériques dans les grands réacteurs de laboratoire appelés chambres de simulation atmosphérique (**Finlayson-Pitts et Pitts, 1986**).

Les chambres de simulation atmosphérique sont de précieux outils scientifiques qui servent d'intermédiaire entre les campagnes sur le terrain et les expériences en laboratoire. En effet, les chambres de simulation permettent de contrôler plus de variables (température, humidité, concentrations...) qu'il n'est possible dans les campagnes de terrain, réduisant la complexité des mesures sur le terrain et les tests des mécanismes d'oxydation des COV. De plus, en ce qui concerne les expériences de cinétique en laboratoire, les chambres offrent la possibilité de réaliser des expériences de cinétique à plus longue échelle que les réacteurs à écoulement, sur une plus large gamme de composés et dans des conditions plus pertinentes sur le plan atmosphérique (**Glowacki et al., 2007**).

Les chambres de simulation sont utilisées depuis plus de 60 ans (**Akimoto, 2014**) et sont toujours construites et développées dans le monde entier. Les composants de base d'une chambre de simulation comprennent le sac de réaction ou le grand récipient réactif, les précurseurs ou les constituants chimiques à étudier, les sources lumineuses et les instruments de surveillance (**Platt, et al., 2009**).

Selon leur source de rayonnement, les chambres de simulation sont placées soit à l'intérieur soit à l'extérieur. Celles de l'intérieur fournissent un contrôle précis de la température et de l'humidité, mais peuvent souffrir de la différence entre les spectres des lumières artificielles couplées et le vrai rayonnement solaire (**Wang, et al., 2014**). D'un autre côté, les chambres placées à l'extérieures, étant généralement plus grandes que celles à l'intérieures, sont capables de fonctionner dans des conditions atmosphériques réelles telles que la lumière naturelle du soleil et la température (**Platt, et al., 2009**).

Les chambres de simulation ont l'avantage d'étudier la formation et l'évolution de composés d'intérêt spécifiques comme les polluants, dans un système fermé séparément de la météorologie et en dehors des autres interférences atmosphériques (**Wang et al., 2011**). Ils sont utiles pour la détection d'espèces multiples en utilisant plusieurs techniques sur de longues échelles de temps qui pourraient être de l'ordre des heures ou des jours (**Glowacki et al., 2007**). En fait, le grand volume de la chambre offre un espace pour les équipements d'analyse tels que le cryo-piégeage des radicaux et la fluorescence induite par laser (LIF). Le grand réacteur favorise également l'application de la spectroscopie d'absorption à long trajet dans les UV, le VIS et l'IR. Les chambres de simulation offrent l'opportunité de comprendre les mécanismes d'oxydation aussi bien en phase gazeuse qu'en phase particulaire.

D'un autre côté, les chambres de simulation présentent certaines limites. La surface de leur paroi représente la plus grande incertitude et pourrait induire des réactions hétérogènes ou des dégagements gazeux inattendus possibles de gaz ou de particules. De plus, des réactions non réalistes pourraient être encouragées dans la chambre, en particulier lorsque la source de lumière est artificielle. Le fond des produits chimiques et des effets de mémoire ne peut pas être nié également; ils peuvent compliquer la composition chimique du mélange étudié et donc la fiabilité des données (**Wang et al., 2011**).

L'utilisation de chambres atmosphériques est une approche importante qui a été adoptée pour comprendre la chimie des composés organiques volatils (COV) et des aérosols atmosphériques et pour étudier les interactions gas-particules dans l'atmosphère (**Finlayson-Pitts et Pitts, 1986**). Un grand nombre de données expérimentales étudiant les processus chimiques et physiques des composés organiques émis ont été obtenues au cours des deux dernières décennies. Cependant, les différentes classes de COV émis dans la troposphère ne sont pas entièrement comprises et il y a beaucoup à savoir. Les COV sont émis par des sources biogéniques et anthropiques. À l'échelle régionale et mondiale, les émissions de COV naturels dépassent celles des émissions anthropiques d'un facteur d'environ 10 (**Lamb et al., 1987; Guenther et al., 1995**). Les importantes émissions de composés organiques volatils biogéniques (COVB) et leur contribution au bilan mondial du carbone atmosphérique ont révélé l'importance de cette classe de composés. Parmi les différentes classes de COVB, les monoterpènes ($C_{10}H_{16}$) dont les structures sont constituées de deux unités d'isoprène (C_5H_8) sont considérés comme d'une grande importance. Les deux monoterpènes les plus naturellement abondants sont l' α -pinène et le β -pinène (**Guenther et al., 1995**). Ceux-ci, en plus d'autres monoterpènes, sont très réactifs dans l'atmosphère et leur durée de vie chimique atmosphérique varie de quelques minutes à quelques heures (**Atkinson et al., 1990a**). L'oxydation de ces COVB peut produire des espèces de pression de vapeur suffisamment faible pour être condensable, conduisant à la formation d'aérosols organiques secondaires (AOS). Ce processus est initié en phase gazeuse par l'attaque du radical hydroxyle pendant la journée et par les radicaux nitrate pendant la nuit (**Finlayson-Pitts et Pitts Jr, 1999**). L'ozone oxyde les COVB pendant la nuit et le jour et l'ozonolyse de ces composés est connue pour être la réaction d'oxydation la plus efficace en termes de génération de produits à faible volatilité pouvant contribuer de manière significative à la formation de AOS (**Bernard et al., 2010**).

L'étude des AOS a été d'un grand intérêt en raison de leur importance dans l'atmosphère. Les AOS représentent une part importante des aérosols troposphériques ambiants. Comme tous les aérosols, les AOS influent sur les processus atmosphériques, le climat et la santé humaine. Par exemple, les AOS ont un impact sur le climat via la diffusion et l'absorption des rayonnements solaires et infrarouges dans l'atmosphère et ont donc un forçage radiatif direct (**IPCC, 2014**). Ils modifient également l'efficacité de formation et de précipitation de l'eau liquide, de la glace et des nuages en phase mixte et affectent ainsi la durée de vie, les quantités et l'albédo des nuages (**Andreae et Crutzen, 1997**). Afin de comprendre l'interaction entre les aérosols atmosphériques

et les nuages, un nombre croissant d'études ont été menées et axées sur le comportement hygroscopique des aérosols. L'hygroscopicité représente la capacité des aérosols à interagir avec la vapeur d'eau dans l'air ambiant. Il explique les conditions dans lesquelles les aérosols de différentes compositions chimiques peuvent servir de CCN (noyaux de condensation des nuages). Des mesures de l'absorption d'eau et de l'activité CCN des particules atmosphériques sont nécessaires pour les modèles climatiques, les modèles de résolution des nuages et les prévisions de la qualité de l'air (Mirrieles et Brooks, 2018).

La difficulté d'étudier l'atmosphère est liée à la diversité des constituants et à la complexité des processus de transformation impliqués dans les phases atmosphériques homogènes et hétérogènes. Cherchant à mieux comprendre ce milieu physico-chimique complexe, des chambres de simulation atmosphérique sont utilisées depuis les six dernières décennies. En 2015, une nouvelle chambre de simulation atmosphérique construite nommée *CHARME* a été développée dans notre laboratoire LPCA (Laboratoire de Physico-Chimie de l'Atmosphère, Dunkerque).

Cette thèse est le premier travail de recherche réalisé au sein de *CHARME*. La nouvelle chambre de simulation (conception, fonctionnalités, instruments...) est représentée pour la première fois et les résultats d'une série de tests de caractérisation sont décrits dans la première partie de ce manuscrit. La deuxième session de cette recherche présente l'étude de la réaction d'ozonolyse du γ -terpinène.

Caractérisation de *CHARME*

La nouvelle chambre de simulation *CHARME* présentée dans la **Figure 1**, est l'acronyme de «CHambre pour l'étude de la Réactivité Atmosphérique et de la Métrologie de l'Environnement». Elle vise à être une plate-forme scientifique pour les travaux de recherche nationaux et internationaux dans le domaine de la chimie physique atmosphérique. Elle est fondée pour étudier la phase gazeuse (mesures cinétiques, mécanismes chimiques et formation de produits...), la phase particulaire (formation des AOS...) et pour développer des instruments optiques dédiés aux mesures d'espèces d'intérêt atmosphérique (IBBCEAS, EC-QCL,...).

CHARME est un réacteur intérieur fermé de forme cylindrique et de structure horizontale linéaire. Elle se compose d'une cuve en acier inoxydable de type 304L de 9,2 m³ avec une surface interne de 30 à 32 m² et un rapport surface / volume S / V d'environ 3,5 m⁻¹. Elle possède une longueur de 4,4 m, une largeur de 2,2 m, une hauteur de 2,2 m, un diamètre intérieur d'environ 1,68 m et un poids moyen de 5850 kg.



Figure 1 : Photographie de la chambre de simulation *CHARME*.

Les caractéristiques de la CSA sont indiquées dans le **Tableau II.1**.

Tableau 1: Caractéristiques de la chambre de simulation atmosphérique *CHARME*.

Nom	<i>CHARME</i>
Acronyme	CHambre pour l'étude de la Réactivité Atmosphérique et de la Métrologie de l'Environnement
Localisation	Intérieur
Forme	Cylindre
Position	Horizontale
Matériau	Inox type 304L - électropoli
Fenêtre	4 fenêtres en quartz
Volume	9,2 m ³
Rapport S/V	3,5 m ⁻¹
Longueur × Diamètre	4,4 m × 1,68 m
Masse	5850 kg
Température*	-20° C < T < +50° C
Pression	0,4 mbar < P < 1013 mbar
Lampes	4 lampes à arc à haute pression au xénon (= 5 kW chacune)

* *Sera opérationnel à l'avenir*

CHARME est équipée de 4 lampes à arc au xénon (5 kW chacune) pour simuler l'irradiation solaire et est couplée (en ligne et hors ligne) à de nombreux instruments analytiques pour la mesure des phases gazeuses et particulaires atmosphériques (Tableau 2).

Tableau 2: Résumé de l'instrumentation couplée à *CHARME* avec leurs paramètres de mesure.

Instrument (Modèle)	Espèce (Paramètre)
Analyseur d'ozone (UV photometric, Thermo Scientific 49i) Générateur d'ozone (Air Tree Ozone Technology C-L010-DTI)	O ₃
Analyseur de NO _x (Chemiluminescence, Thermo Scientific 42i)	NO, NO ₂
IBBCEAS in-situ (660 nm) ¹	NO ₃ , NO ₂
EC-QCL-MPC (8 µm) ^{1,2}	N ₂ O ₅
PTR-ToF-MS, IONICON 1000 Thermodésorbteur – GC (Autosystem XL) – FID / MS (Turbomass), Perkin Elmer Cellule à trajets multiples (cellule Chernin) connectée à FTIR (Bruker)	COV
SMPS (DMA “TS1 3081”, CPC “TSI 3775”) SMPS (Grimm 5.404) OPC (Grimm 1108) Générateur (TSI 3076) et Sécheur (TSI 3062) d'aérosol	Mesure des particules (distribution granulométrique ; concentration en nombre, en volume et en masse) Génération des particules
Sondes : (VAISALA HMT330) et (Sensirion EK-H5 - SensorSHT75)	Humidité, Température
Régulateur de pression avec jauges capacitives MK Baratron (Baratron® Basics)	Pression
Spectroradiomètre (Metcon)	Flux actinique

¹*Développé en LPCA.*

²*Sera couplé à CHARME à l'avenir.*

La nouvelle chambre de simulation *CHARME*, doit être caractérisée et validée afin de vérifier l'absence d'artefacts et de confirmer qu'elle peut être utilisée pour simuler des réactions chimiques atmosphériques.

La caractérisation est essentielle pour évaluer certains paramètres fondamentaux à travers différents tests, notamment:

- La caractérisation du système de pompage pour déterminer la pression la plus basse disponible dans la chambre et le temps pour l'atteindre.
- Tests de fuite pour vérifier l'étanchéité de la chambre.
- Tests de mélange pour vérifier l'homogénéisation des gaz et des particules.
- Tests de perte de paroi pour déterminer la durée de vie des gaz et aérosols sans aucune réaction.
- Tests de lumière pour caractériser le système d'irradiation en mesurant sa distribution spectrale, en déterminant les constantes de photolyse de NO₂ et O (1D) et en vérifiant l'homogénéité de la lumière dans la chambre.
- Expériences d'irradiation propène-NO_x-air pour illustrer l'utilité de la chambre pour l'évaluation des mécanismes auxiliaires.

CHARME présentait une bonne limite de vide et des fuites assez négligeables (~ 40 ppb d'air du laboratoire). Les quatre ventilateurs agitateurs tournant à 190 tr / min permettent un mélange court (~ 3 minutes) et efficace des espèces chimiques. Les propriétés des parois et leurs effets mineurs ont permis des constantes de perte de parois relativement faibles de gaz et des particules, ce qui entraîne des durées de vie de quelques heures pour ces espèces. Le temps relativement court pour le processus de nettoyage (~ 60 minutes) et son efficacité ont montré l'avantage d'effectuer plus d'une expérience par jour (de 1 à 3, selon la durée de chacune). L'irradiation de la chambre à blanc pendant 1 heure a conduit à la formation de gaz (1 ppb d'O₃ et 2 ppb de NO₂) et d'aérosols (15 particules), ce qui est acceptable et comparable à ceux mesurés dans d'autres chambres atmosphériques. Des tests préliminaires ont montré la capacité de faire varier l'humidité relative dans la chambre, mais des travaux supplémentaires sont nécessaires pour définir les conditions et simuler les brouillards ou les nuages. Des expériences sur la formation d'aérosols secondaires à partir de la réaction d'ozonolyse α -pinène ont révélé une bonne reproductibilité et un accord avec les données de la littérature. Concernant le système d'irradiation, bien que la distribution spectrale mesurée (de 315 nm à 650 nm; cette dernière valeur correspondant à la limite supérieure du spectroradiomètre) ne soit pas très proche du spectre d'émission solaire, la photolyse de fréquence NO₂ déterminée (J_{NO_2}) était en le même ordre que ceux mesurés dans d'autres chambres et dans l'atmosphère. Les expériences d'irradiation propène – NO_x – air ont été utilisées pour identifier le mécanisme auxiliaire de la chambre et une concentration initiale en HONO de 1 ppb permet au modèle d'ajuster les concentrations mesurées de gaz. Il est important

de garder à l'esprit que tous ces paramètres doivent être caractérisés régulièrement, car ils peuvent varier en raison de la propreté des parois de la chambre et / ou du vieillissement des lampes, de la pompe, etc.

Ainsi, les différents tests effectués pour caractériser *CHARME* sont réussis et permettent de conclure que cette enceinte peut être utilisée pour simuler des processus physico-chimiques atmosphériques.

L'étude de l'ozonolyse du γ -terpinène

L'étude au sein de la chambre, présentée dans ce travail vise à contribuer à la compréhension du comportement atmosphérique du monoterpène, le γ -terpinène. Ce composé a été sélectionné en fonction de sa réactivité avec les principaux oxydants atmosphériques (O_3 , OH et NO_3), sa capacité à libérer des radicaux OH par réaction avec O_3 et son potentiel à former des aérosols organiques secondaires. Un certain nombre d'études ont rapporté l'oxydation en phase gazeuse du γ -terpinène avec OH (Atkinson et al., 1986; Griffin et al., 1999a; Lee et al., 2006; Rio et al., 2010; Aschmann et al., 2011) et NO_3 (Atkinson et al., 1985a; Martinez et al., 1999; Fouqueau et al., 2017). Cependant, l'ozonolyse de ce composé a été étudiée dans une moindre mesure avec seulement deux publications concernant les études cinétiques (Grimsrud et al., 1975; Atkinson et al., 1990) et des informations limitées sur le produit et la mécanique rapportées par Reissell et al., (1999) et Aschmann et al., (2002). Par conséquent, la connaissance de la réactivité atmosphérique de ce monoterpène étant limitée, il a fallu améliorer les connaissances en chimie atmosphérique, notamment s'intéresser à ses réactions avec l'ozone. De plus, la recherche scientifique s'est récemment concentrée sur l'hygroscopicité des AOS en raison de l'importance de cette propriété sur le climat et la santé. L'examen de l'ozonolyse du γ -terpinène est divisé en trois parties complémentaires. La première section se concentre sur la chimie en phase gazeuse, y compris les études cinétiques et mécaniques. La deuxième partie est dédiée à la phase particulaire, elle concerne la détermination des rendements de formation des AOS et l'identification de leur morphologie et de leur état physique. Enfin, la troisième unité du chapitre met en lumière les propriétés hygroscopiques des AOS.

L'enquête cinétique a été réalisée à 294 ± 2 K, pression atmosphérique, dans des conditions sèches (HR <2%) et en présence de cyclohexane comme piègeur d'OH. Deux méthodes différentes, le pseudo-premier ordre et la méthode relative ont été utilisées pour déterminer la constante de réaction du γ -terpinène avec l'ozone. Les valeurs obtenues avec les deux méthodes sont en bon accord et conduisent à un coefficient de vitesse de $(2,1 \pm 0,11) \times 10^{-16} \text{ cm}^3 \text{ molécules}^{-1} \text{ s}^{-1}$ pour la réaction d'ozonolyse du γ -terpinène. Les produits d'oxydation formés en phase gazeuse ont été analysés avec un PTR-TOF-MS. 20 produits d'oxydation ont été observés et quantifiés et 9 d'entre eux ont été identifiés. Un mécanisme proposant la formation de certains des produits d'oxydation observés a été présenté pour la première fois.

De plus, l'étude de la phase particulaire a révélé un rendement de formation de AOS sur une gamme de masse ($\sim 10 - 890 \mu\text{g m}^{-3}$) en présence ($\sim 49\%$) et en l'absence ($\sim 52\%$) d'un piègeur OH (cyclohexane). L'examen de l'état physique et de la morphologie des particules AOS formées a montré qu'elles sont visqueuses et sphériques. De plus, les propriétés hygroscopiques et l'activité CCN des AOS ont été étudiées en utilisant un HTDMA à HR 93%. Ces paramètres ont été caractérisés dans différentes conditions expérimentales, notamment: (1) l'effet des concentrations initiales de précurseurs, (2) la présence d'un COV anthropique (TMB), (3) la présence d'un piègeur d'OH et (4) la présence de sulfate d'ammonium particules.

Tableau 3: Résumé des expériences réalisées pour caractériser les phases gazeuses et particulaires de la réaction de l'ozone et du γ -terpinène.

Paramètre	Résultat	Commentaire
Phase gazeuse		
Constante de vitesse	$(2,1 \pm 0,11) \times 10^{-16}$ $\text{cm}^3 \text{ molecule}^{-1} \text{ s}^{-1}$	Une nouvelle détermination révélée à partir de 2 méthodes (pseudo premier ordre et relative (avec 3 références) dans 2 chambres différentes
Produits gazeux	20 produits observés et 9 identifiés dont: formaldéhyde, acétaldéhyde, acide formique, acétone, glyoxal, acide acétique	Un rendement total moyen ~ 52%
Phase particulaire		
Rendement AOS	~49 % (Avec du cyclohexane)	La réaction du γ -terpinène et de l'ozone est considérée comme un nouveau contributeur à la formation atmosphérique des AOS.
	~52% (Sans cyclohexane)	
Morphologie	Sphérique	Indépendamment de la concentration initiale du précurseur et de la présence / absence de cyclohexane.
État physique	Visqueux	
Facteur de croissance (HR = 90%)	1,024 – 1,11	En fonction de la concentration initiale du γ -terpinène, de la présence de radicaux OH et de TMB.
	1,20 – 1,44	Affecté par la présence de graines d'AS et la concentration initiale du γ -terpinène
K _{GF}	0,008 – 0,2	En fonction de la concentration initiale du γ -terpinène, de la présence de radicaux OH, TMB et graines.

Conclusion et perspectives

Ce travail de recherche présente *CHARME* avec toutes ses fonctionnalités de base et ses instruments importants. Il vise à caractériser les paramètres techniques et physico-chimiques dont l'intensité de l'irradiation, le temps de mélange des différents composés, la durée de vie des gaz et des particules, l'effet des murs etc. Les tests préliminaires effectués à *CHARME* ont démontré que cette chambre est un outil utile pour étudier les processus physico-chimiques se produisant dans l'atmosphère. D'autres développements sont prévus pour *CHARME* dans un avenir proche. En 2020, une cellule à trajets multiples Chernin sera installée dans la chambre et connectée à un spectromètre FTIR (Bruker) et à une source THz (pour les analyses de spectroscopie rotationnelle). D'autres techniques optiques seront également couplées à *CHARME* (IBBCEAS pour HONO et coefficients d'extinction des aérosols, spectroscopie photoacoustique pour les coefficients d'absorption des aérosols, EC-QCL-MPC pour N₂O₅...). Enfin, une installation pour introduire avec précision les COV dans le réacteur et un système de régulation de la température (de -20 à 50 ° C) seront installés.

De plus, un travail de recherche pour étudier la réaction de l'ozone avec le γ -terpinène, un monoterpène important contenant deux doubles liaisons endocycliques, a été réalisée dans la chambre de simulation *CHARME*. Les résultats obtenus en phase gazeuse comprennent: la détermination de la constante de vitesse, l'identification et la quantification des produits et la suggestion d'un mécanisme conduisant aux produits observés. De plus, la phase particulaire a été étudiée en déterminant les rendements de formation des aérosols organiques secondaires, en caractérisant leurs propriétés chimiques et physiques et en examinant leur hygroscopicité. Les recherches futures concernant cette réaction nécessitent un ensemble d'investigations comprenant: la détermination des rendements de formation d'OH et l'identification / quantification de la composition moléculaire AOS en utilisant différentes méthodes. La caractérisation chimique des AOS formés à partir de l'ozonolyse du γ -terpinène a été provisoirement étudiée. Les analyses ont été réalisées à l'aide de différentes techniques: thermodésorption / GC / MS (en LPCA), extraction au solvant suivie par ES / LC / QToF-MS (en CCM, ULCO) et ToF-SIMS (en PhLAM, Université de Lille). Le premier n'a pas permis de caractériser clairement certains composés organiques en phase particulaire et les deux autres qui ne sont pas réalisés en LPCA ne sont pas encore finis. La dérivatisation suivie d'analyses GC / MS pourrait également être testée pour l'analyse de composés

(multi) fonctionnalisés. Les résultats de l'étude de l'hygroscopicité des AOS à l'aide d'un CCNc sont en cours de traitement, et après il est possible d'avoir une analyse de fermeture pour les valeurs kappa obtenues à partir des données CCNc et HTDMA. En revanche, la réactivité du γ -terpinène avec d'autres oxydants OH, NO₃ et Cl devrait être étudiée dans *CHARME*. De plus, la réactivité des différents précurseurs des COV (Furan, Sesquiterpenes...) des AOS est à étudier dans le futur.

Enfin, *CHARME* est un instrument phare de la région «Hauts-de-France». Il a récemment été associé au projet européen EUROCHAMP 2020 et vise à devenir une plateforme nationale et internationale pour les physico-chimistes de l'atmosphère.

Références

- Aschmann, S.M., Arey, J., Atkinson, R., 2002. OH radical formation from the gas-phase reactions of O₃ with a series of terpenes. *Atmospheric Environment* 36, 4347–4355. [https://doi.org/10.1016/S1352-2310\(02\)00355-2](https://doi.org/10.1016/S1352-2310(02)00355-2)
- Aschmann, S.M., Arey, J., Atkinson, R., 2011. Formation of p-cymene from OH + γ -terpinene: H-atom abstraction from the cyclohexadiene ring structure. *Atmospheric Environment* 45, 4408–4411. <https://doi.org/10.1016/j.atmosenv.2011.05.044>
- Atkinson, Roger, Aschmann, S.M., Winer, A.M., Pitts, J.N., 1985a. Kinetics and atmospheric implications of the gas-phase reactions of nitrate radicals with a series of monoterpenes and related organics at 294 \pm 2 K. *Environmental Science & Technology* 19, 159–163. <https://doi.org/10.1021/es00132a009>
- Atkinson, R., 1986. Kinetics and mechanisms of the gas-phase reactions of the hydroxyl radical with organic compounds under atmospheric conditions. *Chemical Reviews* 86, 69–201. <https://doi.org/10.1021/cr00071a004>
- Atkinson, R., Hasegawa, D., Aschmann, S.M., 1990. Rate constants for the gas-phase reactions of O₃ with a series of monoterpenes and related compounds at 296 \pm 2 K. *International Journal of Chemical Kinetics* 22, 871–887. <https://doi.org/10.1002/kin.550220807>
- Bernard, F., Quilgars, A., Cazaunau, M., Grosselin, B., Daele, V., Mellouki, A., Winterhalter, R., Moortgat, G.K., 2010. Ozonolysis of a series of biogenic organic volatile compounds and secondary organic aerosol formation, in: EGU General Assembly Conference Abstracts. p. 822.
- Finlayson-Pitts, B.J., Pitts, J.N., 1986. *Atmospheric chemistry: fundamentals and experimental techniques*. New York: Wiley.
- Finlayson-Pitts, B.J., Pitts Jr, J.N., 1999. *Chemistry of the upper and lower atmosphere: theory, experiments, and applications*. Elsevier.
- Fouqueau, A., Cirtog, M., Quilleuc, M.L., Cazaunau, M., Pangui, E., Duncianu, M., Doussin, J.-F., Picquet-Varrault, B., 2017. Reactivity of γ -Terpinene with NO₃ radicals: experimental approach for kinetic and mechanistic study. EGU General Assembly 19, 2017-8444.
- Griffin, R.J., Cocker, D.R., Flagan, R.C., Seinfeld, J.H., 1999. Organic aerosol formation from the oxidation of biogenic hydrocarbons. *Journal of Geophysical Research: Atmospheres* 104, 3555–3567. <https://doi.org/10.1029/1998JD100049>
- Grimsrud, E.P., Westberg, H.H., Rasmussen, R.A., 1975. Atmospheric Reactivity of Monoterpene Hydrocarbons, NO_x Photooxidation and Ozonolysis.
- Guenther, A., Hewitt, C.N., Erickson, D., Fall, R., Geron, C., Graedel, T., Harley, P., Klinger, L., Lerdau, M., McKay, W.A., Pierce, T., Scholes, B., Steinbrecher, R., Tallamraju, R., Taylor, J., Zimmerman, P., 1995a. A global model of natural volatile organic compound emissions. *Journal of Geophysical Research* 100, 8873. <https://doi.org/10.1029/94JD02950>
- IPCC, 2013. Anthropogenic and Natural Radiative Forcing — IPCC. URL <https://www.ipcc.ch/report/ar5/wg1/anthropogenic-and-natural-radiative-forcing/> (accessed 5.20.19).
- Lamb, B., Guenther, A., Gay, D., Westberg, H., 1987. A national inventory of biogenic hydrocarbon emissions. *Atmospheric Environment* (1967) 21, 1695–1705. [https://doi.org/10.1016/0004-6981\(87\)90108-9](https://doi.org/10.1016/0004-6981(87)90108-9)
- Lee, A., Goldstein, A.H., Kroll, J.H., Ng, N.L., Varutbangkul, V., Flagan, R.C., Seinfeld, J.H., 2006a. Gas-phase products and secondary aerosol yields from the photooxidation of 16

- different terpenes. *Journal of Geophysical Research* 111. <https://doi.org/10.1029/2006JD007050>
- Martinez, E., Cabanas, B., Aranda, A., Martin, P., Salgado, S., 1999. Absolute Rate Coefficients for the Gas-Phase Reactions of NO₃ Radical with a Series of Monoterpenes at T = 298 to 433 K 18
 - Mirrielees, J.A., Brooks, S.D., 2018. Instrument artifacts lead to uncertainties in parameterizations of cloud condensation nucleation. *Atmospheric Measurement Techniques* 11, 6389–6407. <https://doi.org/10.5194/amt-11-6389-2018>
 - Reissell, A., Harry, C., Aschmann, S.M., Atkinson, R., Arey, J., 1999. Formation of acetone from the OH radical and O₃ initiated reactions of a series of monoterpenes. *Journal of Geophysical Research: Atmospheres* 104, 13869–13879. <https://doi.org/10.1029/1999JD900198>
 - Rio, C., Flaud, P.-M., Loison, J.-C., Villenave, E., 2010. Experimental reevaluation of the importance of the abstraction channel in the reactions of monoterpenes with OH radicals. *Chemphyschem* 11, 3962–3970. <https://doi.org/10.1002/cphc.201000518>

Abstracts

(English and French)

Title: Characterization of the new atmospheric simulation chamber *CHARME*, and study of the ozonolysis reaction of a biogenic VOC, the γ -terpinene.

Keywords: Atmospheric Simulation Chamber, Characterization, γ -terpinene, Ozone, Rate coefficient, Mechanistic study, Secondary Organic Aerosols

The study of atmospheric processes is among the central topics of current environmental research. The most direct and significant way to investigate the transformation of pollutants and the formation of aerosols in the atmosphere, is to simulate these processes under controlled and simplified conditions. In this regard, a new simulation chamber, *CHARME* (CHamber for the Atmospheric Reactivity and the Metrology of the Environment) has been designed in the Laboratory of Physico-Chemistry of the Atmosphere (LPCA) in the University of Littoral Côte d'Opale (ULCO). *CHARME* is also dedicated to the development and validation of new spectroscopic approaches for the metrology of atmospheric species including gases, particles and radicals.

The first aim of this research was to characterize all the technical, physical and chemical parameters of this new chamber and to optimize the methods for studying the atmospheric reactivity of volatile organic compounds (VOCs) and simulating the formation of secondary organic aerosols (SOA). The results of numerous experiments and tests show that *CHARME* is a convenient tool to reproduce chemical reactions occurring in the troposphere

The second research objective was to investigate the reaction of the biogenic VOC, γ -terpinene, with ozone. The rate coefficient at (294 ± 2) K and atmospheric pressure was determined and the gas-phase oxidation products were identified. The physical state and hygroscopicity of the secondary organic aerosols was also studied. To our knowledge, this work represents the first study on SOA formation from the ozonolysis of γ -terpinene.

Titre: Caractérisation de la nouvelle chambre de simulation atmosphérique CHARME et étude de la réaction d'ozonolyse d'un COV biogénique, le γ -terpinène.

Mots-clés: Chambre de simulation atmosphérique, Caractérisation, γ -terpinène, Ozone, Coefficient de vitesse, Etude mécanistique, Aérosols organiques secondaires

L'étude des mécanismes et interactions atmosphériques est un des sujets majeurs actuels de recherches environnementales. La façon la plus directe et pertinente pour étudier la transformation des polluants et la formation des aérosols dans l'atmosphère est de simuler les processus dans des conditions contrôlées et simplifiées. Une nouvelle chambre de simulation CHARME (CHamber for the Atmospheric Reactivity and the Metrology of the Environment) a été développée au Laboratoire de Physico-Chimie Atmosphérique (LPCA) de l'Université du Littoral Côte d'Opale (ULCO). CHARME est également dédiée à la validation de dispositifs optiques utilisés pour la métrologie d'espèces atmosphériques stables et instables (radicaux).

La première partie de ces travaux de recherche concerne la caractérisation de tous les paramètres techniques, physiques et chimiques de cette nouvelle chambre et l'optimisation des méthodes pour étudier la réactivité des composés organiques volatiles (COV) et simuler la formation d'aérosols organiques secondaires (AOS). Les résultats obtenus démontrent que CHARME est un outil adapté pour reproduire les réactions se produisant dans la troposphère.

La deuxième partie est dédiée à l'étude de la réaction d'ozonolyse d'un COV biogénique, le γ -terpinène. La constante de vitesse à (294 ± 2) K et la pression atmosphérique a été mesurée et les produits d'oxydation identifiés dans la phase gazeuse. L'hygroscopicité des aérosols organiques secondaires a également été étudiée. A notre connaissance, ce travail *représente la première étude sur la formation des AOS à partir de l'ozonolyse du γ -terpinène.*